UNIVERSIDAD COMPLUTENSE DE MADRID

FACULTAD DE FARMACIA

Departamento de Química Física II

POLÍMEROS CONJUGADOS FLUORESCENTES PARA EL DESARROLLO DE BIOSENSORES ÓPTICOS DE APLICACIÓN EN CIENCIAS DE LA SALUD

MEMORIA PRESENTADA PARA OPTAR AL GRADO DE DOCTOR

Marco Laurenti

Bajo la Dirección de los Doctores

Prof. Enrique José López Cabarcos

Prof. Jorge Rubio Retama

Madrid 2011

"Al piccolo Matteo, a mia madre e mio padre,

a mio fratello e sua moglie,

a tutta la mia famiglia e amici."

Agradecimientos

Al fin he llegado a escribir la parte más importante de mi Tesis: los agradecimientos. Me ha costado pero estoy seguro de que el trabajo que presento en esta Tesis de Doctorado os gustará. Las primeras personas que quiero agradecer son sin duda mis Directores de Tesis el Prof. Enrique López Cabarcos y el Prof. Jorge Rubio Retama. Habría muchas cosas que decir… Pero a Enrique quiero sobre todo agradecerle la oportunidad de hacer la Tesis en este fantástico grupo de investigación y porque en estos 4 años juntos he tenido la oportunidad de conocer una persona estupenda, que ha aportado mucho a mi forma de pensar tanto en la investigación como en lo personal. Con respecto a Jorge, ya van 5 añitos desde que nos hemos conocido en Dresde, durante mi Máster, y si no me he ido a Londres a hacer el Doctorado es porque me has convencido de venir a Madrid y trabajar en este grupo. He aprendido muchas cosas y si puedo presentar esta Tesis es una buena parte gracias a tu ayuda.

Quiero agradecer todos los compañeros del laboratorio. Mohamad que ha sido un amigo y compañero muy valioso. Me has ayudado con los papeles cuando todavía no sabía hablar ni una palabra de español y me has dado muchos consejos importantes para sobrevivir estos 4 años aquí en Madrid, gracias. A Maha que aunque últimamente no te veo muy a menudo me has hecho reír muchas veces y me has ayudado en estos años en Madrid… Bueno a ver si quedamos para tomar un café (claro invito yo!). A David una persona encantadora, que por mala suerte se ha puesto a investigar con una cosa que odio bastante: las malditas nanoparticulas de hierro! A Julia Y Jatsue las dos últimas chicas que se han quedado en el grupo. Os deseo mucha suerte para vuestra inminente escritura de la Tesis! A Isabel otra chica encantadora que he tenido la suerte de conocer durante este Doctorado. A por cierto te lo juro que en cuanto acabe de escribir me pongo a hacer el trabajo que tenemos pendiente! A Mary que ha sido una compañera y amiga muy preciosa! A Rafa de la Universidad de Almería, me has ayudado un montón en los 4 meses pasados allí con vosotros. Tu también estas con la inminente defensa de la Tesis así que suerte y visca el Barça! Jejejeje! Al próximo Doctor del grupo Ángel Manchón, otra persona valiosa que he conocido durante mi camino aquí en Madrid. A los dos últimos fichajes del grupo Abdullah (el freno de emergencia no se tocaaaa!!!!) y Paulino! Las charlas que hemos tenido han sido muy buenas, me he reído como nunca con vosotros dos y habéis traído una aire nueva en el grupo! Chicos tenéis una buena oportunidad de trabajar en un buen grupo y aprender mucho. Quería agradecer también a las chicas del laboratorio del Prof. Leontidis de la Universidad de Chipre: María, Joanna, y Paulina por haber sido tan pacientes conmigo.

Quería agradecer a todo el Departamento de Química Física II de la Facultad de Farmacia por la estupenda acogida que he recibido desde el principio. Carmen Rueda, Conchita Arias, Pedro Galera, Francisco García Blanco, Marian y Begoña Elorza, Conchita Civera, Piedad Yusta, Visi Sanchéz, Miguel Angel Jimenez, Jesús Ruiz Cabello, Cristina Sainz, Paz Sevilla, Ángeles Heras, José Luis López Lacomba, y Jose González. Al Profesor Gregorio Carcedo de Técnicas por las charlas y los desayunos en su compañía. Gracias a todos vosotros me he sentido de verdad como en familia, hoy más que nunca. A los Profesores Antonio Fernández Barbero y Epaminondas Leontidis por la estupenda oportunidad de trabajar en vuestros laboratorios. A todas las personas de los CAIs de la Universidad Complutense de Madrid que me han ayudado en muchas análisis presentadas en esta Tesis. A José y a tod@s los de la cafetería de Farmacia a los que deberían dar el Doctorado en Psicología honoris causa.

Quería agradecer la Comunidad de Madrid por el contrato de Investigador de apoyo que me ha permitido realizar la Tesis, al Ministerio de Educación y Ciencia por los proyectos MAT2006-13646 y MAT2010-15349, el programa CAM-UCM de “Consolidación de Grupos de Investigación” R45/05-14177 y CCG06-1093, y el programa COST D43.

Quería agradecer a mi familia por todo el apoyo recibido durante estos años fuera de casa y si hoy tengo la oportunidad de conseguir esta etapa la mayor parte del merito es sin duda vuestra. En fin a todas las personas (compañer@s de pisos, amig@s) que directamente o indirectamente han participado en esta aventura que espero sea solo el comienzo de una nueva aventura.

"When you have eliminated the impossible,

whatever remains, however improbable,

must be the truth."

Sherlock Holmes in "The sign of the four".

Index

Abstract

Abstract

There are different materials with unique optical properties that can be used as sensors. However, the fabrication of a selective system towards a specific analyte is a complex task and a lot of investigation is required before the new chemo- or biosensor could be used in the analysis of real sample such as serum, polluted environment, contamination in water, etc.

This PhD thesis is focused on the development of new fluorescent materials and the strategies required for their applications in the field of optical sensing. To achieve this goal were used water-soluble conjugated polymers based on polythiophenes and poly(p-phenylene-vinylene).

The luminescence of conjugated polymers (CPs) can be either amplified using surfactants (surfactochromic effect) or quenched using molecules that deactivate the excited states of the CPs. This work investigates the influence of the surfactant chain length and surfactant concentration on the photoluminescence (PL) response of the water-soluble conjugated polymer poly(3-ethoxy-butyl-sulfonate-thiophene-2,5-diyl) (PTEBS) using N-alkyl-ammonium surfactants with 8, 9, 10, and 12 carbon atoms per hydrocarbon chain. The surfactant concentration was varied from 0.125 the critical micelle concentration (CMC) up to 2 times the CMC. The results show that at premicellar concentrations the polymer PL emission is sharply affected by the surfactant chain length. Thus, the PL is quenched by the surfactants with the shortest tails whereas the surfactants with the longest ones provoke an enhancement of the PL emission. This behavior has been associated with the capacity of the surfactants with the longest hydrocarbon chains to accommodate their tails inside the polymer, hindering the π–π interchain interactions during aggregation and reducing intrachain defects. By contrast, at the CMC, the surfactant chain length does not modify the PL emission, since the excess of surfactant inhibits polymer aggregation, thus enhancing the efficiency of light emissive processes.

The fluorescence amplification or quenching of CPs can be used as tool for the detection of specific molecules making possible the construction of optical sensors constituted of CPs.

Abstract

Thus a nitroaromatic compound sensor was developed combining the fluorescent polymer PTEBS and the microgel poly(N-isopropylacrylamide) (PNIPAM) synthesizing an interpenetrated PNIPAM-PTEBS microgel reticulated with methylene-bis-acrylamide (BA). PNIPAM is a thermoresponsive microgel in which a change of temperature can induce the microgel volume phase transition (VPT) making possible to modify the PL properties of the interpenetrated PNIPAM-PTEBS microgels. When the temperature was below the low critical solution temperature (LCST) of PNIPAM-PTEBS, the PL intensity was higher than that above the LCST. Time-resolved fluorescence measurements indicate that, in the swollen state, the increment of cross-linking increases the fluorescence decay time of PTEBS. By contrast, in the collapsed state, variations in the decay time were attributed to higher rigidity of the PNIPAM−PTEBS system, which was confirmed by neutron scattering measurements. Moreover, the shift in the wavelength of the fluorescence emission peak observed above the LCST indicates that the collapsed PNIPAM matrix was able to interact with the PTEBS chains hindering the formation of π−π interactions. This property is envisaged for developing a picric acid microsensor based on the formation of π−π interactions with the π-conjugated polymer, thus quenching its PL emission. Above the LCST of PNIPAM−PTEBS microgels, the interactions would be broken and the initial PL emission would be recovered. This property could render reusable microsensors for detection of nitro aromatic compounds.

CPs can be used as biosensors being possible to measure the product of a biochemical reaction between two chemical reagents. A new acetaminophen (APAP) biosensor was developed using the catalytic cycle of Horseradish peroxidase (HRP) catalyzed by hydrogen peroxide (H_2O_2). The HRP enzyme was encapsulated within a polyacrylamide microgel. It has been studied the fluorescence decrease of the water-soluble CP poly(2-methoxy-5-propyloxy-sulfonate-1,4-p-phenylene-vinylene) (MPS-PPV) by the catalytic activity of HRP in the presence of H_2O_2. MPS-PPV acts as a donor substrate in the catalytic cycle of HRP where the electron-deficient enzymatic intermediates compounds I (CoI) and II (CoII) can subtract electrons from the

polymer leading to its fluorescence decrease. The addition of the phenolic drug APAP to the former solution favors the decrease of the polymer fluorescence, which indicates the peroxidase-catalyzed co-oxidation of MPS-PPV and APAP. The encapsulation of HRP within polyacrylamide (PAA) microgels allows the isolation of intermediates CoI and CoII from the polymer, leading to a fluorescence decrease that is only due to the product of biocatalytic APAP oxidation. This system could be used to develop a new device for phenolic compounds detection.

A new water-soluble CP poly(3-ethoxy-thiophene-2,5-diyl-dimercaptosuccinic acid) (PTE-DMSA) was synthesized with the aim to have a fluorescent polymer with very specific properties suitable to detect optically the presence of metal ions such as lead and mercury. In order to do that, the fluorescence property of the polythiophene, that constitutes the polymer backbone, was combined with the complexation capacity of the meso-2,3-dimercaptosuccinic acid (DMSA) that constitutes the side chain species of the π–π CP. The method used to polymerize the monomer 2-(3-thienyl)-ethyl-acetate was the iron(III) chloride catalyzed polymerization. After the polymer synthesis, DMSA subunits were covalently attached to the side chains. The specific metal ions complexation produced by the DMSA provokes the variation of the polymer environment that triggers the PL quenching. In addition, it has been investigated the mechanism of the decreasing polymer PL intensity using time resolved fluorescence spectroscopy. The new water-soluble conjugated polymer could be used to develop devices for metal ions detection.

The development of sensors can be achieved combining CPs with microgels or using the free CPs in water. However, CPs are also polyelectrolytes that can be used as reducing and stabilizing agents during the synthesis of nanocrystals. The inclusion of nanoparticles within the microgels could provide materials with new properties such as magnetic or optical response, making them a hybrid material with interesting properties for sensors. A one-pot process to synthesize Au nanocrystals (AuNCs) was reported using the polyelectrolyte PTEBS in

combination with cadmium acetate and lead nitrate. This system allows controlling the shape of AuNCs obtaining them in high yield. The structures obtained present a high anisotropy consisting of triangular, hexagonal or truncated triangular plates with a tail attached to one edge. High resolution transmission electron microscopy (HR-TEM) investigation shows the crystallographic coherence of the as synthesized structures and the chemical composition of these AuNCs was studied using X-Ray Fluorescence (XRF) spectroscopy demonstrating the absence of lead and small traces of cadmium.

When we speak about hybrid materials an important challenge for researchers is the production of hybrid materials with magnetic and optical properties and tailored architectures. First, it has been investigated the mechanism that leads to the formation of core-shell hybrid microparticles based on a magnetic core of Fe_3O_4 and a thermoresponsive PNIPAM shell. To achieve this goal the surface of Fe_3O_4 nanoparticles was modified by the addition of 3-butenoic acid. After that the Fe_3O_4 nanoparticles were dispersed in water and submitted to free radical polymerization at 70 °C in the presence of NIPAM and BA as cross-linking agent. The result of this reaction was the synthesis of monodisperse microgels with a magnetic core of Fe_3O_4 nanoparticles. By varying the amount of 3-butenoic acid it was possible to obtain hybrid microgels with different magnetic core size and different architecture. Furthermore the core size was conspicuously influenced on the hydrodynamic diameter of the microgels in such way that when the smallest magnetic cores were used the biggest microgels were obtained.

Keywords: conjugated polymer, fluorescence quenching, water-soluble polythiophene, poly(p-phenylene-vinylene), MPS-PPV, PNIPAM microgel, interpenetrated microgels, fluorescent microgels, HRP enzyme, optical sensors, APAP detection, heavy metal ions detection, core-shell PNIPAM microgels, gold nanocrystals, and anisotropic gold nanocrystals.

Resumen

Resumen

Existen diferentes materiales con propiedades ópticas definidas que pueden usarse como sensores. Sin embargo la construcción de un sistema selectivo con respecto a un analito específico es una tarea compleja que requiere mucha investigación antes que el nuevo quimiosensor ó biosensor pueda usarse en el análisis de muestras reales como sueros, aguas contaminadas, etc.

Este trabajo de Tesis está enfocado en el desarrollo de nuevos materiales fluorescentes y en las estrategias requeridas para su aplicación en el campo de los sensores ópticos. Para alcanzar esta meta se han utilizado polímeros conjugados solubles en agua basados en politiofenos y polifenilenosvinilenos. La luminiscencia de los polímeros conjugados (CPs) puede ser amplificada usando tensioactivos (efecto surfactocrómico) ó amortiguada utilizando moléculas que desactivan los estados excitados de los CPs. El trabajo de Tesis comienza investigando la influencia de la longitud de la cadena de tensioactivos y de su concentración en la respuesta fotoluminiscente del polímero conjugado soluble en agua poly[2-(3-thienyl)-ethoxy-4-butylsulfonato] (PTEBS). Como tensioactivos se ha usado moléculas de N-alquilamonio con 8, 9, 10 y 12 átomos de carbono en la cadena hidrocarbonada. La concentración de tensioactivo varió entre 0.125 de la concentración micelar crítica (CMC) y 2 veces la CMC. Los resultados muestran que para concentraciones premicelares la emisión PL del polímero es fuertemente afectada por la longitud de la cadena del tensioactivo. Así, en el caso de los tensioactivos con cadenas cortas la PL se amortigua mientras que los tensioactivos con cadenas más largas provocan un aumento de la emisión luminiscente. Este comportamiento se asocia con la capacidad que tienen los tensioactivos de cadenas más largas de acomodarlas dentro del ovillo polimérico obstruyendo de esta manera las interacciones $\pi-\pi$ entre cadenas poliméricas a la vez que contribuyen a reducir los defectos intracadena durante la agregación del polímero. Por el contrario, en la CMC la longitud de la cadena del tensioactivo no modifica la emisión PL del CP ya que el exceso de tensioactivo inhibe la agregación del polímero mejorando así la eficiencia del proceso de emisión.

Tanto la amplificación de la fluorescencia como la amortiguación de la misma pueden ser usadas para detectar moléculas específicas en sensores ópticos. Se ha desarrollado un sensor de compuestos nitroaromáticos combinando el polímero fluorescente PTEBS y microgeles poliméricos de poli(N-isopropilacrilamida) (PNIPAM) sintetizando microgeles interpenetrados PNIPAM-PTEBS. El PNIPAN es un microgel termosensible en el cual un cambio de temperatura puede inducir una transición de volumen lo que permite modificar la PL de estos microgeles. Así cuando la temperatura está por debajo de la temperatura critica inferior de solución (LCST) del PNIPAM, la intensidad de la PL es mayor que cuando está por encima de la LCST. Medidas de fluorescencia resueltas en el tiempo indican que en el estado hinchado el aumento del entrecruzamiento en el microgel aumenta el tiempo de decaimiento de la fluorescencia del PTEBS. Por el contrario, en el estado colapsado del microgel las variaciones en el tiempo de decaimiento se asocian con la mayor rigidez del sistema PNIPAM-PTEBS lo cual parecen confirmar las medidas de dispersión de neutrones. Además el corrimiento en la longitud de onda del pico de emisión fluorescente por encima de la LCST indica que la matriz de PNIPAM colapsado interacciona con las cadenas de PTEBS dificultando la formación de interacciones π–π. Esta propiedad se utilizó para desarrollar un microsensor de ácido pícrico basado en la formación de interacciones π–π del analito con el polímero conjugado que amortiguaría su luminiscencia por este mecanismo. Por encima de la LCST de los microgeles interpenetrados la interacción π–π se rompería recuperándose la emisión fluorescente inicial. Esta propiedad se podría usar para desarrollar microsensores reutilizables para compuestos nitroaromáticos.

Los CPs se pueden usar también como transductores para fabricar un biosenosr que mida el producto de una reacción bioquímica entre dos reactivos. Se ha desarrollado un biosensor de acetaminofeno (APAP) usando el ciclo catalítico de la enzima peroxidasa de rábano (HRP) catalizado por el peróxido de hidrógeno. Se encapsuló la HRP dentro de un microgel de poliacrilamida y se estudió la disminución de la fluorescencia del polímero conjugado soluble en agua poli(2-metoxi-5-propiloxi-sulfonato-1,4-p-fenilenovinileno) (MPS-PPV) debido a la actividad

catalítica de la HRP en presencia de H_2O_2. El MPS-PPV actúa como un sustrato donador de electrones en el ciclo catalítico de la HRP donde los intermediarios enzimáticos deficientes en electrones CoI y CoII pueden substraer electrones desde el polímero causando una disminución de su luminiscencia. La adición del fármaco APAP a esta solución favorece la disminución de la luminiscencia del polímero lo que indica una co-oxidación del MPS-PPV por los intermediarios del HRP y del APAP. La encapsulación de HRP en un microgel de poliacrilamida permite aislar los intermediarios CoI y CoII del polímero conjugado y de esta forma la disminución de la PL que se observa es solo debida al producto de la oxidación del APAP. Este sistema podría servir para desarrollar sensores de compuestos fenólicos.

Con la idea de tener un polímero fluorescente con propiedades ópticas específicas que permitieran detectar iones metálicos, se sintetizó un nuevo polímero luminiscente, poli(3-etoxi-tiofeno-2,5-diyl-acido dimercapto succínico) (PTE-DMSA). Para ello se combinaron las propiedades fluorescentes del tiofeno, que constituye el esqueleto del polímero, con la capacidad de secuestrar iónes del ácido meso-2,3-dimercato succínico (DMSA) que constituye el grupo lateral del nuevo CP. El método usado para polimerizar el monómero, 2-(3-tienil)-etil acetato, fue el de polimerización catalizada por cloruro de hierro (Fe(III)) y una vez obtenido el polímero, las subunidades de DMSA se unieron covalentemente a la cadena principal por sustitución nucleofilica. La especificidad del DMSA para secuestrar ciertos iones provoca la variación del entorno del polímero amortiguando su fluorescencia. Además se ha investigado el mecanismo de disminución de la intensidad luminiscente usando espectroscopia de fluorescencia con resolución temporal. Este nuevo polímero luminiscente podría ser utilizado para detectar iones de metales pesados como plomo ó mercurio.

Hasta aquí se han desarrollado sensores combinando CPs con microgeles o usando directamente alguna propiedad del CP como su facilidad para acomplejar iones metálicos. Sin embargo los CPs también son polielectrolitos que pueden usarse como agentes reductores y

estabilizadores en la síntesis de nanocristales. La inclusión de nanopartículas dentro del microgel puede dotarlo de nuevas propiedades, tales como respuesta mágnetica para facilitar su recuperación ó respuesta óptica, por lo que abordamos la síntesis de materiales híbridos que pudieran usarse como sensores. Se comenzó sintetizando, con un método de un solo paso, nanocristales de Au (AuNCs) utilizando el PTEBS como polímero estabilizador en combinación con acetato de cadmio y nitrato de plomo. Este método permite controlar la forma de las AuNCs y su obtención en cantidades considerables. Algunas de las estructuras que se obtienen presentan gran anisotropía y consisten en placas triangulares, hexagonales ó triangulares truncadas con una cola adherida a uno de sus lados. Con microscopía de alta resolución (HR-TEM) se demostró la coherencia cristalográfica de estas nanoestructuras. Su composición química fue estudiada con fluorescencia de rayos-X (XRF) y se encontró que no contienen plomo y solo presentan tan solo trazas de cadmio.

Cuando se trata con materiales híbridos un desafío importante para los investigadores es controlar su arquitectura. Se finaliza este trabajo investigando los mecanismos de formación de micropartículas híbridas con núcleo inorgánico (Fe_3O_4) y cubierta polimérica (PNIPAM). Para ello la superficie de las nanopartículas de Fe_3O_4 se modificó con ácido 3-butanoico y a continuación las nanoparticulas se dispersaron en agua y se procedió a la polimerización, a 70 °C, del PNIPAM en presencia de bisacrilamida, que se utilizo como entrecruzante. El resultado fueron microgeles monodispersos con un núcleo de nanopartículas magnéticas. Variando la concentración de ácido 3-butanoico fue posible obtener micropartículas hibridas con núcleos de tamaño variable y también controlar la distribución de las nanopartículas de Fe_3O_4 de tal manera que se concentren solo en el núcleo ó se distribuyan de forma uniforme por el microgel. Además se ha observado que el tamaño del núcleo inorgánico determina el diámetro del microgel de tal manera que cuanto más pequeño es el núcleo mayor es el diámetro de la macropartícula híbrida.

Resumen

Palabras clave: polímero conjugados, amortiguación de la fluorescencia, politiofenos soluble en agua, poli(p-fenileno-vinileno), MPS-PPV, PNIPAM microgel, microgeles interpenetrados, microgeles fluorescentes, HRP enzima, sensores ópticos, APAP, detección de iones de metales pesados, PNIPAM microgeles núcleo-corteza, nanocristales de oro, y nanocristales de oro anisotropicos.

Work Hypothesis

Work Hypothesis

The fluorescence response of a water-soluble conjugated polymer, as polythiophenes or poly(p-phenylene-vinylene), can be modified using different analytes that can interact with the polymer in a specific way.

The hypothesis of this work is that we can produce new tailored materials with different architectures for the development of sensors and biosensors combining the optical properties of CPs with the properties of the properties of smart microgels and nanocrystals.

Hipótesis de Trabajo

Hipótesis de Trabajo

La respuesta fluorescente de los polímeros conjugados solubles en agua como politiofenos ó polifenilenosvinilenos puede modificarse usando diferentes analitos que interaccionan con el polímero de forma específica.

La hipótesis de este trabajo es que podemos producir nuevos materiales con diferentes arquitecturas para el desarrollo de sensores y biosensores combinando las propiedades ópticas de los CPs con las propiedades de los microgeles y los nanocristales.

1. *Introduction*

1. *Introduction*

1.1 *Conjugated Polymers*

In 2000 the Nobel Prize in Chemistry was awarded to Alan Heeger, Alan MacDiarmid, and Hideki Shirakawa recognizing their path breaking discovery of high conductivity in polyacetylene in 1977. Professor Bengt Nordén begins the Presentation Speech for the 2000 Nobel Prize in Chemistry with these words: *"We all associate chemistry with test tubes, stinking laboratories and explosions - Alfred Nobel's dynamite was born in such an environment. Perhaps the development of new knowledge in chemistry, more than any other science, has been characterized as a sparkling interplay between theory on one hand, the safe and predictable, and, on the other hand, the explosive and surprising reality"*.[1] This unexpected discovery on CPs gave birth to a research area of great importance. The vast portfolio of new polymer structures with unique and tailored properties and the wide range of applications being pursued are far beyond what we could have envisioned when the field was in its infancy. Nowadays, big efforts have been done to synthesize new conjugated polymers developing new synthesis paths and materials with tailored properties. Examples of the advances on the synthesis and characterization of conjugated polymers are the most known classes of CPs: poly(p-phenylene-vinylene) (PPV), poly(pyrrole) (PPy), poly(thiophene) (PT), poly(aniline) (PANI), and poly(fluorene) (PFO) (see Figure 1).

Conjugated polymers have been extensively investigated due to their unique electronic and optical properties. The advances in semiconducting electronics, memory materials, photovoltaic, and applications directed to biomedicine are emerging as future growth areas while conductivity remains an important property that has undergone significant developments. During the last 10 years, we have witnessed fascinating developments of a wide range of commercial applications in optoelectronics devices.

[1] "The Nobel Prize in Chemistry 2000 - Presentation Speech". Nobelprize.org. 27 Jul 2010 http://nobelprize.org/nobel_prizes/chemistry/laureates/2000/presentation-speech.html

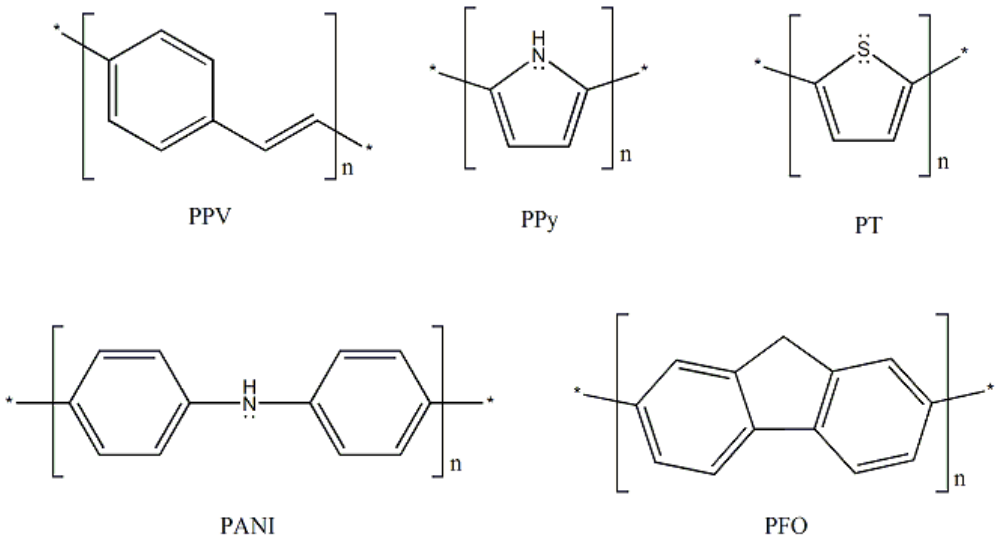

Figure 1. Chemical structure of the most investigated conjugated polymers.

One of the most promising applications of CPs is Polymer Light Emitting Diode (PLED). In October 2007 Sony Corporation presented a new type of display using Organic Light Emitting Diode (OLED) technology.[2] Unfortunately, these kinds of displays were too expensive compared with Light Emitting Diode (LED), and their use is restricted only to the fabrication of small displays. In May 2010, Sony develops a "rollable" OLED display that can be wrapped around a pencil, based on Organic Thin Film Transistors (OTFTs) with a polymeric organic semiconductor material (POSM). This was achieved due to the development of integration technologies of OTFTs and OLEDs on an ultra-thin 20 µm thick flexible substrate. By combining these technologies, Sony successfully demonstrated the world's first OLED panel which is capable of reproducing moving images while being repeatedly rolled-up around a cylinder with a radius of 4 mm and stretched.[3]

[2] Sony Launches World's First OLED TV http://www.sony.net/SonyInfo/News/Press/200710/07-1001E/
[3] Sony Corporation "Rollable" OLED Display http://www.sony.net/SonyInfo/News/Press/201005/10-070E/

1.1.1 *Energy Bands Gap in Conducting Polymers*

A key discovery in the development of conducting polymers was the finding in 1973 that the inorganic polymer polysulfur nitride, $(SN)_x$, is a metallic-like material.[4] The room-temperature conductivity of $(SN)_x$ is of the order of $\approx 10^3$ $(\Omega \cdot cm)^{-1}$, which is closer to the value $\approx 6 \cdot 10^5$ $(\Omega \cdot cm)^{-1}$ of copper than to $\approx 10^{-14}$ $(\Omega \cdot cm)^{-1}$ of polyethylene. Below a critical temperature around 0.3 K, $(SN)_x$ becomes a superconductor.[5] These discoveries were of particular importance because they proved the existence of highly conducting polymers and stimulated the enormous amount of work necessary to synthesize other polymeric conductors.

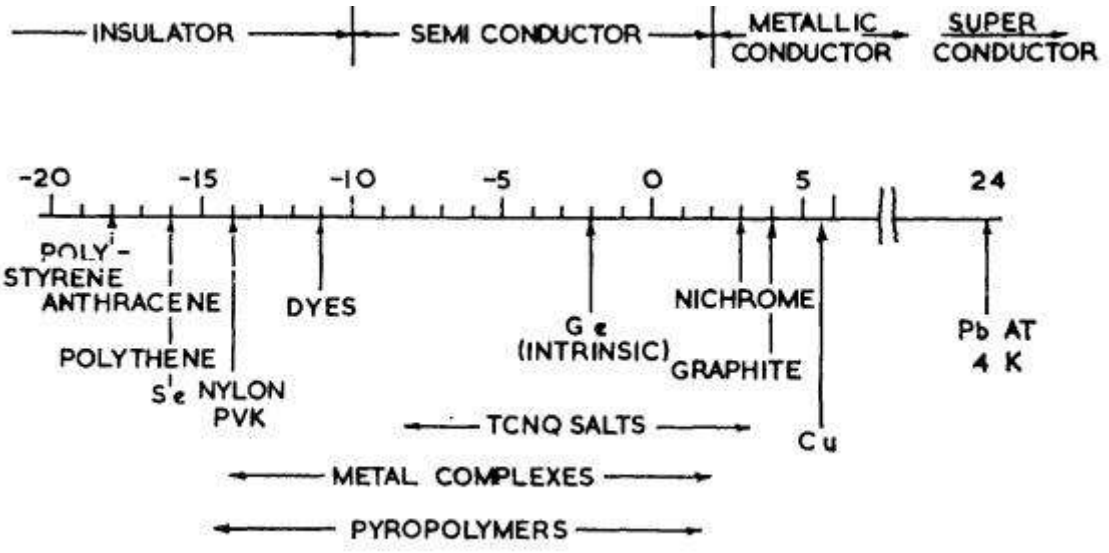

Figure 2. Conductivity ranges of various materials. The scale gives the log of the conductivity $(\Omega \cdot cm)^{-1}$.

The major breakthrough in the area of conducting plastics occurred in 1977 when the same redox chemistry was applied to an intrinsically insulating organic polymer, polyacetylene. It was discovered that polyacetylene, which has an intrinsic conductivity lower than $\approx 10^{-5}$ $(\Omega \cdot cm)^{-1}$

[4] V. V. Walatka, M. M. Labes, and J. H. Perlstein, *Phys. Rev. Lett.*, **1973**, *31*, 1139.
[5] R. L. Greene, G. B. Street, and L. J. Suter, *Phys. Rev. Lett.*, **1975**, *34*, 577.

could be made highly conducting ≈10^3 $(\Omega \cdot cm)^{-1}$ by exposing it to oxidizing or reducing agents.[6] This process is often referred to as "doping" by analogy with the doping of inorganic semiconductors. This is a rather misleading analogy, however, and the process is best viewed as a redox reaction. The insulating neutral polymer is converted into an ionic complex consisting of a polymeric cation (or anion) and a counterion which is the reduced form of the oxidizing agent (or the oxidized form of the reducing agent). In solid-state physics terminology, the use of an oxidizing agent corresponds to p-type doping and that of a reducing agent to n-type doping.[7] An important criterion in selecting potentially conducting polymers is therefore the ease with which the system can be oxidized or reduced. This accounts in part for the choice of π-bonded unsaturated polymers which, like polyacetylene, have small ionization potentials and/or large electron affinities (Figure 2).

In conjugated polymers the sp^2p_z hybridization leads formally to one unpaired electron per carbon atom. As a result the electronic structure is determined by the chain symmetry (e.g. the number and kind of atoms in the repeat unit), with the result that such polymer can be expected to exhibit semiconducting or metallic behavior. For a solid material the electronic band structure describes those ranges of energies that an electron is forbidden or allowed to have (Figure 3).

The band-gap generally refers to the energy difference in electron volts between the top of the valence band and the bottom of the conduction band. For conducting polythiophenes the band-gap ranges are between 2.0 eV and 0.1 eV typical of semiconductors materials.[8]

---

[6] C. K. Chiang, C. R. Fincher, Y. W. Park, A. J. Heeger, H. Shirakawa, E. J. Louis, S. C. Gau, and A. G. McDiarmid, *Phys. Rev. Lett.*, **1977**, *39*, 1098.

[7] T. A. Skotheim, and J. R. Reynolds, "*Handbook of Conducting Polymers*" 3rd Ed., Taylor & Francis Group, CRC Press, New York, **2007**.

[8] A. J. Heeger, *Chem. Soc. Rev.*, **2010**, *39*, 2354.

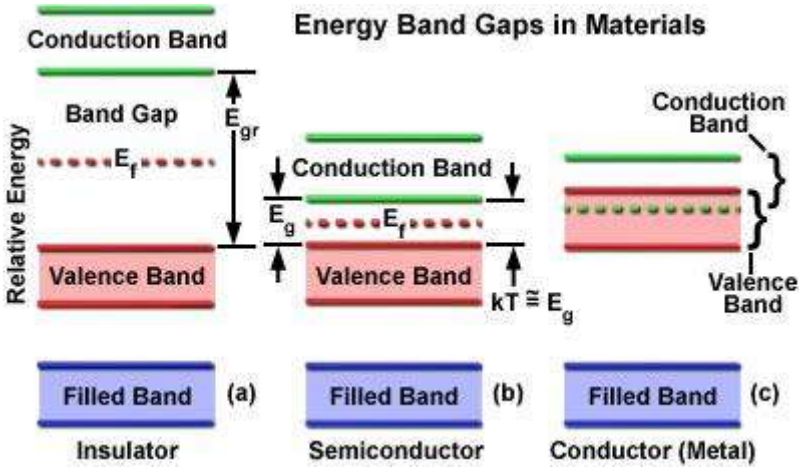

Figure 3. Representation of three general materials: a) insulator, b) semiconductor, and c) conductor. The band-gap energy is represented by the Eg variable, kT is the thermal excitation energy, and Ef is the Fermi energy, the energy of the highest occupied quantum state at 0 K.

The π-band of polyacetylene is half-filled, implying the possibility of metallic conductivity. Because of the strong intrachain bonding, and weak interchain interactions, characteristic of such polymers, the π electrons are delocalized along the polymer chain, making them essentially quasi-one-dimensional conductors. Quasi-one-dimensional metals tend to distort spontaneously[9] such that the spacing between successive atoms along the chain is modulated with period $2\pi/Q = 2\pi/k_F$, where k_F is the Fermi wave number. When the band is half-filled, the tendency toward spontaneous symmetry breaking is particularly strong, and the distortion leads to a pairing of successive sites along the chain or dimerization. This dimerization opens an energy gap at the Fermi surface, thereby lowering the energy of the occupied states and stabilizing the distortion. The competition between the lowering of the electronic energy and the increase of the elastic energy of the polymer caused by the distortion leads to an equilibrium bond-length modulation which is of order 0.03-0.04 Å in polyacetylene. Thus the lattice instability removes the high density of states at the Fermi surface and renders the system

[9] R. E. Peierls, *Quantum Theory of Solids*, **1955**, Cambridge.

a semiconductor, in contrast to the metallic behavior expected of a corresponding three-dimensional system with a half-filled band.

1.1.2 *Characteristics of Fluorescence Emission*

Luminescence is the emission of light from any substance, and occurs from electronically excited states. The lifetime (τ) of a fluorophore is the average time between its excitation and return to ground state. In excited singlet states, the electron in the excited orbital is paired (by opposite spin) to the second electron in the ground-state orbital. Consequently, return to the ground state is spin allowed, and occurs rapidly by emission of a photon (see Figure 4). The emission rates of fluorescence are typically 10^8 s^{-1}, so that a typical fluorescence lifetime is near 10 ns.[10]

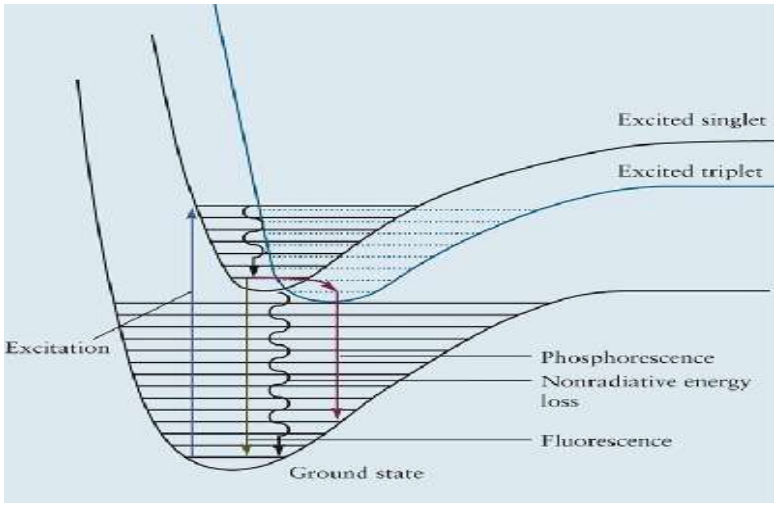

Figure 4. Illustration of how a singlet excited state can convert to a triplet excited state.

Phosphorescence is the emission of light from a triplet excited state, in which the electron in the excited orbital has the same spin orientation as the ground state electron (see

[10] J. R. Lakowicz, "*Principles of Fluorescence Spectroscopy*" 3rd Ed., Springer Science, New York, **2006**.

Figure 4). Thus, the transition to the ground state is forbidden and the emission rate is slow (10^3 to 10^0 s^{-1}), so that the phosphorescence lifetime are typically milliseconds to seconds.[10] It should be noted that the distinction between fluorescence and phosphorescence is not always clear since transition metal-ligand complexes (MLCs), which contain a metal and one or more organic ligands, display mixed singlet-triplet states.

In order to understand the fluorescence phenomena we need to know the processes that occur between the absorption and emission of light that is usually illustrated by the Jablonski diagram.

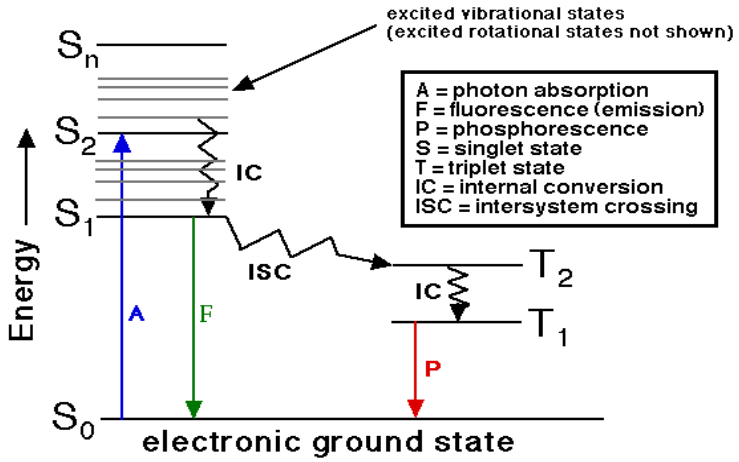

Figure 5. The Jablonski diagram summarized the process behind fluorescence and phosphorescence.

A molecule can absorb energy as electromagnetic radiation; there are a number of routes by which it can return to ground state (see Figure 5). The singlet ground, first, second, and *n* electronic states are depicted by S_0, S_1, S_2 and S_n, respectively. At each of these electronic energy levels the fluorophore can exist in a number of vibrational energy levels, depicted by 0, 1, 2 etc. In this Jablonski diagram we excluded a number of interactions that can promote the emission of energy from the excited molecule without the release of a photon, such as

quenching, energy transfer, and solvent interactions. The transitions between states are depicted as vertical lines to illustrate the instantaneous nature of light absorption. Electronic transitions occur in about 10^{-15} s, a time too short for significant nuclei displacement that is known as the Frank-Condom principle.[10] Following light absorption, a fluorophore may be excited to some higher vibrational level of either S_1 or S_2. With a few rare exceptions, molecules in condensed phase rapidly relax to the lowest vibrational level of S_1. This process is called internal conversion and generally occurs within 10^{-12} s or less. Since fluorescence lifetimes are typically near 10^{-8} s, internal conversion is generally complete prior to emission. Hence, fluorescence emission generally results from a thermally equilibrated excited state that is the lowest energy vibrational state of S_1. The return to ground state, S_0, typically occurs to a higher excited vibrational ground state level, which then quickly reaches thermal equilibrium. An interesting consequence of emission to higher vibrational ground states is that the emission spectrum is typically a mirror image of the absorption spectrum of the $S_0 \rightarrow S_1$ transition. This similarity occurs because electronic excitation does not greatly alter the nuclear geometry.

Molecules in the S_1 state can also undergo a spin conversion to the first triplet state T_1. Emission from T_1 is termed phosphorescence, and is generally shifted to longer wavelengths relative to fluorescence. Conversion of S_1 to T_1 is called intersystem crossing. Transition from T_1 to the singlet ground state is forbidden, and as a result the rate constants for triplet emission are several orders of magnitude smaller than those for fluorescence.

Molecules containing heavy atoms such as bromine and iodine are frequently phosphorescent. The heavy atoms facilitate intersystem crossing and thus enhance phosphorescence quantum yields. Examination of the Jablonski diagram (Figure 5) reveals that the energy of the emission is typically less than that of absorption since fluorescence typically occurs at lower energies or longer wavelengths. This phenomenon was first observed by Sir. G. G. Stokes, and is known as the Stokes Shift. In 1852, he described the phenomenon of

fluorescence, as exhibited by fluorite and uranium glass, materials which he viewed as having the power to convert invisible ultra-violet radiation into radiation of longer wavelengths that are visible. The process is summarized in Figure 6.

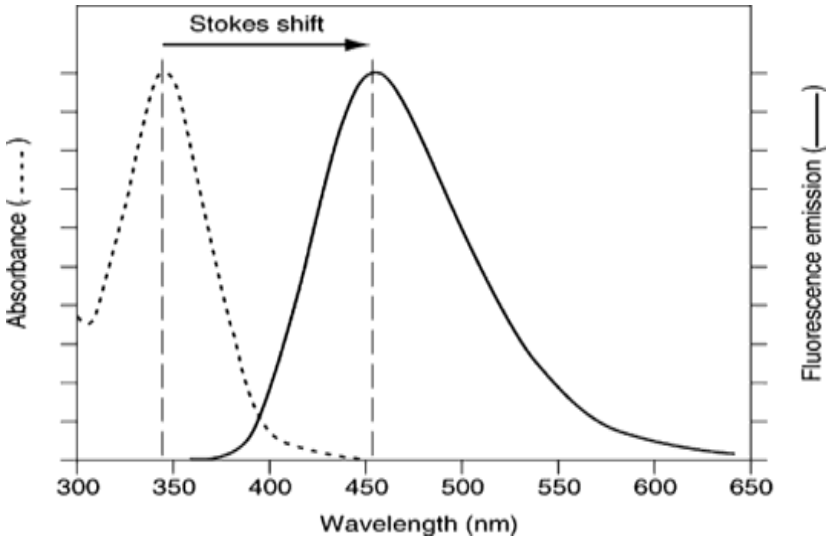

Figure 6. The emission from the fluorophore occurs always at a longer wavelength than the absorbance.

Another property of fluorescence is that the emission spectrum is generally independent by the excitation wavelength and this is known as Kasha's rule. Upon excitation into higher electronic and vibrational levels, the excess of energy is quickly dissipated leaving the fluorophore in the lowest vibrational level of S_1 (Figure 5). The relaxation occurs in about 10^{-12} s and is the result of a strong overlap among numerous states of nearly equal energy. Because of this rapid relaxation the emission spectra are usually independent by the excitation wavelength.

In fluorescence there are other two important factors to keep in consideration: i) the fluorescence lifetime; ii) and quantum yields. The lifetime is important as it determines the time available for the fluorophore to interact or diffuse in its environment, and hence the information available from its emission. Quantum yield is the number of emitted photons relative to the

number of absorbed photons. Substances with largest quantum yields, approaching unity, display the brightest emission.

1.1.3 *Luminescent Materials and Their Applications*

Luminescence is formally divided into different subcategories such as chemiluminiscence, electroluminescence, and photoluminescence, depending by the effect that produces the emission of light. As described in **Chapter 1.1.2** photoluminescence is divided into fluorescence and phosphorescence, depending on the nature of the excited states. Chemiluminiscence is the emission of light as the result of a chemical reaction, while electroluminescence is the phenomenon by which a material emits light in response to an electric current that passed through it, or to a strong electric field.

One powerful application of luminescence is on the Enzyme-Linked Immunosorbent Assay test (ELISA) that is used as a diagnostic tool in medicine.[11] In simple terms, in ELISA, an unknown amount of antigen is fixed onto a surface, and then a specific antibody is applied over the surface so that it can bind to the antigen. This antibody is linked to an enzyme, and in the final step a substance is added that the enzyme can convert to some detectable signal. Thus, in the case of fluorescence ELISA, when light of the appropriate wavelength is shone upon the sample, any antigen/antibody complexes will give fluorescence so that the amount of antigen in the sample can be inferred through the magnitude of the fluorescence.[12]

Another well-known example of the utilization of luminescence as chemosensor is luminol, used frequently in crime scene investigations. Luminol is a versatile molecule that mixed with an appropriate oxidizing agent exhibit striking blue glow due to the

[11] X. Duburcq, C. Olivier, F. Malingue, R. Desmet, A. Bouzidi, F. Zhou, C. Auriault, H. Gras-Masse, and O. Melnyk, *Bioconjugate Chem.*, **2004**, *15*, 307.
[12] K. D. McReynolds, M. J. Hadd, and J. Gervay-Hague, *Bioconjugate Chem.*, **1999**, *10*, 1021.

chemiluminiscence reaction. Luminol is used to detect trace amounts of blood left at crime scenes as it reacts with iron found in hemoglobin. It is also used by biologists in cellular assays for the detection of copper, iron, and cyanides. In Figure 7 is shown the chemiluminiscence of luminol mixed together with hydrogen peroxide and a catalyst, typically iron.[13]

Figure 7. Luminol is a well-known example of chemiluminiscence.

In order to increase the performance of optical sensors the field of chemical sensing is becoming very dependent upon novel materials. Polymers, crystals, glasses, particles, and nanostructures have made a profound impact and have endowed modern sensory systems with superior performance. CPs are luminescent and promising application are emerging for their use as optical sensors taking advantage of their fluorescence properties. In addition, CPs have emerged as an important transduction materials since they readily transform a chemical signal into an easily measured electrical or optical event. Before using CPs as biosensors is important to recognize that the extraordinary sensory performance of biological systems originates from an

[13] M. Lowry, S. O. Fakayode, M. L. Geng, G. A. Baker, L. Wang, M. E. McCarroll, G. Patonay and I. M. Warner, *Anal. Chem.*, **2008**, *80*, 4551.

interactive system wherein the receptor is served by analyte delivery and/or removal mechanisms, selectivity is derived from receptors, and sensitivity is the result of analyte-triggered biochemical cascades. In Figure 8 is shown an example of fluorescent CPs that typically occurs from aromatic molecules since they possess a large $\pi-\pi$ conjugation between the aromatic rings making possible the stabilization of the excited electronic state.

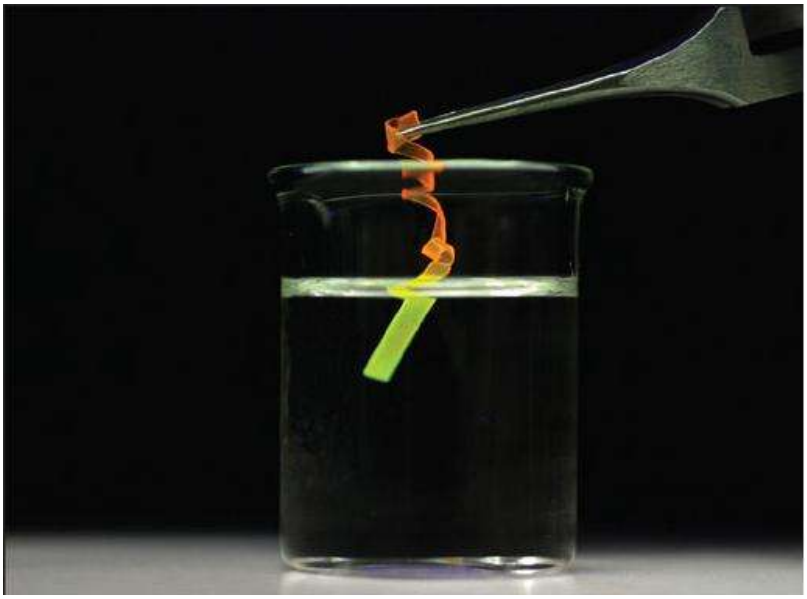

Figure 8. Blend of poly(*p*-phenylene-vinylene) and cross-linked poly(cyclooctene).

The CP in Figure 8 was prepared by incorporating a fluorescent poly(*p*-phenylene-vinylene) into a cross-linked poly(cyclooctene) (PCO) matrix *via* guest diffusion. Exposure of these phase-separated blends to temperatures above the melting point (T_m) of the PCO leads to dissolution of the dye molecules, and therefore causes a pronounced change of their absorption and fluorescence color.[14]

[14] **J. Kunzelman, T. Chung, P. T. Mather, and C. Weder, *J. Mater. Chem.*, 2008, *18*,** 1082.

1.1.4 *Fluorescence Quenching in Conjugated Polymers*

Probably one of the most interesting properties of fluorescent compounds is the possibility to modify this fluorescence intensity by the addition of molecules, called quenchers (see Figure 9). One of the most known types of quenching is the collisional quenching that occurs when the excited state of the fluorophore is deactivated upon contact with other molecules in solution. During this process the fluorophore is not chemically altered and returned to the ground state during a diffusive encounter with the quencher.

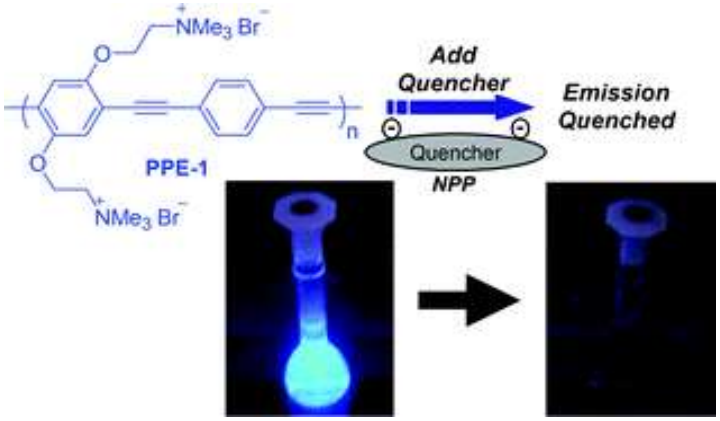

Figure 9. In this picture it can be seen a fluorescence quenching example. The vial on the left does not contain the quencher and it is fluorescent, while the vial on the right contains quencher and does not show any fluorescence.[15]

Collisional quenching is described by the Stern-Volmer equation:

$$F_0/F = 1 + K_{SV}[Q] = 1 + k_q\tau_0[Q] \qquad [1]$$

In this expression K_{SV} is the Stern-Volmer quenching constant, k_q is the bimolecular quenching constant, τ_0 is the unquenched lifetime, and [Q] is the quencher concentration. The Stern-Volmer quenching constant K_{SV} indicates the sensitivity of the fluorophore to a quencher.

[15] W. N. George, M. Giles, I. McCulloch, J. C. de Mello, and G. J. H. Steinke, *Soft Matter*, **2007**, ***3***, 1381.

Aside from collisional quenching, fluorescence quenching can occur by a variety of other process. Thus, the fluorophore can form no-fluorescent complexes with quenchers and this process is referred to as static quenching since it occurs in the ground state and does not rely on diffusion of molecular collisions. The expression that describes the static quenching is represented by equation (2):

$$F_0/F = 1 + K_S[Q] \qquad [2]$$

where K_S is the Stern-Volmer constant and [Q] is the quencher concentration. The dependence of F_0/F on [Q] is linear which is identical for dynamic quenching, except that the quenching constant is now an association constant. Another important factor to take into account is that for static quenching $\tau_0/\tau = 1$, while for dynamic quenching $\tau_0/\tau = F_0/F$.

1.1.5 *Resonance Energy Transfer*

Another important process that occurs in the excited state is the resonance energy transfer (RET) which is a distance-dependent excited state interaction where the emission of one fluorophore is coupled to the excitation of another. It occurs primarily because the acceptor dipole interacts or resonates with the donor dipole. RET is used to obtain structural maps of complex biological structures, primarily proteins and other macromolecular assemblies such as ribosomes and nucleosomes. Measurements of energy transfer can provide intra- or intermolecular **distance** data for proteins and their ligands in the range of 10-100 Angstrom. This process occurs whenever the emission spectrum of the fluorophore, called the donor, overlaps with the absorption spectrum of another molecule, called the acceptor. Such overlap is illustrated in Figure 10. To observe RET the acceptor does not need to be fluorescent since does not involve emission of light by the donor. The donor and acceptor are coupled by a dipole-

dipole interaction. For these reasons the term RET is preferred over the term fluorescence resonance energy transfer (FRET), which is also in common use.

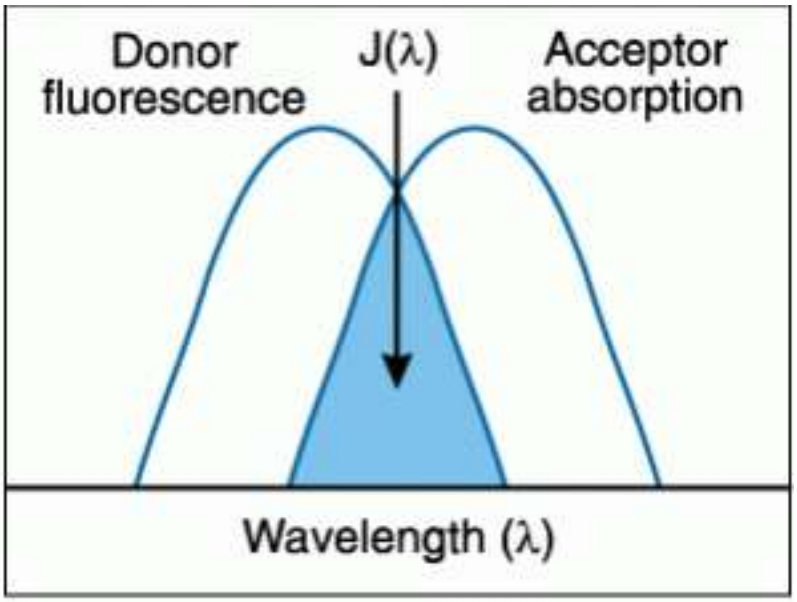

Figure 10. Spectral overlap of resonance energy transfer (RET).

The extent of energy is determined by the distance between the donor and acceptor, and the extent of spectral overlap. For convenience the spectral overlap (Figure 10) is described in terms of the Foster distance (R_0). The rate of energy transfer $k_T(r)$ is given by the equation:

$$k_T(r) = \frac{1}{\tau_D}\left(\frac{R_0}{r}\right)^6 \qquad [3]$$

where τ_D is the lifetime of the donor in the absence of energy transfer and r is the distance between the donor (D) and acceptor (A).

1.1.6 *Conjugated Polymers as Fluorescent Sensors*

CPs offer the opportunity to couple analyte receptor interactions, as well as nonspecific interactions, into observable responses. The advantage of CPs-based sensors over devices using small molecule (chemosensor) elements is the potential of the CPs to exhibit collective properties, making the system more sensitive to minor perturbations such as transport properties, electrical conductivity or rate of energy migration.[16] In general, CPs in their pristine (neutral) states are wide band gap semiconductors.[17,18] The luminescence efficiency in many cases is related to the delocalization and polarization of the electronic structure. For example, poly(p-phenylene-vinylene) is a strongly luminescent material wherein absorption of photons creates excitons, which are bound electron-hole pairs.[16] A more polarizable and delocalized polymer such as polyacetylene is only very weakly luminescent.

A vast number of studies on oligomers confirm that the electronic states in a CP have limited delocalization and the electronic structure of a given CP is often determined by 7-13 repeating units.[19] This is particularly prevalent in systems containing aromatic rings since the aromatic character localizes the electronic wave functions.

One important field where CPs have been employed is in the detection of explosives based on highly nitrated organic compounds such as nitroaromatics, nitramines, or nitrates which renders them electron-deficient. This electron deficiency has been important in explosives detection using CPs that posses a high electron density. Yang and Swager used a fluorescence quenching transduction mechanism together with the amplifying nature of conjugated polymers

[16] T. M. Swager, *Acc. Chem. Res.* **1998**, *31*, 201.
[17] I. D. W. Samuel, G. Rumbles, C. J. Collison, R. H. Friend, S. C. Moratti, and A. B. Holmes, *Synth. Met.* **1997**, *84*, 497.
[18] L. Smilowitz, A. Hays, A. J. Heeger, G. Wang, and J. E. Bowers, *J. Chem. Phys* **1993**, *98*, 6504.
[19] K. Mullen, and G. Wegner, "*Electronic Materials: The Oligomer Approach*", Wiley-VCH, Weinheim, **1998**.

to design a highly sensitive material to 2,4,6-trinitrotoluene (TNT) vapor, RDX, and PTEN.[20] More recently, ICx Nomadics Inc., has developed a sensory device with femtogram sensitivity to TNT.[21]

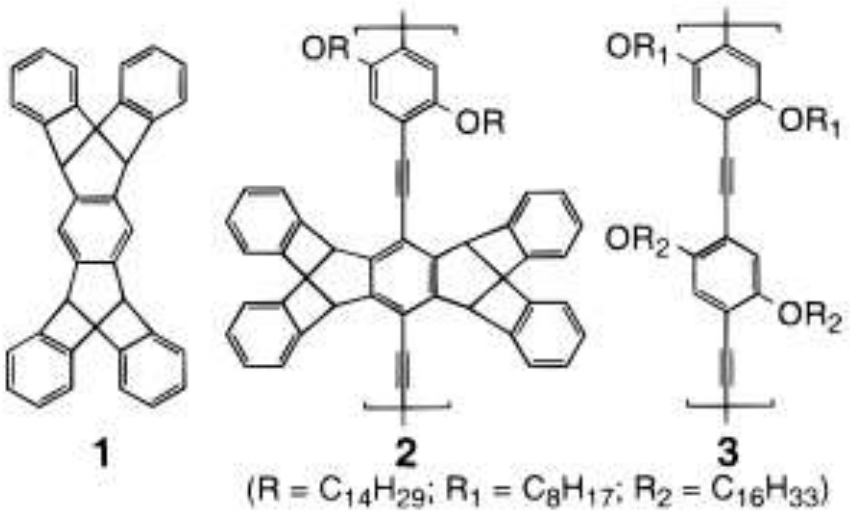

Figure 11. Monomer and CPs used to detect nitroaromatic compounds. **1** is the rigid pentiptycene group, which prevents the polymer chains from aggregation and self-quenching in the solid state. **2** and **3** are the CPs with the different alkyl groups and monomer.

1.1.7 *Fluorescent Polymer as Cations and Anions Sensory Material*

An important field of application of CPs is ion sensing, such as heavy metal ions or small molecules with biological importance. In fact these polymers can be used to detect by fluorescence quenching small amounts of heavy metal ions like Hg^{+2} and Pb^{+2}, which are toxic for living organism. In 2006 Wang and coworkers developed a mercury sensing strategy based on Hg^{2+} induced aggregation of conjugated polymer and subsequent fluorescence self quenching.[22] A thymine moiety (T) is covalently linked to the side chain of the CP. In the absence of Hg^{2+} ions,

[20] T. L. Andrew, and T. M. Swager, *J. Am. Chem. Soc.*, **2007**, *129*, 7254.
[21] C. J. Cumming, C. Aker, M. Fisher, M. Fox, M. J. la Grone, D. Reust, M. G. Rockley, T. M. Swager, E. Towers, and V. Williams, *IEEE Trans. Geosci. Remote Sensing*, **2001**, *39*, 1119.
[22] Y. Tang, F. He, M. Yu, F. Feng, L. An, H. Sun, S. Wang, Y. Li, and D. Zhu, *Macromol. Rapid Commun.* **2006**, *27*, 389.

the CP chain remains extended and the CP exhibits strong fluorescence emission. Upon adding Hg^{2+} ions, the formation of interpolymer π-stacking aggregation, induced by specific thymine–Hg–thymine interactions, results in the fluorescence quenching of the CP (see Figure 12).

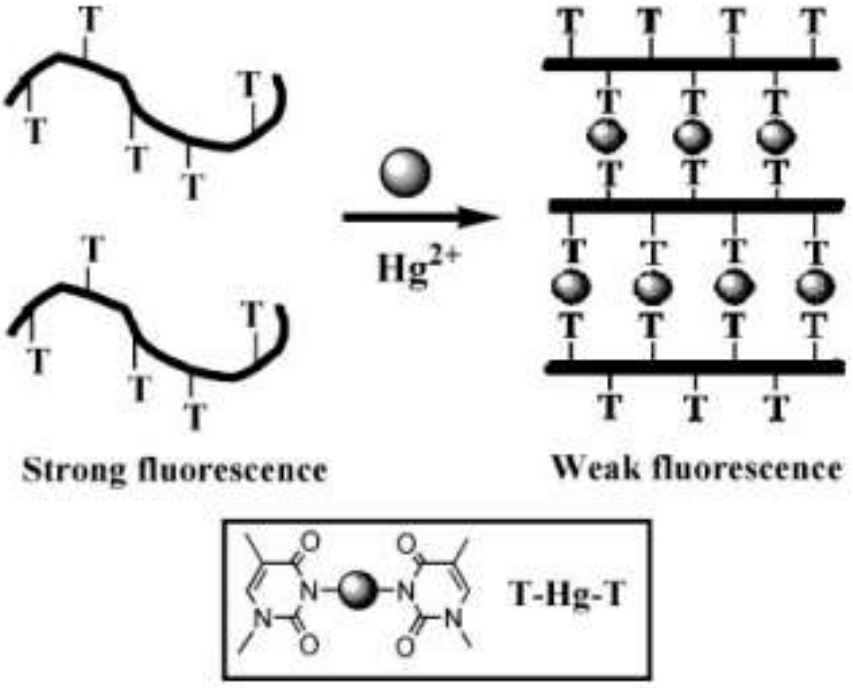

Figure 12. Schematic representation of the Hg^{2+} assay proposed by Wang and coworkers.

Leclerc and coworkers reports a new water-soluble cationic polythiophene derivative which can optically detect the presence of iodide over a wide range of other anions (F^-, Cl^-, Br^-, CO_3^{2-}, HCO_3^-, $H_2PO_4^-$, HPO_4^{2-}, CH_3COO^-, $EDTA^{4-}$, SO_4^{2-}, $(C_6H_5)_4B^-$).[23] This simple, rapid, and versatile methodology is based on the different interaction (self-assembly of two opposite charges) and the conformational change of the cationic poly(3-alkoxy-4-methyl-thiophene-2,5-diyl) (see Figure 13).

[23] H. A. Ho, and M. Leclerc, *J. Am. Chem. Soc.*, **2003**, *125*, 4412.

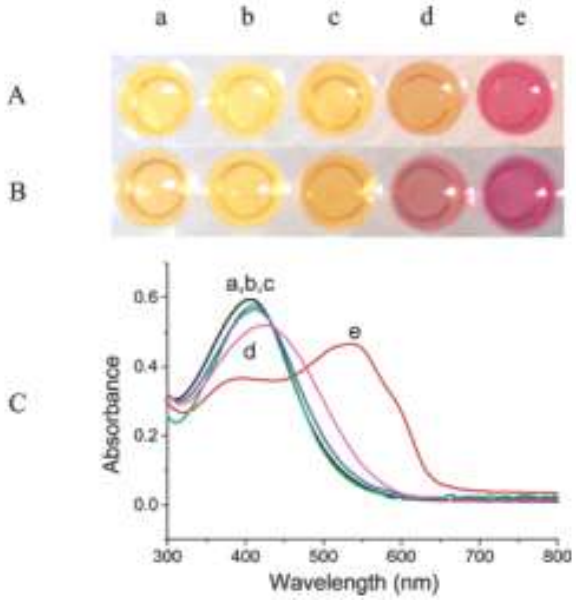

Figure 13. (A) Photographs of solutions of (a) cationic polythiophene, (b) +NaF, (c) +NaCl, (d) +NaBr, (e) +NaI. (B) Assays of photographs A, 4 days after. (C) UV-Vis absorption spectra corresponding to the different assays in photograph A.

More recently, Skinkai and coworkers have found a new approach that could improve the simplicity, selectivity, and sensitivity of adenosine triphosphate (ATP) detection.[24] In their work they used a cationic water-soluble polythiophene that displays colorimetric and fluorescent responses to ATP through electrostatic and hydrophobic cooperative interactions. Upon adding increasing amounts of ATP, the absorption maximum is gradually red-shifted to 538 nm with an observed dramatic color change from yellow to pink-red. This shift and the appearance of two vibronic bands are characteristic of the aggregation of the PT backbone (see Figure 14).[25,26,27,28,29] These results indicate that water-soluble CPs could be used as a

[24] C. Li, M. Numata, M. Takeuchi, and S. Shinkai, *Angew. Chem. Int. Ed.*, **2005**, *44*, 6371.
[25] M. Chayer, K. Faïd, and M. Leclerc, *Chem. Mater*. **1997**, *9*, 2902.
[26] F. Brustolin, F. Goldoni, E. W. Meijer, and N. A. J. M. Sommerdijk, *Macromolecules* **2002**, *35*, 1054.
[27] B. M. W. Langeveld-Voss, R. A. J. Janssen, M. P. T. Christiaans, S. C. J. Meskers, H. P. J. M. Dekkers, and E. W. Meijer, *J. Am.Chem. Soc.*, **1996**, *118*, 4908.
[28] B. M. W. Langeveld-Voss, R. A. J. Janssen, and E. W. Meijer, *J. Mol. Struct.*, **2000**, *521*, 285.
[29] F. J. M. Hoeben, P. Jonkheijm, E. W. Meijer, and A. P. H. J. Schenning, *Chem. Rev.*, **2005**, *105*, 1491.

colorimetric sensor for ATP. To validate the specificity of the PT derivative toward anionic guests, the changes in the absorption spectra of the poly[(3-N-N'-dimethylpropoxy-1-amine)-4-methyl-thiophene-2,5-diyl)] (**4**) in water upon addition of biologically important anions such as adenosine monophosphate (AMP), adenosine diphosphate (ADP), and uridine triphosphate (UTP), as well as chloride, carboxylate, phosphate, and triphosphate ions (as sodium salts) were studied. After the addition of an equimolar amount of these anions to aqueous solutions of **4**, most of the solutions remained yellow with $\lambda_{max} < 435$ nm except for those that contained ADP and UTP which gave orange solutions with shifts of the absorption maxima to 435 and 461 nm, respectively. The most remarkable effect was noted, however, upon addition of ATP, which gave a pink-red solution (Figure 14).

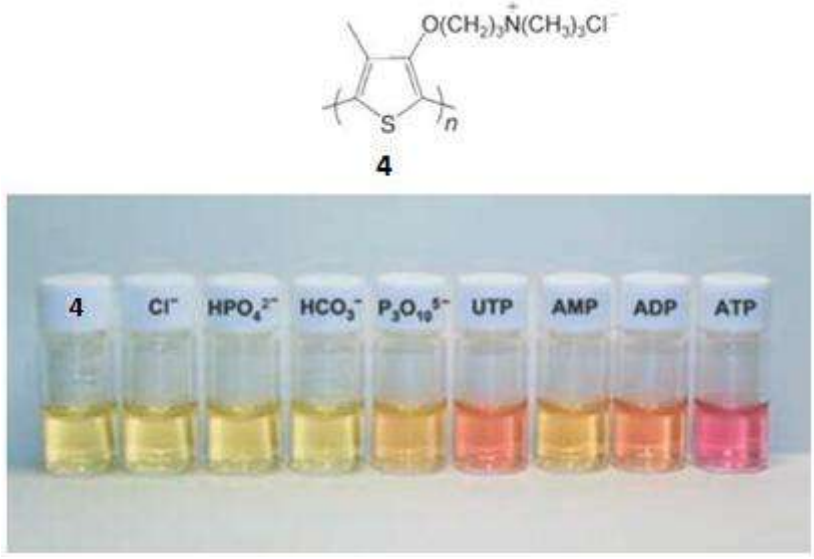

Figure 14. The vials show the changes in the color of the solutions of **4** in water induced by the addition of equimolar amounts of various anions.

Bunz and co-workers develop a more sensitive lead sensor that further exploits the benefits of multivalent interactions between a functionalized conjugated polymer and a metal

cation (Figure 15).[30] The fluorescence of the carboxylated, water-soluble poly(p-phenylene-ethynylene) **5** was quenched by metal ions in aqueous solution.

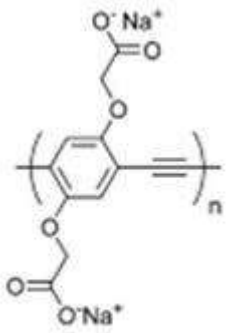

5

Figure 15. Water-soluble poly(p-phenylene-ethynylene) synthesized by Bunz and coworkers.

The authors examined a variety of divalent cations including Pb^{2+}, Ca^{2+}, Zn^{2+}, Hg^{2+}, Mg^{2+}, Cu^{2+}, Mn^{2+}, and dimethyl-viologen. Polymer **5** was most sensitive to Pb^{2+} salts and exhibited more than 10-fold higher sensitivity toward $Pb(NO_3)_2$ (K_{SV} = 8.8x10^5) and $Pb(OAc)_2$ (K_{SV} = 6.9x10^5) than any other cation investigated. The sensitivity of the conjugated polymer was ascribed to a combination of the transport properties of the conjugated polymer and a multivalency effect through which the Pb^{2+} cation could be simultaneously bound by more than one carboxylate from the same polymer chain.

1.1.8 *Detection of Biological Molecules Using Conjugated Polymers*

Many conjugated polymer-based biosensors rely on indirect detection of the target analyte. This is especially true for the detection of biological macromolecules such as proteins. The sensory response usually requires a quencher that is not part of the biological

[30] I. B. Kim, A. Dunkhorst, J. Gilbert, and U. H. F. Bunz, *Macromolecules*, **2005**, *38*, 4560.

macromolecule of interest. Heeger and co-workers reported the direct detection of cytochrome *c* (cyt *c*), an iron-containing protein.[31] Cyt *c* quenched the fluorescence of the conjugated poly(lithium-5-methoxy-2-(4-sulfobutoxy)-1,4-phenylene-vinylene) (MBL-PPV) (Figure 16) in 10 mM potassium phosphate buffer (pH 7.4) with a K_{SV} = 3.2x10^8. The authors attributed the quenching response to electron transfer from the photoexcited polymer to cyt *c* (Scheme 1). In addition, they attributed the large Stern-Volmer constant to the formation of an electrostatic complex between the polyanionic conjugated polymer and the polycationic protein. MBL-PPV was most sensitive to quenching by cyt *c* at low pH, conditions under which cyt *c* was positively charged. Nevertheless, cyt *c*, which carries an overall negative charge at pH 10, was still able to quench polymer emission at relatively high pH, albeit with reduced efficiency (K_{SV} = 2.6 x 10^6 at pH 10).

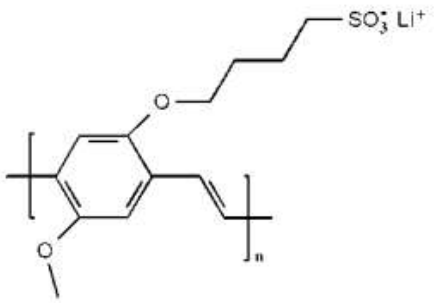

Figure 16. Chemical structure of poly(lithium-5-methoxy-2-(4-sulfobutoxy)-1,4-phenylene-vinylene) (MBL-PPV).

Scheme 1. Mechanism Proposed by Heeger et al. to Explain the Quenching of MBL-PPV.

$$\text{MBL-PPV} \xrightarrow{h\nu} \text{MBL-PPV*}$$

$$\text{MBL-PPV*} + \text{cyt } c \text{ Fe(III)} \rightarrow \text{MBL-PPV} + \text{cyt } c \text{ Fe(II)}$$

[31] C. Fan, K. W. Plaxco, and A. J. Heeger, *J. Am. Chem. Soc.*, **2002**, *124*, 5642.

where MBL-PPV* stands for the excited state of the CP.

In comparison to cyt *c*, lysozyme quenched conjugated polyelectrolyte fluorescence with similar, though slightly lower, efficiency. However, lysozyme, a polycationic protein, was unable to quench conjugated polyelectrolyte fluorescence via electron transfer. On first inspection, the fluorescence quenching response of MBL-PPV to cyt *c* permits to directly detect this protein with high sensitivity using a simple, unfunctionalized conjugated polyelectrolyte. However, the quenching responses to the cyt *c* and lysozyme present a problem of specificity associated with the use CPs as biosensors.

A new emerging application of CPs is their use in medical diagnostic. In 2005, Nilsson and co-workers reported a new approach to the detection of amyloid fibril formation with a zwitterionic conjugated oligomer **6** (Figure 17).[32] In the presence of native bovine insulin (5 μM), **6** showed only a small increase in emission intensity. Upon addition of insulin, that had been incubated at 65 °C for several hours to cause amyloid fibril formation the authors observed a strong blue-shift (from 600 to 560 nm) and an increase in fluorescence intensity. The authors attributed these changes to the twisting and disaggregation of **6** upon binding to the fibril.

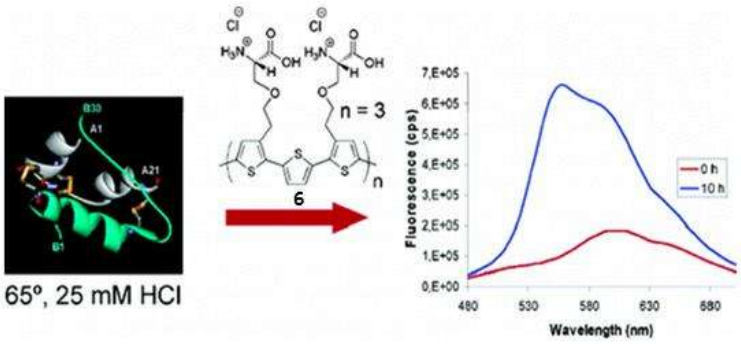

Figure 17. Illustration of the assay utilized by Nilsson and coworker to identify the amyloid fibril formation. In the fluorescence graph is visible the large blue-shift that identify the fibril formation.

[32] A. Herland, K. P. R. Nilsson, J. D. M. Olsson, P. Hammarström, P. Konradsson, and O. Inganäs, *J. Am. Chem. Soc.*, **2005**, *127*, 2317.

1.2 *Microgels*

CPs can be combined with other polymers to produce interpenetrated systems in the form of microgels or macrogels. Thermo-responsive aqueous colloidal microgels form an interesting subset of polymer colloids since they have properties in common with water-soluble polymers, water-swollen macrogels, and with swollen microgels. Like water-soluble polymers, the properties of microgels depend upon the subtle balance of polymer-polymer vs. polymer-water interactions. Like macroscopic aqueous gels, colloidal microgels are characterized by a degree of swelling, an average cross-link density and characteristic time constants for swelling and shrinking. Like hydrophobic polymer colloids, colloidal microgels can be prepared to have monodisperse particle size distributions. Microgels can be characterized by standard colloidal techniques including electrophoresis, dynamic light scattering, rheology and transmission or scanning electron microscopy (TEM or SEM).

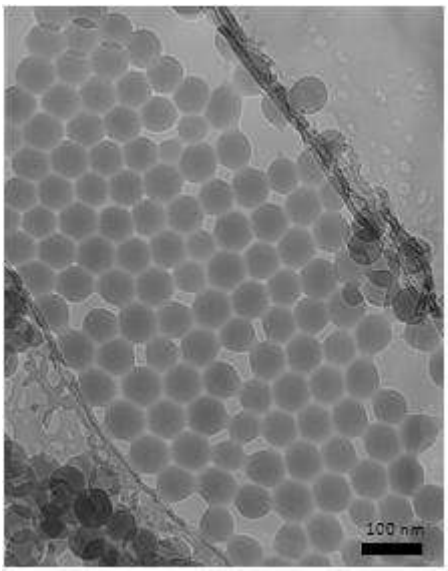

Figure 18. The TEM image shows polystyrene microgels with a monodisperse size.

1.2.1 *Microgels and LCST*

One of the most studied microgels is the cross-linked PNIPAM, a polymer which has a lower critical solution temperature in water of 32 °C.[33,34] At room temperature, the gels have high water content, a low refractive index difference with water, and a few electrically charged groups on the chain ends. By contrast, at elevated temperatures the particle collapses and the volume decreases up to 10-times; the density of electrically charged groups is higher and the refractive index difference with water is greater. An important measure for the state of swelling is the so-called swelling ratio α, which is defined as the ratio between the volume of collapsed particles $V_{collapsed}$ and the volume of the particles in the totally swollen state $V_{swollen}$. Since, we are dealing with microgels of near spherical shape in solution one can use the radii in order to calculate α.

$$\alpha = {\text{Vcollapsed}}/{\text{Vswollen}} = (Rc|Rs)^3 \qquad [4]$$

where *Rc* is the radii of the collapsed microgel and *Rs* for the swollen microgel.[35] The surfactant-free emulsion polymerization that is usually used for the synthesis led to spherical microgels with rather low polydispersity. There have been many publications describing the preparation, characterization and application of temperature-sensitive microgels, most based on PNIPAM. This activity reflects the current interest in "switchable" or "intelligent" materials[36,37,38] making NIPAM one of the major building block for temperature-sensitive microgels. In aqueous solution

[33] M. Heskins, and J.E. Guillet, *J. Macromol. Sci. Chem. A2*, **1968**, 1441.
[34] H. G. Schild, *Prog. Polym. Sci.*, **1992**, *17*, 163.
[35] M. Karg, I. Pastoriza-Santos, B. Rodriguez-González, R. von Klitzing, S. Wellert and T. Hellweg, *Langmuir*, **2008**, *24*, 6300.
[36] M. Agrawal, J. Rubio-Retama, N. E. Zafeiropoulos, N. Gaponik, S. Gupta, V. Cimrova, V. Lesnyak, E. López-Cabarcos, S. Tzavalas, R. Rojas-Reyna, A. Eychmüller, and M. Stamm, *Langmuir*, **2008**, *24*, 9820.
[37] A. Garcia, M. Marquez, T. Cai, R. Rosario, Z. Hu, D. Gust, M. Hayes, S. A. Vail, and Choong-Do Park *Langmuir*, **2007**, *23*, 224.
[38] N. MacKinnon, G. Guérin, B. Liu, C. C. Gradinaru, J. L. Rubinstein, and P. M. Macdonald, *Langmuir*, **2010**, *26*, 1081.

it undergoes rapid free radical polymerization to give high molecular weight polymers.[39,40] Gels, either micro or macro, are temperature-sensitive if most of the polymer in the gel network displays has temperature-sensitive phase behavior in the swelling solvent. A linear polymer that displays cloud point behavior when heated can be cross-linked to give a temperature-sensitive microgel network. Upon heating such a microgel, one observes the microgel to shrink by expelling water over a narrow temperature range, usually called the volume phase transition. PNIPAM based aqueous microgels are temperature-sensitive because PNIPAM has a lower critical solution temperature of 32 °C.

1.2.2 *Microgel Synthesis*

The first published account of PNIPAM based microgels described a "surfactant-free emulsion polymerization" of aqueous NIPAM and BA.[41] This recipe was essentially the same as that used to prepare monodisperse, surfactant-free polystyrene latex.[42] The polymerization was conducted at 60-70 °C in order to generate free radicals by the decomposition of the persulfate initiator. However, elevated temperature was also required so that growing PNIPAM chains are phase separated to form colloidal particles and some authors call this procedure "precipitation polymerization". This simple polymerization procedure can produce remarkably uniform particles as shown with TEM micrograph in Figures 18 and 19. The TEM sample was prepared by placing a dilute drop of aqueous particles onto the sample grid and allowing it to dry. Microgel particle formation occurs by homogenous nucleation that is known sometimes to give latex dispersions with a narrow particle size distribution.[43]

---

[39] X. Wu, R.H. Pelton, A.E. Hamielec, D.R. Woods, and W. McPhee, *Colloid Polym. Sci.*, **1994**, *272*, 467.
[40] G. Bokias, A. Durand, and D. Hourdet, *Macromol. Chem. Phys.*, **1998**, *199*, 1387.
[41] R.H. Pelton, and P. Chibante, *Colloids Surf.*, **1986**, *20*, 247.
[42] J.W. Goodwin, R.H. Ottewill, and R. Pelton, *Colloid Polym. Sci.*, **1979**, *257*, 61.
[43] R. G. Gilbert, *Emulsion Polymerization: A Mechanistic Approach*, Academic Press, London, **1995**.

According to this mechanism a water-soluble sulfate radical initiates a water-soluble NIPAM monomer which then grows in solution until it reaches a critical chain length after which the growing chain collapses to become a colloidally unstable “precursor particle”.

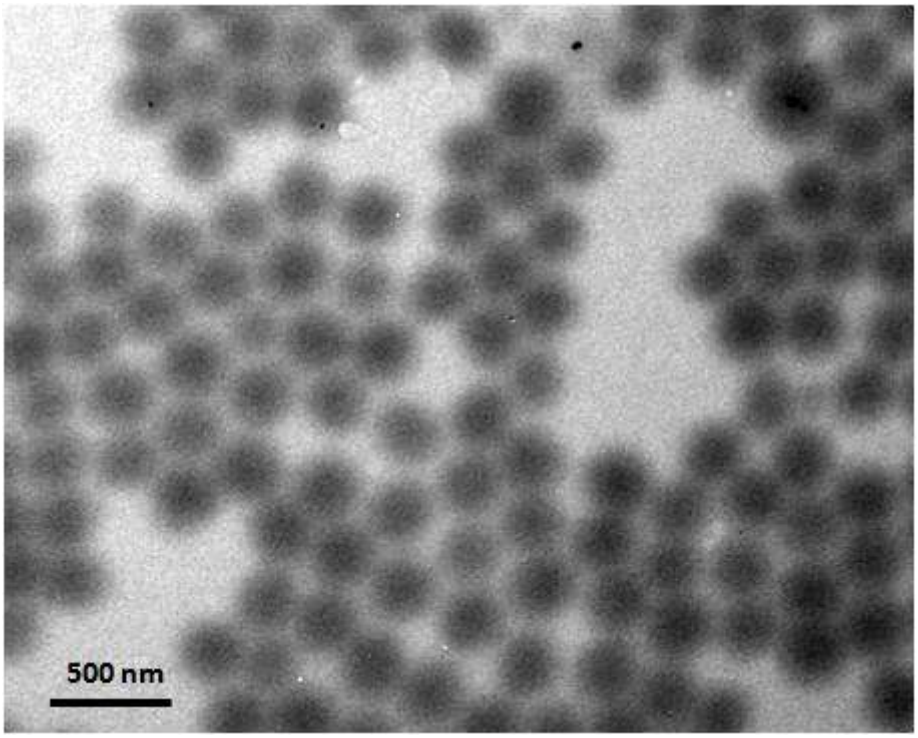

Figure 19. TEM micrograph of uniform PNIPAM microgels.

The precursor particles follow one of two competing processes. Either they deposit onto an existing colloidally stable polymer particle or they aggregate with other precursor particles until they form a particle sufficiently large to be colloidally stable. At the polymerization temperature 60-70 °C which is well above the LCST, the growing PNIPAM microgel particles are colloidally stabilized by electrostatic interactions originating from sulfate groups introduced by the persulfate initiator.

1.2.3 *Microgels as Containers*

Polymer microgels can be used to encapsulate or entrap different substances within their volume. Polyacrylamide gels have been widely used as matrix of electrophoresis and they have found applications as support for enzyme immobilization and drug encapsulation.[44] To obtain microgels, new methods of polymerization have been developed in recent years like polymerization in micelles,[45] concentrated microemulsions and nanoemulsions.[46,47]

Polymerization in W/O concentrated emulsion is less common than polymerization in emulsion but has attracted attention in recent years because it reduces the large quantities of surfactants required in microemulsion polymerization. The preparation of PAA microgels by this method yields microgels with similar size to the globule of the precursor concentrated emulsion. The microgel is produced in a bead shape and the degree of cross-linking determines the water uptake, pore size and the molecular exclusion limit. This method allows the entrapment of drugs, enzymes and macromolecules inside microgel particles and opens new possibilities in fields like control drug release and fabrication of new biosensors since the enzymes retain their activity.

One example of enzyme confinement into microgels has been published by Rubio et al.[48] They report the use of cross-linked PAA microgels to immobilize glucose oxidase (GOx), the modifications induced by the enzyme in the microstructure of the gels and with this system they prepared an amperometric biosensor. The choice of cross-linking content leads to microgels with different degree of swelling, which influences the amount of GOx immobilized within the polymer matrix. The microparticles with GOx were used to fabricate an amperometric biosensor able to detect glucose. The current response of the biosensor is based on the formation of

[44] P. Bera, and S. K. Saha, *Polymer*, **1998**, *39*, 1461.
[45] H. Jingcheng, Z. Liqiang, L. Ganzuo, W. Hanqing, and D. Zhengwei, *Polymer*, **1996**, *37*, 3117.
[46] H. R. Lin, *Eur. Polym. J.*, **2001**, *37*, 1507.
[47] M. E. S. R. Silva, E. R. Dutra, V. Mano, and J. C. Machado, *Polym. Degradation Stability*, **2000**, *67*, 491.
[48] J. Rubio-Retama, B. López-Ruiz, and E. López-Cabarcos, *Biomaterials*, **2003**, *24*, 2965.

hydrogen peroxide during the enzyme-catalyzed reaction which is subsequently oxidized. The detection scheme is summarized in the following equations:

$$\text{Glucose} + O_2 - (\text{glucose oxidase}) \rightarrow H_2O_2 + \text{Gluconolactone}$$

$$H_2O_2 \rightarrow O_2 + 2H^+ + 2e^-$$

The current response resulting from the oxidation of hydrogen peroxide is detected by amperometry.

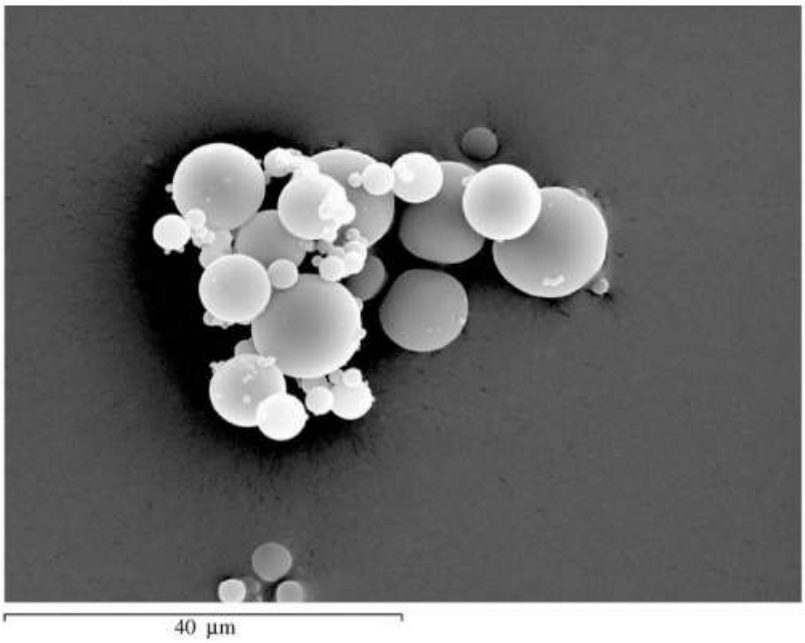

Figure 20. SEM micrograph of microgel particles with GOx immobilized within the polymer matrix.

1.2.4 *Copolymers and Interpenetrated Microgels*

It is important to find ways to control microparticles swelling and phase transition temperature when dealing with microgels applications. A powerful tool to influence the swelling behavior is to copolymerize with organic comonomers such as acrylic acid, vinylacetic acid,

styrene, and others.[49,50,51,52,53] The change of the chemical composition of the network can affect the transition temperature as well as the swelling properties and the local network dynamics.[54] Hence, the use of comonomer moieties within the microgel synthesis is a pathway to design versatile systems with specific properties. Considering pure PNIPAM particles the swelling can be understood as a result of the balance between polymer elasticity and the osmotic pressure. Both are responsible for the state of extension of the network. An additional contribution to the osmotic pressure appears when charged functionalities are incorporated into the network.[55] Like typical polyelectrolytes, such charged networks are sensitive to changes of pH, which defines the degree of dissociation and also to changes of the ionic strength, which affects the Debye screening length.

In 2008 Karg et al. studied the VPT of a series of poly(NIPAM-co-allylacetic acid) copolymers with different contents of allylacetic acid (AAA) that were synthesized by means of a simple radical polymerization. They found that these copolymers were much more sensitive to external stimuli such as pH and ionic strength than their pure PNIPAM counterparts. They investigated the VPT at two different pH values and various salt concentrations and at pH 10 for the copolymer microgels with the highest AAA content, they found a significant shift of the VPT temperature toward higher values. Furthermore, for higher AAA content, a change in pH from 8 to 10 can induce a change in radius of up to 100 nm making the particles interesting as pH controlled actuators.

[49] A. Fernandez-Nieves, A. Fernandez-Barbero, and F. J. de las Nieves, *J. Chem. Phys.*, **2001**, *115*, 7644.
[50] Y. Levin, A. Diehl, A. Fernandez-Nieves, and A. Fernandez-Barbero, *Phys. Rev . E*, **2002**, *65*, 1.
[51] J. D. Debord, and L. A. Lyon, *Langmuir*, **2003**, *19*, 7662.
[52] I. Berndt, and W. Richtering, *Macromolecules*, **2003**, *36*, 8780.
[53] T. Hoare, and R. Pelton, *Macromolecules*, **2004**, *37*, 2544.
[54] T. Hellweg, K. Kratz, S. Pouget, and W. Eimer, *Colloids Surf. A*, **2002**, *202*, 223.
[55] K. Kratz, T. Hellweg, and W. Eimer, *Colloids Surf. A,* **2000**, *170*, 137.

1.2.5 *Core-Shell Microgels*

Another interesting way to control the particle swelling and the phase transition temperature of microgels is to synthesize core-shell microgels. They usually consist of a water-insoluble latex particle coated with a gel layer. The composite particles have properties characteristic of both the core and the shell. The core dominates light scattering turbidity behavior whereas the colloid stability is determined by the hydrogel shell. For example, latex with temperature-sensitive colloidal stability can be achieved with a PNIPAM shell.

The first reported preparation of PNIPAM coated core-shell particles was by Pelton who described both the one-step surfactant-free preparation of polystyrene-PNIPAM gels and the grafting of PNIPAM onto existing latex particles.[56] Unlike the homogenous microgel preparations, these polymerizations are conducted below the LCST so that PNIPAM does not phase separate. Similar core-shell microgel structures were obtained by Bradley et al. They prepared microgel core-shell particles with temperature-responsive PNIPAM shell and pH-responsive poly(2-vinylpyridine) core.[57] Their studied the uptake and release of an anionic surfactant from the microgels as a function of the solution pH and temperature. The results indicate that electrostatic attraction between the anionic surfactant and the cationically charged core of the microgel particles is the dominant mechanism for absorption of the surfactant into the core-shell particles.

Berndt et al. have published the synthesis of a multiresponsive core-shell microgel composed by NIPAM and N-isopropylmethacrylamide (NIPMAM).[58] This microgel presents two different VPT at two distinct different temperatures. These particles show a two-step shrinking process of hydrodynamic radius *Rh* upon heating in aqueous solution. The transitions at 34 °C and 44 °C are assigned to core and shell collapse, respectively.

---

[56] R.H. Pelton, *J. Polym. Sci.*, **1988**, *26*, 9.
[57] M. Bradley, and B. Vincent, *Langmuir*, **2008**, *24*, 2421.
[58] I. Berndt, J. S. Pedersen, and W. Richtering, *J. Am. Chem. Soc.*, **2005**, *127*, 9372.

More recently PNIPAM has been employed in the synthesis of core-shell hybrid microparticles constituted of a core of metal nanoparticles and a PNIPAM shell. Contreras et al.[59] have developed a simple two-step procedure for the encapsulation of cetyltrimethylammonium bromide (CTAB) stabilized metal nanoparticles within PNIPAM. The first step comprises the growth of a polystyrene (PS) shell onto the metal nanoparticles (promoted by the CTAB bilayer), which serves to avoid aggregation and make the surface of the particles fully compatible with PNIPAM. The second step consists in the precipitation polymerization of NIPAM on the surface of the Au nanocrystals.

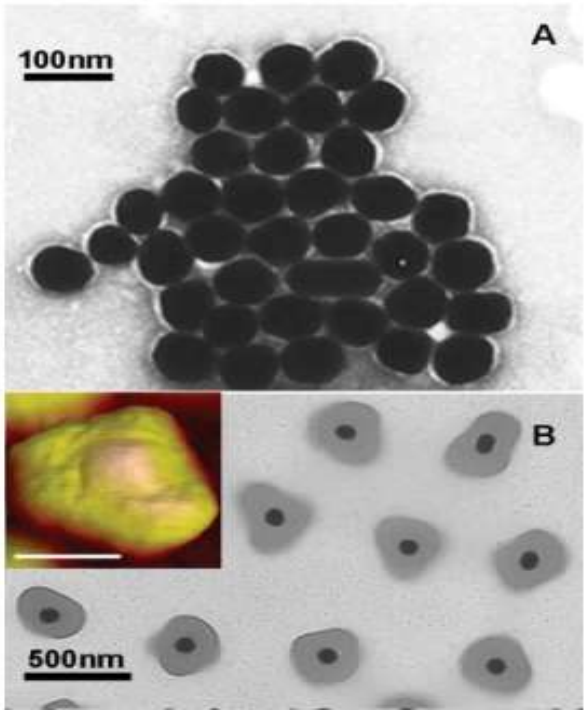

Figure 21. TEM images showing A) PS-DVB coated Au nanoparticles and B) Au–PNIPAM core-shell microgels. The inset in (B) is a tapping-mode atomic force microscopy image of one composite particle. The scale bar is 200 nm.

[59] R. Contreras-Cáceres, A. Sánchez-Iglesias, M. Karg, I. Pastoriza-Santos, J. Pérez-Juste, J. Pacifico, T. Hellweg, A. Fernandez-Barbero, and L. M. Liz-Marzán, *Adv. Mater.*, **2008**, *20*, 1666.

1.3 *Gold Nanocrystals*

Noble metal nanoparticles have been intensively studied within the past 15 years for materials applications,[60,61,62] as well as biochemical or biomedical usage.[63] Some of the interest in gold nanoparticles is due to the prominent optical resonance in the visible range and their sensitivity on environmental changes, size, and shape of the particles as well as the local field enhancement of light interacting with the resonant system. Therefore, applications require synthesis protocols, which deliver well-defined shapes and sizes.[64,65]

Several classes of synthesis routes exist, which display different characteristics of the final products. Besides the strength of the reductant, the action of a stabilizer in the solution phase synthesis is critical. Examples of widespread usage are the organic phase synthesis involving a two phase process,[66] or the single phase water based reduction of a gold or silver salt by citrate, introduced by Turkevich et al.[67,68,69,70] and refined by Frens,[71] which produces almost spherical particles over a tunable range of sizes (see Figure 22).

The kinetics of the Turkevich process has been addressed in a publication from Chow and Zukoski[72] focusing on the stabilization mechanism. The reduction of a gold salt in the presence of a complexing surfactant[73,74,75,76] allows us to obtain elongated, crystallographically

[60] Q. Q. Wang, J. B. Han, D. L. Guo, S. Xiao, Y. B. Han, H. M. Gong, and X. W. Zou, *Nano Lett.*, **2007**, *7*, 723.
[61] R. P. Andres, J. D. Bielefeld, J. I. Henderson, D. B. Janes, V. R. Kolagunta, C. P. Kubiak, W. J. Mahoney, and R. G. Osifchin, *Science*, **1996**, *273*, 1690.
[62] S. Abalde-Cela, S. Ho, B. Rodríguez-González, M. A. Correa-Duarte, R. A. Álvarez-Puebla, L. M. Liz-Marzán, and N. A. Kotov, *Angew. Chem., Int. Ed.*, **2009**, *48*, 5326.
[63] L. R. Hirsch et al., *Proc. Natl. Acad. Sci. U.S.A.*, **2003**, *100*, 13549.
[64] C. Burda, X. Chen, R. Narayanan, and M. A. El-Sayed, *Chem. Rev.*, **2005**, *105*, 1025.
[65] B. L. Cushing, V. L. Kolesnichenko, and C. J. O'Connor, *Chem. Rev.*, **2004**, *104*, 3893.
[66] M. Brust, M. Walker, D. Bethell, D. J. Schiffrin, and R. J. Whyman, *Chem. Soc., Chem. Commun.*, **1994**, 801.
[67] J. Turkevich, P. C. Stevenson, and J. Hillier, *Discuss. Faraday Soc.*, **1951**, *11*, 55.
[68] B. V. Enüstün, and J. Turkevich, *J. Am. Chem. Soc.*, **1963**, *85*, 3317.
[69] J. Turkevich, *Gold Bull.*, **1985**, *18*, 86.
[70] J. Turkevich, *Gold Bull.*, **1985**, *18*, 125.
[71] G. Frens, *Nat. Phys. Sci.*, **1973**, *20*, 241.
[72] M. K. Chow, and C. F. Zukoski, *J. Coll. Interface Sci.*, **1994**, *165*, 97.
[73] B. Nikoobakht, and M. A. El-Sayed, *Chem. Mater.*, **2003**, *15*, 1957.

aligned, nanorods. In this procedure, the gold ions are complexed by a surfactant molecule as CTAB and not directly reduced by ascorbic acid.

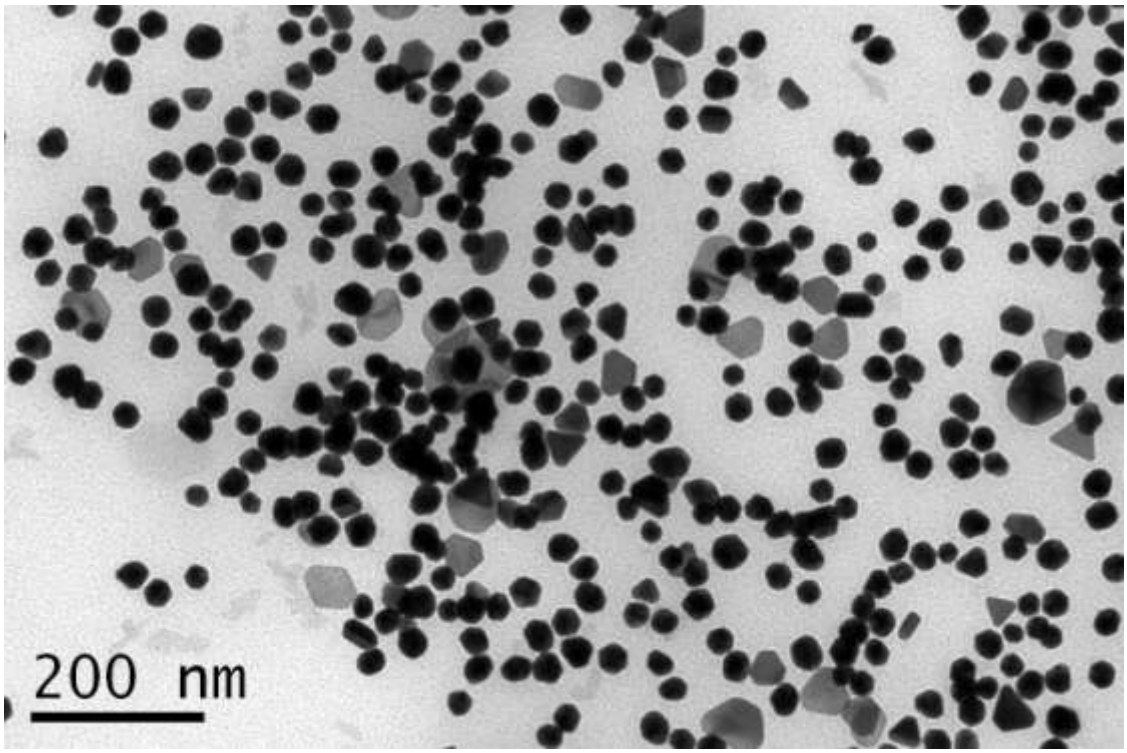

Figure 22. TEM image of Au nanoparticles synthesized using a slightly modified Turkevic method.

Only the addition of gold particle seeds allows the growth of crystallographically oriented rods. It is important to recognize that the conditions necessary for nucleation of nanocrystals are exactly the opposite to those required for selective growth of facets. Small seed particles of gold are generated under conditions of high chemical supersaturation[77] and this leads to the fastest nucleation rate and almost invariably to spherical nuclei with sizes between 1 and 5 nm. Such conditions ensure rapid growth of all crystal surfaces but are contraindicated for shape control. Shape control is commonly achieved through a two-step process, termed

[74] N. R. Jana, L. Gearheart, and C. J. Murphy, *J. Phys. Chem. B*, **2001**, *105*, 4065.
[75] N. R. Jana, L. Gearheart, and C. J. Murphy, *Adv. Mater.*, **2001**, *13*, 1389.
[76] D. B. Busbee, S. O. Obare, and C. J. Murphy, *Adv. Mater.*, **2003**, *15*, 414.
[77] J. W. Mullin, *"Crystallization"* 4th Edition, Butterworth-Heinemann, **2001**.

''seed-mediated growth''. In the first step, very small, reasonably uniform, spherical seed particles are generated. The reaction conditions are then altered and in the second step more gold ions and a different reductant are added, together with some shape templating surfactant or molecule. The seeds are grown then into larger particles of particular morphologies or habits and growth stage is much slower and proceeds under milder reducing conditions than the nucleation stage.

1.3.1 *Surface Plasmon Resonance*

Although, Faraday's best known contributions were in Electromagnetism, he posed the central problem of small particles optics in 1857 for the Bakerian lecture.[78] Faraday's purpose in exploring colloidal phenomena followed his concerns with the interaction between light and matter. Faraday thought that there might be some value in observing the interaction of light with material particles, which, in turn, were also small compared with the wavelength of light. He thought on gold because samples could be prepared with particles smaller than the wavelength of the visible light and because known phenomena appeared to indicate that a variation in the size of gold particles gives a variety of colors. Despite Faraday's appreciation was only in 1908 that Gustav Mie explained the red color of the gold nanoparticles in solution by solving Maxwell's equations.[79] Bulk gold has a yellow color, caused by a reduction in reflectivity for light at the end of the spectrum. Whenever gold or silver is obtained as colloidal dispersion of nanoparticles a variety of colors appears depending on the size of the nanoparticles, as shown in Figure 23.

[78] M. Faraday, *Philos. Trans. R. Soc. Ser. A*, **1857**, *147*, 145, London.
[79] G. Mie, *Ann. Phys.*, **1908**, *25*, 377.

When the particles of gold are small enough, their color is ruby red, due to their strong absorption of green light at about 520 nm, corresponding to the frequency at which a plasmon resonance occurs with the gold.

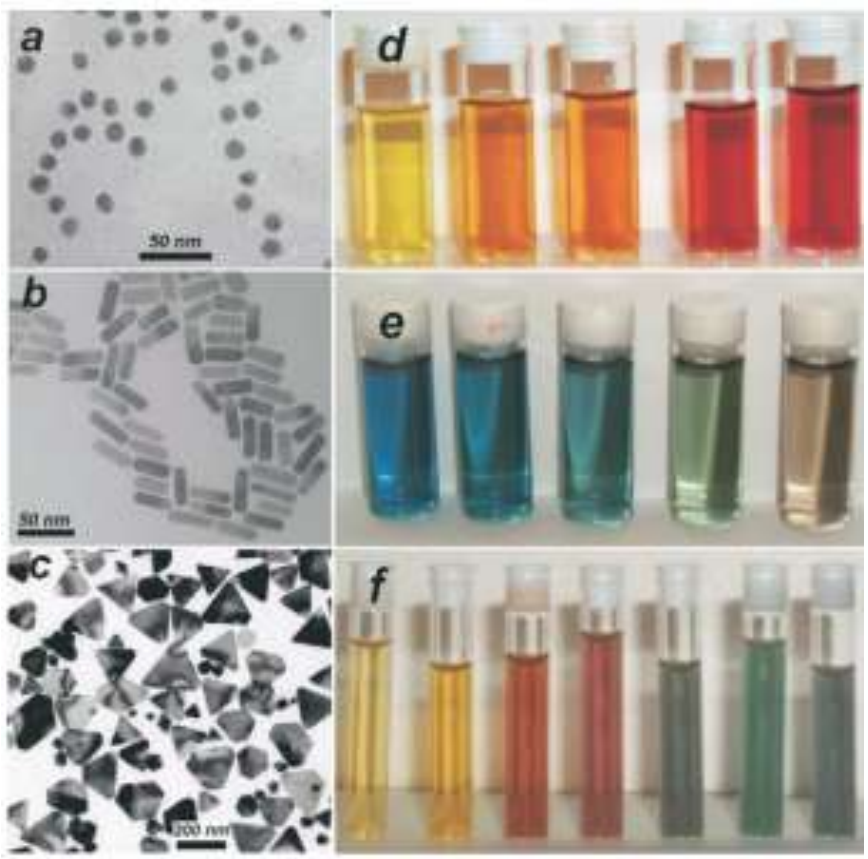

Figure 23. Left: TEM micrographs of Au nanospheres and nanorods (a,b) and Ag nanoprisms (c, mostly truncated triangles) formed using citrate reduction, seeded growth, and DMF reduction, respectively. Right: Photographs of colloidal dispersions of AuAg alloy nanoparticles with increasing Au concentration (d), Au nanorods of increasing aspect ratio (e), and Ag nanoprisms with increasing lateral size (f).[80]

The physical origin of the light absorption by metal nanoparticles is the coherent oscillation of the conduction band electrons induced by the interacting electromagnetic field.

[80] L. M. Liz-Marzán, *Materials Today*, **2004**, *7*, 26.

1. *Introduction*

The electromagnetic surface waves can propagate along the interface between conducting materials and a dielectric over a broad range of frequencies, ranging from dc and radio frequencies up to the visible.[81] The oscillation modes comprise an electromagnetic field coupled to the oscillations of conduction electrons and are called surface plasmons. They are characterized by strong field enhancement at the interface, while the electric field vector decays exponentially away from the surface (in the nanometer range).[82,83,84] When the dimensions of the conductor are reduced, boundary and surface effects become very important, and for this reason, the optical properties of small metal nanoparticles are dominated by collective oscillation of conduction electrons.[85,86,87] An absorption band results when the incident photon frequency is resonant with the collective oscillation of the conduction band electrons and is known as the surface plasmon resonance (SPR). The resonance frequency of the SPR is strongly dependent upon the size, shape, interparticle interactions, dielectric properties, and local environment of the nanoparticle.[88,89]

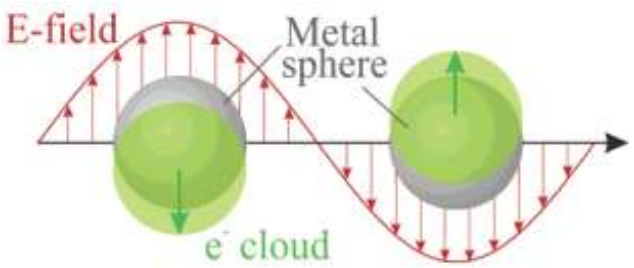

Figure 24. Schematic representation of plasmon oscillation for a sphere, showing the displacement of the conduction electron charge cloud relative to the nuclei.[90]

[81] R. Collin, *"Field Theory of Guided Waves"*, 2nd Ed., Wiley, New York, **1990**.
[82] R. H. Ritchie, *Phys. Rev.*, **1957**, *106*, 874.
[83] H. Raether, "*Surface Plasmons*", Springer-Verlag, Berlin, **1988**.
[84] W. L. Barnes, A. Dereux, and T. W. Ebbesen, *Nature*, **2003**, *424*, 824.
[85] M. Moskovits, *Rev. Mod. Phys.*, **1985**, *57*, 783.
[86] H. Metiu, and P. Das, *Annu. Rev. Phys. Chem.*, **1984**, *35*, 507.
[87] H. Metiu, *Prog. Surf. Sci.*, **1984**, *17*, 153.
[88] C. A. Mirkin, and M. A. Ratner, *Annu. Rev. Phys. Chem.*, **1997**, *101*, 1593.
[89] M. A. Rampi, O. J. A. Schueller, and G. M. Whitesides, *Appl. Phys. Lett.*, **1998**, *72*, 1781.
[90] K. L. Kelly, E. Coronado, L. L. Zhao, and G. C. Schatz, *J. Phys. Chem. B*, **2003**, *107*, 668.

The oscillation frequency is critically determined by four factors: the density of electrons, the effective electron mass, and the shape and the size of the charge distribution. Actually, many other metals such as, Te, Pb, In, Hg, Sn, and Cd, display this type of spectrally selective resonance, but in general the resonance frequency could be found in the near UV and nanoparticles do not display strong color effects.[91] Furthermore, such small metal particles are also readily oxidized making surface plasmon experiments difficult, while gold is one of the very few metals noble enough to survive as nanoparticles under atmospheric conditions making gold one of the most investigated system for nanoparticles synthesis (Figure 25).

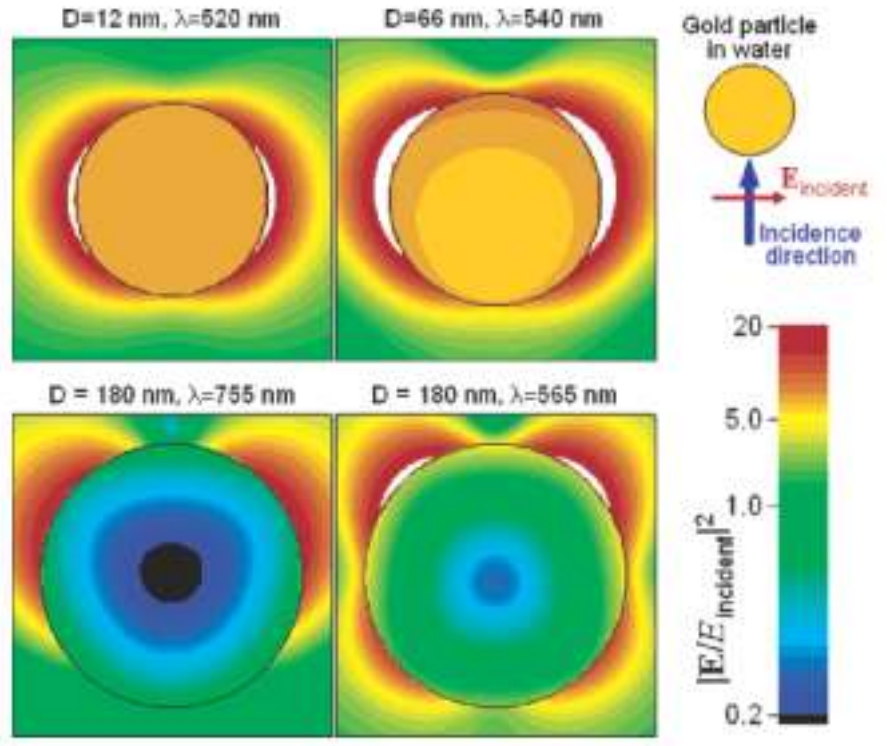

Figure 25. Near field enhancement at spherical gold nanoparticles of various size in water, when illuminated at their corresponding plasmon wavelengths. The polarization and illumination directions are schematically shown.[92]

[91] A. Sanchez-Iglesias, M. Grzelczak, B. Rodríguez-González, R. A. Álvarez-Puebla, L. M. Liz-Marzán, and N. A. Kotov, L*angmuir*, **2009**, *25*, 11431.
[92] J. Rodríguez-Fernández, J. Pérez-Juste, F. J. García de Abajo, and L. M. Liz-Marzán, *Langmuir*, **2006**, *22*, 7007.

1.3.2 *Anisotropic Gold Nanocrystals*

Although the syntheses of spherical nanoparticles have been well developed for many materials, the fabrication of anisotropic nanocrystal is still a challenge nowadays. For colloidal gold nanorods and nanoprisms the preferred synthetic route is the seed-mediated growth and, therefore, the chemicals presented in this methodology such as ascorbic acid, CTAB, chloroaurate ion have been extensively studied.[73,75,93,94] Researchers have also pointed to synthetic additives such halide ions as major factors in directing crystal growth for the shape control of metal nanostructures.[95,96] Their specific adsorption is well-documented in the field of surface chemistry and electro-chemistry since all the halide ions are specifically adsorbed onto low-indexed gold surfaces (i.e., Au(111), Au(110), and Au(100)) except for the fluoride ion.[95] Another interesting new approach comprises the use of metal ions to control the morphology of metal nanostructures.

Chen et al. have reported a modified seed-mediated technique for fabricating gold nanorods/wires wherein the shape of the gold nanomaterials evolved from fusiform into 1D rods and other geometries.[97,98] The presence of silver ions strongly dominated the formation of fusiform nanoparticles, and they were able to synthesize nanoparticles with different shapes. Sun et al, used the replacement reaction between silver nanostructures and an aqueous $HAuCl_4$ solution to generate metal nanostructures with hollow interiors.[99] This approach is very interesting since the method could be seen as a post-functionalization of the synthesized nanostructure.

---

[93] T. H. Ha, H. J. Koo, and B. H. Chung, *J. Phys. Chem. C*, **2007**, *111*, 1123.
[94] H. M. Chen, R. S. Liu, and D. P. Tsai, *Crystal Growth & Design*, **2009**, *9*, 2080.
[95] J. E. Millstone, W. Wei, M. R. Jones, H. Yoo, and C. A. Mirkin, *Nano Lett.*, **2008**, *8*, 2526.
[96] O. M. Magnussen, *Chem. Rev.*, **2002**, *102*, 679.
[97] H. M. Chen, H. C. Peng, R. S. Liu, K. Asakura, C. L. Lee, J. F. Lee, and S. F. Hu, *J. Phys. Chem. B*, **2005**, *109*, 19553.
[98] H. M. Chen, R. S. Liu, and D. P. Tsai, *Crystal Growth & Design*, **2009**, *9*, 2079.
[99] Y. Sun, and Y. Xia, *J. Am. Chem. Soc.*, **2004**, *126*, 3892.

In 2007, Sun et al. have demonstrated the role played by Cu^{2+} on the selective synthesis of gold cuboids and decahedral nanoparticles.[100] They have shown the importance and the influence of different concentration of Cu^{2+} on the preparation of gold nanostructures using the seed-mediated growth method (Figure 26).

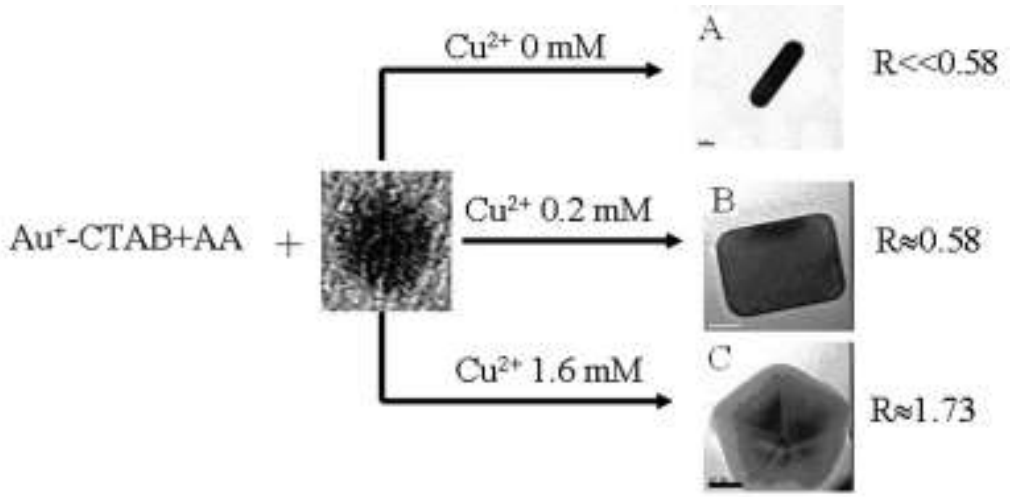

Figure 26. Shape control of Au nanoparticles by changing the concentration of Cu^{2+}. R = $G_{\{100\}}/G_{\{111\}}$

A different new way to control the morphology of the gold nanocrystals is to use polymers as templates, reducing agents or both function. Recently, Tang et al, reported the synthesis of dendritic gold in a one-step hydrothermal reduction of $HAuCl_4$ using ammonium formate as a reducing agent in the presence of poly(vinyl-pyrrolidone) as template (see Figure 27). They found a relationship between an excess of ammonium formate and the dendritic Au particle shape, besides poly(vinyl-pyrrolidone) acts as a stabilizer and may serve not only as a reductant but also as a capping reagent.[101] It seems that the use of two or more capping reagents with different adsorption abilities could be beneficial for the formation of hyperbranched Au nanoparticles.

[100] J. Sun, M. Guan, T. Shang, C. Gao, Z. Xu, and J. Zhu, *Crystal Growth & Design*, **2008**, *8*, 906.
[101] X. L. Tang, P. Jiang, G. L. Ge, M. Tsuji, S. S. Xie, and Y. J. Guo, *Langmuir*, **2008**, *24*, 1763.

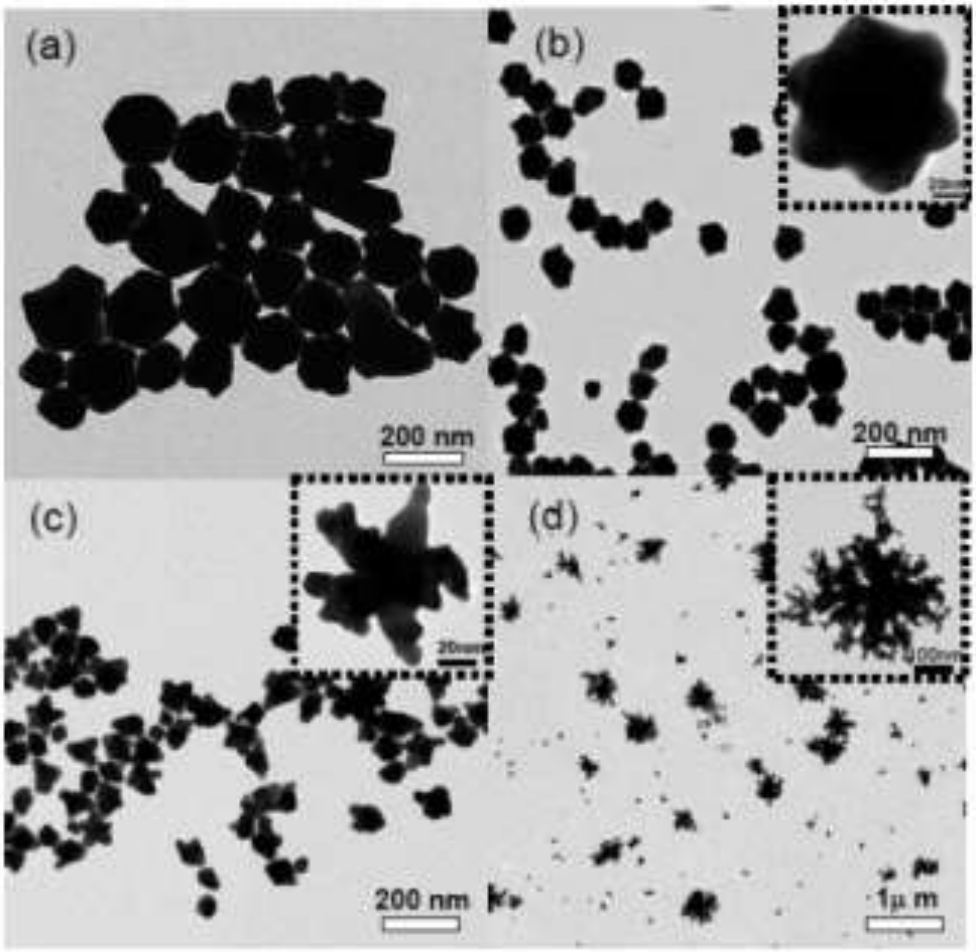

Figure 27. TEM images of obtained Au particles at various ammonium formate concentrations: (a) 0.06, (b) 0.1, (c) 0.3, and (d) 0.5 M. The insets in the TEM images represent individual typical Au particles prepared under corresponding reaction conditions.

Furthermore, poly(vinyl-pyrrolidone) could be used as stabilizing and reducing agent at the same time. Lim et al,[102] describe a simple approach to synthesize anisotropic Au nanostructures with various shapes by reducing $HAuCl_4$ with poly(vinyl-pyrrolidone) in aqueous solutions without the use of any additional capping agent or reductant. The morphology of Au nanostructures evolved from nanotadpoles to nanokites and then triangular and hexagonal microplates (see Figure 28). They concluded that the slow reduction rate associated with the mild reducing power of

[102] B. Lim, P. H. C. Camargo, and Y. Xia, *Langmuir*, **2008**, *24*, 10437.

poly(vinyl-pyrrolidone) plays a critical role to obtain nanoplates during nucleation as well as their growth into anisotropic nanostructures.

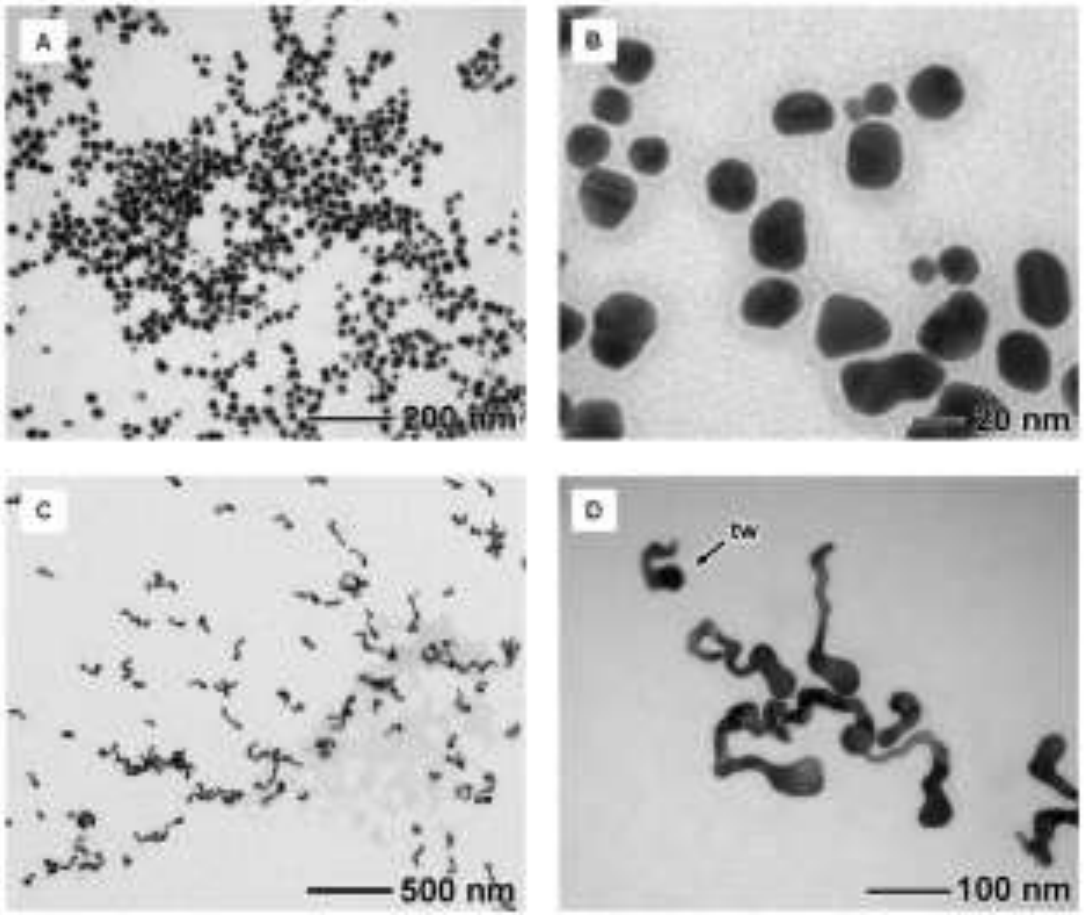

Figure 28. TEM images of Au samples prepared with the addition of (A, B) 0.05 and (C, D) 0.1 mL of 8.7 mM $HAuCl_4$ solution, respectively. The reactions were conducted in boiling water for 1 h with poly(vinyl-pyrrolidone) serving as a reductant and stabilizer. (D) The head indicated by tw has a nonplanar, multiple-twinned structure.

A new possibility to reduce the $HAuCl_4$, reported by Zhai et al. in 2003, is based on the stabilization of gold nanoparticles mediated by poly(3-hexyl-thiophene) in organic solvent.[103] The synthesis of regioregular poly(3-hexyl-thiophene) stabilized gold nanoparticles was accomplished using a room temperature, two-phase, one-pot reaction involving the reduction of

[103] L. Zhai, and R. D. McCullough, *J. Mater. Chem.*, **2004**, *14*, 141.

tetrachloroauric acid by sodium borohydride in the presence of regioregular poly(3-hexyl-thiophene). They prevent the oxidation of the polymer by the tetrachloroauric acid solution using a large amount of the surfactant tetraoctylammonium bromide. The stabilization of the gold nanoparticles was possible since the thiophene rings attach the gold surface and the lateral polymer chains prevent aggregation, stabilizing the nanoparticles in the organic solvent.

2. *Aims of the Work*

2. *Aims of the Work*

The aims of this work are:

1. To study the influence of the surfactant chain length on the PL of a water-soluble CP. For this purpose has been selected a water-soluble fluorescent polythiophene as model CP and N-alkyl-ammonium chloride molecules with different length of the aliphatic chain as model surfactants.

2. Synthesis of an interpenetrated microgel with a CP and development of an optical sensor with this new material. The sensor should be recoverable and with no memory-effect.

3. Development of an optical biosensor coupling an enzyme of the peroxidase family with a water-soluble fluorescent polymer based on p-phenylene-vinylene.

4. Synthesis of a new water-soluble CP with tailor made properties with the purpose to fabricate a heavy metal ions sensor.

5. Fabrication of new hybrid materials combining inorganic nanocrystal with CP as stabilizing and reducing agent. In addition this new hybrid material will be used for the synthesis of a new hybrid material with a core-shell architecture.

3. *Objetivos de Trabajo*

3. *Objetivos de Trabajo*

Los objetivos de este trabajo son:

1. Estudiar la influencia de la longitud de la cadena alifática de tensioactivos sobre la luminiscencia de los polímeros conjugados soluble en agua. Se utilizará un politiofeno modelo soluble en agua y como tensioactivos moléculas de cloruro de N-alquilamonio con diferente longitud de la cadena alifática.

2. Síntesis de un microgel interpenetrado con un polímero conjugado y desarrollo de un sensor óptico con este nuevo material. El sensor deberá ser recuperable y sin efecto de memoria.

3. Desarrollo de un biosensor óptico acoplando una enzima de la familia de la peroxidasa con un polímero fluorescente soluble en agua, basado en para-fenileno-vinileno.

4. Síntesis de un nuevo polímero fluorescente soluble en agua con el objetivo de fabricar un sensor hecho a medida para la detección de iones de metales pesados.

5. Fabricación de nuevos materiales híbridos combinando nanopartículas inorgánicas con polímeros conjugados como agente reductor y estabilizante. Además se investigará el utilizo de dicho material en la síntesis de nuevos materiales híbridos con arquitectura de núcleo-corteza.

4. *Materials and Methods*

4.1 *Chemicals*

The following products were bought from Sigma-Aldrich Inc (Saint Louis, MO, USA). and used without further purification: 3-Thiophene ethanol 99%, dodecylamine 99%, decylamine 99.5%, nonylamine 99.5%, octylamine 99.5%, meso 2,3-dimercaptosuccinic acid 98%, anhydrous iron(III) chloride 99.99%, acetyl chloride 99%, anhydrous magnesium sulfate 99%, N-Isopropylacrylamide 97%, N,N'-methylene-bis-acrylamide 98% (BA), sodium acrylate 97%, p-Toluenesulfonyl chloride 99%, lead(II) nitrate 99%, sodium dihydrogen phosphate 99%, disodium hydrogen phosphate 99%, sodium chloride 99%, mercury(I) nitrate dihydrate 97%, silver nitrate 99%, sodium nitrate 99%, zinc chloride 98%, mercury(II) acetate 98%, potassium carbonate 99%, cesium carbonate 99%, 2,2'-Azobis(2-methylpropionamidine) dihydrochloride 97%, gold(III) chloride trihydrate 99.9%, hexadecyltrimethylammonium bromide 99%, picric acid 98% moistened with water, methyl viologen dichloride hydrate 98%, peroxidase from horseradish type II 150-250 units/mg solid, acrylamide 97%, N,N,N',N'-Tetramethylethylenediamine 99%, dodecane 99%, 4-Acetamidophenol 98%, anhydrous THF 99% contains 250ppm BHT as inhibitor, THF 98% contains 250ppm BHT as inhibitor, hexane 99%, N,N'-dimethylformamide 99.8%, ethyl acetate 99.5%, dimethyl sulfoxide 99.9%, deuterated chloroform 99.8 atom % contains 0.03% (v/v) TMS, deuterated THF 99.5 atoms % contains 0.03% (v/v) TMS, deuterium oxide 99.99 atom%, and deuterated dimethyl sulfoxide 99.96 atom % contains 0.03% (v/v) TMS.

The following products were bought from Merck (Whitehouse Station, NJ, USA) and used without further purification: lead(II) nitrate 99%, sodium dihydrogen phosphate 99%, disodium hydrogen phosphate 99%, sodium chloride 99%, mercury(I) nitrate dihydrate 97%, silver nitrate 99%, sodium nitrate 99%, zinc chloride 98%, mercury(II) acetate 98%, potassium carbonate 99%, cesium carbonate 99%.

The following products were bought from Panreac (Barcelona, Spain) and used without further purification: acetone 99.5%, ethanol 96% (v/v), methanol 99.8%, absolute ethanol 99.5% (v/v), sodium hydroxide 98%, potassium hydroxide > 86%, sodium bicarbonate 99.5%, hydrogen peroxide solution 33% (v/v), hydrochloric acid 37%, sulfuric acid 97%, nitric acid 69%, diethyl ether 99% with 1ppm BHT as inhibitor, chloroform 99.8% with ethanol as stabilizer, and dichloromethane 99.5% with 50 ppm amylene as stabilizer.

Silica gel on TLC plates with fluorescent indicator at 254 nm, Span® 80, and ammonium persulfate 98% were bought from Fluka (Saint Louis, MO, USA). Silica gel 130-270 mesh with pore size 60 Å, molecular sieves 4 Å, and potassium persulfate 99% were bought from Merck and used with further purification. ADS2000 or poly[2-(3-thienyl)ethyloxy-4-butylsulfonate] sodium salt was purchased from American Dye Source Inc (Baie-D'Urfe, QC, Canada). Copper TEM grids with holey carbon or formvar films were bought from Structure Probe Inc (West Chester, PA, USA). Distilled water was produced with a Millipore Elix 20 (Billerica, MA, USA).

In this work, where indicated dry solvent means the solvent was prior distillated in vacuum and stored in nitrogen atmosphere with activated molecular sieves 4 Å.

4.2 *Methods and Instrumentation Used*

4.2.1 *Nuclear Magnetic Resonance Spectroscopy*

Every nuclide that posses a spin quantum number *S* different from zero is observable using NMR. When a nuclide is immersed in a constant magnetic field the atom absorbs and re-emits (resonance) electromagnetic energy at a particular wavelength and the wavelength depends by the chemical environment experimented by the nuclides. In addition, the resonance frequency (RF) is proportional to the strength of the magnetic field.

The molecular structures of the synthesized molecules were analyzed by NMR using a Bruker AVANCE AV-500 (500 MHz) and Bruker AVANCE 250 (250 MHz) (Karlsruhe, Germany). The probes used were TXI ^{1}H and ^{13}C, and QNP ^{1}H, and ^{13}C. The NMR tubes used for the experiments were Wildman® 3mm diameter, limit 500 MHz frequency, and were bought from Sigma-Aldrich. The samples were prepared dissolving 2-4 mg of the desired substance in a deuterated solvent containing an internal standard.

4.2.2 *Ultraviolet-Visible Spectroscopy*

The base of this technique is the absorption of a photon by the target molecules. In fact, in this region of the electromagnetic spectrum a molecule can absorb a photon and provoke the electronic transition from a no excited electronic ground-state to the first excited electronic state. This technique is complementary to the fluorescence spectroscopy since fluorescence deals with transitions from the first electronic excited state to the ground state.

The UV-Vis measurements were performed using a Varian Cary 300 Bio (Palo Alto, CA, USA) and a Shimadzu UV1601 (Kyoto, Japan). The cuvettes used have a path of 1 cm and bought from Hellma (Müllheim, Germany).

4.2.3 *Fluorescence and Lifetime Spectroscopy Measurements*

Fluorescence spectroscopy was done using two spectrometers: i) Jasco FP 6300 coupled with a Jasco ETC-273T temperature controller (Mary's Court Easton, MD, USA), and ii) a QuantaMaster™ 40 Photon Technology International (PTI) (Birmingham, NJ, USA). For the fluorescence lifetime measurement we used an Easylife PTI (Birmingham, NJ, USA) instrument equipped with source laser diodes of 420 nm and 460 nm wavelengths. The cuvettes used have a path of 1 cm and bought from Hellma (Müllheim, Germany).

4.2.4 *Elemental Analysis*

The measurements were done using as instrument a LECO CHNS-932 (St. Laurent, Quebec, Canada) that permits the simultaneous determination of carbon, hydrogen, sulfur and nitrogen content.

4.2.5 *Scanning Electron Microscopy*

The microgels topography and morphology were studied using scanning electron microscopy. The SEM is a type of electron microscope that creates the image by focusing a beam

of electrons onto the surface of a sample and detecting signals from the interaction of the incident electrons with the sample's surface. The type of signals gathered in a SEM can include secondary electrons, characteristic X-rays, and back scattered electrons. Due to the manner in which the image is created, SEM images have great depth of field yielding a characteristic three-dimensional appearance useful for understanding the surface structure of a sample. This great depth of field and the wide range of magnifications are the most familiar imaging mode for specimens in the SEM. Usually, the electron beam energy range varying from 0.5 kV to 40 kV.

The SEM microscope used is a JEOL JSM-6400 (Akishima, Tokio, Japan) working at a potential of 15 kV. The specimens were prepared by drop casting a fine dispersion of the sample solution with a concentration of 1% in weight over a conductive specimen holder of bronze alloy. Subsequently the sample was dried and covered by sputtering with a small layer of gold, using a Blazer SCD-004 in a 0.05 torr argon atmosphere and a current of 20 mA during 30 seconds.

4.2.6 *Transmission Electron Microscope*

Microgels and nanoparticles morphology as well as particle size distribution were analyzed using Transmission Electron Microscopy. In this technique the image is formed from the interaction of the electrons transmitted through an ultra thin specimen. The image is focused onto an imaging device such as a fluorescent screen or by a sensor such as a CCD camera. The voltage of the beam gun is typically in the range of 80-300 kV, and the gun will begin to emit electrons by thermionic or field electron emission. Manipulation of the electron beam is performed using typically three stages of lensing: condenser lenses, the objective lenses, and the projector lenses. Due to the manner in which the image is created, TEM permits to reach in high-resolution TEM (HR-TEM) the resolution limit of 1.7 Å (0.17 nm). The diameter size of standard TEM grid is 3.05 mm and grid materials are usually copper, nickel, gold or platinum.

The TEM microscopes used for these investigations were a JEOL (Akishima, Tokio, Japan) JEM-2100 operating at 200 kV, JEM-3100F operating at 300 kV, and a JEM-1010 with an accelerating voltage of 80 kV. The TEM grids used were copper covered with holey carbon films. The specimen was prepared by drop casting 20 μL of a well-dispersed solution on a TEM grid, and dried at room-temperature.

4.2.7 *Dynamic Light Scattering*

The molecular weight of the synthesized water-soluble conjugated polymer PTE-DMSA was calculated using the Debye plot obtained by dynamic light scattering (DLS). In addition, DLS was used to study the size distribution of CPs nanoparticles, metal nanoparticles and microgels. DLS measures Brownian motion and relates this to the size of the particles. It does this by illuminating the particles with a laser and analyzing the intensity fluctuations in the scattered light. When a solution with small particles is illuminated by a light source such as a laser, the particles will scatter the light following a precise pattern. The pattern will consist of areas of bright light and dark areas where no light is scattered. The reason about this precise pattern is that the scattered light undergoes either constructive or destructive interference by the neighboring particles. The particles are constantly moving due to the Brownian motion and the analysis of the time dependence intensity fluctuation can therefore yield the diffusion coefficient of the particles, and via the Stokes-Einstein equation, knowing the solvent viscosity, the hydrodynamic diameter of the particles can be calculated. Data are typically collected over a time range of 100ns to several seconds depending upon the particle size and solvent viscosity. Analysis of the autocorrelation function in terms of particle size distribution is done by numerically fitting the data with calculations based on assumed distributions. A truly monodisperse sample would give rise to a single exponential decay to which fitting a calculated

particle size distribution is relatively straightforward. In practice, real samples need a series of exponentials and several quite complex schemes that have been devised for the fitting process.

The DLS instrument used was a Malvern (Malvern, Worcs, UK) Zetasizer Nano S equipped with a laser of He-Ne with a wavelength of 633 nm.

4.2.8 *Elastic and Quasi-Elastic Neutron Scattering*

The study of polymer chain dynamics within the microgels was performed using elastic and quasi-elastic neutron scattering. In a neutron scattering experiment, neutrons are scattered by the atomic nuclei changing momentum and energy. The momentum transfer, $\hbar Q$, contains information about the spatial distance which is important for the scattering process, and the energy change, $\hbar\omega$, provides information about the time scale of motions in the sample. The outcome of the experiment is the scattering function $S(Q,\omega)$ that describes the probability of the momentum and energy transfer between neutron and sample. Thus, $S(Q,\omega)$ contains information about the sample structure and dynamics.

The experiments were carried out at the Institute Laue Langevin (ILL) in Grenoble, France, using the cold neutron backscattering spectrometers IN10. The analyzed neutron wavelength was kept always fixed at 6.271 Å using Si(111) crystals, while the incident neutron wavelength was set using two different monochromators. For “fixed energy window” scans centered at zero energy transfer (elastic scans) the incident wavelength was equally set to 6.271 Å by an equivalent Si(111) crystal. Thereby, an energy resolution of 1 μeV FWHM was obtained. The quasi-elastic measurements were performed by applying a Doppler shift to the incident neutrons through a movement of the monochromator.

Measurements were carried out at seven scattering vectors covering the Q range between 0.5 and 2 $Å^{-1}$ where Q is the momentum transfer defined by the equation

$$Q = {}^{4\pi}/_{\lambda}\ \sin\theta \qquad [5]$$

being 2θ the scattering angle. Quasi-elastic spectra were recorded at 290 K and 327 K for every Q. The geometry of the sample holder was double wall hollow cylinder which was sealed to avoid D_2O evaporation during the measurements. The thickness and concentration of the sample was selected to yield a transmission of about 85%. Standard ILL procedures and programs were used for corrections (empty cell), normalization and quasi-elastic peak fit.

For the analysis of data the incoherent scattering function can be written as:

$$S_{inc}\,(Q,\omega) = \exp\left(-\langle u^2\rangle\ {}^{Q^2}/_{3}\right)\delta\omega \otimes \frac{1}{\pi}\,\frac{DQ^2}{(DQ^2)^2+\omega^2} \qquad [6]$$

where $\otimes$ is the convolution product in ω, the displacement mean square amplitude is $\langle u^2\rangle^{1/2}$, and D is the diffusion constant. From the fitting of the quasi-elastic component, measured at different Q, with a Lorentzian function, we obtain the full-width at half-maximum (FWHM), $\Gamma(Q) = DQ^2$, for the collapsed and swollen microgels y subsequently we derived the diffusion coefficient of the polymer chain segments.

4.2.9 *X-Ray Fluorescence Spectroscopy*

X-Ray Fluorescence (XRF) spectroscopy is a non destructive technique used to determine the chemical composition of gas, liquid, or solid samples. The material is excited by bombarding with high-energy X-Ray and the detector measures the characteristic emission of radiation from the material. When the sample material is exposed to this high-energy X-Ray the electrons in the

inner sphere (lower orbital) of the atom can be removed making the electronic structure of the atom unstable. The instability provokes that the electrons from the outer shell (higher orbital) fall into the lower orbital occupying the hole left behind. During this falling the energy is released in the form of a photon and the energy is equal to the energy difference of the two orbitals involved. Thus, the material emits radiation, which has energy characteristic of the atoms present.

The XRF measurements was carried out on an automated AXIOS (PANalytical, Almelo, The Netherlands) X-ray fluorescence spectrometer equipped with an Rh X-ray tube, and 4 kW generator.

4.2.10 *Thermogravimetric Analysis*

The thermogravimetric analysis (TGA) is a technique that permits to determine the decomposition temperature of an organic material and in case of hybrid materials TGA can be used to determine the organic/inorganic ratio inside the material. TGA can be performed either in oxygen or inert atmosphere like nitrogen. The sample is placed in a small electrically heated oven with a thermocouple to accurately measure the temperature and a quartz crystal microbalance measures the weight variations.

The TGA instrument used was a Mettler-Toledo (L'Hospitalet de Llobregat, Barcelona, Spain) TGA/DSC 1 Star System equipped with a Mettler-Toledo ultra microbalance.

4.3 *Material Synthesis*

2-(3-thienyl)-ethyl-acetate (1)

In a 100 mL three neck round bottom flask are placed 5 mL of 2-(3-thienyl) ethanol (45 mmol), 30 mL of dry $CHCl_3$, 9.8 mL of dry tri-ethylamine (70 mmol) and 5 mL of CH_3COCl (70 mmol). The reaction is stirred at 20 °C for 12 hours, and then the solution is washed (2 x 30 mL) with deionised water saturated with $NaHCO_3$. The crude oil is passed through a silica column using as eluent EtOAc/hexane (respectively 2/8), giving the product **1** as yellow pale oil with a yield of 85%. Rf = 0.65 EtOAc/Hexane (3/7).

^{1}H-NRM ($CDCl_3$) δ: 2.08 (s, 3H), 3.00 (t, 2H, J = 5.8 Hz), 4.30 (t, 2H, J = 5.8 Hz), 7.01 (dd, 1H, J_{1-2} = 4.9 Hz, J_{1-3} = 1.5 Hz), 7.06 (dd, 1H, J_{1-2} = 4.6 Hz, J_{1-3} = 1.7 Hz), 7.31 (dd, 1H, J_{1-2} = 4.9 Hz, J_{1-3} = 1.9 Hz).

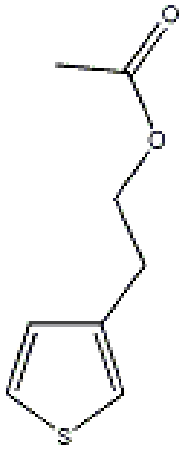

4. *Materials and Methods*

Poly(3-ethyl-acetate-thiophene-2,5-diyl) PTEAc (2)

200 mg of **1** (1.2 mmol) are placed in a 100 mL three neck round bottom flask with 10 mL of dry $CHCl_3$, 780 mg of $FeCl_3$ (4.8 mmol) are dissolved in 40 mL of dry $CHCl_3$ and added with a dropping funnel over a period of 30 minutes under nitrogen flow. The reaction is stirred at 20 °C and stopped after 24 hours. The solution was filtered and the excess of $FeCl_3$ was removed by Soxhlet extraction procedure using methanol as solvent. The polymer was dried under vacuum to afford 85 mg of **2** (yield 42%) as reddish-brown powder.

^{1}H-NRM ($CDCl_3$) δ: 2.10 (s, 3H), 3.00 (t, 2H, J = 5.9 Hz), 4.35 (t, 2H, J = 5.5 Hz), 7.11 (s, 1H).

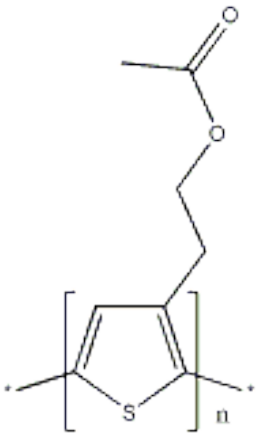

Poly(3-ethanol-thiophene-2,5-diyl) PTEOH (3)

85 mg of **2** (0.5 mmol of repeat units) are placed in a 100 mL three neck round bottom flask with 50 mL of THF and the solution is refluxed. After 10 minutes, 20 mL of a 0.1 M KOH solution in methanol was added under stirring to the flask. The mixture was refluxed at 70 °C for 6 hours. Subsequently, the reaction mixture was neutralized with 0.1 M HCl and poured into 250 mL methanol. The very fine dark brown powder thus obtained was collected by centrifugation, washed first with water and then with methanol. The obtained polymer **3** was dried under vacuum giving 43 mg of PTEOH, with a yield of 50%.

^{1}H NRM ($CDCl_3$) δ: 2.08 (br, 1H), 2.74 (br, 2H), 3.60 (br, 2H), 7.10 (br, 1H).

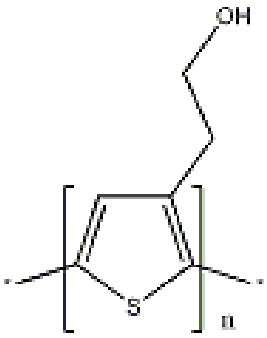

4. *Materials and Methods*

Poly(3-ethoxy-thiophene-2,5-diyl-p-toluenesulfonate) PTETS (4)

42 mg of **3** (0.3 mmol of repeat units) are placed in a 100 mL three neck round bottom flask with 50 mL of dry $CHCl_3$ and cooled to 0 °C; 0.2 mL of dry tri-ethylamine (1.4 mmol) and 270 mg of p-toluenesulfonyl chloride (1.4 mmol) are added to the solution. After 24 hours the reaction is quenched by adding water. The organic layer was washed with 1 M HCl (2x40 mL), sat. $NaHCO_3$ (aq. 2x40 mL), and H_2O (2x40 mL). The organic phase is dried with anhydrous Mg_2SO_4, filtered, and the solvent is removed by reduced pressure giving 41 mg of **4** as an orange-yellow solid (yield 48%).

^{1}H NRM ($CDCl_3$) δ: 2.46 (br, 3H), 3.01 (br, 2H), 4.07 (br, 2H), 7.08 (br, 1H), 7.32 (d, 2H, J = 7.5 Hz), 7.72 (d, 2H, J = 7.5 Hz).

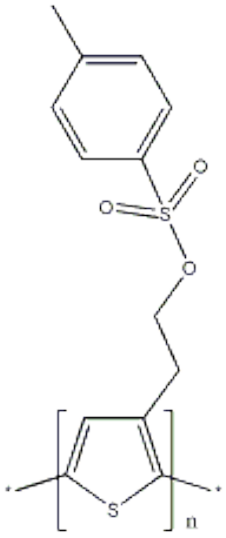

Poly(3-ethoxy-thiophene-2,5-diyl-dimercaptosuccinic-acid) PTE-DMSA (5)

41 mg of **4** (0.14 mmol of repeat units) are placed in a 100 mL three neck round bottom flask with 50 mL of dry DMF, 98 mg of K_2CO_3 (0.7 mmol), and 55 mg of 2,3-meso dimercaptosuccinic acid (0.3 mmol), and the solution is heated to 35 °C. After 30 hours, 20 mL of H_2O are added to quench the reaction. The solution was diluted with acetone (25 mL), and concentrated HCl was added dropwise until the polymer precipitated. After 1 hour the mixture was centrifuged (20 min at 2500 rpm) and the yellow precipitate was washed with acetone twice, and then dissolved in NaOH 2 M (40 mL) and precipitated again adding acetone, filtered and vacuum dried to obtain 20 mg of **5** (yield 50%).

^{1}H NRM (D_2O) δ: 3.00 (br, 2H), 3.44 (br, 1H), 3.50 (br, 1H), 4.32 (br, 2H), 7.1 (s, 1H).

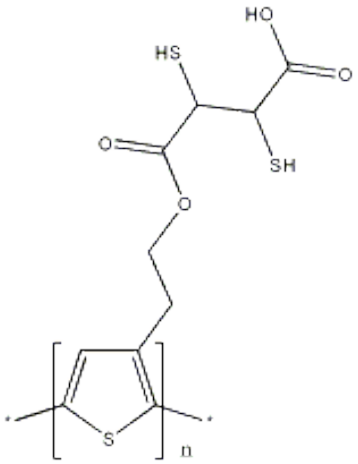

4. *Materials and Methods*

Synthesis of the PNIPAM-PTEBS Microgels

PNIPAM interpenetrated microgels were synthesized using the free surfactant polymerization method[35,41,104] of an aqueous solution (50 mL) of NIPAM (0.1 M), PTEBS ($4.3x10^{-4}$ M, in monomer repetitive units), and cross-linker BA. The cross-linking content, given as [BA(g)]/[NIPAM(g)+BA(g)]x100, was varied between 2.5 and 10% in order to obtain microgels with different swelling properties. During the preparation of the microgels, it is extremely important to dissolve perfectly the photoluminescent polymer. Due to the low solubility of PTEBS, this was obtained at polymer concentrations between 10^{-4} and 10^{-5} M. At higher concentrations, the polymer aggregates, hampering to obtain monodisperse microgels due to the formation of PNIPAM coagulum. The solution was heated up under N_2 atmosphere, and when the temperature reached 70 °C, the polymerization was started by adding 250 mg of ammonium persulfate. The mixture was refluxed for 4 hours in N_2 atmosphere, and, subsequently, the microgels were filtered and dialyzed against distilled water for 2 days. Finally, the microgels were centrifuged at 15000 rpm, redispersed in water several times, freeze-dried, and stored at room temperature.

Synthesis of the Polyacrylamide Microgels

Polyacrylamide microparticles with BA as a cross-linker and HRP entrapped (HRP-PAA) were prepared using the concentrated emulsion polymerization method.[48,105] The cross-linking degree, η, given as the ratio between the cross-linker weight and the monomer, was 8%. The concentrated emulsion was prepared with 16.67% of the oil phase (the continuous phase) and 83.33% of the aqueous phase (dispersed phase). To obtain the W/O concentrated emulsion, 5 mL of an aqueous solution, consisting of 1.25 g of acrylamide, 100 mg of BA, 9 mg of ammonium

[104] M. J. Snowden, and B. Z. Chowdhry, *Chem. Br.*, **1995**, *31*, 943.
[105] M. I. Gonzalez-Sanchez, J. Rubio-Retama, E. Lopez-Cabarcos, and E. Valero, *E. Biosen. Bioelectron.*, **2011**, *26*, 1883.

persulfate, and 1.4 mg of HRP, was added by dropwise addition using a syringe until the continuous oil phase (750 μL of dodecane and 250 μL Span 80). The emulsion was homogenized by magnetic stirring and purged with N_2 to remove residual oxygen. Polymerization was started by adding 63 μL of TEMED to the emulsion. Polymerization of the gel-like emulsion produced entrapped enzyme microgels. During polymerization, the temperature was controlled and kept below 35 °C to maintain enzyme activity and to avoid protein denaturation. After 1 hour microgel particles were precipitated and washed several times with phosphate buffer at pH 7 until no enzymatic activity was detected in the supernatant. Subsequently, they were isolated by centrifugation at 10000 rpm for 10 minutes at 8 °C and freeze-dried. This protocol generated PAA microparticles with diameters of between 1 and 32 μm.

Synthesis of the Magnetic Nanoparticles

Two synthesis methods have been used for the fabrication of magnetic nanoparticles: thermal decomposition of Fe(III) acetylacetonate and a coprecipitation of $FeCl_2$ and $FeCl_3$ in a stochiometric ratio.

Method I Thermal Decomposition

In this case the synthesis of the magnetic nanoparticles was a modification of a previously described method.[106,107] For the synthesis of 13 nm edge length particles, 353 mg (1 mmol) of Fe(III) acetylacetonate were mixed with 688 mg (4 mmol) of 10-undecenoic acid in 25 mL of dibenzyl-ether. After one hour under vacuum in a Schlenk line, the solution was heated up to 200 °C with a constant heating rate of 6-7 °C/min under an argon blanket flow and vigorous stirring. After 2 hours at 200 °C, the solution was heated up to reflux with a constant heating rate of 5.2 °C/min and kept at this temperature for 1 hour. After cooling to room temperature, a

[106] P. Guardia, N. Pérez, A. Labarta, and X. Batlle, *Langmuir*, **2010,** 26, 5843.
[107] P. Guardia, J. Pérez-Juste, A. Labarta, X. Batlle, and L. M. Liz-Marzán, *Chem.Commun.*, **2010**, *46*, 6108.

mixture of toluene and acetone was added to the solution and then centrifuged to precipitate. The precipitate was washed several times with a mixture of toluene and acetone. Finally, the particles were stored in ethanol.

Method II Fe^{+3} and Fe^{+2} Coprecipitation

The particles are synthesized using a modified coprecipitation recipe reported previously.[108] Tetramethyl-ammonium-oxide (TMAOH) is used as alkaline molecule instead of sodium hydroxide. 25 mL of TMAOH 1M and 22 mL of H_2O are mixed under mechanic stirring at 70 °C. After that, a solution containing 3 mL of water, $FeCl_3$ 650 mg and $FeCl_2$ 250 mg is added drop wise. The stirring stands for 30 minutes. After this time the nanoparticles are recover by magnetic decantation and washed several times with distilled water.

Surface Modification of the Magnetic Nanoparticles

The modification of the magnetic nanoparticles was carried out as follows. In a vial of 15 mL, 350 μL of magnetic nanoparticles were diluted in 10 mL of water and sonicated during 15 minutes to reduce the particle aggregation subsequently, the vial was immersed in a water bath at 70 °C and different amounts of 3-butenoic acid (3-bt) were added. This solution was stood for 1 hour at these conditions and then the nanoparticles were centrifuged to remove the 3-bt acid excess at 4000 rpm during 30 minutes. With the aim of reducing the aggregation effects during the centrifugation, 200 μL of CTAB 0.2M were added before starting the centrifugation. After that, the supernatant was discarded and the precipitate was diluted to 10 mL with water and redispersed by sonication during 15 minutes.

Synthesis of Thermoresponsive Microgels with Magnetic Cores

The previous solution was put into a three neck round bottom flask and heated up to 70 °C, under mechanical stirring (350 rpm) and N_2 atmosphere. Subsequently, 226 mg of NIPAM

[108] R. Massart, *IEEE Trans Magn.*, **1981**, *17*, 1247.

and 31 mg of BA were added to the magnetic nanoparticles dispersion. The mixture was stirred during 15 minutes and the polymerization was initiated by adding 100 μL of 2,2′-azobis(2-methylpropionamidine) dihydrochloride 0.1 M, the N_2 flow was removed and the polymerization was kept for 2 hours. Finally, the milk like dispersion was cooled down and the magnetic microgels were collected by placing the reaction flask on a neodymium magnet of 0.6 T during 24 hours. A brown precipitate appears on the bottom of the flask, which was collected and re-dispersed in 10 mL of water.

Synthesis of Gold Nanostructures with PTEBS

In a typical experiment, 1 mL of PTEBS, 1 mM, is diluted with Millipore water to 9.8 mL and sonicated for 1 minute. Subsequently, 186 μL of $HAuCl_4$, 26 mM, is added to the solution and stirred for 1 minute. After 2 hours at room temperature, the reaction is stopped by centrifugation at 4000 rpm and the precipitated solid is redispersed with 10 mL of Millipore water.

Synthesis of Gold Nanostructures with PTEBS and $Cd(CH_3COO)_2$ or $Pb(NO_3)_2$

In a typical experiment, 1 mL of PTEBS 1 mM, is diluted with Millipore water to 9.5 mL, then added 300 μL of $Cd(CH_3COO)_2$ 26 mM, and sonicated for 1 minute. After that, 186 μL of $HAuCl_4$, 26 mM, is added to the solution and stirred for 1 minute. After 3 days at room temperature, the reaction is stopped by centrifugation at 4000 rpm and the precipitated solid is redispersed with 10 mL of Millipore water.

4. *Materials and Methods*

Synthesis of Gold Nanostructures with PTEBS, $Cd(CH_3COO)_2$, and $Pb(NO_3)_2$

In a typical experiment, 1 mL of PTEBS with a molar concentration of 1 mM is diluted with Millipore water to 9.5 mL, then added 300 μL of $Cd(CH_3COO)_2$ 26 mM, 300 μL of $Pb(NO_3)_2$ and sonicated for 1 minute. Subsequently, 186 μL of $HAuCl_4$, 26 mM, is added to the solution and stirred for 1 minute. After 3 days at room temperature, the reaction is stopped by centrifugation at 4000 rpm and the precipitated solid is redispersed with 10 mL of Millipore water.

Synthesis of N-Alkylammonium Chloride Surfactants

Surfactants N-dodecylammonium chloride (C12), N-decylammonium chloride (C10), N-nonylammonium chloride (C9), and N-octylammonium chloride (C8) were synthesized by bubbling gaseous hydrogen chloride through a solution of the corresponding N-alkylamine in diethyl ether. In a typical reaction at room temperature, 10 ml of N-octylamine (0.06 mol) was diluted in 20 mL of diethyl ether. H_2SO_4 98% solution was dropped over an HCl solution generating gaseous hydrogen chloride and by nitrogen flow purged in the solution containing the N-octylamine. The solution changes from transparent to turbid and the final white precipitate was filtered and washed several times with diethyl ether in order to eliminate the N-alkylamine excess. Subsequently, the surfactant was recrystallized dissolving the surfactant in a mixed solvents solution of acetone/ethanol (respectively 1/1) inducing the precipitation by adding diethyl ether.[109] Finally they were vacuum-dried overnight and stored.

[109] A. Terreros, P. Galera Gomez, and E. López-Cabarcos, *Prog. Colloid Polym. Sci.*, **2000**, *115*, 50.


H
Cl
N+
H

5. *Results and Discussions*

5.1 *Water-Soluble Conjugated Polymers Fluorescence Enhancement by the Addition of Surfactants: Influence of the Surfactant Chain Length.*

5.1.1 *Introduction*

Water-soluble conjugated polymers provide a new environment to investigate the properties of π-conjugated polymers that can lead to deeper understanding of the luminescence in these systems and to theoretical descriptions of charge-transfer reactions. Fluorescence methods are highly sensitive, easy to operate, and provide a tool to investigate how the electronic states of the luminescent polyelectrolyte are affected by the geometrical changes of the solvated photoluminescent polymer. For these reasons we decided to take as model polymer the water-soluble PTEBS to study the factors able to change its emission.

PL enhancement of CPs due to the presence of surfactant is called surfactochromicity. This phenomenon was described by Haamed and co-workers[110] as a set of actions which could be summarized as follows. First, the surfactant induces the disruption of the polymer aggregates, reducing interchain quenching and increasing the PL and the quantum yield.[111] Second, the surfactant provokes changes in the polymer structure conformation,[112] extending the effective electron delocalization, which leads to red spectral shifts of the absorption and emission maxima. This effect increases the PL quantum efficiency by inhibiting the folding of the polymer chains, with the subsequent reduction of conformational disorder and of the number of defects acting as trapping and nonradiative recombination sites. Finally, the incorporation of polymer chains into micelles reduces the fluorescence quenching by water preventing

[110] A. Haamed, A.Attar, and A. Monkman, *J. Phys. Chem. B*, **2007**, *111*, 12418.
[111] M. Yan, L. Rothberg, E. Kwock, and T. Millar, *Phys. Rev. Lett*., **1995**, *75*, 1992.
[112] L. Chen, S. Xu, D. McBranch, and D. Whitten, *J. Am. Chem. Soc*., **2000**, *122*, 9303.

nonradiative processes.[113] The investigation of the influence of the cationic surfactant chain length on the PL of PTEBS might help to better understand the interaction between water-soluble CP and cationic surfactants with different chain length.

5.1.2 *Results*

As can be observed in Figure 29 PTEBS is a conjugated polymer with a sulfonate group on the lateral side chain to confer water solubility. This negative charge and the presence of oxygen permit to dissolve the hydrophobic thiophene backbone in water due to the formation of hydrogen bonds with molecules of water.

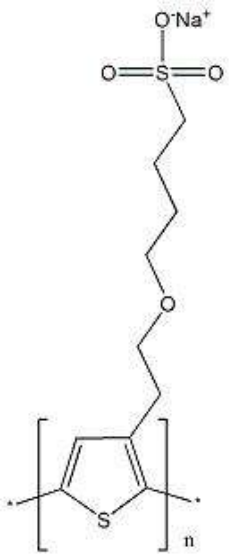

Figure 29. Chemical structure of the model conjugated polymer PTEBS.

In Figure 30 is shown the generic structure of the N-alkylammonium surfactants chloride and they were synthesized by bubbling gaseous hydrogen chloride through a solution of the N-alkylamine in diethyl ether.[109]

[113] A. Chakrabarty, P. Das, A. Mallick, and N. Chattopadhyahy, *J. Phys. Chem. B*, **2008**, *112*, 3684.

5. *Results and Discussions*

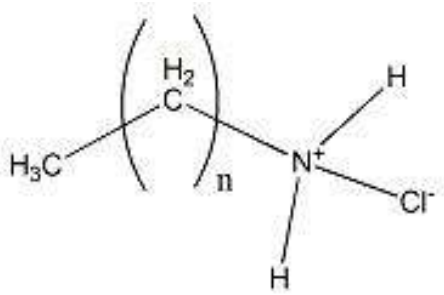

Where n= 7,8,9,11

Figure 30. Schematic chemical structure of the N-alkylammonium surfactants used in the investigation. The n represents the number of carbon atoms.

Once obtained the cationic surfactants, aqueous PTEBS solution with a concentration of 1.8×10^{-5} M was prepared dissolving the polymer in MilliQ water. The polymer concentration is expressed in monomer repeating units.

The first experiment has been the determination of the size of polymer clusters and the polymer-surfactant clusters that was derived from the intensity correlation function measured with DLS, and is shown in Figure 31 as a function of the surfactant concentration: C8 (upper panel left), C9 (upper panel right), C10 (bottom panel left), and C12 (bottom panel right). In aqueous solution, the water-soluble CP PTEBS tend to form aggregates because of the inherent hydrophobicity of the thiophene moieties, which establish π–π and van der Waals interactions with other thiophene groups. The resulting polymer particles have hydrophilic groups in the outer part, whereas the hydrophobic thiophene groups are buried in the inner part of the particle.[29]

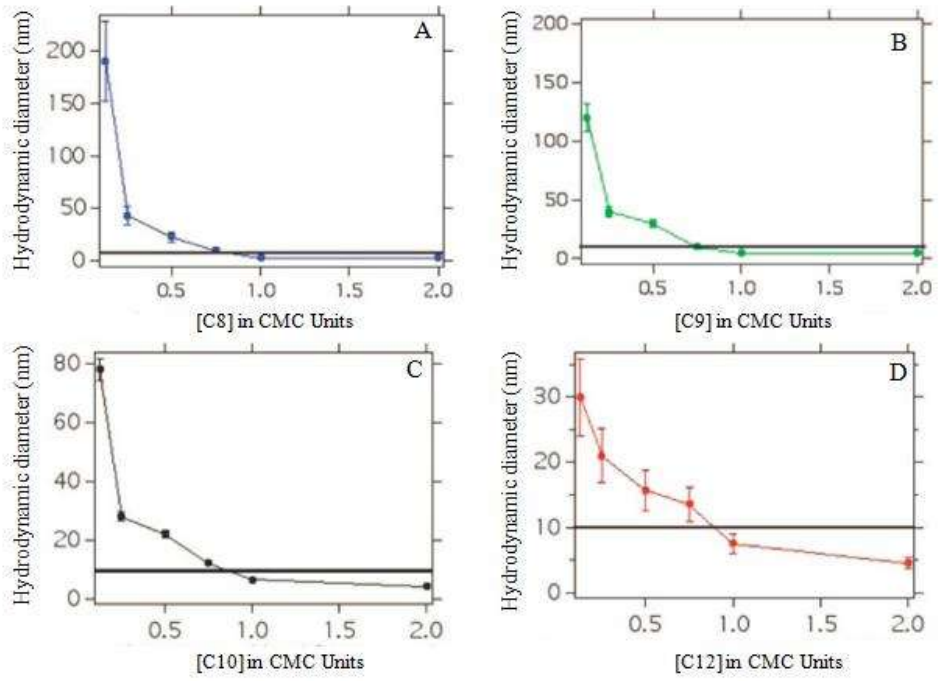

Figure 31. DLS measurements of PTE-BS solutions in the presence of surfactant at different ratios of the CMC: (A) N-octylammonium chloride (C8), (B) N-nonylammonium chloride (C9), (C) N-decylammonium chloride (C10), and (D) N-dodecylammonium chloride (C12). The continuous line in each panel represents the cluster size of the PTEBS in pure water.

As can be seen in Figure 31, the addition of surfactant produces a dual effect on the size of the polymer cluster. Independently of the surfactant chain length, at a low concentration of surfactant (0.125 and 0.25 times the CMC), the polymer aggregates with the surfactant, forming particles with a diameter much greater than 10 nm, which is the size for the PTEBS particles in pure water. This fact indicates that the increment in the hydrodynamic diameter should be due to polymer aggregation rather than to a change from coil to rod. Furthermore, it is also shown that the ability of coagulation depends on the surfactant chain length and this effect is less pronounced for the surfactant with the longest chain. This result could indicate that at low surfactant concentration the ammonium polar head-group interacts with the sulfonate side chain of the polymer through columbic interactions, rendering a polymer-surfactant complex

with low colloidal stability that tends to coagulate.[114] However, as the surfactant concentration is increased, the size of the aggregates sharply decreases leveling at an average diameter close to 5 nm. This result indicates that at surfactant concentrations above 0.5 CMC the polymer cluster breaks up into smaller particles. The reduction in the size of the polymer-surfactant cluster above the CMC with respect to the pure polymer would indicate that for these concentrations the polyelectrolyte charges are effectively screened by the surfactant polar head-groups which lead to the collapse of the polymer particle.

The formation of the polymer-surfactant complex could modify the absorption and emission spectra in a way that depends on the surfactant chain length. As shown in Figure 32, the addition of the cationic surfactant C8 with concentration of 0.125 CMC provokes an abrupt decrease in the PL intensity.

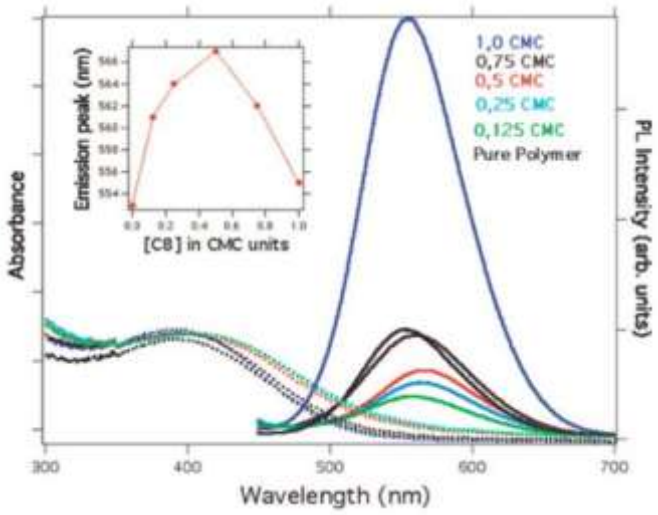

Figure 32. Absorption (dashed line) and emission (continuous line) spectra of PTEBS using different concentrations of C8. The inset shows the shift of the PL maximum (red-shift up to 0.5 CMC followed by a blue-shift at higher surfactant concentrations) as a function of C8 concentration (in CMC units). The excitation wavelength was 425 nm.

[114] W. MacKnight, E. Ponomarenko, G. Leising, and D. Tirrell, *Acc. Chem. Res.*, **1998**, *31*, 781.

This quenching of the PL emission as well as the red-shift at low surfactant concentrations are attributed to the aggregation of the polymer, which increases the π–π interaction between neighbor thiophene rings, inducing interchain excitation quenching. Nevertheless, further increments in the surfactant concentration enhance the PL emission. Such effect is attributed to the rupture of the polymer aggregates with the subsequent reduction of the interchain excitation quenching. These results are in agreement with the variations observed in the hydrodynamic diameter of the polymer-surfactant cluster, which became smaller when the surfactant concentration increased. Furthermore, at low concentration of surfactant, one can observe a red-shift of the PL emission (see inset in Figure 32) that can be explained by the surfactant aggregation effect on the PTEBS. However, further increments in the surfactant concentration break up the polymer cluster (see A panel in Figure 31), shifting the emission peak further to the red. This behavior could be attributed to the transition from coil to rod[115] in the polymer induced by the surfactant that would increase the polymer conjugation.[110,116] This explanation assumes the competition between two effects: the extension of the polymer chain and the breaking up of the polymer cluster, with the polymer chain extension being the dominant effect at premicellar concentrations. Thus, when the surfactant concentration increases, the red-shift reaches a maximum at 0.5 CMC and further increments in the surfactant concentration provoke a blue-shift that can be attributed either to the breaking up of the polymer-surfactant complex or to the enhancement of the hydrophobicity of the media.

A similar behavior to that reported for C8 was observed after the addition of C9, as shown in Figure 33. Nevertheless, in this case, the quenching of the PL disappeared upon addition of the surfactant at concentrations above 0.25 CMC.

[115] M. Knaapila, A. Laszlo, V. Garamus, C. Pearson, S. Pradhan, M. Petty, U. Scherf, H. Burrows, and A. Monkman, *J. Phys. Chem B*, **2006**, *110*, 10248.
[116] A. Najari, H. A. Hoang, J. F. Gravel, P. Nobert, D. Boudreau, and M. Leclerc, *Anal. Chem.*, **2006**, *78*, 7896.

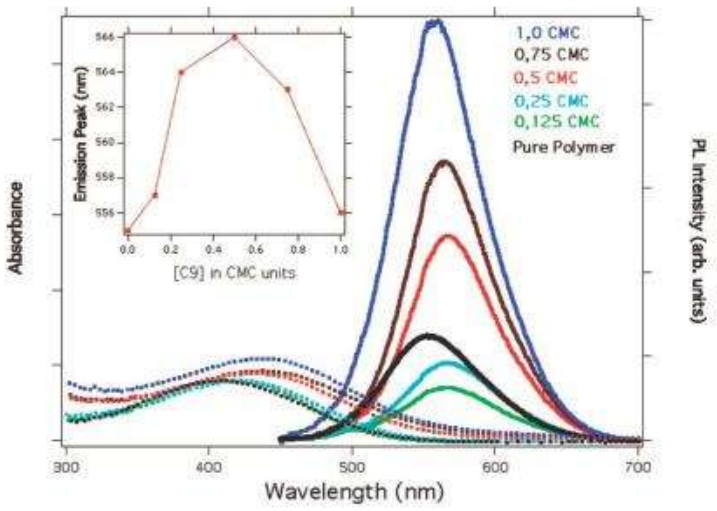

Figure 33. Absorption (dashed line) and emission (continuous line) spectra of PTEBS in using different concentrations of C9. In the fluorescence measurements, the excitation wavelength was 425 nm. The inset shows the shift of the PL peak as a function of C9 concentration (in CMC units).

The sequence of processes described above (aggregation, extension, breaking up, and environmental polarity reduction) is summarized in Scheme 2, which depicts the proposed model for the polymer surfactant complex at different concentrations of C8 and C9. As is illustrated in Scheme 2, the initial addition of surfactant induces the aggregation of the photoluminescent polymer, leading to the formation of a polymer cluster with low, and red-shifted, PL emission. Further increments in the surfactant concentration induce the breaking up of the polymer cluster and the extension of the polymer chain, enhancing the PL emission. Finally, at the CMC, the polymer clusters are completely disaggregated, yielding the minimum surfactant-polymer cluster size with the maximum PL emission.

Scheme 2. Proposed Model for the Interaction between PTE-BS and Surfactant at Different C8 and C9 Concentrations.

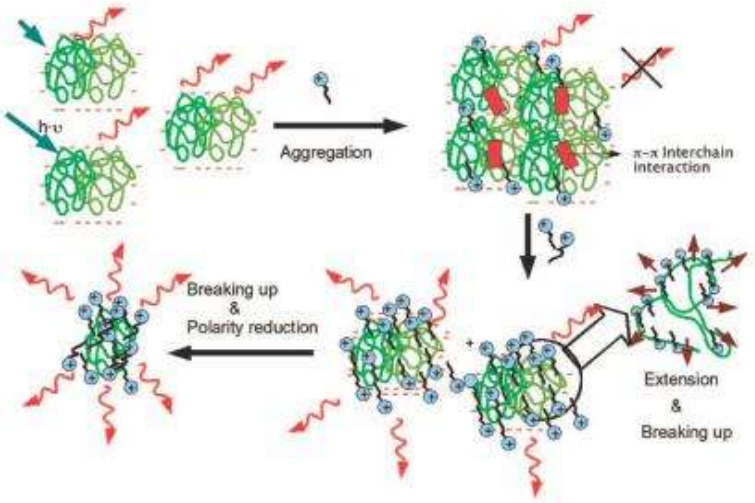

As can be seen in Figure 34, the situation is different in the case of the surfactant C10. At low concentration of C10 (0.125 CMC), the intensity increases instead of being quenched as it was in the case of C8 and C9 (Figure 32 and 33).

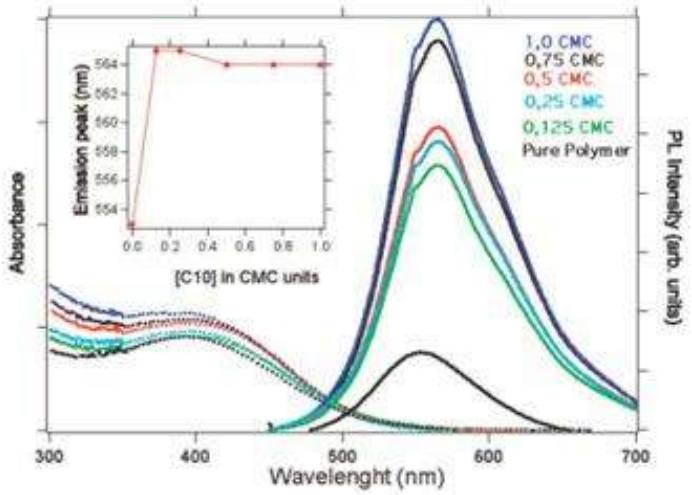

Figure 34. Absorption (dashed line) and emission (continuous line) spectra of PTEBS using different concentrations of C10. The excitation wavelength was 425 nm.

A similar behavior was also obtained for C12 (Figure 35), the polymer-surfactant solution with lowest concentration of surfactant presents an enhancement in the fluorescence emission.

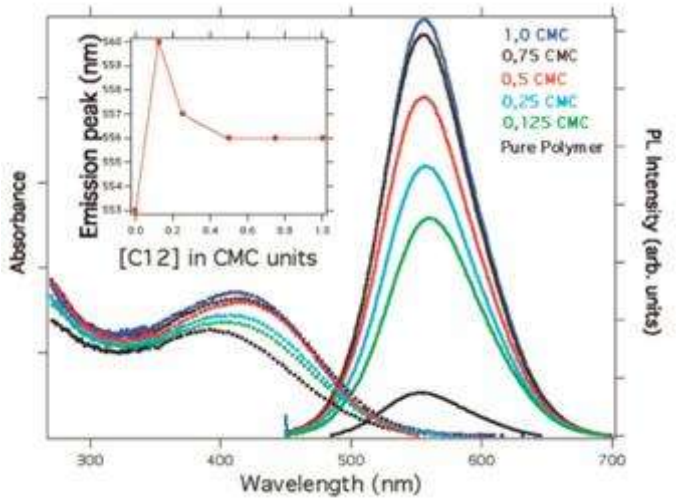

Figure 35. Absorption (dashed line) and emission (continuous line) spectra of PTEBS in the presence of different concentrations of C12. The excitation wavelength was 425 nm.

The PL red-shift is a common aggregation effect that was observed for all the surfactants investigated. Furthermore, the aggregation was confirmed by the large values of the hydrodynamic radius obtained in these systems. However, as is shown in Figure 36, at low surfactant concentrations, the behavior of the PL intensity depends on the surfactant chain length: for C8 and C9, the PL intensity decreases with respect to the PL of the pure polymer, while for C10 and C12 the PL increases.

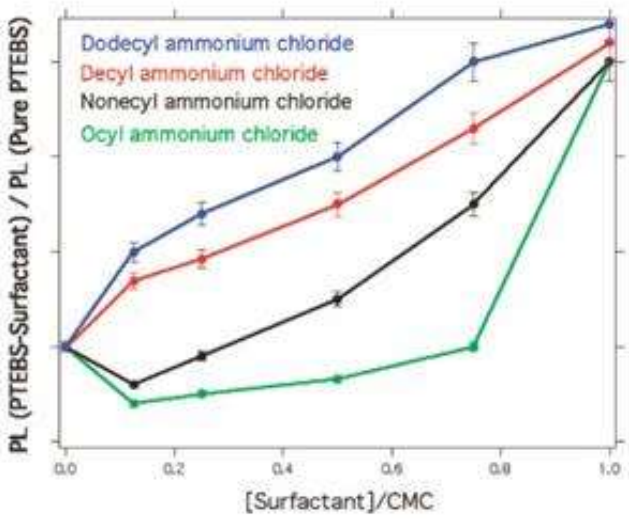

Figure 36. PL emission as a function of the ratio of the CMC for surfactants with different chain length.

The influence of the ionic strength of the solution on the PL of PTEBS has been previously reported and it was found that the PL decreases with increasing the ionic strength.[117] This effect was attributed to the lower solubility of the polymer at high ionic strengths due to the screening effect of cations on the polyelectrolyte charged groups. Thus, the decrease of the PL intensity, with respect to the pure polymer, observed at low concentrations of C8 and C9 can be attributed to a screening effect that favors the aggregation. However, there is a threshold in the surfactant carbon chain length (around 10 carbons) for which the screening effect of the head-group charge is overcome by the hydrophobic interactions between the surfactant tails that favor the formation of polymer-surfactant-like micelle structures that are thermodynamically stable. When the chain length increases, the aggregation capacity of the surfactants is less pronounced and the formation of hydrophobic domains reduces the number of the $\pi-\pi$ interchain interactions accounting for the quenching of the PL emission. Nevertheless, the size difference between the aggregates formed by C9 and C10 at 0.125 CMC

[117] E. López-Cabarcos, and S. Carter, *Macromolecules*, **2005**, *38*, 10537.

(120 and 80 nm respectively) would not fully justify the opposite effect on the PL intensity induced by both surfactants and points to an additional effect.

We can estimate the maximum length (nm) of a fully extended hydrocarbon chain from

$$l_c = 0.15 + 0.27n_c \qquad [7]$$

where n_c is the total number of carbon atoms per chain, 0.15 is the van der Waals radius (in nm) of the terminal methyl group, and 0.127 is the carbon-carbon bond length (in nm) projected onto the direction of the chain in the all-trans configuration.[118] Using this equation, we obtained the l_c value of 1.29 nm for C9 and 1.42 nm for C10. It seems that this small difference of chain length between C9 and C10 can reduce the polymer interchain charge transfer by a steric hindrance, inhibiting the self-polymer quenching and thus increasing PL intensity.

Scheme 3 depicts the proposed model showing the different effects on the interchain interaction upon addition of the surfactants with the shortest and the longest tails at different concentrations.

Scheme 3. Proposed Model for the Interaction between the PTE-BS and the Surfactant with Different Chain Lengths at the Premicellar and Micellar Regimes

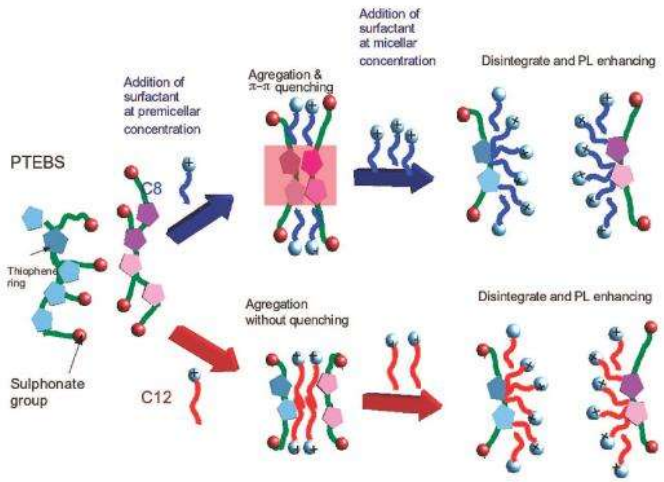

[118] "*The Colloidal Domain*" 1st Ed., F. D. Evans, and H. Wennerström, VHC Publishers Inc., New York, **1994**.

Scheme 3 shows that at premicellar concentrations both surfactants can screen the charge of the sulfonate groups inducing the aggregation of the polymer. However, the main difference between both surfactants is that C12 could be intercalated between two thiophene moieties and C8 could not. Hence, C12 could hinder the interchain charge transfer or π–π interactions, reducing the polymer quenching. By contrast, in the presence of C8, the polymer interchain interactions favor the formation of structures that compete with the light emission processes. Furthermore, the PL emission at 0.125 CMC for C10 and C12 surfactants is almost double the PL emission of the pure polymer. This result indicates that these surfactants not only prevent the formation of polymer interchain interactions during aggregation but also play a role in extending the polymer chain. The accommodation of the large hydrocarbon chains of the surfactant in the hydrophobic polymer regions could reduce the number of defects and the π–π interactions that compete with the radiative emission processes.

Time-resolved fluorescence measurements were carried out to further check the above hypothesis and to find out whether the chain length is a crucial parameter to understand the PL of the π-conjugated polyelectrolytes in the surfactant solutions. Figure 37 shows the PL intensity decay profiles for the pure polymer and the polymer-surfactant solutions. For fitting the decay-time profiles, two exponential decay functions were necessary to describe the experimental data fit (χ^2 between 1.1 and 1.3, residuals < 2.5%, and DW > 1.7) for all samples.

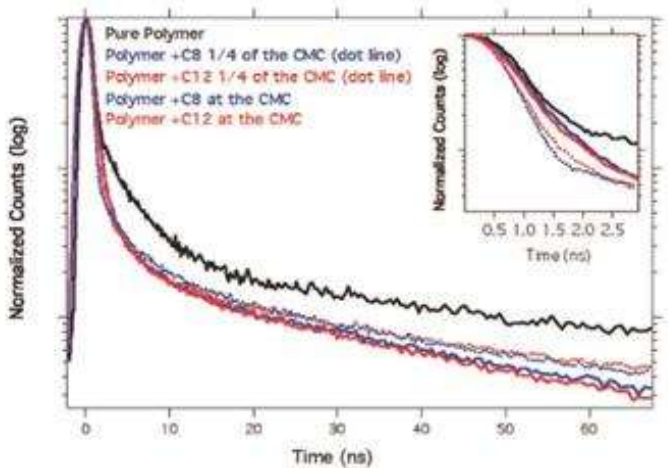

Figure 37. Selected intensity decay-time profile of pure PTEBS (1.8×10^{-5} M) in water (black line) and PTEBS surfactant complexes at different concentrations of C8 and C12. The inset shows the initial decay profile. λ_{exc} = 460 nm.

This indicates that early fluorescence decay is dominated by a double exponential component. Thus, the intensity represented in Figure 37 is assumed to decay as the sum of individual exponential decays

$$I(t) = \sum_{i=1}^{2} A_i e^{(-t/\tau_i)} \qquad [8]$$

where *I(t)* is the intensity, A_i represents the amplitude of the components at t = 0, and τ_i is the decay time of component *i*.[119]

Fluorescence lifetime measurements in polyelectrolytes are the result of a complex distribution of the decay times in the system. In order to get the lifetime distribution as well as the fractional contribution of each component to the steady state photoluminescence intensity,[120] the data were analyzed using the multiexponential method. The decay times obtained for pure PTEBS in water of 2.65 ± 0.08 ns and 0.78 ± 0.02 ns. The addition of surfactant changes this scenario in such a way that, at the lowest concentration of C8, when the polymer is

[119] J. R. Lakowicz, "Principles of Fluorescence Spectroscopy" 2nd Ed., Plenum Publishers, New York, **1999**.
[120] A. Siemiarczuk, B. Wagner, and W. Ware, *Phys. Chem. Lett.*, **1990**, *94*, 1661.

aggregated, both decay times became larger: 10 ± 0.3 ns and 1.8 ± 0.04 ns, respectively. A similar behavior was observed upon addition of C12, for which values of 10 ± 0.3 ns and 0.9 ± 0.02 ns were obtained. Figure 38 shows the smaller decay time and its percentage contribution to the steady state intensity as a function of the surfactant concentration for C8 and C12.

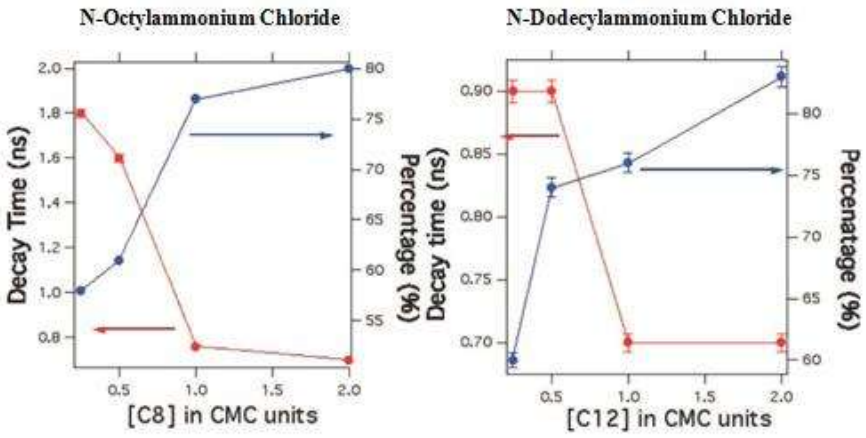

Figure 38. Slower fluorescence decay time of PTEBS and percentage contribution to the steady state intensity as a function of the surfactant concentration: (a) PTEBS and C8 complex and (b) PTEBS and C12 complex.

The smaller decay times increase its relative contribution to the steady state intensity upon increasing the surfactant concentration. Figure 38 shows that the smaller lifetimes fell down from 1.8 to 0.76 ns after increasing the concentration of C8, and from 0.9 to 0.76 ns in the case of addition of C12. According to our model, this lifetime decrease would be related to the reduction of the polarity of the polymer environment, due to the increase of water screening as the surfactant concentration is increased.[121] It is interesting to note that the relative contribution of the slower lifetime increases abruptly in both samples from 55% to 80%.

[121] K. E. Achyuthan, T. S. Bergstedt, L. Chen, R. M. Jones, S. Kumaraswamy, S. A. Kushon, K. D. Ley, L. Lu, D. McBranch, H. Mukundan, F. Rininsland, X. Shi, W. Xia, and D. Whitten, *J. Mater. Chem.*, **2005**, *15*, 2648.

5. *Results and Discussions*

The higher decay times for C8 and C12 are shown in Figure 39. They are associated with the thiophene groups that take part, via π–π stacking, in the interchain interactions. The reduction of this contribution to the steady state intensity (see Figure 39) as surfactant concentration is increased is attributed to the decrease of the π–π interchain interactions induced by the surfactant.

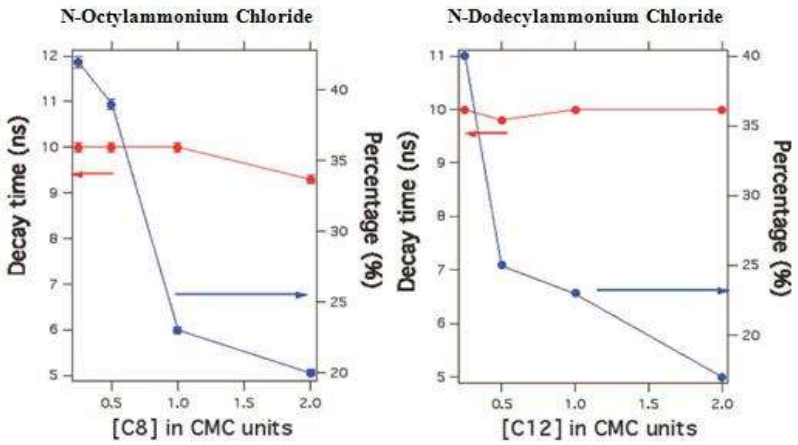

Figure 39. Profile of the higher fluorescence decay time of PTEBS and relative contribution to the steady state intensity as a function of the surfactant concentration: (a) PTEBS and C8 complex and (b) PTEBS and C12 chloride complex.

The time-resolved fluorescence measurements indicate that in the polymer-surfactant complex two different fluorophore environments could account for the two exponentially decay processes observed in the time decay profile. Additionally, at premicellar concentrations, the surfactant with the longest chain length presented shorter lifetimes than those obtained upon addition of the surfactant with the smallest chain length. These results were associated with the elimination of nonradiative decay pathways as well as with increments in the media hydrophobicity. However, at the critical micelle concentration and above, the surfactant chain length loses importance, since the surfactant breaking up process is the dominant effect that

prevents the π–π interchain interaction. In this regime, the size of the polymer-surfactant clusters and the decay time became independent of the surfactant chain length.

5.1.3 *Conclusions*

The results show that at premicellar concentrations, the surfactant chain length influences strongly the PL emission of the PTEBS. In fact, depending on the surfactant chain length, it is possible to quench or enhance the PL emission of the polymer. At premicellar concentrations, the variations in PL intensity are related to the capacity of the surfactants with the shortest chain length (C8 and C9) to aggregate the PTEBS. This effect is overcome by the hydrophobic interactions of the longer surfactant tails (C10 and C12). This scenario changes completely at the CMC and above for which the PL increases. Under these conditions the breaking up effect of the surfactant is maximum and it reduces the mean polymer-surfactant cluster size and consequently the π–π interactions and other effects such as chain kinks, folding, and so forth, which could be involved in quenching phenomena. In summary the polymer-surfactant interaction at premicellar concentrations plays an important role in the emission efficiency of PTEBS, in such a way that by changing the surfactant chain length can be induced variations in the PL emission.

5.2 *Preparation and Characterization of Interpenetrated Microgels as Sensors*

5.2.1 *Introduction*

During the last 10 years the interest over polymer microgels has grown rapidly due to their fast response to external stimuli. They have prompted out within applications as drug delivery systems, molecular entrapment matrices, oil recovery devices, or catalytic media.[122,123,124,125,126] Depending on the environment conditions such as pH, ionic strength, or temperature, the polymer Flory-Huggins parameter can change, leading to a steep variation of the microgel hydrodynamic radius.[127,128] In microgels, this response is fast and has been used to create smart materials of which PNIPAM is, by far, the most investigated system. PNIPAM is a water-soluble polymer with LCST at 32 °C that shrinks or swells in response to changes in temperature.[41,104] Thus, PNIPAM particles swell in water at room temperature, ordering water molecules around the amide group by means of hydrogen bonding. When the temperature increases above the LCST, molecular agitation disrupts these H-bonds and leads to a breakdown of local water structure around PNIPAM chains that triggers hydrophobic attraction among isopropyl groups, with the consequent dehydration of polymer chains. Swelling of microgels depends on the type and concentration of monomer (and/or comonomer),[35] its affinity for the solvent, inclusion of nanoparticles within the microgel, and cross-linking.[41] Thus, the

[122] L. Benee, M. J. Snowden, and B. Z. Chowdhry, "*Encyclopedia of Advanced Materials*", John Wiley & Sons Ltd, New York, **2002**.
[123] A. Hoffman, *J.Controlled Release*, **1987**, *6*, 297.
[124] C. Ramkisson-Ganorkar, F. Liu, M. Baudys, and S. W. Kim, *J. Controlled Release*, **1999**, *59*, 287.
[125] M. Serrano Ruiz, A. Romerosa, B. Sierra-Martin, and A. Fernandez-Barbero, *Angew Chem. Int .Ed.*, **2008**, *47*, 8665.
[126] Y. Nakayama, *Prog. Org. Coat.*, **1998**, *33*, 108.
[127] G. Filipcsei, J. Feher, and M. Zrinyi, *J. Mol. Struct.*, **2000**, *554*, 109.
[128] B. R. Saunders, and B. Vincent, *Adv. Colloid Interface Sci.*, **1999**, *80*, 1.

combination of PNIPAM with other materials as inorganic nanoparticles[129] or conducting polymers[130] can modify the LCST, and this variation has to be taken into account when dealing with applications. Recently, it has been reported the preparation of PNIPAM microgels that combine thermoresponsive and fluorescent properties in one material, using quantum dots as fluorescent emitter.[36]

A different way to synthesize fluorescent microgels is the polymerization of NIPAM in the presence of photoluminescent polymers to produce an interpenetrated network with the photoluminescent polymer entrapped inside the microgel. The PNIPAM particles monodispersity allows the preparation of thermoresponsive surface coatings with controlled thickness.[131] Due to the previous results obtained from the study of the interactions of the CP PTEBS with N-Alkylammonium surfactant it would be possible to prepare fluorescent sensors producing an interpenetrated microgel with PTEBS and PNIPAM.

5.2.2 *Results*

The interpenetrated microgel was synthesized using the free-radical polymerization method.[35,104,128] The PTEBS concentration used in the preparation of the interpenetrated microgel was 1.8×10^{-4} M. Higher concentration of CP was responsible of the NIPAM coagulation during the polymerization giving a polydisperse material. This effect could be due to the high ionic strength of the initiator ammonium persulfate. The cross-linking content, given as [cross-linker(g)]/[NIPAM(g)+cross-linker(g)]x100, was varied between 2.5 and 10% in order to obtain microgels with different swelling properties, using as cross-linker BA.

---

[129] A. Pich, and H. J. P. Adler, *Polym. Int.*, **2007**, *56*, 291.
[130] E. López-Cabarcos, D. Mecerreyes, B. Sierra-Martín, M. S. Romero-Cano, P. Strunz, and A. Fernandez-Barbero, *Phys. Chem. Chem. Phys.*, **2004**, *6*, 1396.
[131] S. Schmidt, H. Motschmann, T. Hellweg, and R. von Klitzing, *Polymer*, **2008**, *49*, 749.

5. *Results and Discussions*

Dynamic light scattering measurements were performed on a dispersion of PTEBS, and the results indicated that, in water, the polymer forms small particles with 10 nm of hydrodynamic diameter (see inset of Figure 40).

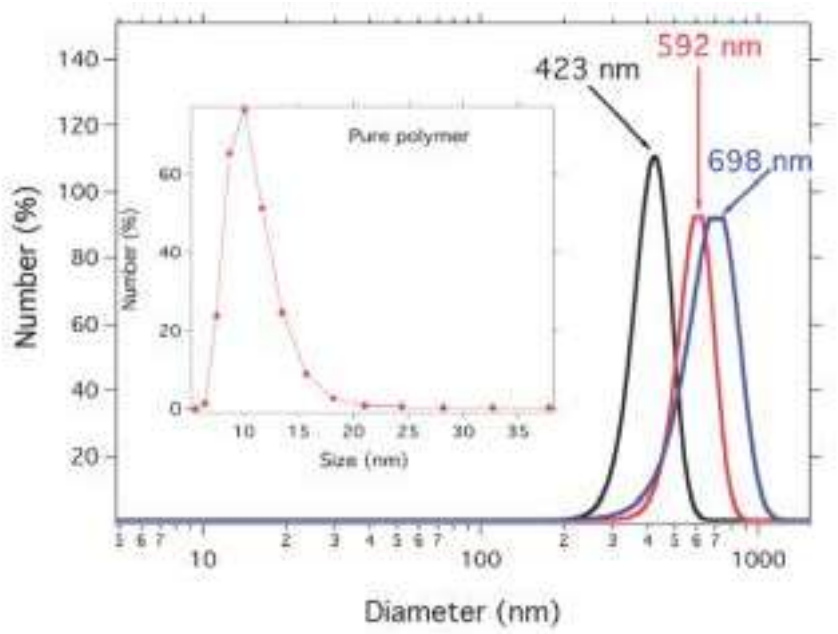

Figure 40. Hydrodynamic diameter of PNIPAM-PTEBS microgels with different cross-linking rates: (black line) 10% of BA, (red line) 5% of BA, and (blue line) 2.5% of BA. The inset depicts the hydrodynamic diameter of the PTEBS particles.

However, after the synthesis of the PNIPAM microgels in the presence of PTEBS, only microgel particles are observed as is shown in Figure 40. The hydrodynamic diameter of the microgels depends on cross-linking content and the values obtained by DLS were 420 ± 50 nm (for 10% BA), 590 ± 60 nm (for 5% BA), and 700 ± 100 nm (for 2.5% BA). These results indicate that during the microgel formation PTEBS interacts with the PNIPAM growing chains, leading to interpenetrated polymer particles in which the CP is entrapped inside the PNIPAM matrix microgel. The driving force for this interaction would be the inherent hydrophobicity of thiophene moieties, which permits the formation of van der Waals interactions between PTEBS

and the incipient PNIPAM chains that are hydrophobic at the reaction temperature (70 °C). This sort of interaction has previously been reported for polythiophene moieties with N-alkylammonium surfactants.[110,112,132]

The chemical composition of PTEBS and PNIPAM is very different (see Scheme 4). This feature has been used to determine the amount of PTEBS within the microgels using elemental analysis, and it was found to be around 0.7% (w/w). The amount of PTEBS immobilized within the microgels does not depend on cross-linking percentage.

Scheme 4. **Chemical Structure of (a) PTEBS and (b) PNIPAM.**

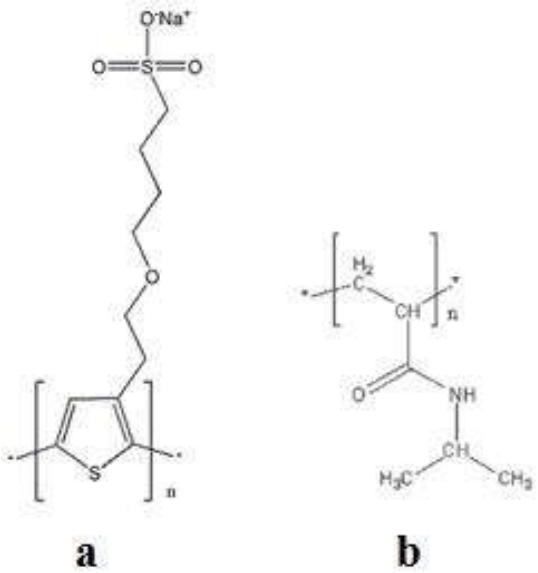

a **b**

In Figure 40 can be observed that the microgels with higher cross-linking rates present smaller hydrodynamic diameters (≈423nm). This is due to the increment of the elastic tension introduced by the cross-linker that hinders the microgel swelling and reduces its size. The SEM micrograph of the synthesized particles (see Figure 41) showed that the microgels are spherical and quite monodisperse, with a collapsed diameter close to 250 nm.

[132] M. Laurenti, J. Rubio-Retama, F. García-Blanco, and E. López-Cabarcos, *Langmuir*, **2008**, *24*, 23.

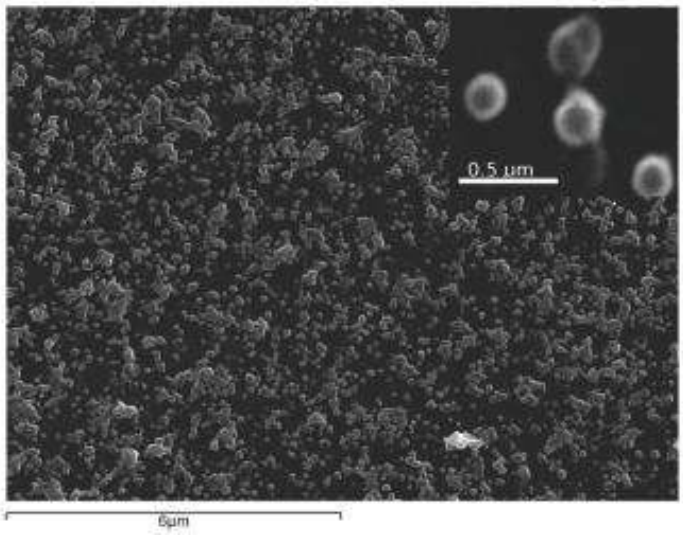

Figure 41. SEM micrograph of PNIPAM-PTEBS microgels prepared with a cross-linking content of 10%. The inset shows microgels at high magnification.

The microgels can be easily redispersed in water, giving a colloidal suspension which is stable for several days and presents fluorescence emission when illuminated by UV radiation (see Figure 42).

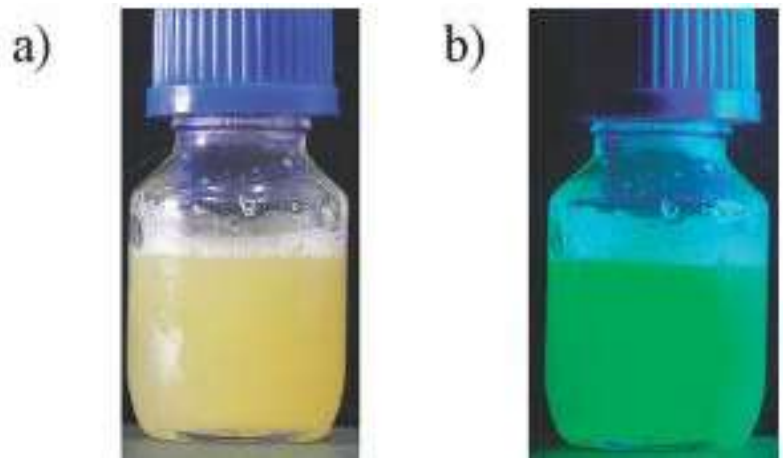

Figure 42. a) PNIPAM-PTEBS microgels with 10% of cross-linker BA dispersed in water under visible light, and b) illuminated with a UV-lamp with excitation wavelength of 350 nm.

The swelling behavior of the interpenetrated microgels was evaluated by studying the change of the hydrodynamic diameter, D_h, as a function of temperature (Figure 43). As can be evaluated the variation of D_h during the volume transition depends on the cross-linking rate of the interpenetrated microgels, as it occurred in pure PNIPAM microgels. This effect is due to the increment of the microgel rigidity introduced by the cross-linker, which hinders the polymer swelling.

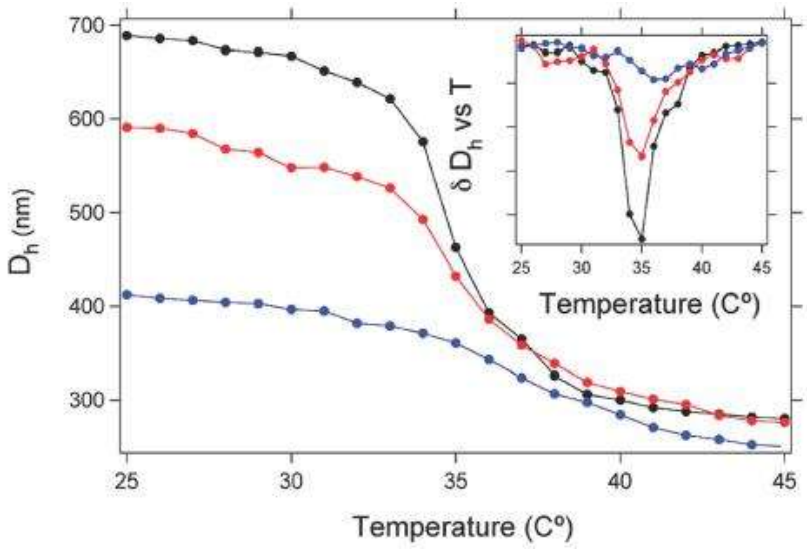

Figure 43. Hydrodynamic diameter of microgels with different cross-linking content as a function of the temperature: (black filled circle) PNIPAM-PTEBS microgels with 2.5% of cross-linker, (red filled circle) PNIPAM-PTEBS microgels with a 5% of cross-linker, (blue filled circle) PNIPAM-PTEBS microgels with 10% of cross-linker. The inset depicts the derivative of the D_h versus temperature.

The inset in Figure 43 shows that, independently of the cross-linking content, the microgels present a volume transition at 34 °C, slightly higher than the LCST for pure PNIPAM. This change is attributed not only to the steric hindrances that the conjugated polymer introduces during PNIPAM chain aggregation but also to the electrostatic repulsion of the PTEBS

sulfonate groups in the polymer matrix. Similar results were obtained after immobilizing nanoparticles[133] or introducing charged monomers inside PNIPAM microgels.[55]

Recently it has been reported, using IQNS, that PNIPAM chain dynamics exhibits striking differences in the swollen and collapsed states.[134,135] The backscattering spectrometer IN10 at ILL (France, Grenoble) was used to study the IQNS of the interpenetrated microgels (Figure 44), with the aim to investigate if the entrapment of PTEBS modifies the dynamics of the PNIPAM chains since the DLS reveals a different LCST.

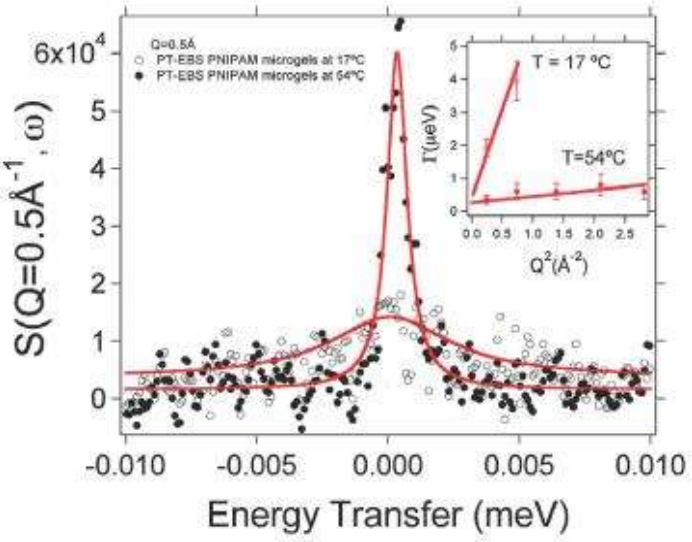

Figure 44. S(Q,ω) function clearly showing the different dynamics of the 5 wt % cross-linked PNIPAM-PTEBS network in the swollen (17 °C) and collapsed (54 °C) states. The solid lines through the points represent the fitting with a Lorentzian function. The inset shows the full-width at half-maximum of the quasielastic component as a function of Q^2 for the microgels in the swollen and collapsed states.

[133] J. Rubio-Retama, N. E. Zafeiropoulos, C. Serafinelli, R. Rojas-Reyna, B. Voit, E. López-Cabarcos, and M. Stamm, *Langmuir,* **2007**, *23*, 10280.
[134] J. Rubio-Retama, B. Frick, T. Seydel, M. Stamm, A. Fernandez-Barbero, and E. López-Cabarcos, *Macromolecules*, **2008**, *41*, 4739.
[135] J. Rubio-Retama, B. Frick, T. Seydel, B. López-Ruiz, A. Fernandez-Barbero, and E. López-Cabarcos, *Colloids Surf. A*, **2008**, *319*, 149.

The incoherent scattering function S(Q,ω) in the swollen (17 °C) and collapsed states (54 °C) of the 5% cross-linked PTEBS-PNIPAM microgels (Q is the scattering vector and ω is the energy in $\hbar$ units). The incoherent scattering function given by equation [6] was used to fit the experimental data. From the fitting of the quasi-elastic component, measured at different Q, with a Lorentzian function obtaining the full-width at half-maximum (FWHM), $\Gamma(Q)$, for the collapsed and swollen microgels. As is illustrated in the inset of Figure 44, the dependence is linear, $\Gamma = DQ^2$, and from the slope can be calculated the diffusion constant of the polymer chains with respect to the microgel center of mass. In the swollen state the diffusion value obtained was $D = 1.3 \times 10^{-11}$ m^2/s, while in the collapsed state $D = 4.5 \times 10^{-13}$ m^2/s.

These results are very close to those obtained for pure PNIPAM microgels, indicating that the presence of the PTEBS within the PNIPAM microgels does not alter significantly the dynamics of the polymer chains.[134] On the other hand, the big difference of the PNIPAM chain dynamics between the swollen and the collapsed states indicates that microgels present a sol-like behavior below the LCST, whereas they behave as solid-like systems above the LCST.[135]

The PL properties of the thermoresponsive interpenetrated microgels were evaluated as a function of the temperature. As can be seen in Figure 45, the PL intensity is partially quenched when PNIPAM is above the LCST and the collapsed microgel resembles a solid material.

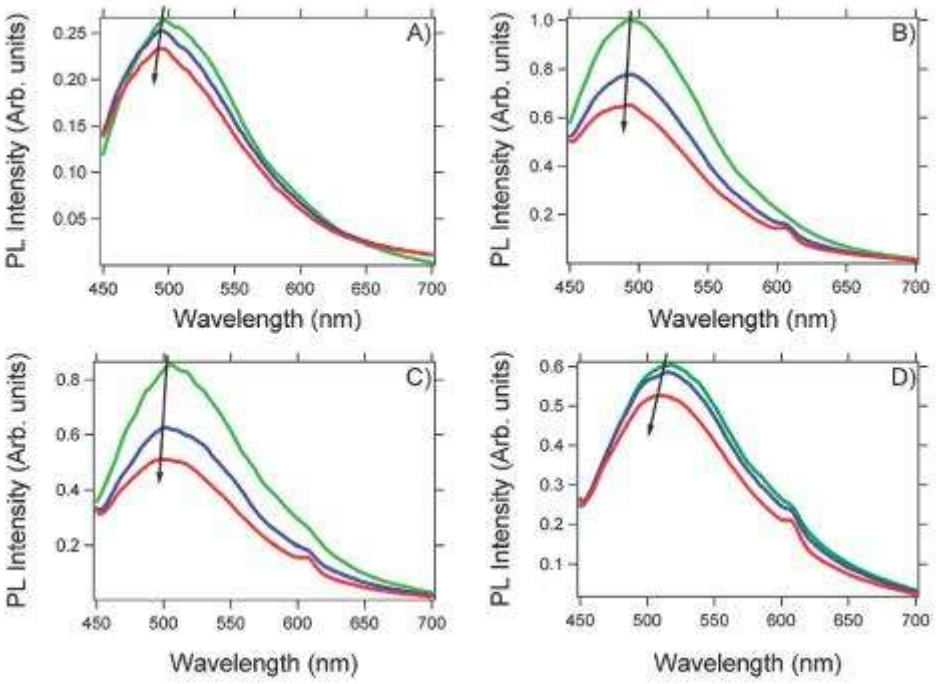

Figure 45. Emission spectra of PTEBS and PNIPAM-PTEBS microgels at different temperatures (green line 25 °C, blue line 35 °C, and red line 45 °C) measured with microgel concentration of 0.02% (w/w). A) pure PTEBS ($4.3x10^{-4}$ M), B) PNIPAM-PTEBS microgel with 2.5% BA, C) PNIPAM-PTEBS microgel with 5% BA, and D) PNIPAM-PTEBS microgel with 10% BA. All spectra were recorded with excitation wavelength of 425 nm.

In such state, the reduction of microgel particle size with the consequent increase of its refractive index will diminish the number of photons that can reach the entrapped PTEBS, since a fraction of them are scattered.[136,137] Thus, the reduction of the PL emission peak is due not only to the greater chain-chain interaction between the polythiophenes in the collapsed microgel but also to the smaller amount of photons reaching the luminescent polymer. The effect is more intense when the amount of cross-linker in the microgels decreases, and this is attributed to the higher changes in the refractive index experienced by low cross-linked

[136] J. L. X. Hong, Y. Liu, D. Li, Y. W. Wang, J. H. Li, Y. B. Bai, and T. J. Li, *Adv. Mater.*, **2005**, *17*, 163.
[137] Y. Gong, M. Gao, D. Wang, and H. Möhwald, *Chem. Mater.*, **2005**, *17*, 2648.

microgels at the volume transition. Another consequence of the PTEBS immobilization is the shift in the PL emission of the polymer. Figure 46 shows the shift of the PL emission maximum in microgels with different cross-linking content at several temperatures.

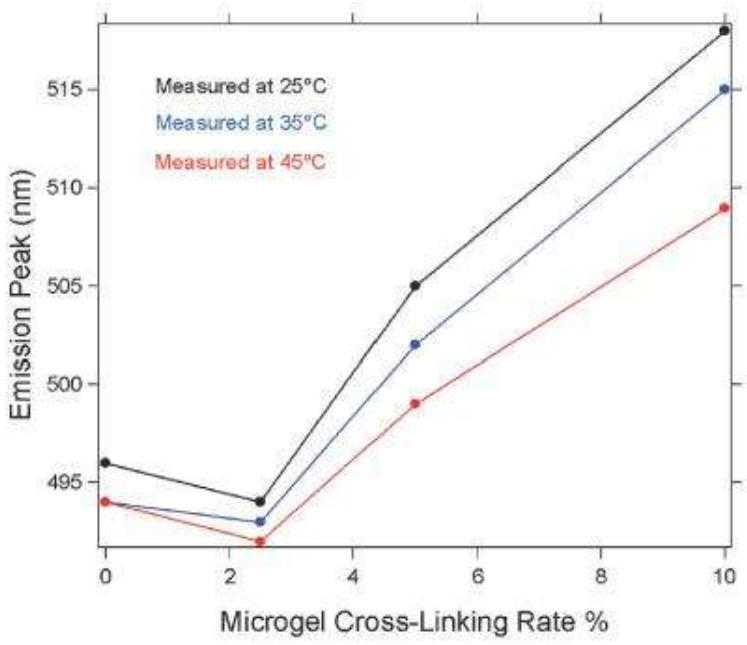

Figure 46. Shift of the emission peak as a function of the cross-linking content measured at (black filled circle) 25 °C, (blue filled circle) 35 °C, and (red filled circle) 45 °C.

It can be seen that the emission peak is slightly shifted from 492 nm to 490 nm when the PTEBS is entrapped inside the PNIPAM microgels with 2.5% cross-linker at 25 °C. This tiny blue-shift could be attributed to the change of polarity around the entrapped PTEBS. However, when the cross-linking content increases, the PL emission is red-shifted by an amount approximately proportional to the cross-linking. This effect can be attributed to the stretching of the PTEBS chains in the hydrophobic environment provided by the higher PNIPAM concentrations inside the higher cross-linked microgels. A more stretched and consequently planar backbone will give a red-shift of the emission peak.[117,138,139,140] On the other hand, above the LCST, one would

[138] E. López-Cabarcos, and S. Carter, *Macromolecules*, **2005**, *38*, 4409.

expect an intensification of the red-shift, since in this environment the volume fraction of the PNIPAM matrix increases, promoting major structure compactness. On the contrary, the PL emission suffers a considerable blue-shift with the increasing temperature. This unexpected behavior could arise from the different viscoelastic properties of PNIPAM above and below the LCST. As it has been previously demonstrated, the chain dynamics of the PNIPAM microgels show a sol-gel-like behavior below the LCST while above the LCST the dynamics is compatible with a solid-like behavior and the collapsed microgel would hinder the rearrangement of the PTEBS chain segments. Thus, the greater flexibility of the polythiophene backbone below the LCST might facilitate a greater delocalization of the relaxed excited state (exciton).

By contrast, above the LCST the tight PNIPAM environment might increase the rigidity of the polythiophene backbone reducing the length of the π-conjugated segments.[141,142] Furthermore, the hydrophobic character of the PNIPAM chains above the LCST could permit them to interact with the hydrophobic polythiophene moieties of the PTEBS, breaking up the π-π intrachain interaction which would also shift the emission to the blue.[112,143]

Time-resolved fluorescence measurements were carried out to better understand the PL emission process of the interpenetrated microgel network (Figure 47). The decay time profiles were fitted with equation [8] for all the samples.

In order to get the lifetime distribution as well as the fractional contribution of each component to the intensity the data were analyzed using the multiexponential method.

---

[139] S. W. Thomas, G. D. Joly, and T. M. Swager, *Chem. Rev.*, **2007**, *107*, 1339.
[140] A. H. Hoang, N. Ahmed, and M. Leclerc, *Acc. Chem. Res.*, **2008**, *41*, 168.
[141] M. Wang, S. Zou, G. Guerin, L. Shen, K. Deng, M. Jones, G. C. Walter, G. D. Acholes, and M. A. Winnik, *Macromolecules*, **2008**, *41*, 6993.
[142] Y. Kanemitsu, K. Masuda, A. M. Tanaka, T. Kushida, K. S. Min, and A. H. Atwater, *Phys. Status Solidi*, **2002**, *190*, 529.
[143] G. Kwak, W. E. Lee, H. Jeong, T. Sakaguchi, and M. Fujiki, *Macromolecules*, **2009**, *42*, 20.

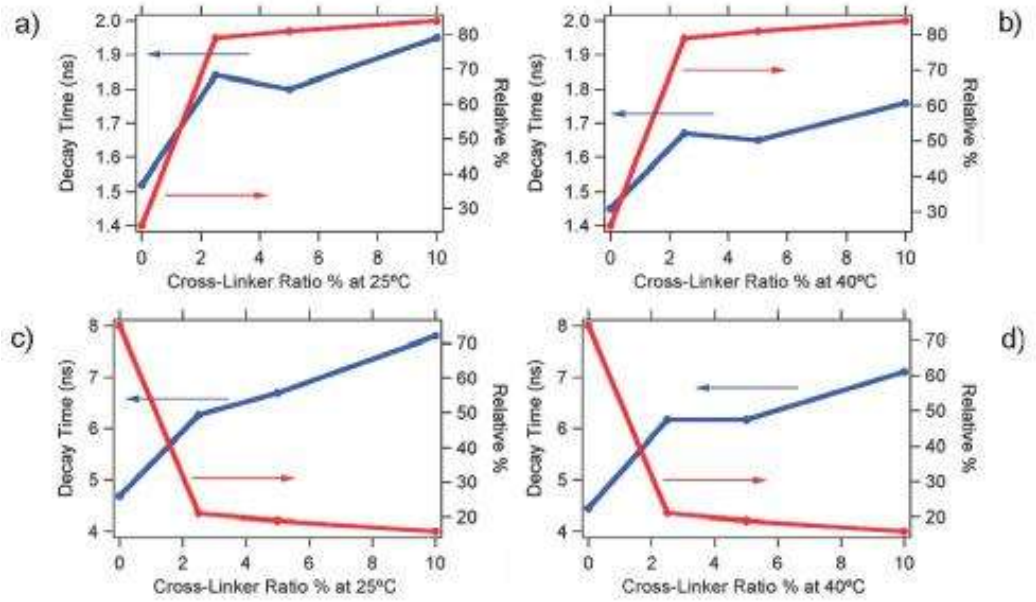

Figure 47. Two fluorescence decay times (blue) and percentage contribution to the steady state intensity (red) as a function of cross-linker content of PTEBS-PNIPAM microgels in the swollen (a, c) and collapsed states (b, d). The fast component is shown in the upper panel, and the slow one in the bottom panel.

Figure 47 represents the decay times obtained for the microgels with varying cross-linking rate above and below the LCST. The existence of two decay times would indicate the presence of polythiophene moieties in two different environments. Furthermore, the decay time of entrapped PTEBS increases with respect to the nonencapsulated polymer, and the increment is proportional to the cross-linking rate. This fact could be related to the reduction of the water content inside the microgels and the consequent increase of the polymer volume fraction as the cross-linking becomes higher (see upper part of Scheme 5).

Scheme 5. Proposed Mechanism to Explain the Decay Time Behavior[a]

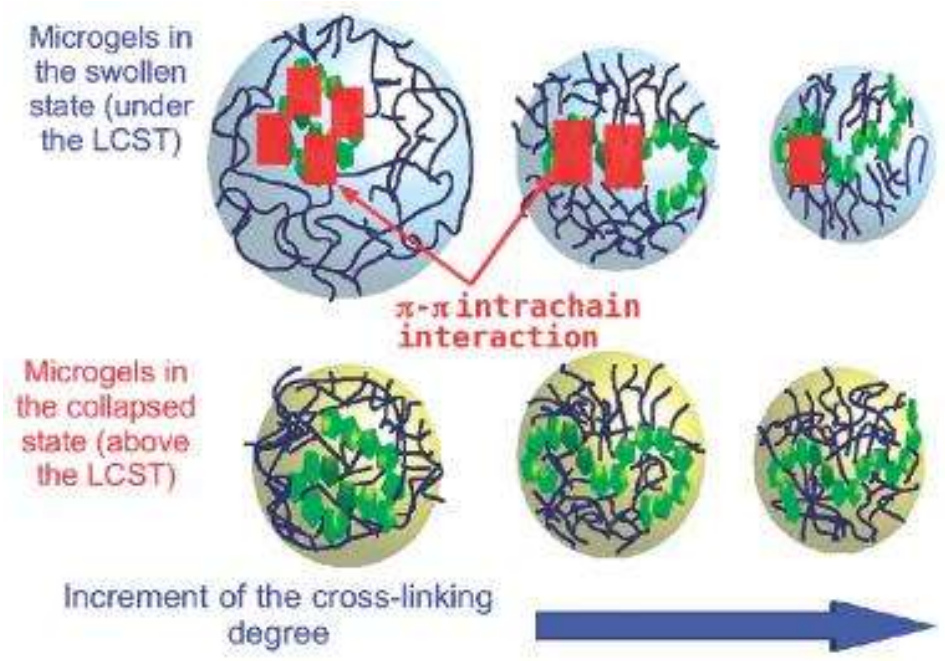

[a]Poly(thiophene) chains are hydrophobic, forming π–π intrachain interactions below the LCST. The π–π interactions are favored by the reduction of water content as the cross-linking increases. However, above the LCST, the PNIPAM chains become hydrophobic and interact with the polythiophene moieties, breaking up the π–π intrachain interactions.

Moreover, is worth pointing out the shortening of the PL decay time when the microgel collapsed, which is attributed to the reduction of delocalization of the exciton along the PTEBS chain, due to the higher rigidity of the conjugated polymer chain in the collapsed microgel[140] (see bottom part of Scheme 5). The detection of nitro aromatics by quenching of conjugated polymers is well established after the original work of the Swager group.[20,139,144] Above the LCST, the capacity of the PNIPAM chain to break up the π–π interaction of PTEBS opens the possibility of using this system to dissociate similar interactions between polythiophene and quenching molecules such as 2,4,6-nitrotoluene, picric acid, or dimethyl-viologen. For instance, below the

[144] A. Narayanan, O. Varnavski, T. M. Swager, and T. Goodson, *J. Phys. Chem. C*, **2008**, 112, 881.

LCST, the addition of increasing concentrations of picric acid, ranging from $1x10^{-7}$ M to $1x10^{-4}$ M, to the interpenetrated microgels provokes the quenching of the PL emission (see Figure 48), which indicates the formation of a complex between the quencher and the π-conjugated polymer.

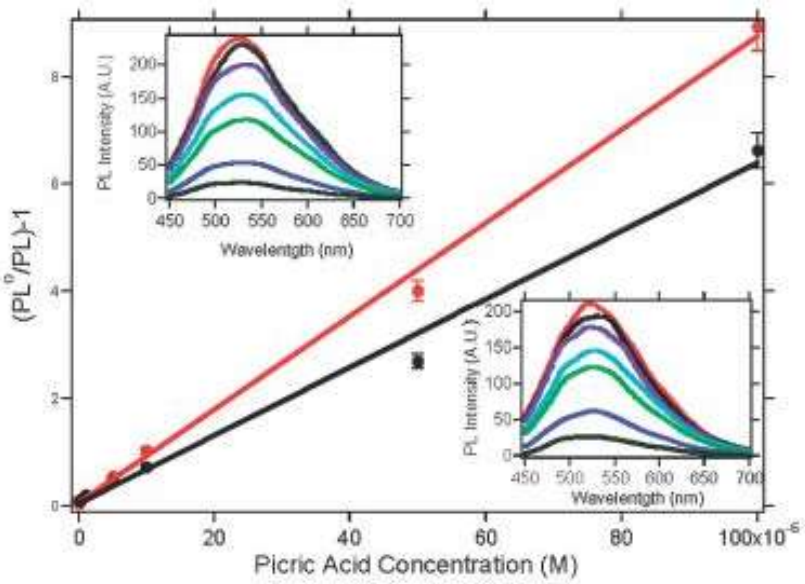

Figure 48. Stern-Volmer plot of PL quenching with picric acid at 25 °C (red line) and 45 °C (black line). The upper inset shows the PL emission of PNIPAM-PTEBS microgels at different concentrations of picric acid at 25 °C, while the inset on the bottom depicts the PL emission at 45 °C for different concentrations of picric acid.

The quenching of the PL emission by the nitro aromatic compound is 92% of its initial value at 25 °C. The quantitative measure of PL quenching is given by the Stern-Volmer constant K_{SV}, defined by equation [1]. For entrapped PTEBS quenched by picric acid, $K_{SV} = 1x10^5$ at 25 °C and at 45 °C $K_{SV} = 7x10^4$. These values have been compared with the nonencapsulated PTEBS, being $K_{SV} = 8x10^4$ and $K_{SV} = 7x10^4$ at 25 and 45 °C, respectively. As can be seen, at 25 °C the differences in the K_{SV} capacity are slightly bigger in the interpenetrated microgels, which could be due to the capacity of PNIPAM to stretch the PTEBS chain below the LCST. This fact could

facilitate the accessibility of quencher to the fluorophores, increasing the K_{SV} value at lower temperatures.

When the temperature of the microgels is raised above the LCST, the interactions between quencher and PTEBS are hindered due to the collapse of the microgels, and the PL emission partially recovers, even in the presence of the quencher in the microgel dispersion (see Figure 49).

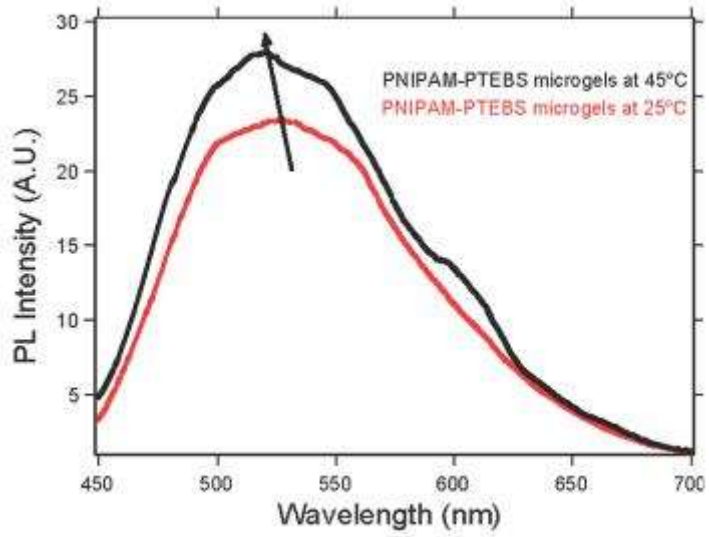

Figure 49. PL emission of the PTEBS-PNIPAM microgels in the presence of $1x10^{-4}$ M picric acid at 25 and 45 °C.

This phenomenon can be used to collect the microgels free of quencher. Thus, by recovering the microgels in the collapsed state, and redispersing them in pure water at 25 °C, 100% of the initial PL emission is recovered (see Figure 50).

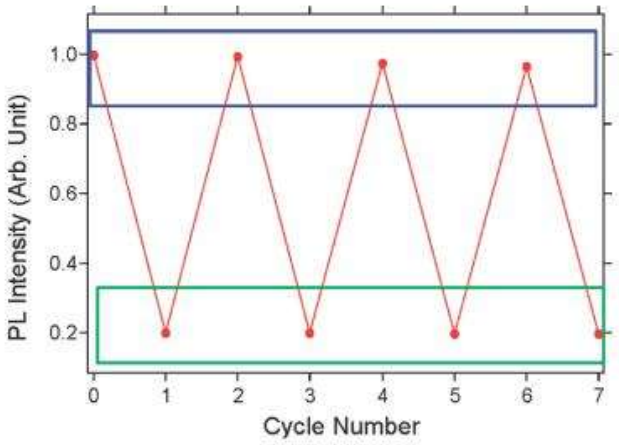

Figure 50. PL intensity measured during repeated cycles of quencher addition and subsequent recovering of collapsed microgels.

Scheme 6 summarizes the mechanism of fluorescence quenching and recovering for interpenetrated microgels. In the swollen state, the microgels are fluorescent, but after the addition of the nitro aromatic compound the PL is quenched because picric acid forms a nonfluorescent complex with the π-conjugated polymer.

Scheme 6. Mechanism of PL Quenching and Recovering of the Initial Fluorescence of Interpenetrated Microgels.

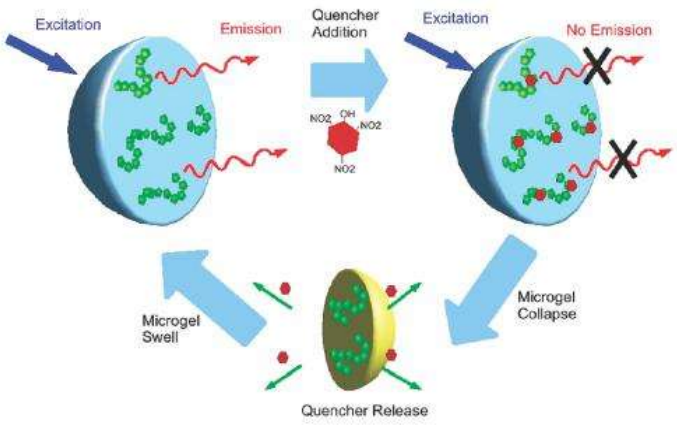

However, above the LCST, the PNIPAM matrix interacts with the polythiophene moieties, breaking partially the quencher-polythiophene complex and releasing the quencher. Subsequently, the microgels are collected and reswelled, recovering its initial fluorescence. The whole procedure could be use to recover the fluorescence microgels and reuse them again.

5.2.3 *Conclusions*

The work of this section shows an easy way for the synthesis of fluorescence microgels based on PNIPAM and PTEBS. The PL properties of the interpenetrated microgels were studied as a function of cross-linking degree, temperature, and rigidity of the polymer matrix. The results confirmed the close relationship between the environment and the PL emission of the encapsulated π-conjugated polymer. Furthermore, it was observed that above the LCST the PNIPAM chain was able to interact with the π-conjugated polymer, breaking π–π interactions. This characteristic was used to prepare a reusable microsensor suitable for detecting nitro aromatic compounds.

5.3 *Fluorescence Decrease of Conjugated Polymers by the Catalytic Activity of HRP and Its Application in Phenolic Compounds Detection*

5.3.1 *Introduction*

Chen et al.[145] proposed a novel fluorescent biosensor based on the luminescent polyelectrolyte MPS-PPV. They showed that the PL of MPS-PPV was very efficiently quenched by an electron acceptor dimethyl-viologen. By tethering the quencher to a ligand that is sequestered by binding it to a specific biorelevant target, they created a novel and sensitive class of biosensors. More recently, Fan et al.[31] reported that cytochrome *c* (cyt *c*) acts as an efficient PL quencher of MBL-PPV, which is an example of fluorescence quenching of CPs by a protein. These authors attributed the high efficiency of the polymer fluorescence decrease to a combination of PET between cyt *c* and the CP, and also to the formation of the polymer-quencher complexes driven by attractive Coulomb interactions.

Based on the previous work about the investigation of the PL quenching due to the interaction of the PTEBS with the molecules of picric acid, it has been decided to prepare a new biosensor based on a water-soluble CP and a peroxidase enzyme. In this work has been proposed a mechanism to detect phenolic compounds based on the oxidation of MPS-PPV by the catalytic activity of HRP in the presence of H_2O_2, which brings about a conspicuous drop in PL. The heme-containing protein HRP (donor: hydrogen-peroxide oxidoreductase, EC 1.11.1.7) catalyzes the oxidation of substrates at the expense of H_2O_2 or lipid peroxides. The enzyme catalytic cycle is initiated by the rapid $2e^-$ oxidation ($k > 10^7\ M^{-1}s^{-1}$)[146] of the met enzyme (i.e., in

[145] L. Chen, D. W. McBranch, L. H. Wang, R. Helgeson, F. Wudl, and D. Whitten, *Proc. Natl. Acad. Sci. U.S.A.*, **1999**, *96*, 12287.
[146] J. N. Rodríguez-Lopez, J. Hernandez-Ruiz, F. García-Canovas, R. N. F. Torneley, M. Acosta, and M. B. Arnao, *J. Biol. Chem.*, **1997**, *272*, 5469.

the Fe(III) heme state, native enzyme, metHRP) by hydrogen peroxide to give the green enzymatic intermediate CoI, with the heme iron oxidized to the oxyferryl state (Fe^{IV}=O) and a π-cation radical on the porphyrin ring. Phenols or aromatic amines reduce CoI in a one-electron step to CoII, and CoII back to the native enzyme in a sequential one-electron step, as shown in Scheme 7. However, in the presence of an excess of H_2O_2, CoII transforms to compound III (CoIII) (formal oxidation state of +6), which involves a protective mechanism against the suicide inactivation of HRP. Donor substrates also show a protective effect on the H_2O_2-induced suicide inactivation of HRP, as long as the [substrate]/[H_2O_2] ratio is high.[147] Thus, rich electron molecules such as π–π conjugated polymers may act as substrates in the HRP action mechanism to provide a protective effect.

Scheme 7. Classic Peroxidase Cycle Using H_2O_2 as an Oxidizing Substrate Where S is a Reducing Substrate and S• is the Free Radical Product.

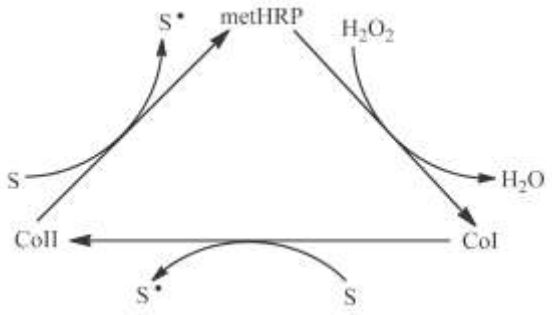

Polymer oxidation conveys an increase in the polymer HOMO-LUMO band gap by decreasing fluorescence quantum efficiency and provoking a blue-shift of the signal. The change in fluorescence emission offers the possibility of detecting the radical molecules generated by a peroxidase-like activity, which can occur in living organisms under oxidative stress conditions.

[147] J. Hernández-Ruiz, M. B. Arnao, A. N. Hiner, F. García-Cánovas, and M. Acosta, *Biochem. J.*, **2001**, *354*, 107.

For instance, HRP catalyzes the one-electron oxidation of the analgesic and antipyretic drug APAP, which is safe for humans at normal doses but can lead to liver damage and renal impairment if ingested in excess.[148] The HRP-catalyzed oxidation of APAP in the presence of H_2O_2 yields N-acetyl-p-benzosemiquinonimine (NAPSQI•), a very reactive radical[149,150] that lowers the polymer's fluorescence emission and makes it possible to detect APAP at micromolar concentrations. This feature may lead to the development of new sensory devices that use the optical and electronic properties of CPs.

5.3.2 *Results*

The PL decrease of MPS-PPV by the catalytic activity of HRP in the presence of H_2O_2 was investigated. The emission spectrum of an MPS-PPV solution (80 μM) was measured in both the absence and presence of H_2O_2 (Figure 51A), and no difference between them was observed. The emission spectrum of an MPS-PPV solution in the presence of HRP is shown in Figure 51B (curve 1) and, in comparison with Figure 51A, no shift of the maximum wavelength or decrease in the fluorescence of MPS-PPV was observed.

However, when H_2O_2 was added to this solution, fluorescence intensity decreased conspicuously as a function of time, as shown in Figure 51B. Moreover, this decrease of PL intensity was concomitant with a blue-shift of the maximum from 547 to 517 nm (Figure 51B). Polymer fluorescence was not restored after the end of the biocatalytic reaction, which suggests a permanent change in the MPS-PPV structure.

---

[148] S. H. Thomas, *Pharmacol. Ther.*, **1993**, *60*, 91.
[149] D. W. Potter, and J. A. Hinson, *Drug. Metab. Rev.*, **1989**, *20*, 341.
[150] M. I. González-Sánchez, M. C. Manjabacas, F. García-Carmona, and E. Valero, *Chem. Res. Toxicol.*, **2009**, *22*, 1841.

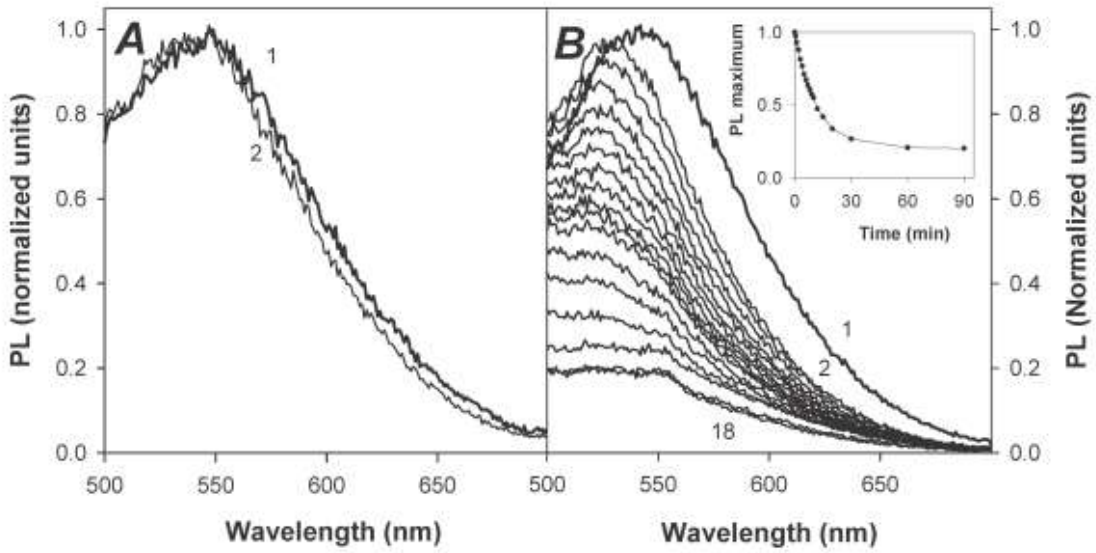

Figure 51. (A) Emission spectra of 80 μM MPS-PPV (curve 1) and 80 μM MPS-PPV plus 0.5 mM H_2O_2 (t = 5 min after the addition of H_2O_2, curve 2). (B) Repetitive emission spectra of 80 μM MPS-PPV in the presence of HRP and H_2O_2. Curve 1 corresponds to the emission spectrum of a solution of 80 μM MPS-PPV and 3.0 μM HRP. Curves 2-18 are the emission spectra of 80 μM MPS-PPV and 3.0 μM HRP taken after the addition of 0.5 mM H_2O_2 at the times indicated in the inset where it is shown the evolution of the PL maximum as a function of time. Scan speed was 600 nm/min. The excitation wavelength was 466 nm.

Figure 52 shows the UV-Vis spectrum of native HRP in an aqueous solution (curve 1) with an intense peak at 403 nm (Söret band), which is characteristic of pigmented heme-containing moieties, and three weak bands assignable to Q_v, Q_0, and porphyrin → iron charge-transfer bands at 504, 537, and 645 nm, respectively.[151]

The absorbance spectrum of MPS-PPV in the aqueous solution (curve 2) shows two maxima at 358 and 453 nm. Curve 3 in Figure 52 corresponds to the absorbance spectrum of a solution of HRP and MPS-PPV.

[151] Q. Huang, W. Al-Azzam, K. Griebenow, and R. Schewertzer-Stenner, *Biophys. J.*, **2003**, *84*, 3285.

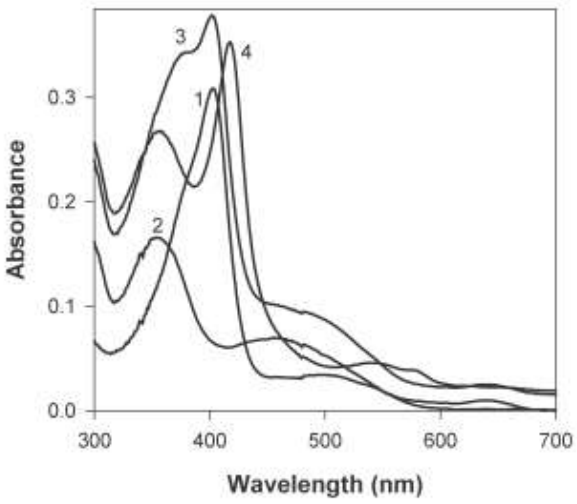

Figure 52. Absorption spectra of an aqueous solution of 3.0 μM HRP (curve 1), 80 μM MPS-PPV (curve 2), 3.0 μM HRP with 80 μM MPS-PPV (curve 3), and 3.0 μM HRP with 80 μM MPS-PPV, 1 min after the addition of 0.5 mM H_2O_2 (curve 4). Scan speed was 1000 nm/min.

This curve coincides with the sum of curves 1 and 2, indicating that there is no reaction between the polymer and the protein. However, when an excess of H_2O_2 is added to this latter solution, the maximum wavelength of the Söret band of HRP red-shifted from 403 to 417 nm (curve 4) owing to the formation of CoIII (Söret band at 418 nm and two absorbance peaks at 544 and 577 nm) under the condition of an excess of H_2O_2 used in this experiment.[152] In addition, the 453 nm peak corresponding to MPS-PPV disappeared at 1 min after the addition of H_2O_2.

The change in absorbance during the reaction of HRP with H_2O_2 is shown in the insets of Figure 53 in both the absence (A) and presence (B) of MPS-PPV. Given our aim to better illustrate the evolution of absorbance during the reaction, in Figure 53 are presented the results obtained in both cases from a spectral differential analysis.

[152] V. F. Ximenes, L. H. Catalani, and A. Campa, *Biochem. Biophys. Res. Commun.*, **2001**, *287*, 130.

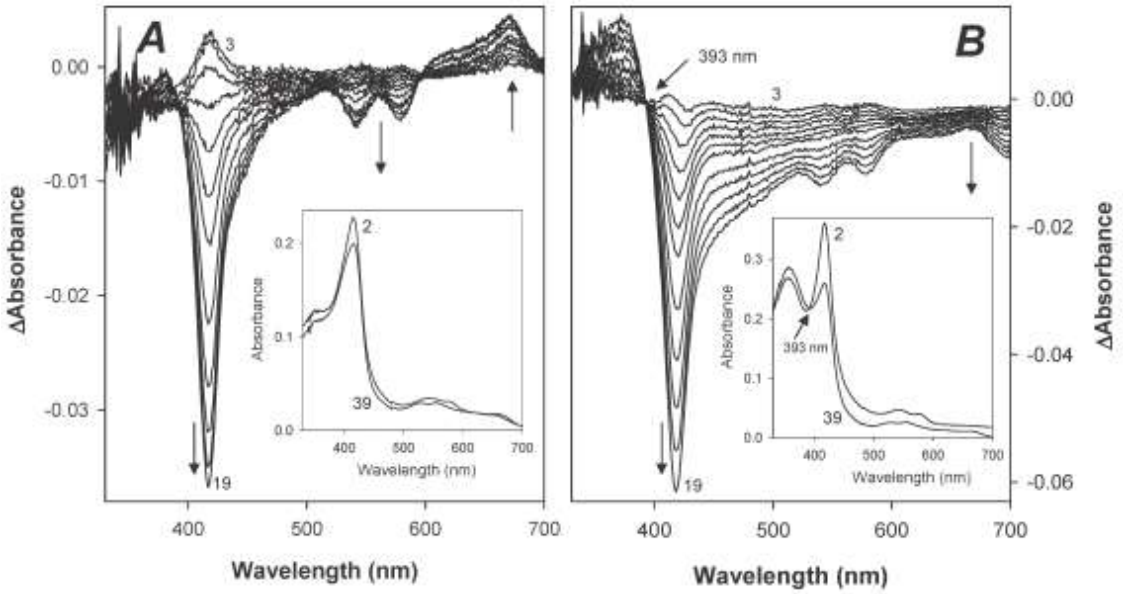

Figure 53. Spectral differential analysis of the reaction of native ferric HRP (metHRP) (3.1 μM) with H_2O_2 (0.5 mM) in the absence (A) and presence (B) of MPS-PPV (80 μM). The spectrum obtained 2 min after the addition of H_2O_2 has been subtracted from all the spectra to show maxima differences. (A) Spectra were taken at 1 min intervals from t = 3 min (spectrum 3) up to 9 min after the addition of H_2O_2, and at 2 min intervals from t = 11 min up to 19 min (spectrum 19). The scan speed was 600 nm/min. The inset shows the direct spectra obtained at 2 min (curve 2, predominance of CoIII) and 39 min (curve 39, predominance of CoII) after the addition of H_2O_2. (B) The spectra shown were taken as in (A). The inset shows the direct spectra obtained at 2 min (curve 2, predominance of CoIII) and 39 min (curve 39, predominance of CoII) after the addition of H_2O_2.

Upon the addition of H_2O_2 to native HRP, the Söret band shifted from 403 (Figure 52, curve 1) to 417 nm (curve 2 in the inset of Figure 53A and B) due to the predominance of species CoIII under the experimental conditions described herein. The characteristic CoIII spectrum reached its maximum at 2 min after the reaction began (insets in Figure 53A and B, curve 2) and subsequently decayed with time (Figure 53A and B). In the absence of the polymer (Figure 53A),

CoIII evolved toward the formation of the inactive species of HRP, as observed by the increase in absorbance at 670 nm, and the CoII spectrum could be seen at longer reaction times (Söret band at 420 nm and two absorbance peaks at 527 and 554 nm) (Figure 53A inset, curve 39). When MPS-PPV was included in the reaction medium, the absorbance at 417 nm showed faster decay (Figure 53B). Moreover, no increase in absorbance was observed at 670 nm, indicating a protective effect of the polymer on H_2O_2-induced HRP suicide inactivation. During the course of the reaction, an isosbestic point at 393 nm was maintained, indicating the coexistence of species CoI and CoII (Figure 53B).[153] The characteristic CoII spectrum could be seen at longer reaction times (Figure 53B inset, curve 39). Based on these results, it is feasible to decrease polymer fluorescence using the free radicals generated by enzymatic oxidation of aromatic compounds to therefore detect those molecules that are substrates of HRP. In the presence of H_2O_2, HRP catalyzes the oxidation of APAP to NAPSQI•,[149,150] an electron-deficient molecule which reacts with nucleophilic molecules (Scheme 8).

Scheme 8. Production of NAPSQI• from APAP via HRP-Catalyzed Oxidation in the Presence of H_2O_2.

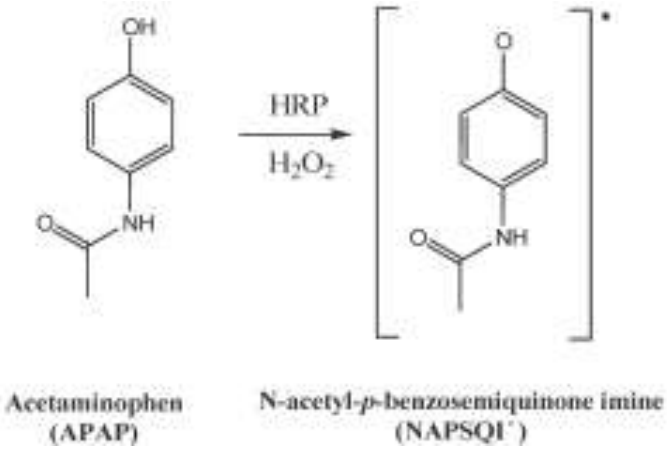

[153] H. B. Dunford, "*Peroxidases and Catalases. Biochemistry, Biophysics, Biotechnology and Physiology*" 2nd Ed., John Wiley & Sons, New York, **2010**.

5. *Results and Discussions*

To prove the effect of NAPSQI•, the fluorescence emission of MPS-PPV was measured in the presence of HRP, H_2O_2, and APAP. The results are shown in Figure 54.

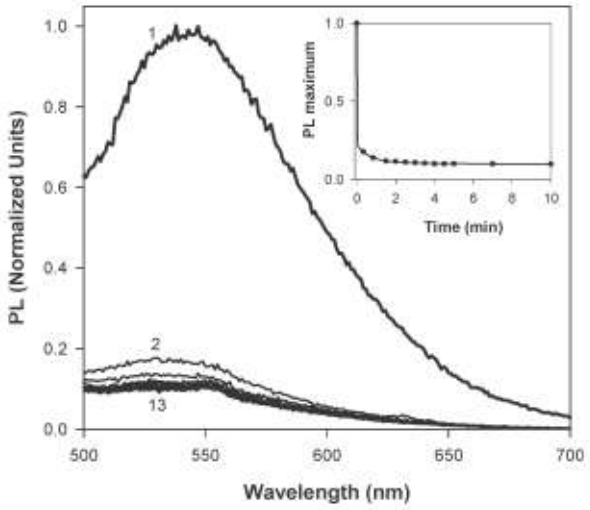

Figure 54. Curve 1 is the fluorescence spectrum of a solution containing 80 μM MPS-PPV, 3 μM HRP, and 0.6 mM APAP. Curves 2–13 correspond to the spectra of the previous solution after the addition of 0.5 mM H_2O_2 at the times indicated in the inset. The scan speed was 600 nm/min. The excitation wavelength was 466 nm.

If one compares the inset in Figure 51 with the inset in Figure 54, it can be seen that the presence of APAP yielded an almost instantaneous fluorescence decrease, which indicates the appearance of NAPSQI•. In addition, the color of the samples changed from pale pink to orange as a result of the reaction (Scheme 9). Under these experimental conditions, there were three molecules responsible for the decrease in fluorescence: CoI, CoII, and NAPSQI•. For the purpose of isolating the contribution of the different agents, HRP was immobilized in PAA with 8% of the cross-linking degree.[48,105] Figure 55A depicts an SEM micrograph of the microgels with HRP entrapped inside. Microgels were spherical in shape with a mean hydrodynamic diameter of 6.8 μm when dispersed in water (Figure 55B).

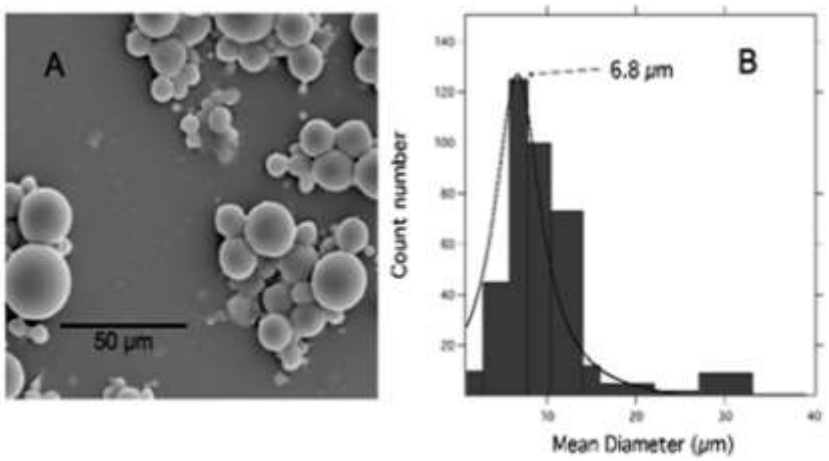

Figure 55. (A) SEM micrograph of microgels with HRP entrapped inside with a cross-linking degree of 8%. (B) Size distribution of the microgels dispersed in the aqueous solution.

HRP immobilization within the microgels prevents contact between both ferryl states of HRP (CoI and CoII intermediates) and MPS-PPV, thus avoiding the effect of the activated enzyme on the CP. At the same time, the reticulated polymer microgel allows a good diffusion of small molecules such as H_2O_2 and APAP which, after being transformed within the microgel into NAPSQI•, can diffuse to the bulk solution where MPS-PPV is dissolved. In this scenario, fluorescence intensity reduction is related with the presence of NAPSQI• in the bulk solution.

To prove the isolation of the enzyme from MPS-PPV, the fluorescence emission spectrum of MPS-PPV in the presence of the HRP encapsulated in the microgels (HRP-PAA) was measured in both the absence (Figure 56A, curve 1) and presence of H_2O_2 (Figure 56A, curve 2); the difference was negligible.

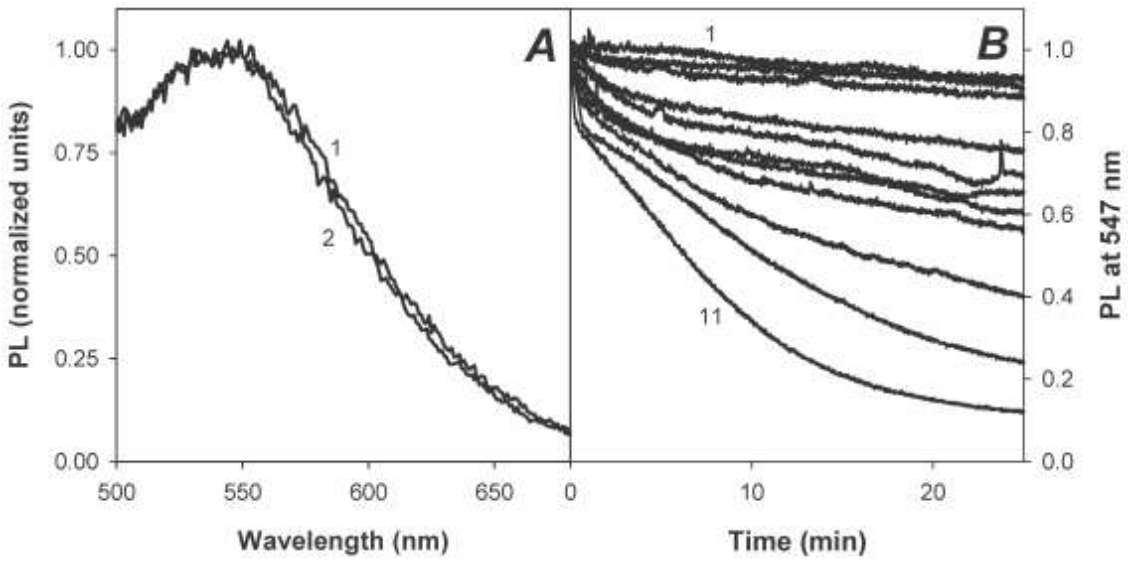

Figure 56. (A) Emission spectra of an MPS-PPV aqueous solution (80 μM) in the presence of 1 mg of HRP-PAA (curve 1), 1 mg of HRP-PAA and H_2O_2 0.5 mM (t = 10 min after the addition of H_2O_2, curve 2). (B) Fluorescence intensity at 547 nm of 80 μM MPS-PPV aqueous solutions recorded in the presence of 1 mg of HRP-PAA at a fixed H_2O_2 concentration (0.5 mM) and different APAP concentrations. Curve 1 corresponds to a solution containing 80 μM MPS-PPV and 1 mg of HRP-PAA, in the absence of H_2O_2. Curves 2-11 were obtained in the presence of H_2O_2 at the following APAP concentrations: $6x10^{-8}$ M, $1x10^{-7}$ M, $6x10^{-7}$ M, $1x10^{-6}$ M, $6x10^{-6}$ M, $1x10^{-5}$ M, $3x10^{-5}$ M, $6x10^{-5}$ M, and $1x10^{-4}$ M.

The corresponding variation of fluorescence emission at the maximum wavelength as a function of time is shown in Figure 56B, curves 1 and 2, respectively. Both time courses were in parallel, indicating that, under these conditions, the effect of H_2O_2 on the fluorescence emission was slight and, therefore, the confinement of HRP inside the PAA microgels was effective. Subsequently, H_2O_2 was added to different solutions consisting of HRP-PAA, MPS-PPV, and a range of APAP concentrations, while fluorescence emission was measured as a function of time (Figure 56B, curves 3-11). The degree of PL decrease is dependent upon the APAP concentration, a fact that could be used to detect APAP (or other phenolic compounds substrates of HRP) by

optical means. Thus, setting the detection limit to equal 3 times the fluctuation of the signal is possible to be able to detect APAP concentrations above $1x10^{-7}$ M under the experimental conditions described herein.

The water-soluble π–π conjugated polymer MPS-PPV is able to act as a donor substrate in the catalytic cycle of HRP in the presence of H_2O_2. There are two facts that support this statement: (i) MPS-PPV has electron donor character[154] and (ii) the active HRP site offers good accessibility,[155] which facilitates interaction with the polymer. Thus, MPS-PPV behaves as a substrate of HRP by reducing both CoI and CoII in agreement with the action mechanism of HRP27 (Scheme 7). Both intermediates, CoI and CoII, are powerful oxidants with redox potentials close to +1V,[156] and each one can subtract an electron from the polymer, provoking its oxidation and decreasing its fluorescence.

In CPs, there is a red-shift of the emission spectra when the electron density is injected into the polymer chain and a blue-shift when the electron density is removed.[119,157] Therefore, the blue-shift observed from 547 to 517 nm (Figure 51) correlates with both the oxidation of the polymer chain and the corresponding decrease of π–π conjugation. Oxidation of MPS-PPV would explain not only the blue-shift of the PL maximum reported in Figure 51 but also the disappearance of the maximum at 453 nm in the absorbance spectra (Figure 52, curve 4). Furthermore, the isoelectric point of HRP is 7.2,[158] which means that HRP is not charged under our experimental conditions (pH 7.0). For this reason, the decrease in fluorescence could not be attributed to the formation of a polymer-protein complex driven by attractive Coulomb interactions.

---

[154] S. J. Toal, and W. C. Trogler, *J. Mater.Chem.*, **2006**, *16*, 2871.
[155] P. R. Ortiz de Montellano, *Annu. Rev. Pharmacol. Toxicol.*, **1992**, *32*, 89.
[156] N. C. Veitch, *Phytochemistry*, **2004**, *65*, 249.
[157] S. W. Thomas, and T. M. Swager, *Macromolecules*, **2005**, *38*, 2716.
[158] A. C. Maehly, *Arch. Biochem. Biophys.*, **1955**, *56*, 507.

The spectra shown in Figure 53B indicate that MPS-PPV has a protective effect against the H_2O_2-induced inactivation of HRP. This behavior is characteristic of electron donors that reduce CoI and CoII to the so-called met state of the protein.[147,150] Moreover, the CoII spectrum is clearly noted with long reaction times (Figure 53A, B, insets), thus providing proof that CoI has been reduced. The reduction of CoII back to the ferric state of the protein usually takes place at a slower rate than the reduction of CoI,[159] thus the rate-limiting step in the catalytic cycle of HRP. A feasible model in which MPS-PPV behaves as a substrate of HRP would be the following:

$$\text{HRP (Fe(III))} + H_2O_2 \rightarrow \text{CoI} + H_2O$$

$$\text{CoI} + \text{MPS-PPV} \rightarrow \text{CoII} + \text{MPS-PPV}\bullet$$

$$\text{CoII} + \text{MPS-PPV} \rightarrow \text{HRP (Fe (III))} + \text{MPS-PPV}\bullet$$

where MPS-PPV• stands for the oxidized state of MPS-PPV. When APAP was included in the reaction medium, an almost instantaneous fluorescence decrease took place. There have been reports that in the peroxidase-catalyzed oxidation of two substrates, activation (or inhibition) of the reaction of one substrate for another is often observed (co-oxidation).[160] For example, the oxidations of both NADPH[161] and rifampicin[162] catalyzed by HRP and H_2O_2 are markedly increased by the presence of APAP. This phenomenon is explained by an electron-transfer mechanism of the following type:

$$S1\bullet + S2 \rightarrow S1 + S2\bullet$$

[159] H. B. Dunford, and J. S. Stillman, *Coord. Chem. Rev.*, **1976**, *19*, 187.
[160] O. V. Lebedeva, and N. N. Ugaroya, *Russ. Chem. Bull.*, **1996**, *45*, 18.
[161] R. J. Keller, and J. A. Hinson, *Drug Metab. Dispos.*, **1991**, *19*, 184.
[162] F. J. N. Dos Santos, V. F. Ximenes, L. M. Da Fonseca, O. M. De Faria Oliveira, and I. L. Brunetti, *Biol. Pharm. Bull.*, **2005**, *28*, 1822.

where S1 and S2 are substrates of HRP, and S1• and S2• are their corresponding oxidized products. In such cases, the better substrate (S1) is oxidized first by CoI and CoII, and its product (S1•) is the oxidizing agent for the second substrate (S2).

In our case, S1 is APAP, while S2 is MPS-PPV since APAP is oxidized by HRP with good catalytic efficiency.[149,150] Furthermore, the accessibility of MPS-PPV to the active site of the enzyme is more difficult. The encapsulation of HRP inside PAA microgels confirms this surmise since it prevents any contact between the protein and the CP, and consequently, no drop in fluorescence was observed in the absence of APAP (Figure 56A). However, small molecules such as H_2O_2 and APAP can diffuse through the microgel and reach the enzyme catalytic site to generate NAPSQI•, which then diffuses outward the microgel, oxidizing MPS-PPV and decreasing the fluorescence emission. In Scheme 9 is summarized the steps involved in the fluorescence decrease of MPS-PPV using HRP-PAA in the presence of H_2O_2 and APAP.

Scheme 9. Summary of the APAP Detection Mechanism. (A) Sample showing the pink color of the solution before the addition of hydrogen peroxide to the system and (B) yellow color after the addition of hydrogen peroxide to the system.

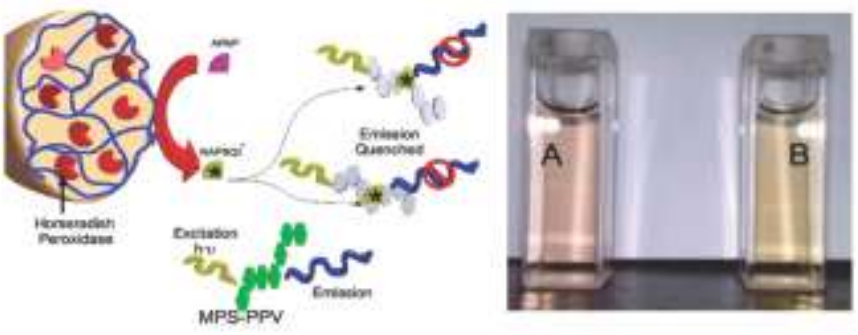

5.3.3 *Conclusions*

HRP intermediates CoI and CoII act as efficient one-electron oxidizing agents of MPS-PPV, which lead to a drop in its fluorescence emission. This is an example of photoluminescence decrease of a CP due to the catalytic action of HRP, which can be applied to the detection of specific molecules. The addition of a phenolic compound to the reaction medium, such as APAP, leads to an increased MPS-PPV oxidation rate due to the phenomenon of substrate-substrate activation, which is typical of HRP-catalyzed reactions (cooxidation). For the purpose of substantiating our model, HRP has been immobilized within PAA microgels to separate the protein from the polymer. This new system can be used to detect phenolic compounds since it responds to APAP at micromolar concentrations.

5.4 *Synthesis of a New Water-Soluble Polythiophene with the Express Purpose to Detect Heavy Metal Ions*

5.4.1 *Introduction*

The synthesis of tailored π–π CPs depends on the application for which the conjugated polymer is intended. There is a growing interest in the development of new chemical sensors for heavy metal ions that appear as pollutants in the environment and are toxic for living organisms.[163,164,165,166,167] Nowadays, these toxic ions are waste of the electronic industry and their concentration in the environment has to be controlled because their accumulation in the human body can cause serious illnesses.[168] Thus, the development of chemo and biosensors for detection of heavy-metal ions has received considerable attention in recent years. Several small molecules have been reported to successfully detect heavy metal ions, even though most of them suffer drawbacks such as low sensitivity or low water solubility.[164,169,170,171,172,173] Water soluble CPs offer the opportunity to couple analyte-receptor interactions into observable and measured responses with the advantage, over devices using small molecules, of their enhanced

[163] X. Peng, J. Du, J. Fan, J. Wang, Y. Wu, J. Zhao, S. Sun, and T. Xu, *J. Am. Chem. Soc.*, **2007**, *129*, 1500.
[164] Q. He, E. W. Miller, A. P. Wong, and C. J. Chang, *J. Am. Chem. Soc.*, **2006**, *128*, 9316.
[165] A. B. Descalzo, R. Martínez-Máñez, R. Radeglia, K. Rurack, and J. Soto, *J. Am. Chem. Soc.*, **2003**, *125*, 3418.
[166] L. Marbella, B. Serli-Mitasev, and P. Basu, *Angew. Chem. Int. Ed.*, **2009**, *48*, 3996.
[167] R. Krämer, *Angew. Chem. Int. Ed.*, **1998**, *37*, 772.
[168] C. N. Alpers, M. P. Hunerlach, J. Y. May, and R. L. Hothem, *U.S. Geological Survey.*, **2005**.
[169] Z. Xu, K. H. Baek, H. N. Kim, J. Cui, X. Qian, D. R. Spring, I. Shin, and J. Yoon, *J. Am. Chem. Soc.*, **2010**, *132*, 601.
[170] L. Zeng, E. W. Miller, A. Pralle, E. Y. Isacoff, and C. J. Chang, *J. Am. Chem. Soc.*, **2006**, *128*, 10.
[171] R. H. Yang, W. H. Chan, W. A. Lee, P. F. Xia, H .K. Zhang, and K. Li, *J. Am. Chem. Soc.*, **2003**, *125*, 2884.
[172] E. M. Nolan, and S. J. Lippard, *J. Am. Chem. Soc.*, **2003**, *125*, 14270.
[173] E. M. Nolan, J. Jaworski, K. Okamoto, Y. Hayashi, M. Sheng, and S. J. Lippard, *J. Am. Chem. Soc.*, **2005**, *127*, 16812.

sensitivity which allows detecting trace elements of analytes,[174] and different attempts to use CPs for heavy metal ions detection have already been reported.[175,176,177]

In 2004 Bunz and co-workers explored the use of sugar-functionalized poly(p-phenylene-ethynylene) as fluorescent sensor for Hg^{2+} and Pb^{2+} in N-N'-dimethyl-formamide solution.[178] The polymer exhibited the highest sensitivity toward Hg^{2+}, since its emission was efficiently quenched by $HgCl_2$ and the Stern-Volmer constant $K_{SV} = 1.1x10^4$, with $Hg(OAc)_2$ the $K_{SV} = 1.6x10^4$, with $Hg(NO_3)_2$ the $K_{SV} = 3.8x10^4$, and with $Hg(tfa)_2$ the $K_{SV} = 4.8x10^4$. The sugar residues of the polymer were critical for achieving this high sensitivity toward Hg^{2+} salts since the polymer lacking sugar functionalization was unresponsive to $HgCl_2$ and $Hg(OAc)_2$. However, Hg^{2+} salts containing easily dissociated counterions, such as $Hg(NO_3)_2$ and $Hg(tfa)_2$, quenched the emission of the non-functionalized polymer even though its sensitivity was 10-fold less than the sugar-functionalized one. Furthermore, poly(p-phenylene-ethynylene) containing two sugar moieties per repeat unit was sensitive to Pb^{2+} ($K_{SV} = 7.2x10^4$, for $Pb(OAc)_2$) but was almost unresponsive to Hg^{2+} salts.

In 2006, Wang and co-workers developed a mercury-sensing strategy based on Hg^{2+} induced aggregation of a conjugated polymer and the subsequent fluorescence self-quenching.[22] They functionalized a thiophene monomer with thymine, and the exposure of this CP to Hg^{2+} resulted in a 5 nm red-shift of the absorption maximum and substantial fluorescence quenching. These changes were attributed to the polymer aggregation induced via the coordination of thymine residues to Hg^{2+} ions which provokes interpolymer π-stacking aggregation. The assay permitted the determination of Hg^{2+} over a concentration range from $3x10^{-5}$ to $3x10^{-4}$ M. Moreover, the fluorescence quenching response of the PTT (thymine-functionalized

[174] J. Zheng, and T. M. Swager, *Macromolecules*, **2006**, *39*, 6781.
[175] A. Alvarez-Diaz, A. Salinas-Castillo, M. Camprubí-Robles, J. M. Costa-Fernandez, Rosario Pereiro, R. Mallavia, and A. Sanz-Medel, *Anal. Chem.*, **2011**, *83*, 2712.
[176] A. Ono, and H. Togashi, *Angew. Chem. Int. Ed.*, **2004**, *43*, 4300.
[177] C. Qin, X. Wu, B. Gao, and H. Tong, *Macromolecules*, **2009**, *42*, 5427.
[178] I. B. Kim, B. Erdogan, J. N. Wilson, and U. H. F. Bunz, *Chem. Eur. J.*, **2004**, *10*, 6247.

polythiophene) was selective for Hg^{2+} over Mg^{2+}, Ca^{2+}, Mn^{2+}, Co^{2+}, Ni^{2+}, Cu^{2+}, and Zn^{2+} since the fluorescence quenching efficiency of PTT by Hg^{2+} ions is approximately eight times higher than that of Zn^{2+}, and 2.5 times higher than that of Cu^{2+}.

The above results indicate that metal sensing with CPs should involve a chelating agent on the CP able to transducer the metal sensing. The first chelator to come into clinical use was EDTA, initially employed to treat lead intoxication and for the removal of radionuclides.[179] Other chelators used in clinical treatments were D,L-2,3-dimercapto-1-propanesulfonic acid (DMPS), and DMSA.[180,181,182] The later was used in the treatment of heavy metals intoxication due to its low toxicity and great ability to chelate lead, mercury, and organic mercury.[183]

In this section is reported the synthesis of a new water-soluble polythiophene (Figure 57) which can be used to optically detect the presence of heavy metal ions such as lead and mercury. For this, it has combined the fluorescence properties of polythiophene with the chelation ability of DMSA that can provoke a variation of the polythiophene backbone enhancing the PL self-quenching of the polymer. In addition, the PL behaviour of the new water-soluble polythiophene it has been studying, as well as the PL emission quenching by the addition of K^{+}, Sr^{2+}, Ca^{2+}, Cd^{2+}, Pb^{2+}, and Hg^{2+}.

[179] H. Foreman, and J. G. Hamilton, *AECD-3247*, **1951**, 1.
[180] T. D. Hoover, and H. V. Aposhian, *Toxicol. Appl. Pharmacol.*, **1983**, *70*, 160.
[181] E. A. H. Friedheim, and C. Corvi, *J. Pharm. Pharmacol.*, **1975**, *27*, 624.
[182] M. M. Jones, A. D. Weaver, and M. A. Basinger, *J. Inorg. Nucl. Chem.*, **1981**, *43*, 2175.
[183] G. Rischitelli, P. Nygren, C. Bougatsos, M. Freeman, and M. Helfand, *Pediatrics*, **2006**, *118*, 1867.

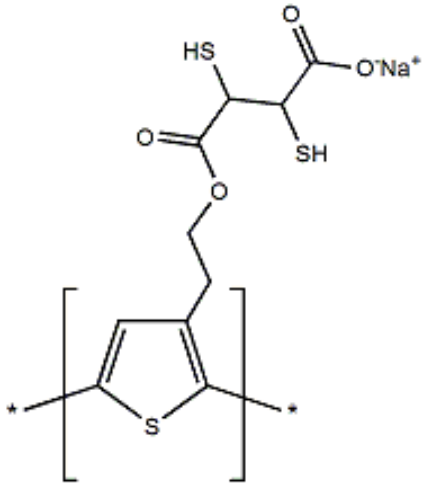

Figure 57. Monomer structure of the synthesized π-π conjugated polymer.

5.4.2 *Results*

The new fluorescent water-soluble conjugated polymer PTE-DMSA is based on a polythiophene backbone functionalized with DMSA that creates complexation sites for heavy ions like Pb^{2+}, Cd^{2+} and Hg^{2+}. The method used to polymerize the monomer 1 is the iron(III) chloride catalyzed polymerization proposed by Sugimoto et al. This method permits obtaining good molecular weight and good regioregularity.[184] The synthetic route to obtain PTE-DMSA is summarized in Scheme 10, and the coloured polymer solutions obtained during the different steps of the polymer functionalization are shown in Figure 58.

The PTE-DMSA solubility in water is quite satisfactory after the addition of a small volume (around 2% v/v) of tetrahydrofuran, ethanol, or acetone as can be seen in Figure 58 (forth vial from the left). Figure 59 shows the UV-Vis spectrum of an aqueous solution of PTE-DMSA ($1.3x10^{-5}$ M).

[184] R. Sugimoto, S. Taketa, H. B. Gu, and K. Yoshino, *Chem. Express*, **1986**, *1*, 635.

Scheme 10. Schematic Illustration of the Synthetic Route Used to Obtain the PTE-DMSA.

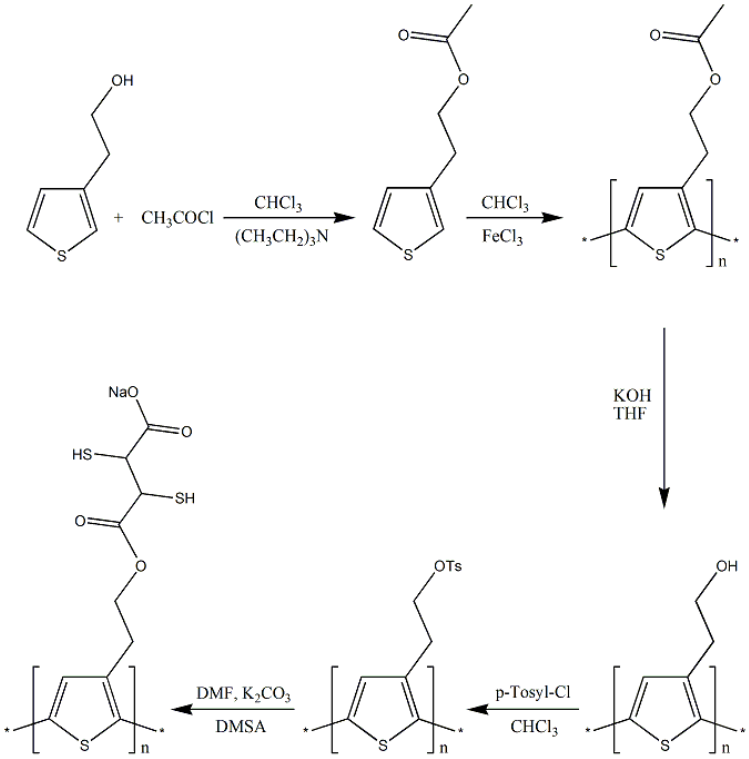

Figure 58. Dispersions of the synthesized polymers during the different synthesis steps under UV illumination (350 nm). From the left, the first vial contains the polythiophene with ester group in chloroform (PTEAc), the second vial corresponds to the polythiophene with hydroxyl group in THF (PTEOH), the third vial contains the polythiophene with the p-toluensulfonate group in methanol (PTETS), and the forth vial contains the polythiophene functionalized with DMSA in water (PTE-DMSA).

5. *Results and Discussions*

The spectrum presents a broad absorption maximum at 410 nm which is attributed to transitions within the conjugated π-orbital system. The emission spectrum, also shown in Figure 59, presents a maximum at 530 nm when PTE-DMSA is excited at 410 nm, close to the wavelength of the absorption maximum.

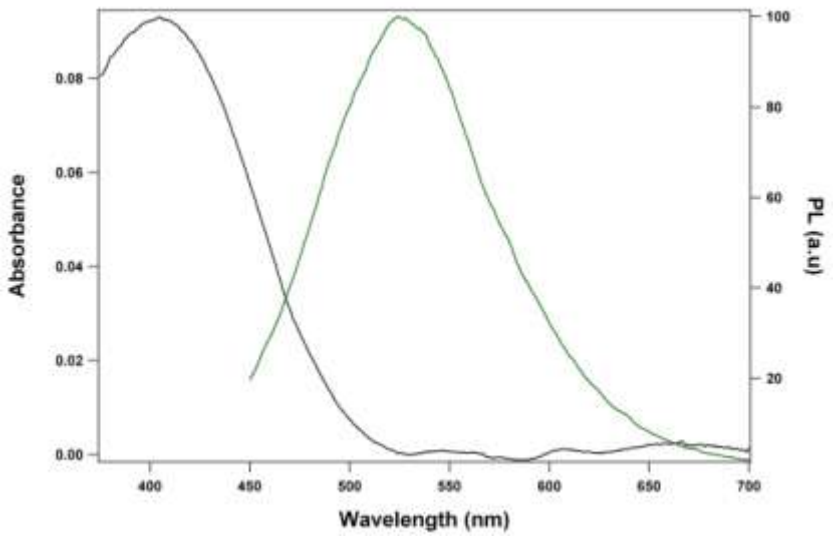

Figure 59. The black line is the UV-Vis spectrum of the PTE-DMSA in aqueous solution with a concentration of 1.3×10^{-5} M. The green line is the emission spectrum of the former PTE-DMSA solution excited at 410 nm.

The binding of metal ions to DMSA decreases the colloidal stability of the polymer and provokes a variation in its chain configuration causing the aggregation of the polymer and the subsequent decrease in the PL emission. The quantitative measure of the PL quenching efficiency by the addition of metal ions is given by the Stern-Volmer equation [1].

It can be assumed that quenching occurs by the formation of a complex between the polymer and metals ions, thus the quenching can be described by static quenching. In such case the linear dependence of F_0/F on [*Q*] given in equation [1] can be easily derived by consideration of the association constant for complex formation K_S and in this case $K_{SV} = K_S$. It has

been measured the PL behaviour of PTE-DMSA in presence of a series of metal ions such as K^+, Sr^{2+}, Ca^{2+}, Cd^{2+}, Pb^{2+}, and Hg^{2+} whose standard reduction potential relative to the standard hydrogen electrode increases from K^+ (-2.93 V) up to Hg^{+2} (+0.85 V). The standard reduction potential is an important parameter to take into account when measuring the PL quenching with metals since the polymer could suffer electron transfer to the metal cation.

Figure 60 shows the absorbance (left side) and the PL quenching (right side) of PTE-DMSA by K^+ (Figure 60A), Sr^{2+} (Figure 60B), and Ca^{2+} (Figure 60C) in aqueous solutions with polymer concentration $1.3x10^{-5}$ M. The concentration of the metal ions is indicated in the insets of Figure 60 and varies between the initial concentration of $2.5x10^{-5}$ M up to the final concentration of $1.2x10^{-4}$ M.

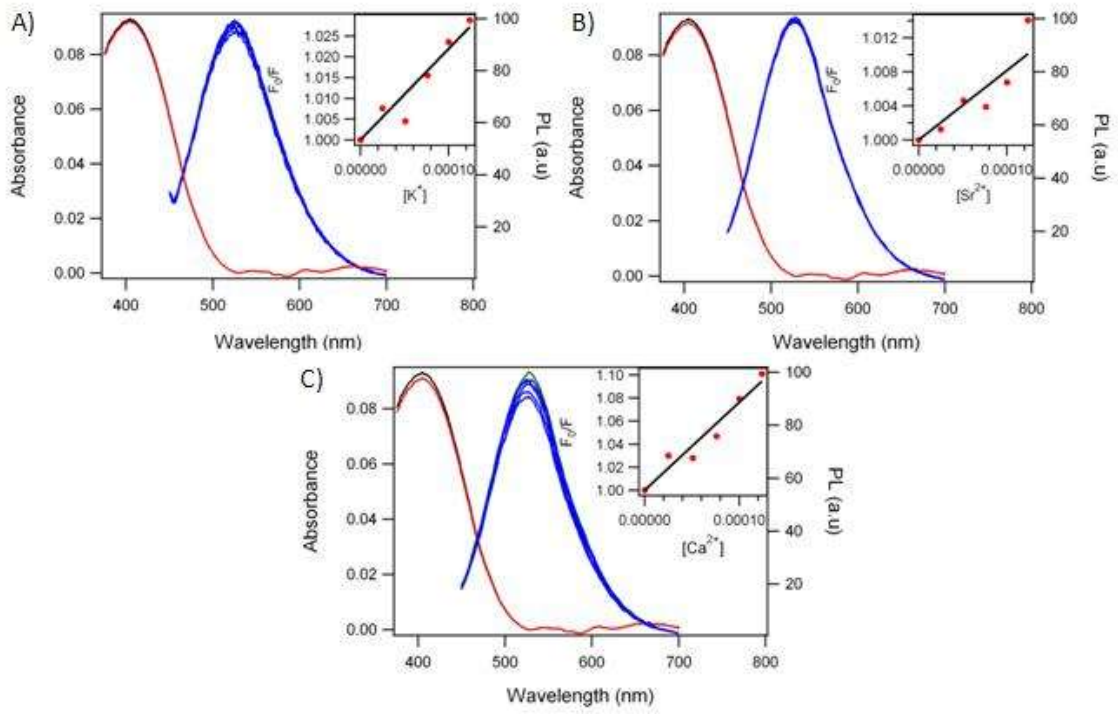

Figure 60. A) The black line is the UV-Vis spectrum of an aqueous solution $1.3x10^{-5}$ M of PTE-DMSA and the red line is after the addition of KNO_3 ($1.2x10^{-4}$ M). The green line represents the PL emission (λ_{exc} = 425 nm) of the former polymer solution before the addition, and the blue lines after the addition of KNO_3 from the initial concentration $2.5x10^{-5}$ M to the final

concentration of $1.2x10^{-4}$ M. B) The same polymer and metal ion concentrations but with $Sr(NO_3)_2$, and C) with $Ca(NO_3)_2$. In the inset is represented the Stern-Volmer plot for fluorescence quenching by the respective metal ion.

As can been appreciate from Figure 60, the PL emission of PTE-DMSA is scarcely quenched after the addition of K^+, Sr^{2+}, and Ca^{2+}. The K_{SV} values derived from the Stern-Volmer plot are given in Table 1. The small K_{SV} values obtained seems to indicate that these cations slightly interact with the CP since the PL quenching is small indicating they cannot decrease the stability of the PTE-DMSA in water.

Figure 61 shows the absorbance (left side) and the PL quenching (right side) of PTE-DMSA after the addition of Cd^{2+}, Pb^{2+}, and Hg^{2+} in aqueous solutions with polymer concentration $1.3x10^{-5}$ M. On the contrary to what happened to the previous set of ions the addition of Cd^{2+}, Pb^{2+}, and Hg^{2+} provoke a conspicuous PL quenching of the PTE-DMSA solution. This fact can be attributed to the capacity of the DMSA group which is able to interact with these three cations changing the PL emission of the polymer.

After the addition of cadmium acetate the maximum of the UV-Vis spectrum decreases its intensity, this effect is concomitant with the formation of particles in the solution that can be seen with the naked eye, which indicates the polymer aggregation. In addition to the PL quenching it can be observed a blue-shift emission from 530 nm to 521 nm (Figure 61A). The aggregation of PTE-DMSA induced by Cd^{2+} could change the polymer conformation, creating kink defects that reduce the electrons $\pi-\pi$ delocalization. That increases the HOMO-LUMO energy gap relative to that of the uncomplexed polymer chain.[185] Therefore, the collapse of the conjugated chain induced by Cd^{2+} would explain the blue-shift.

[185] T. Q. Nguyen, V. Doan, and B. J. Schwartz, *J. Chem. Phys.*, **1999**, *110*, 4068.

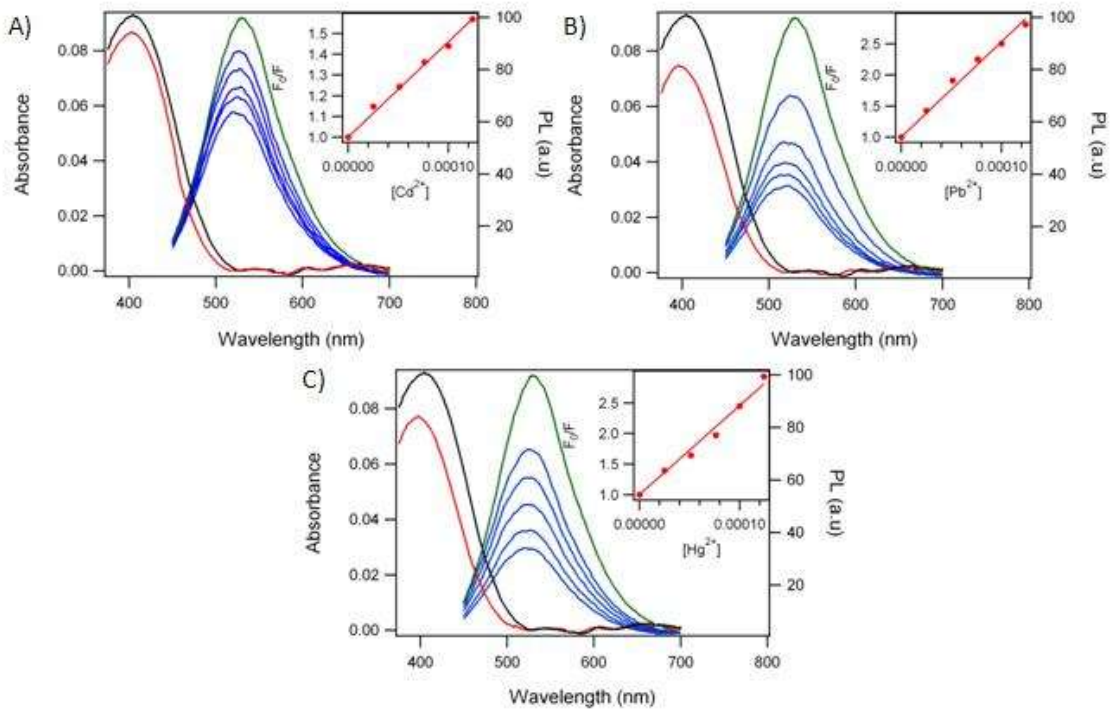

Figure 61. A) The black line is the UV-Vis spectrum of an aqueous solution $1.3x10^{-5}$ M of PTE-DMSA and the red line is after the addition of KNO_3 ($1.2x10^{-4}$ M). The green line represents the PL emission (λ_{exc} = 425 nm) of the former polymer solution before the addition, and the blue lines after the addition of cadmium acetate from the initial concentration $2.5x10^{-5}$ M to the final concentration of $1.2x10^{-4}$ M. B) The same polymer and metal ion concentrations but with lead nitrate, and C) with mercury acetate. In the inset is represented the Stern-Volmer plot for fluorescence quenching by the respective metal ion.

The association constant (K_{SV} = K_S), derived from the Stern-Volmer plot, of PTE-DMSA with Cd^{2+} is $K_{SV} = 4.3x10^3$ which is much higher than K_{SV} calculated for K^+, Sr^{2+}, and Ca^{2+} (Table 1) indicating the preference of PTE-DMSA for Cd^{2+}.

As can be seen in Figure 61B, the addition of lead nitrate to the CP solution provokes higher PL quenching respect the addition of cadmium acetate, and the corresponding K_{SV} is $1.5x10^4$. This value is more than 3 times higher than the K_{SV} obtained with Cd^{2+}. The PL maximum

is blue-shifted ≈11 nm, while the UV-Vis peak is blue-shifted ≈8 nm. The higher blue-shift observed in this case can be attributed to the higher affinity of PTE-DMSA for Pb^{2+} that is able to induce a bigger conformational change in the polymer. [185,186] Similarly to what happen with cadmium and lead, the addition of mercury acetate provokes a change in the PL emission of PTE-DMSA (Figure 61C). The absorbance peak is blue-shifted ≈8 nm and the PL maximum ≈10 nm. However, as can be seen in the inset of Figure 61C the dependence of F_0/F on $[Hg^{2+}]$ shows a small upward curvature.

This could indicate that two processes are responsible of the observed quenching that could be treated as a combination of dynamic and static quenching. However, since the upward curvature is small it can be possible use the linear fitting to obtain K_{SV} = 1.4x10^4. The standard reduction potential of Hg^{2+} is +0.85 V vs. SHE indicating that it is a strong oxidant agent. Furthermore, if it takes into account that the polymer is rich in electron it can be assumed that an oxidative doping (p-type) process could take place after the addition of Hg^{2+}. Thus, for the Hg^{2+}, the blue-shift would be attributed to two factors: i) the conformational PTE-DMSA change due to the polymer aggregation induced by mercury cations, and ii) the partial polymer oxidation.

Life-time PL measurements were performed to elucidate the processes responsible of the observed quenching (pure static or a combination of dynamic and static) and are shown in Figure 62. For dynamic quenching $F_0/F = \tau_0/\tau$, while for static quenching $\tau_0/\tau = 1$ since the life time is τ_0.[10] Figure 62 shows in logarithmic scale the normalized counts for the solution of pure PTE-DMSA, and after the addition of Cd^{2+} (blue line), and Hg^{2+} (red line).

[186] B. J. Schwartz, *Annu. Re*V. *Phys. Chem.*, **2003**, *54*, 141.

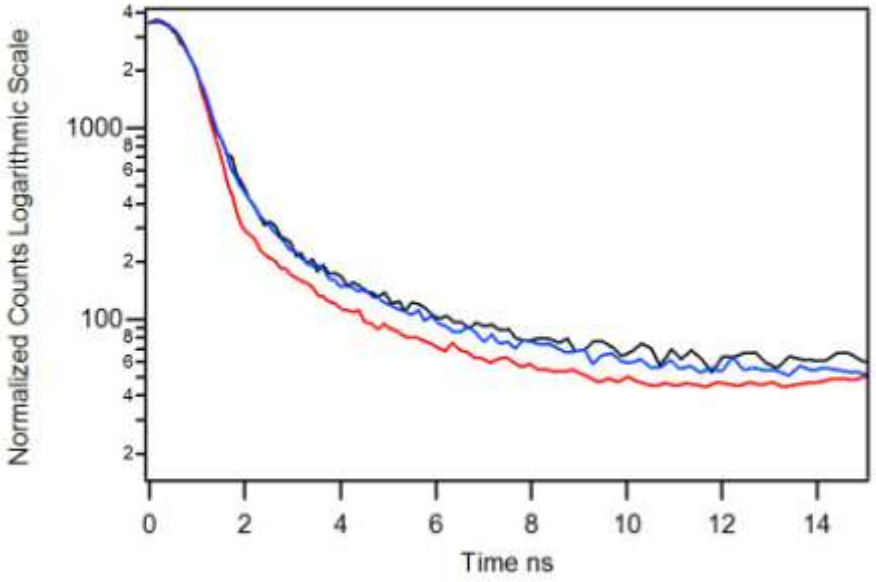

Figure 62. The black line represents the decay time profile of an aqueous solution $1.3x10^{-5}$ M of PTE-DMSA, the blue line represents the decay time profile of the polymer solution after the addition of Cd^{2+} ($1.2x10^{-4}$ M), and the red line represents the decay time profile of the polymer solution after the addition of Hg^{2+} ($1.2x10^{-4}$ M). The excitation wavelength was 410 nm.

Fluorescence lifetime measurements in polyelectrolytes are the result of a complex distribution of the decay times in the system. For fitting the decay-time profiles two exponential decay functions were necessary for the three samples. This indicates that early fluorescence decay is dominated by a double exponential component. Thus, the intensity is assumed to decay as the sum of individual exponential decays as expressed by equation [8].

The data were analyzed using the multiexponential mode and the life-times for pure PTE-DMSA were calculated 0.58 ± 0.06 ns and 3.08 ± 0.22 ns with a $\chi^2 = 0.82$, residuals 2.5%, and DW = 2.1. After the addition of Cd^{2+} the polymer life-time does not change since the smaller life-time is 0.58 ± 0.04 ns and the higher is 2.91 ± 0.15 ns with a $\chi^2 = 0.97$, residuals 3.6%, and DW = 1.8. This result confirms that the observed quenching is driven by static process. On the other

hand, the PTE-DMSA life-times after the addition of Hg^{2+} considerably changes: the smaller life time is 0.29 ± 0.01 ns, and the higher is 1.86 ± 0.09 ns, with a χ^2 = 0.90, residuals 1.5%, and DW = 2.1. The upward curvature in the Stern-Volmer plot together with the change measured in the life times indicate that when Hg^{2+} is present the PL quenching is a combination of static and dynamic quenching.

Table 1. Resume of the Photoluminescence Quenching of PTE-DMSA by Metal Cations.

Quencher	Emission λ_{max} shift (nm)	K_{sv}
K^+	0	200
Sr^{2+}	0	80
Ca^{2+}	0	700
Cd^{2+}	9	4.300
Pb^{2+}	11	15.000
Hg^{2+}	10	15.000

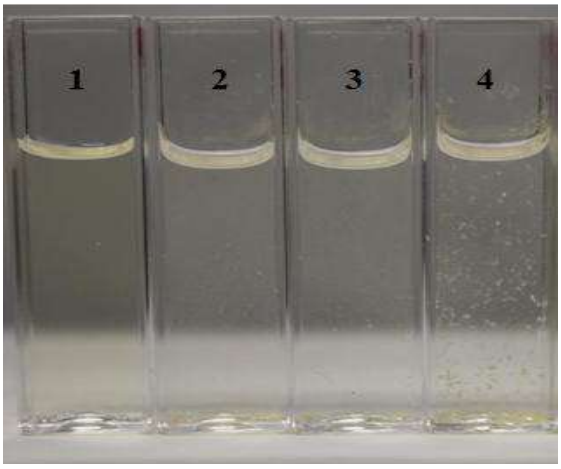

Figure 63. The cuvette 1 contains the pure PTE-DMSA solution; the cuvette 2 is the polymer solution after the addition of Cd^{2+}; cuvette 3 is the polymer solution after the addition of Pb^{2+}, and cuvette 4 is the polymer solution after the addition of Hg^{2+}. In all samples the polymer concentration is $1.3x10^{-5}$ M and the cation concentration is $1.2x10^{-4}$ M.

In Table 1 is summarized the shift of the PL maximum, and the K_{SV} obtained when PTE-DMSA is quenched by the different cations investigated in this work. The K_{SV} values indicate that PTE-DMSA exhibits good selectivity towards cations such as Pb^{2+} and Hg^{2+} in comparison with K^{+}, Sr^{+2}, and Ca^{+2}. On the other hand, even though the K_{SV} of Pb^{2+} and Hg^{2+} is ≈4 times higher than that of Cd^{2+} these later ions would interfere in the detection of Pb^{2+} and Hg^{2+} with PTE-DMSA. However as is shown in Figure 63 (cuvette 4), the presence of Hg^{+2} induce the formation of aggregates than can be visualized with the naked eye.

5.4.3 *Conclusion*

The new water-soluble conjugated polymer PTE-DMSA exhibits good fluorescence properties and could be used as chemosensor of Pb^{2+} and Hg^{2+}. The main process involved in the cations sensing is the aggregation process that induces the photoluminescence quenching of the CP. However, for the detection of the mercury (II) ions the results indicate that process involved during the quenching is the combination of the aggregation process between the ion and the DMSA lateral chain and the oxidation process provoked by the mercury (II) ions. The PTE-DMSA polymer exhibits very good Stern-Volmer constant for the ions of lead (II) and mercury (II).

5.5 *CPs as Reducing and Stabilizing Agent in the Synthesis of Multiresponsive Hybrid Materials*

5.5.1 *Use of CPs to Control the Shape of Au Nanocrystals: Synthesis of Highly Anisotropic Nanocrystals*

5.5.1.1 *Introduction*

The controlled synthesis of nanocrystals have attracted considerable attention because of their widespread use in catalysis, photonics, electronics, optoelectronics, biological labeling, imaging, sensing, and surface-enhanced Raman scattering (SERS).[187,188,189,190,191,192,193] Although the syntheses of spherical nanoparticles have been well developed for many materials, the fabrication of nanocrystals with other shapes is still a challenge nowadays. The morphological control of the asymmetric Au nanostructures permits to tune the localized surface plasmon resonance in the visible and near-IR regions.

From all the above studies it seems clear that the mechanism of crystal growth plays an important role in the size and shape obtained and therefore is of major importance if one aims to obtain tailored nanostructures.[75,73,93,94,95,96,97,98,99,100,101,102] In this work, it has been studied the synthesis of Au nanostructures using the water-soluble conjugated polymer PTEBS for the reduction of $HAuCl_4$ and the stabilization of the Au nanocrystals, and the effect of cadmium and lead ions on the later synthesis. PTEBS is a polymer whose polythiophene backbone could serve

[187] T. S. Ahmadi, Z. L. Wang, T. C. Green, A. Henglein, and M. A. El-Sayed, *Science*, **1996**, *272*, 1924.
[188] S. A. Maier, L. M. Brongersma, P. G. Kik, S. Meltzer, A. A. G. Requicha, and H. A. Atwater, *Adv. Mater.*, **2001**, *13*, 1501.
[189] X. Teng, D. Black, N. J. Watkins, Y. Gao, and H. Yang, *Nano Lett.*, **2003**, *3*, 261.
[190] T. A. Taton, C. A. Mirkin, and R. Letsinger, *Science*, **2000**, *289*, 1757.
[191] A. G. Tkachenko, H. Xie, D. Coleman, W. Glomm, J. Ryan, M. F. Anderson, S. Franzen, and D. L. Feldheim, *J. Am. Chem. Soc.*, **2003**, 125, 4700.
[192] X. Zhang, M. A. Young, O. Lyandres, and R. P. Van Duyne, *J. Am. Chem. Soc.*, **2005**, *127*, 4484.
[193] J. Chen, F. Saeki, B. J. Wiley, H. Cang, M. J. Cobb, Y. Z. Li, L. Au, H. Zhang, M. B. Kimmey, X. Li, and Y. Xia, *Nano Lett.*, **2005**, *5*, 473.

as a tail group (hydrophobic) whereas the sulfonate group could act as a head group (hydrophilic).[194] In addition the thiophene ring can bind the surface of the Au nanoparticles stabilizing them in water more efficiently than poly(vinyl-pyrrolidone). Furthermore, the PTEBS is a polymer rich in electrons that can be used to reduce the $HAuCl_4$ in water without the need to use capping agents or surfactants. First, It was studied the synthesis of Au nanocrystals using the conjugated polymer PTEBS; subsequently the effect of adding to the previous polymer solution $Cd(COOCH_3)_2$ or $Pb(NO_3)_2$; and finally the effect of adding together PTEBS, $Cd(COOCH_3)_2$ and $Pb(NO_3)_2$.

5.5.1.2 *Results*

In a typical synthesis conducted with PTEBS alone, the reaction is performed at room temperature and a PTEBS stock solution is diluted in 9.8 mL of water with a final concentration of $1x10^{-4}$ M (in monomer repeating units), and finally a small aliquot of $HAuCl_4$ (186 μL, $1x10^{-4}$ M) is added to the flask. Figure 64A shows the TEM of a grid prepared with an aliquot withdrawn from the solution after 10 minutes from the beginning of the reaction. In Figure 64A the Au colloidal size is comprised between 20 and 200 nm. After 1 day reaction, a new grid was prepared with an aliquot withdrawn from the solution and the result, presented Figure 64B, shows monodisperse nanoparticles with a diameter varying from 8 nm up to 12 nm.

[194] M. Laurenti, J. Benito-Retama, F. Garcia-Blanco, B. Frick, and E. Lopez-Cabarcos, *Langmuir*, **2009**, *25*, 9579.

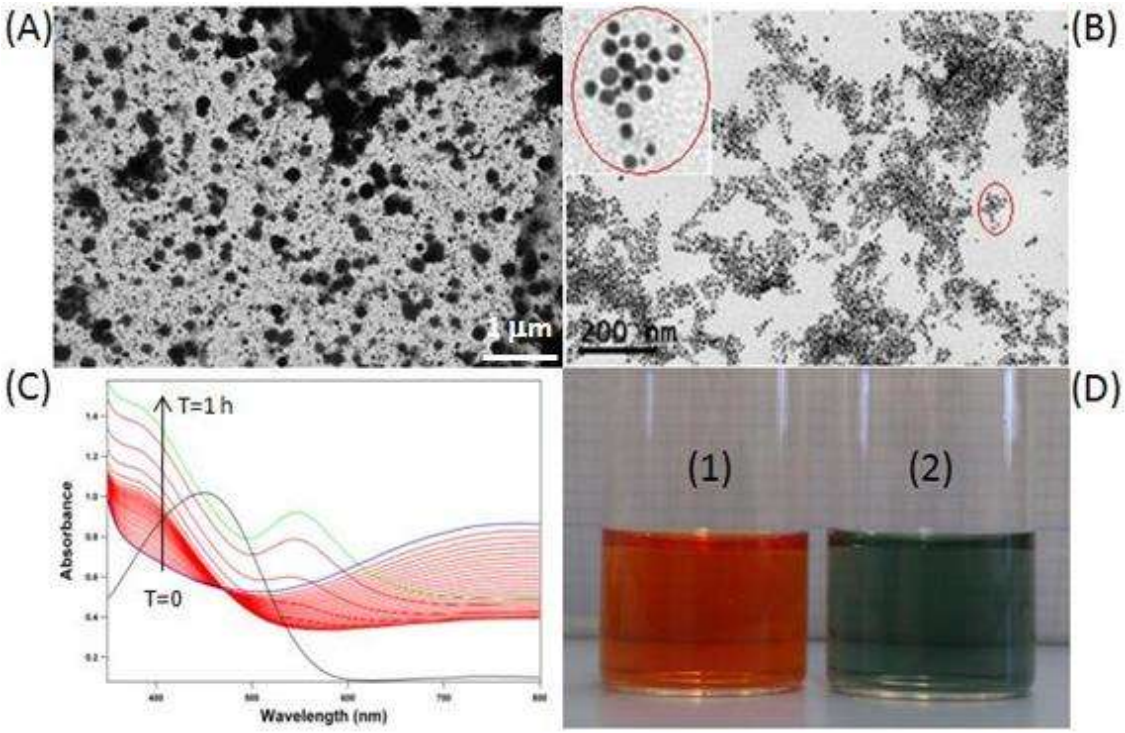

Figure 64. (A) TEM micrograph of the nanoparticles obtained using PTEBS 1mM and $HAuCl_4$ 1mM recorded after 10 minutes from the beginning of the reaction. The size of the Au colloids comprises between 200 nm and 20 nm. The scale bar is 1 µm. (B) TEM image of the particles obtained in the previous reaction recorded after 1 day from the beginning of the reaction. Surprisingly, there are only spherical gold nanoparticles with diameter between 8 and 12 nm. The scale bar is 200nm. (C) UV-Vis kinetic experiment showing the evolution of the absorbance as a function of the time (black arrow). The black line represents the absorbance spectrum of pure PTEBS, 1 mM, in water which presents a maximum at 450 nm. In this solution is added the $HAuCl_4$, 1mM, and the blue line represents the UV-Vis absorbance recorded immediately after the salt addition. The spectrums were taken every two minutes (red lines) for one hour. (D) The vial **(1)** shows the typical orange color of the PTEBS in water, while vial **(2)** represents the color of the solution immediately after the addition of $HAuCl_4$ (blue-green).

Figure 64C shows the evolution of the absorbance as a function of time during one hour after the PTEBS was mixed with $HAuCl_4$. In Figure 64C the black line represents the absorbance of a PTEBS solution (1mM) showing an intense peak at 440 nm typical of this polymer. After the addition of $HAuCl_4$ (1mM) to this solution the peak at 440 nm instantaneously blue-shift due to the oxidation and a new band appears at ≈800 nm (green line taken 10 seconds after the addition of $HAuCl_4$). This later peak gradually disappears and the blue line is the absorbance of the solution 1 hour after the beginning of the reaction whereas the red lines are the absorbance of the solution taken every two minutes. The black arrow indicates the time-course of the reaction taking place between the PTEBS and $HAuCl_4$. In fact, the intense band at ≈800 nm decreases while at ≈535 nm appears the surface plasmon resonance (SPR) of the Au nanocrystals. This result is consistent with the TEM images (Figure 64A and 64B) since the band at ≈800 nm could be the SPR of the Au colloids visible in Figure 64C and the SPR at ≈530 nm is typical for spherical gold nanocrystals. Vial 1 in Figure 64D shows the typical intense orange color of the PTEBS in water, vial **2** shows the blue-green color of the solution shortly after the addition of $HAuCl_4$ to the aqueous PTEBS solution.

As was previously indicated, the size of the objects in Figure 64A (taken after 10 minutes) is much bigger than those in Figure 64B (taken after 1 day). In 2003, Prased et al. reported the digestive-ripening of highly polydisperse gold colloids by alkylthiols, alkylamines, alkylsilanes, and alkylphosphines ligands molecules.[195,196] The digestive ripening process can narrow the size distribution of a polydisperse colloid significantly. Unlike the well known Ostwald ripening in which large particles grow at the expense of small particles, this process narrows the distribution by sharing the material among different sizes of particles until a thermodynamically stable size is reached in the colloid. Thiophenes molecules are similar to

[195] B. L. V. Prasad, S. I. Stoeva, C. M. Sorensen, and K. J. Klabunde, *Langmuir*, **2002**, *18*, 7515.
[196] B. L. V. Prasad, S. I. Stoeva, C. M. Sorensen, and K. J. Klabunde, *Chem. Mater.*, **2003**, *15*, 935.

alkylthiols and the phenomenon observed in the TEM investigation could be attributed to the digestive-ripening induced by thiophene molecules at room temperature.

The investigation of the influence of cadmium acetate and lead nitrate on the synthesis of gold nanocrystals using PTEBS and $HAuCl_4$ was done using the same reaction condition used previously with PTEBS alone. Moreover, to understand and separate the effects of the two metal ions they will be studied separately. The concentration of $Cd(COOCH_3)_2$ used for the investigation was 1.6 mM and the addition of the aliquot to reaction medium was done before the addition of the 186 μL of $HAuCl_4$ ($1x10^{-4}$ M) in order to avoid possible time dependent effects of the cadmium ions. The TEM micrograph presented in Figure 65A shows that the presence of Cd ions induces a huge change on the morphology of the Au nanostructure. In comparison with the synthesis performed with PTEBS alone, the colloidal gold lost its spherical shape (Figure 64B), the majority of the structures do not have well-defined geometrical contours, and the nanostructures show anisotropy. The Cd^{2+} also modifies the rate of the reaction which now takes 3 days to be completed indicating a slowdown of the crystal growing rate.

A parallel study was performed to investigate the effect of lead nitrate on the gold nanoparticles synthesis. As well as cadmium, the effect of lead ions over the synthesis of Au nanocrystals is not well known. Since 1930, lead nitrate is used in the gold cyanidation process; by contrast the knowledge of the effect of lead nitrate on the surfaces of gold is still fragmentary. However, it seems that the lead nitrate is able to make the oxidative etching of the gold nanocrystals in combination with the dissolved molecular oxygen[197]. In our case, the reaction needs 3 days to be completed as it occurred in the presence of Cd^{2+} and the result obtained is shown in Figure 65B. It can be seen the lead nitrate effect on the synthesis is completely different from the cadmium acetate and from PTEBS alone. The TEM picture shows irregular colloidal gold crystals with some planar structure. The white rectangle remarks the

[197] G. Deschenes, R. Lastra, J. R. Brown, S. Jin, O. May, and E. Ghali, *Minerals Engineering*, **2000**, *13*, 1263.

possible effect of gold re-dissolution and re-crystallization due the oxidative etching and the evolution of the colloid structure from a 2D platelet (gray zone with fringes) to 3D colloids (dark zone).

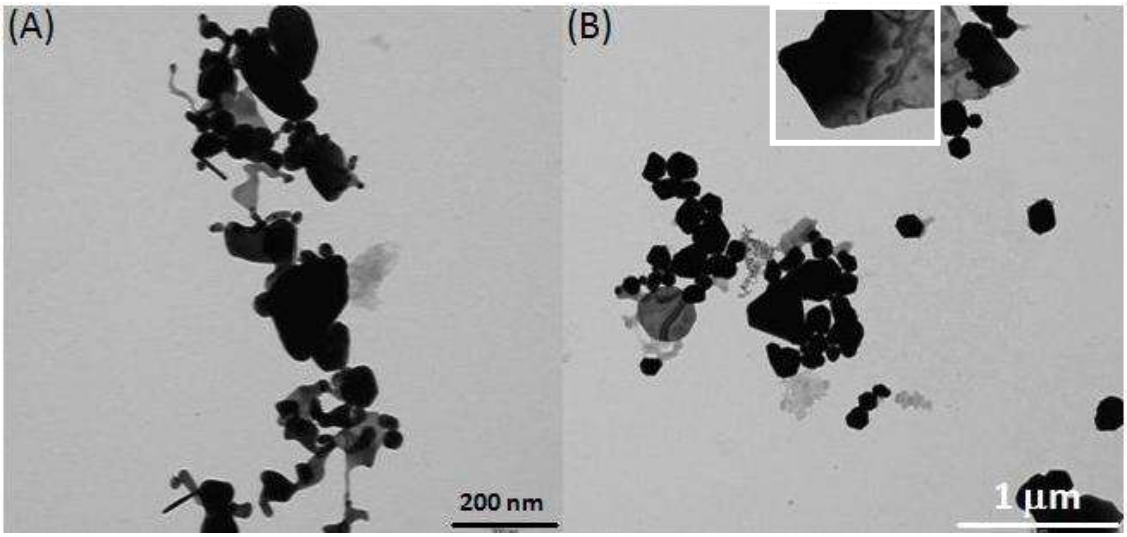

Figure 65. (A) The TEM picture shows Au nanocrystals obtained using a concentration of cadmium acetate of 1.6 mM. The scale bar is 200 nm and the accelerating voltage is 100kV. (B) This picture shows Au nanocrystals synthesized using a concentration of lead nitrate of 1.6 mM. The white rectangle indicates the possible effect of the lead ions on the Au nanocrystals. The scale bar is 1 µm and the accelerating voltage is 100kV.

Since it has been produced three different nanostructures using PTEBS alone or in combination with Cd or Pb ions, it has been decided to synthesize gold nanocrystals using PTEBS together with Cd and Pb ions. The reaction was carried out using the same recipe used for cadmium or lead with the difference that the lead nitrate and cadmium acetate aliquots were added together. Three concentrations of cadmium and lead were assayed (0.53, 1.06, and 1.6 mM) and a ratio 1:1 between cadmium and lead was maintained.

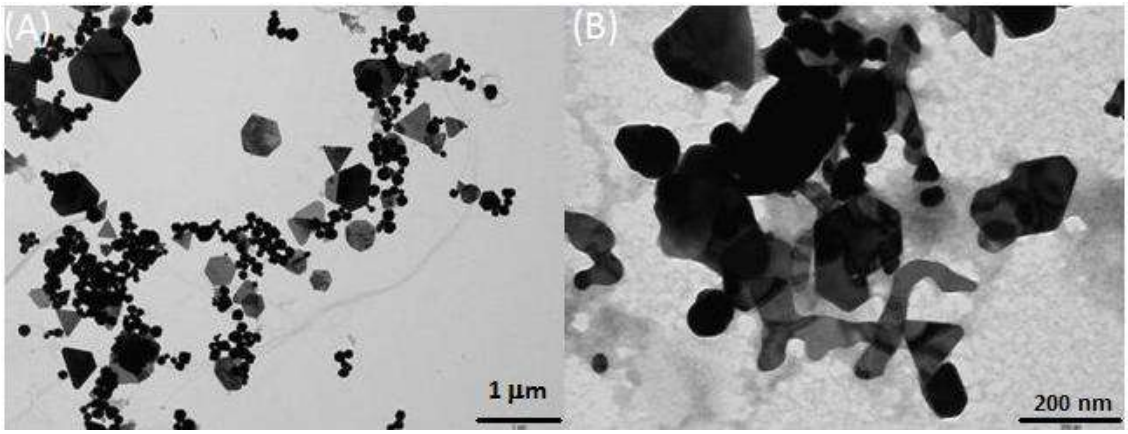

Figure 66. (A) TEM image of the synthesized Au nanostructures using a concentration of 0.53 mM of lead nitrate and cadmium acetate. The scale bar is 1 µm and the accelerating voltage is 100kV. (B) TEM image of the synthesized Au nanostructures using a concentration of 1.06 mM of lead nitrate and cadmium acetate. The scale bar is 200 nm and the accelerating voltage is 100kV.

Figure 66A shows the Au nanostructures obtained mixing cadmium and lead with a concentration of 0.53 mM. The synthesized colloids present two kinds of morphology: a platelet 2D structure and a 3D colloidal structure. The hexagonal and triangular nanoplates have a size between 150 nm and 1 µm and the average size is around 450 nm, while the remaining gold has polydisperse polyhedral shape. Figure 66B shows the Au nanostructures obtained when the concentration is increased up to 1.06 mM and as can be seen the nanocrystals obtained have a different morphology. The structures present high anisotropy and can be separated into two kinds of shapes: an anisotropic platelet structure, and 3D irregular colloids.

The synthesis of gold nanocrystals when the concentration of Cd^{2+} and Pb^{2+} is increased up to 1.6 mM is shown in Figure 67. The obtained Au nanocrystals are highly anisotropic and they present an interesting morphology with hexagonal, triangular, and truncated geometry with tails attached to one edge of the Au nanostructures.

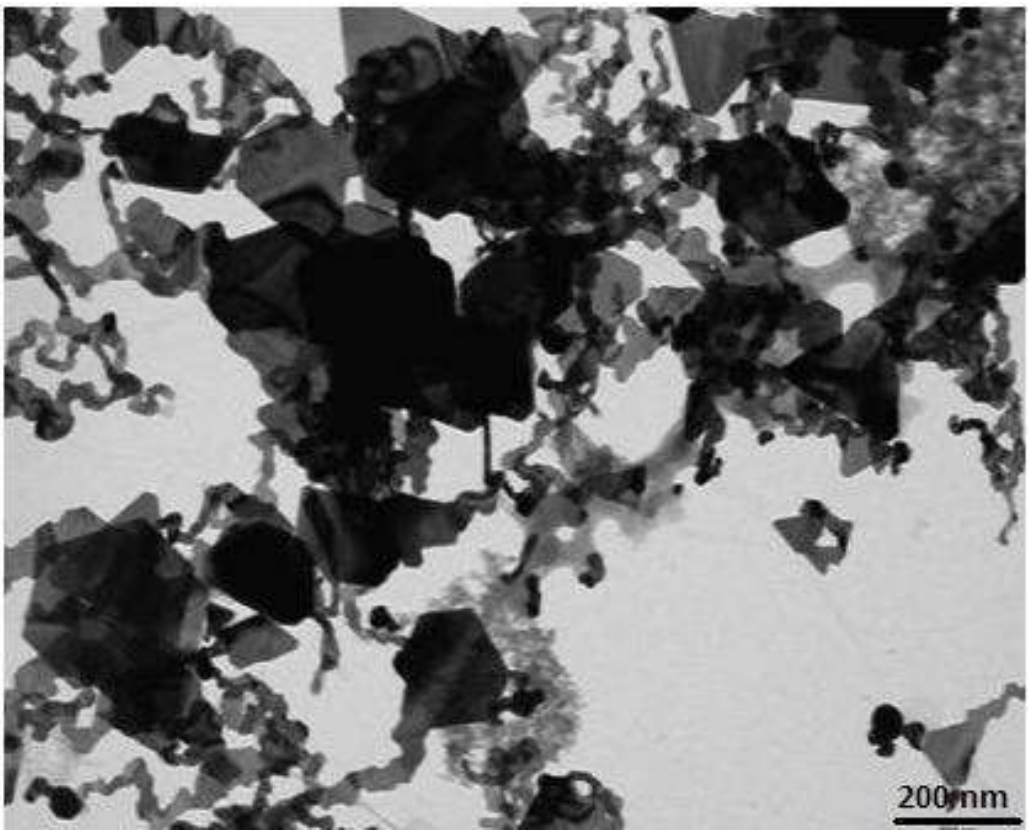

Figure 67. The TEM picture shows the synthesized Au nanocrystals with a concentration of Cd^{2+} and Pb^{2+} of 1.6 mM. The Au nanocrystals obtained present a high content of anisotropy and the majority of them are hexagons, triangles, and truncated triangles with tails. The scale bar is 200 nm and the accelerating voltage 100kV.

The presence of these two ions with a concentration bigger than 1.06 mM conspicuously change the morphology obtained as is illustrated in Figures 66A, 66B, and 67. The ion effect on the synthesis of Au nanostructures can be explained looking the different ratio [Ions]/[Au^{3+}]. A ratio close to 1:2 produces structures with platelet and 3D shapes, but when the ratio is increased up to 1.06:1 the effect on the anisotropy is remarkable indicating that the threshold ratio to observe anisotropy is around 1:1. An increase of the ratio [Ions]/[Au^{3+}] to 1.6:1 induces dramatic changes and the structures obtained are highly anisotropic (Figures 67 and 68). It is important to point out the synergistic effect of both ions when they are used together in the

synthesis of the gold nanoparticles. In fact, if one compares the synthesis showed in Figure 65A with that showed in Figure 67, the amount of cadmium is the same in both cases, but the anisotropy of the nanostructures is much higher when cadmium is used in combination with lead. Moreover, when cadmium is used alone the structures do not present a platelet structure.

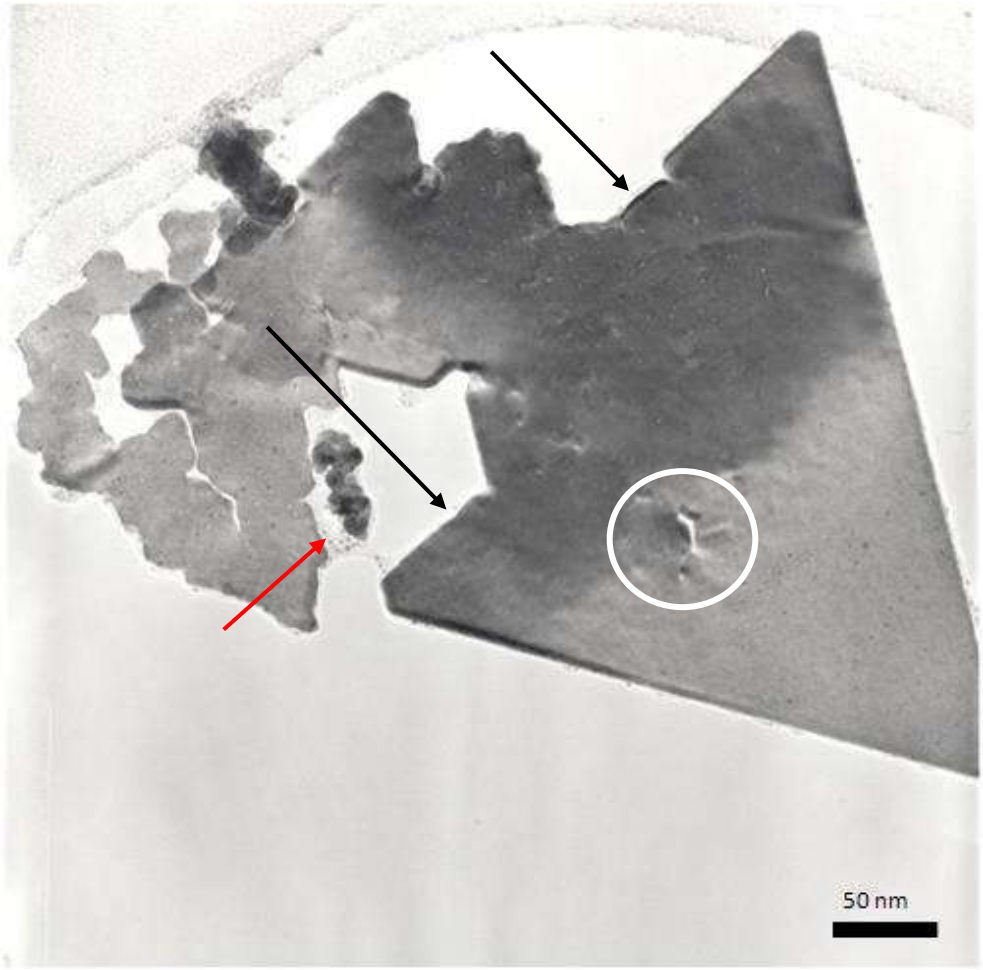

Figure 68. The TEM image shows a single Au nanoplate with tail surrounded by small Au nanoparticles. The white circle indicates a part of the Au sheet where the structure is not totally formed. The red arrow shows some nanoparticles close to the growing tail, while the black arrows differentiate the different height of the same triangle edge. The scale bar is 50 nm and the accelerating voltage is 200 kV.

A typical particle isolated from those presented in Figure 67 is shown in Figure 68 with relevant information concerning the formation mechanism of these anisotropic nanostructures. The white circle remarks the presence of tiny holes that seems to indicate that the triangle plate is the product of attachment of two previously formed Au plates. The black arrows in the Figure 68 substantiate this interpretation pointing out different thickness on the same edge of the plate that only would be possible when two different plates attach together. Moreover, the tails are present only on one edge of the nanoplates indicating somewhat like "fusion" of two nanosnakes. The red arrow shows very small gold nanoparticles (diameter 1.6 nm) close to the formed nanostructure which would facilitate the fusion of the small plate to the tail.

In order to better understand this mechanism a TEM investigation was performed preparing a grid withdrawing an aliquot after 2 hours from the beginning of the reaction with Cd^{2+} and Pb^{2+} (1.6 mM). Figure 69A and B shows the formation of growing nanosnakes that gradually assemble into nanoplates with triangular or hexagonal geometries and a pendant tail attached to one edge. The length of these nanosnakes is considerable and is comprised between 50 nm and 500 nm, while the Au nanoparticles present a more monodisperse size and both structures are embedded inside the PTEBS matrix (grayer zone). If one compares the UV-Vis experiment in Figure 69C with the one in Figure 64C can be distinguished a difference in the behavior of the reaction. In the case with PTEBS alone after 1 hour the SPR of the Au nanocrystals is already visible, while in the case with Cd^{2+} and Pb^{2+} (1.6 mM) the spectrum taken after 3 hours does not show any SPR of spherical Au nanoparticles.

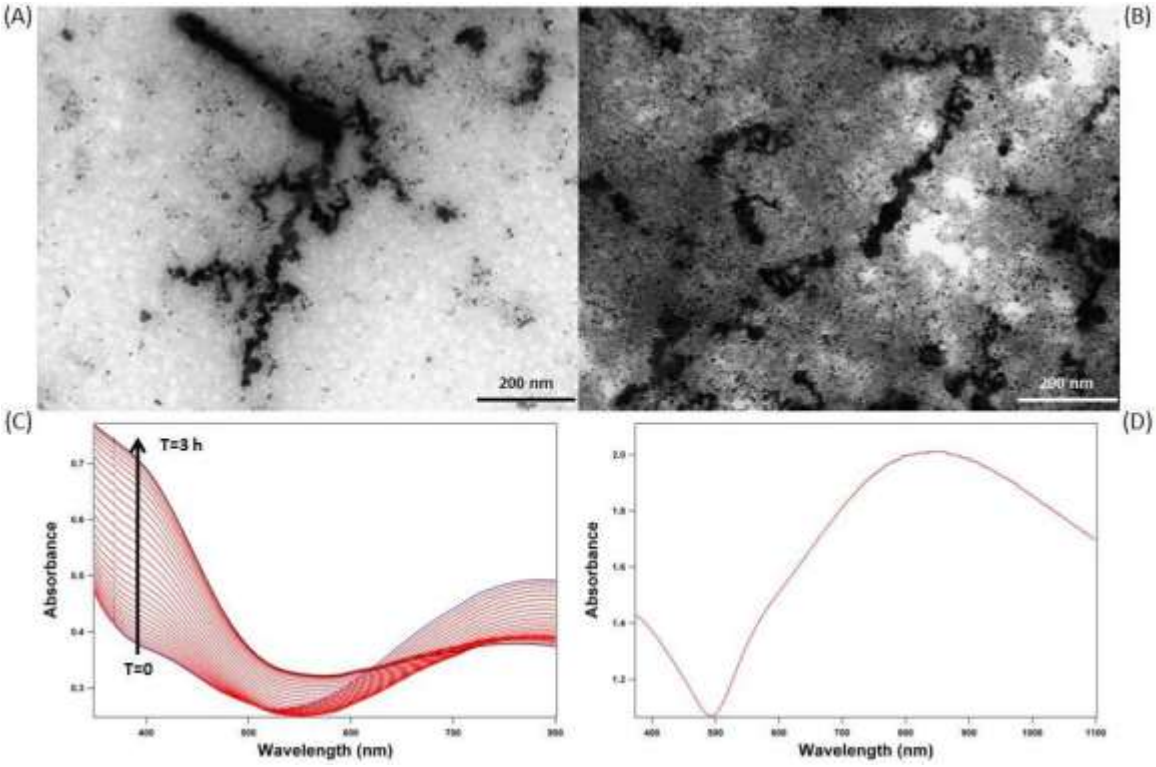

Figure 69. (A) and (B) TEM grid prepared withdrawing an aliquot from the reaction with Cd and Pb with a concentration of 1.6 mM, after 2 hours from the beginning of the reaction. The scale bar is 200 nm and the accelerating voltage is 100Kv. (C) UV-Vis kinetic experiment showing the evolution of the absorbance as a function of the time (black arrow). The experiment is carried out mixing PTEBS in water with a concentration of 1 mM, Cd^{2+} 1.6 mM, Pb^{2+} 1.6 mM, and $HAuCl_4$ 1 mM. The blue line represents the UV-Vis absorbance shortly after the addition of Au and the black line is the absorbance after 3 hours. The spectrums are taken every 3 minutes (red lines) for 3 hours. (D) Final SPR of the Au anisotropic nanocrystals obtained after 3 days. The maximum of the SPR is at 870 nm.

The SPR of the final nanocrystals was recorded after 3 days from the beginning of the reaction and the maximum is at 870 nm making these nanostructures interesting for application in near infrared spectroscopy. Similar Au structures as showed in Figure 67 and 68 were reported in 2008 by Lim et al[102] using poly(vinyl-pyrrolidone). In 2008 Muñoz et al. also

synthesized core-shell silver@polypyrrole nanosnakes[198,199] that they attribute to the presence of pyrrole. These nanostructures are metastable at the reaction conditions and undergo bending and folding while they preserve the crystallographic coherence. They propose "nanomalleability" to explain how such extraordinary "coherent" shape evolution may be taking place.[199] However, in our case the oriented attachment takes place between adjacent snakes of the same structure and small gold nanoparticles until it forms a triangle or hexagonal structure. Nevertheless, the most important factor that induces these conformation is the effect of $Cd(COOCH_3)_2$ and $Pb(NO_3)_2$ when they are used with the conjugated polymer PTEBS. The use of conjugated polymer to stabilize gold nanostructure was reported in 2005 by Ah et al.[200] They proposed a novel method to obtain monodisperse size-controlled gold nanoplates with high purity from the reduction of $HAuCl_4$ by reduced amount of sodium citrate, which kinetically controls the reaction pathway, in the presence of poly(vinyl-pyrrolidone).

Extensive HR-TEM investigation was performed on the gold nanostructure synthesized using the concentration 1.6 mM of Cd^{2+} and Pb^{2+}. Figure 70 shows a typical HRTEM image taken by directing the electron beam perpendicular to the flat faces of a single anisotropic nanostructure. The inset shows the related selected area electron diffraction (SAED) pattern obtained by focusing the electron beam on a nanoplate lying flat on the TEM grid. The SAED pattern reveals the hexagonal symmetry diffraction spot pattern, demonstrating that the gold nanostructure is a single crystal, with the preferential growth direction along the Au {111} plane.[201] Three sets of spots can be identified based on d-spacing calculated from the SAED image. The inner set (circle) with a lattice spacing of 2.4 Å could correspond to the forbidden 1/3{422} reflection. The set (box) with a spacing of 1.4 Å could be assigned to the {220} reflection of the *fcc* Au. It indicates that the prepared nanoplates are single-crystalline with {111}

[198] D. Muñoz-Rojas, J. Oró-Solé, O. Ayyad, and P. Gómez-Romero, *Small*, **2008**, *4*, 1301.
[199] D. Muñoz-Rojas, J. Oró-Solé, O. Ayyad, and P. Gómez-Romero, *J. Phys. Chem. C*, **2008**, *112*, 20312.
[200] C. S. Ah, Y. J. Yun, H. J. Park, W. J. Kim, D. H. Ha, and W. S. Yun, *Chem. Mater.*, **2005**, *17*, 5558.
[201] X. P. Sun, S. J. Dong, and E. K. Wang, *Angew. Chem., Int. Ed.*, **2004**, *43*, 6360.

lattice planes as the basal planes. The outer set (triangle) with a lattice spacing of 0.8 Å could be indexed to the {422} Bragg reflection. These two sets of reflection are both allowed by an *fcc* lattice.[202,203] This phenomenon has been observed by many authors in Au or Ag plate-like crystals, and a number of explanations for the occurrence of such forbidden reflections have been suggested.

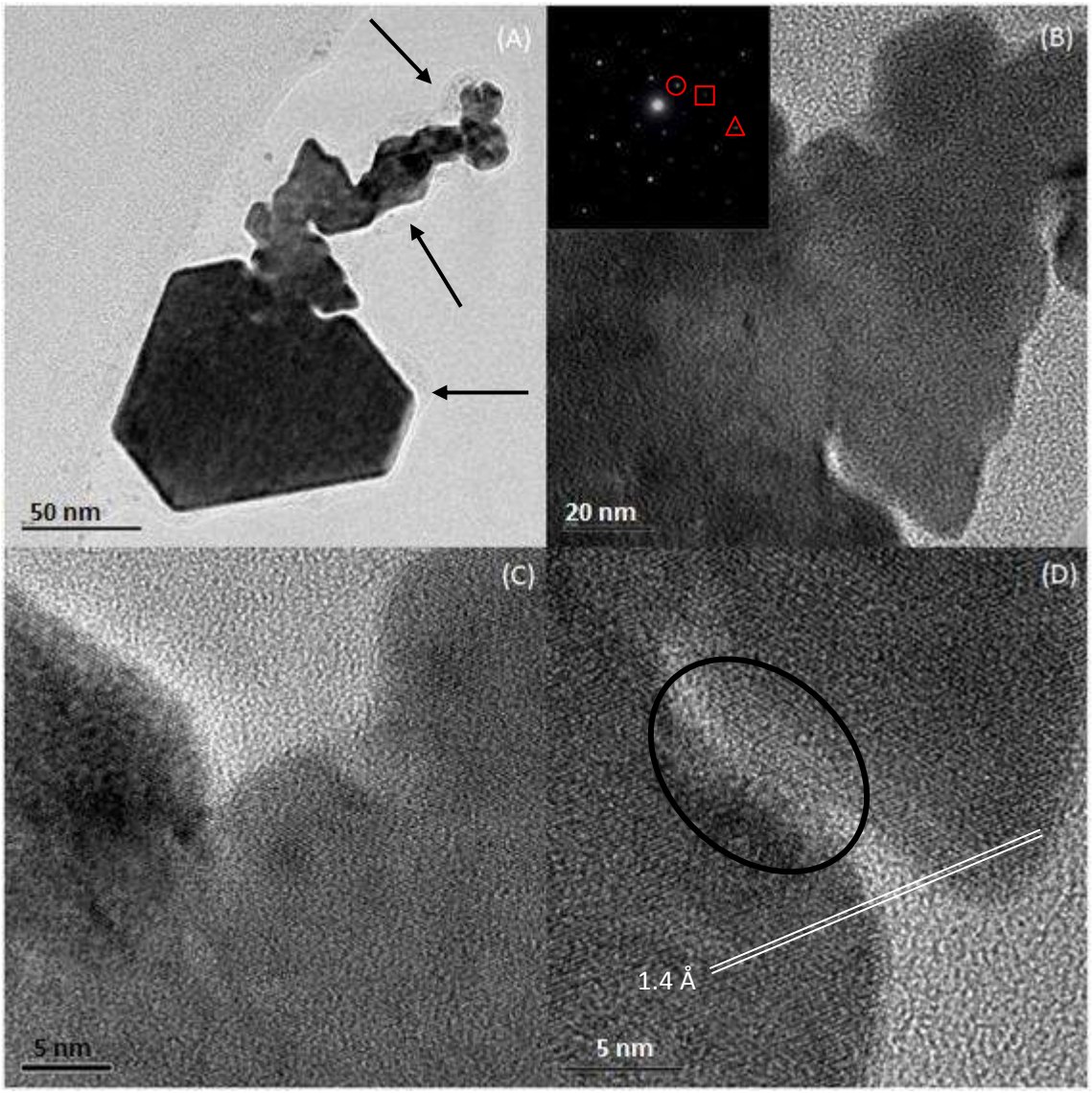

Figure 70. (A) HRTEM of a single Au anisotropic truncated triangle with tails. The black arrows indicate the PTEBS covering the nanostructure and at the end of the tail small Au nanoparticles

[202] I. Washio, Y. J. Xiong, Y. D. Yin, and Y. N. Xia, *Adv. Mater.*, **2006**, *18*, 1745.
[203] R. C. Jin, Y. W. Cao, C. A. Mirkin, K. L. Kelly, G. C. Schatz, and J. G. Zheng, *Science*, **2001**, *294*, 1901.

embedded into the polymer. The scale bar is 50 nm. (B) Close-up of (A) showing the part of the tail attached to the nanostructure. In the inset is shown the related SAED pattern obtained by focusing the electron beam on the nanoplate. The SAED pattern reveals the hexagonal symmetry diffraction spot pattern demonstrating that the Au nanoplate is a single crystal. The spots circled, squared, and triangled could be indexed respectively to the forbidden 1/3{422}, {220}, and {422} Bragg reflection. The scale bar is 20 nm. (C) and (D) is the close-up of image (B) at the top and the bottom of the structure, respectively. The scale bar is 5 nm and the accelerating voltage is 300kV.

HRTEM results confirmed that all the nanoplates have the same crystallographic structure. According to the results of Pileni et al. such 1/3{422} forbidden reflections observed on the plate-like structures of Au or Ag could be attributed to (111) stacking faults lying parallel to the (111) surface and extending across the entire nanosheet.[204] The close-up in Figure 70B shows that the nanotail is attached to the truncated triangle forming a unique structure. In addition the fringes are separated by 1.4 Å (Figure 70D) that can be ascribed to the {220} reflection for an *fcc* lattice of gold and it is also visible the partially formed Au layer between the tail and the truncated triangle (black ellipse). Moreover, the presence of the same distance between the fringes on the tail and the truncated triangle demonstrates crystallographic coherence, proven also by the SAED. It is important to notice that XRF does not detect any trace of Pb^{2+} on the Au nanostructures while detects trace of Cd^{2+}, but its signal is very weak for a quantitative estimation. Scheme 11 resumes the different structures obtained when the Au nanocrystals are synthesized using the PTEBS; PTEBS and Cd; PTEBS and Pb; and PTEBS with Cd and Pb together.

[204] V. Germain, J. Li, D. Ingert, Z. L. Wang, and M. P. Pileni, *J. Phys. Chem. B*, **2003**, *107*, 8717.

Scheme 11. Resume of the different Au structures obtained using PTEBS 1 mM, 1.6 mM of Cd, and 1.6 mM of Pb together.

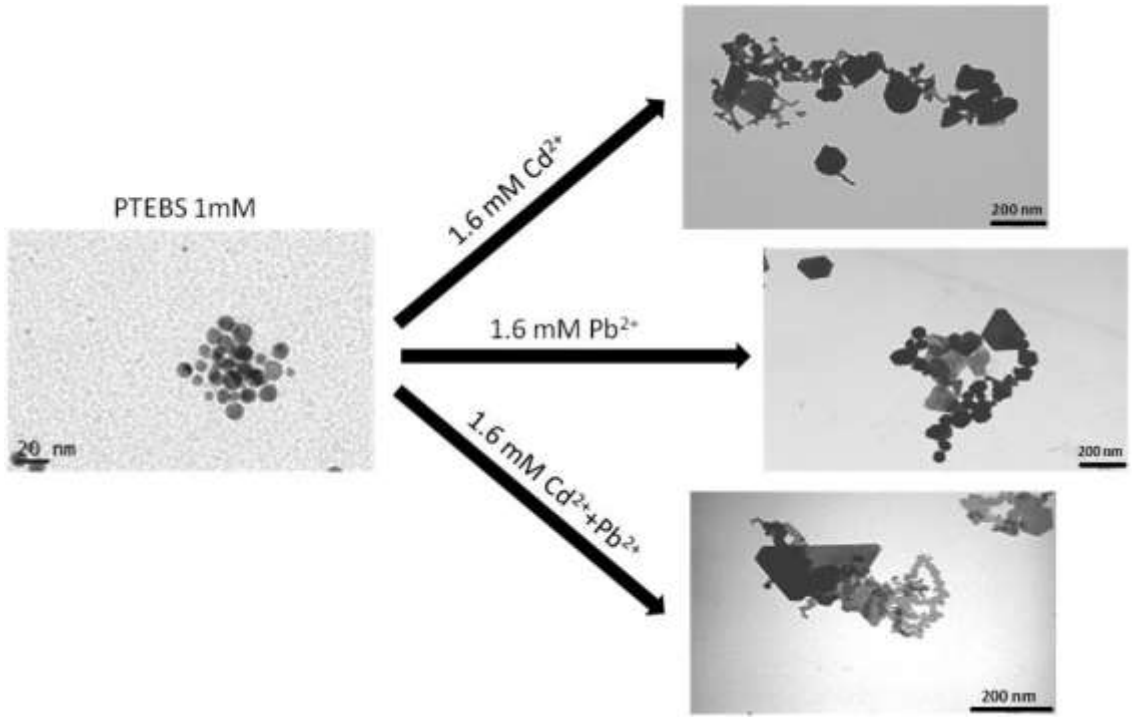

5.5.1.3 *Conclusions*

It has been developed a one-pot method strategy for the fabrication of complex Au nanoarchitecture using the water-soluble conjugated polymer PTEBS. The CPs gave spherical Au nanoparticles with a diameter comprised between 8 and 12 nm and could act as stabilizer and reductant agent. The conjugated polythiophene seems to induce the digestive-ripening of the Au colloids until the nanoparticles reach a diameter between 8-12 nm. The addition of $Cd(COOCH_3)_2$ with a concentration of 1.6 mM changes dramatically the morphology of the Au nanocrystals inducing partial anisotropy, while the addition of $Pb(NO_3)_2$ with a concentration of 1.6 mM

produces polydisperse Au colloids. However, when both ions are used together their effect is to induce high anisotropy and the nanostructures obtained present triangular and hexagonal morphology with tails attached to one edge. The production of these nanostructures is of interest for their potential application in the field of the NIR and IR.

5.5.2 *Mechanism of Formation of Hybrid Microparticles*

5.5.2.1 *Introduction*

Thermosensitive microgels can be combined with inorganic components like quantum dots,[205] silver,[206] gold,[207] or magnetic nanoparticles[208] to yield nanostructured and multifunctional hybrid material. The combination between the organic and the inorganic components establishes a symbiotic relation in which the microgels give colloidal stability as well as stimuli responsive features while the inorganic counterpart provide quantum properties like photoluminescence,[36,209] surface plasmon resonance,[210] or magnetism.[211]

In some works the localization of the inorganic material is on the outer part of the microgels. This sort of decoration can be produced by either exploiting charge interactions between the nanoparticles and the microgels[210] or by covalent bonds between the microgels and the magnetic material.[212] However, one of the major drawbacks concomitant with this strategy is a reduction of the colloidal stability which leads to nanoparticles aggregation. This approach usually leads to the homogeneous distribution of the nanoparticles within the microgels.[213] Nevertheless this sort of decoration presents two major disadvantages; firstly, not all the inorganic nanoparticles can be done in the presence of microgels and this limits the strategy only for synthesis performed at mild conditions. Secondly, the high specific surface of the nanoparticles can favor interactions between the nanoparticles and the microgel matrix, which normally affect the thermal response of the microgels being possible to block the LCST

---

[205] D. Jaczewski, N. Tomczak, M. Y. Han, and G. J. Vancso, *Macromolecules*, **2009,** *42*, 1801.
[206] H. Xu, J. Xu, Z. Zhu, H. Liu, and S. Liu, *Macromolecules*, **2006**, *39*, 8451.
[207] T. Kawano, Y. Niidome, T. Mori, Y. Katayama, and T. Niidome, *Bioconjugate Chem.*, **2009**, *20*, 209.
[208] B. Luo, X. J. Song, F. Zhang, A. Xia, W. L. Yang, J. H. Hu, and C. C. Wang, *Langmuir*, **2010**, *26*, 1674.
[209] S. Bai, C. Wu, K. Gawlitza, R. Von Klitzing, M. Ansorge-Schumacher, and D. Wang, *Langmuir*, **2010**, *26*, 12980.
[210] M. Karg, Y. Lu, E. Carbo-Argibay, I. Pastoriza-Santos, J. Pérez-Juste, L. M. Liz-Marzán, and T. Hellweg, *Langmuir*, **2009**, *25*, 3163.
[211] S. Schachschal, A. Balaceanu, C. Melian, D. Demco, T. Eckert, W. Richtering, and A. Pich, *Macromolecules*, **2010**, *43*, 4331.
[212] F. Zhang, and C. C. Wang, *Langmuir*, **2009,** *25*, 8255.
[213] A. Pich, S. Bhattacharya, Y. Lu, V. Boyko, and H. J. P. Adler, *Langmuir*, **2004**, *20*, 10706.

when high amount of inorganic nanoparticles are loaded within microgels and for this reason, only microgels with a limited amount of inorganic material are produced using this method.[133,214]

To overcome the previous disadvantages many efforts have been done to produce hierarchical microgels in which the inorganic nanoparticles are locate in the core of the system.[215,216,217,218] However these methodologies have not been successfully applied with Fe_3O_4 nanoparticles, since its surface inhibits the polymerization reaction. This impediment has been related with the capacity to mediate in redox process and thus to transfer an electron to the radical, which subsequently stops the polymerization.[219] This is the reason why some authors cover the surface of the magnetic nanoparticles with SiO_2 to overcome this problem but this solution present two mayor disadvantages, firstly the process turns into a tedious multistep procedure and secondly the incorporation of a second inorganic material diminishes the maximum magnetic moment of the final material. These problems have been recently solved[220] just by covering the nanoparticles with 3-bt, which hinders the nanoparticles surface oxidation. With this molecule is possible to create a simple method that yields thermosensitive microgels, which present a magnetic core, formed by cluster of Fe_3O_4 nanoparticles.

5.5.2.2 *Results*

In this work it has been performed a parametric study about the role of 3-bt molecule as well as the hydrophobic-hydrophilic character of the nanoparticles during the synthesis of the microgels and how they influence on the architecture of the final hybrid material. Figure 71

[214] J. Rubio-Retama, N. E. Zafeiropoulos, B. Frick, T. Seydel, and E. López-Cabarcos, *Langmuir*, **2010**, *26*, 7101.
[215] C. Dagallier, H. Dietsch, P. Schurtenberger, and F. Scheffold, *Soft Matter*, **2010**, *6*, 2174.
[216] R. Contreras-Cáceres, J. Pacifico, I. Pastoriza-Santos, J. Pérez-Juste, A. Fernandez-Barbero, and L. M. Liz-Marzán, *Adv. Funct. Mater.*, **2009,** *19*, 3070.
[217] R. Contreras-Cáceres, I. Pastoriza-Santos, R. A. Alvarez-Puebla, J. Pérez-Juste, A. Fernández-Barbero, and L. M. Liz-Marzán, *Chem. Eur. J.*, **2010**, *16*, 9462.
[218] A. Sánchez-Iglesias, M. Grzelczak, B. Rodríguez-González, P. Guardia-Girós, I. Pastoriza-Santos, J. Pérez-Juste, M. Prato, and L. M. Liz-Marzán, *ACS Nano*, **2009**, *3*, 3184.
[219] R. L. Rebodos, and P. J. Vikesland, *Langmuir*, **2010** early view DOI: 10.1021/la102461z.
[220] R. Contreras-Cáceres, S. Abalde-Cela, P. Guardia-Girós, A. Fernández-Barbero, J. Pérez- Juste, R. A. Alvarez-Puebla, and L. M. Liz-Marzán, *Langmuir,* **2011**, *27*, 4520.

shows a representative TEM image of the synthesized magnetic nanoparticles. As one can observe the size of the nanoparticles obtained by thermal decomposition was 13 nm while the size for those nanoparticles produced by coprecipitation was around 6 nm. These two different syntheses permitted to obtain magnetic nanoparticles with different hydrophobic-hydrophilic character that was exploited to control the magnetic core of the hybrid microgels.

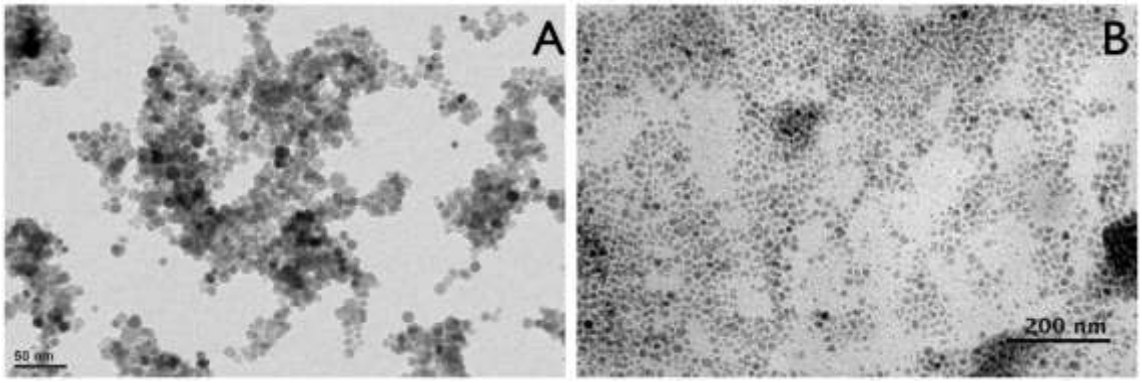

Figure 71. TEM image of (A) 13 nm edge length iron oxide nanoparticles synthesized by thermal decomposition and (B) 6 nm edge length iron oxide nanoparticles synthesized by coprecipitation method.

The dispersion in water of the magnetic nanoparticles synthesized using the thermal decomposition produced nanoparticle aggregates[221] with a mean hydrodynamic diameter of 188 ± 27 nm. With the aim of getting magnetic cluster with smaller sizes, magnetic nanoparticles were treated with different amounts (µL) of 3-butenoic acid. In this way and after incubating these nanoparticles with 3-bt during one hour at 70 °C, it was possible to reduce the mean hydrodynamic diameter of the clusters (see Figure 72).

[221] P. Qiu, C. Jensen, N. Charity, R. Towner, and C. Mao, *J. Am. Chem. Soc.*, **2010**, *132*, 17724.

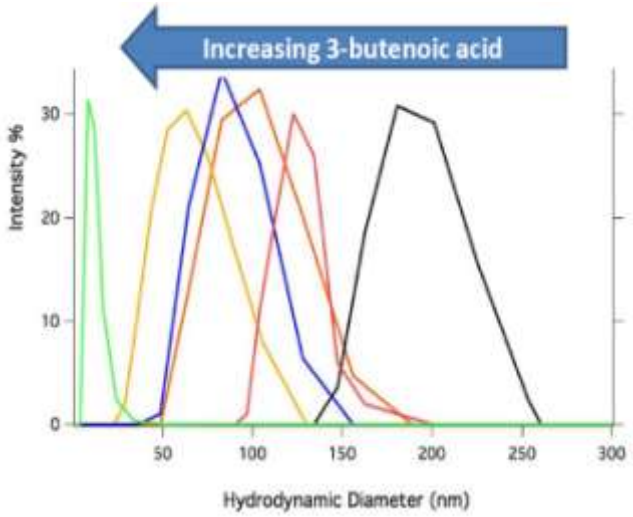

Figure 72. Evolution of the cluster size distribution, after addition of 3-bt: 0, 10, 20, 40, 100 µL. The left hand distribution curve shows the size distribution for the magnetic nanoparticles obtained by method II with 160 µL of 3-bt.

Figure 72 depicts the hydrodynamic diameter of the clusters treated with different concentrations of 3-butenoic acid. From this study can be inferred that 3-bt was able to disaggregate the magnetic clusters and reduce their size. The driving force of the size reduction would be the increment of the superficial charge of the magnetic nanoparticles that occurs when 3-bt is added. The scheme 1 summarizes the process that is involved in the nanoparticle segregation.

Scheme 12. (A) Representation of the iron nanoparticles surface modification and the effect on the hydrodynamic diameter. (B) TEM of nanoparticles cluster obtained after the process.

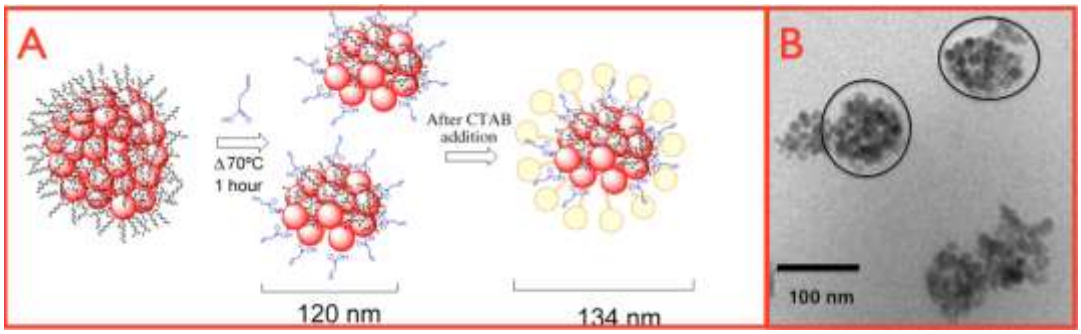

5. *Results and Discussions*

Disaggregation is a consequence of the extra surface charge provided to the particles by the 3-bt as confirmed by electrophoretic mobility that changes from $3.8x10^{-8}$ $m^{-2}V^{-1}s^{-1}$ for untreated particles (sample S0I) to $5.3x10^{-8}$ $m^{-2}V^{-1}s^{-1}$ sample S100I. For 3-bt amounts higher than about 100 µL, the charge bared by the particles saturates and cluster segregation stops being impossible to obtain single nanoparticles. In order to get the smallest magnetic cluster, nanoparticles produced by co-precipitation were modified by adding 3-bt. These nanoparticles without treating with 3-bt showed a hydrodynamic diameter of 20 ± 10 nm. When 160 µL of 3-bt was added to an aqueous dispersion of these nanoparticles the cluster size reduces to a hydrodynamic diameter of 12 ± 7 nm (See Table 1).

Table 2. Amount of 3-bt acid added for surface treatment, electrophoretic mobility (µ), hydrodynamic diameter for both, the magnetic cluster (Dh) and pNIPAM@Fe_3O_4 (Dh) and colloidal stability. Samples S0I to S100I are synthesized by method I and S160II by method II.

Sample	3-bt(µL)	µ (10^{-8} $m^{-2}V^{-1}s^{-1}$)	Dh (nm) magn. cluster	Dh (nm) Fe_3O_4@PNIPAM	Colloidal Stability
S0I	0	3.8 ± 0.1	188 ± 27	No measured	< 2 hours
S10I	10	4.2 ± 0.1	134 ± 12	600 ± 21	> 2 weeks
S20I	20	4.4 ± 0.1	110 ± 21	630 ± 23	> 2 weeks
S40I	40	5.2 ± 0.1	78 ± 15	674 ± 28	> 2 weeks
S100I	100	5.2 ± 0.1	55 ± 13	724 ± 32	> 2 weeks
S160II	160	-	12 ± 7	4800 ± 120	> 2 weeks

When NIPAM is polymerized in the presence of the magnetic clusters hybrid microgels were obtained. Figure 73 shows the shape of the hybrid microgels obtained after using different magnetic clusters.

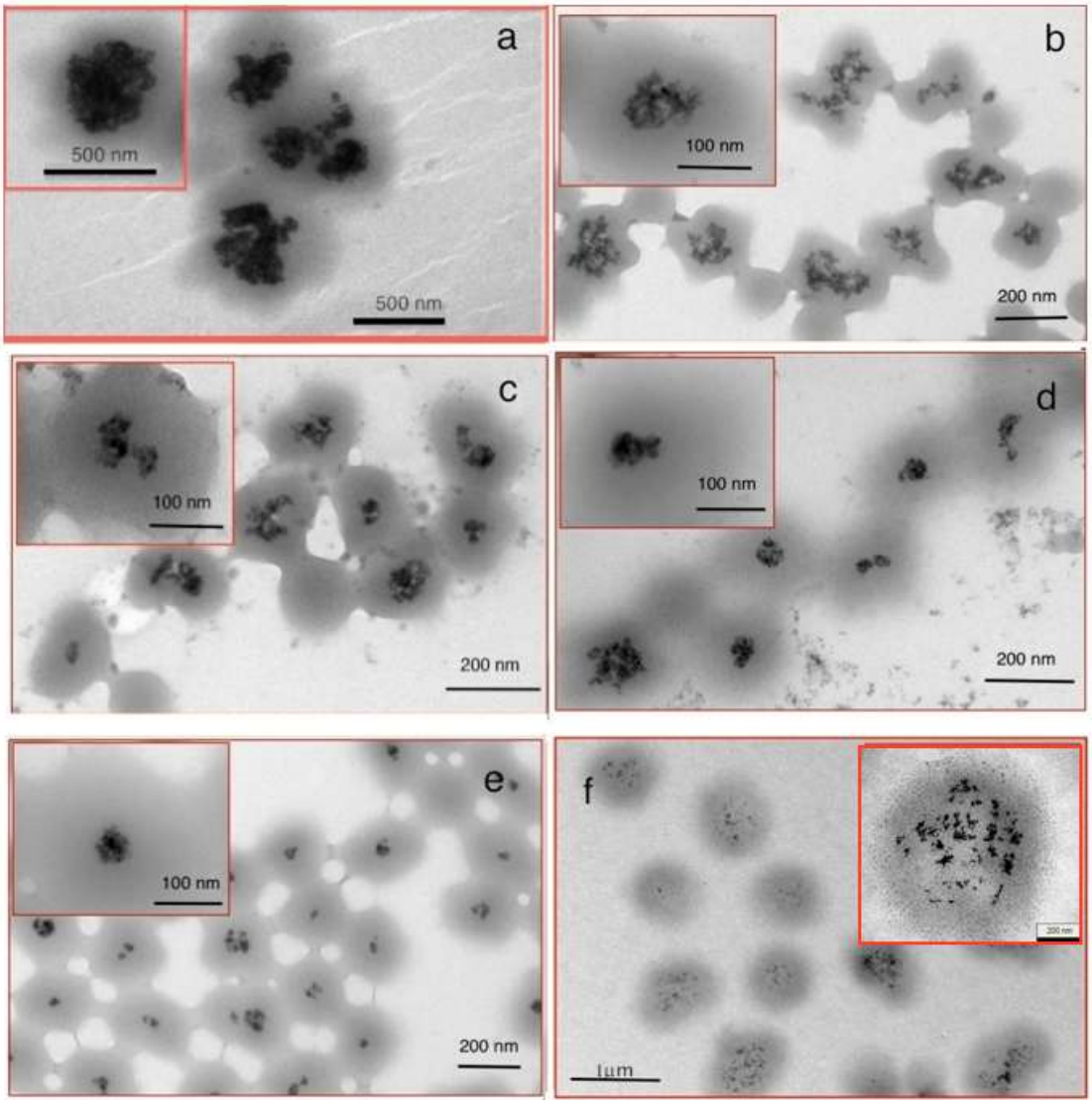

Figure 73. TEM pictures of core-shell Fe_3O_4@PNIPAM microgels. Magnetic core reduction for increasing 3-bt; a) 0 µL (S0I); b) 10 µL (S10I); c) 20 µL (S20I), d) 40 µL (S40I), e) 100 µL (S100I) and f) 160 µL (S160II).

The microgel synthesis in absence of 3-bt (sample S0I) leads to large aggregates of the magnetic material, resulting in irregular clusters covered by PNIPAM. These hybrid particles show poor stability, provoking colloidal aggregation and strong sedimentation. The average particle size for Fe_3O_4@PNIPAM in sample S0I is about 500 nm, as determined by TEM, being impossible to measure by DLS due to their poor colloidal stability. The use of magnetic clusters modified with 3-bt and polymerized with NIPAM leads to stable hybrid microgels with size

ranged between 220 to 250 nm (in the collapsed state) for samples S10I to S100I at TEM chamber conditions. In Figure 73 one can observe that the PNIPAM reaction carried out in the presence of magnetic cluster with size above 55 nm (samples from S10I to S100I) produced hybrid microgels with the inorganic material located in the center, forming an inorganic core, which maintains the magnetic cluster formed prior the microgels synthesis. Furthermore the shape of the clusters evolved from irregular to pseudo-spherical when the amount of the 3-bt was increased. By contrast when the smallest magnetic clusters were used (S160II) hybrid particles with mean size of 1 μm were obtained. In this case the PNIPAM microgels present the magnetic nanoparticles randomly distributed in the inner part of the microgels (Figure 73f) with multiple magnetic cluster per microgels subunit. These results indicate that there is a strong influence of the aggregation state of the magnetic nanoparticles on the final microgel architecture.

As can be inferred from the previous results, the variation of the amount of 3-bt influences the aggregation state of the magnetic clusters used during the synthesis permits controlling the size of the magnetic cluster allowing to entrap different amounts of magnetic material, (see Figure 74).

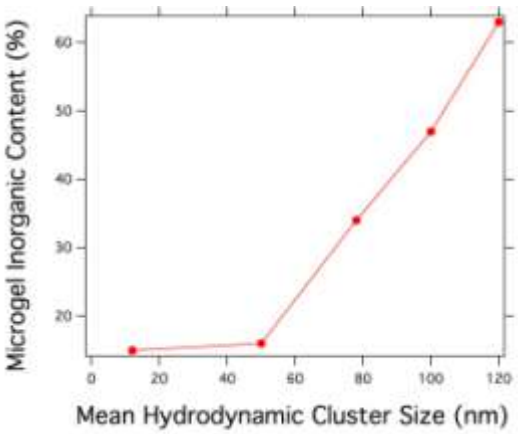

Figure 74. The microgel inorganic content (%) as a function of the magnetic cluster precursors as determined by thermogravimetry.

As can be observed in Figure 74, the sample S10I reaches 63% of inorganic content as determined by thermogravimetric analysis being colloidally stable. Despite the localization of the magnetic nanoparticles all the samples present VPT (see Figure 75).

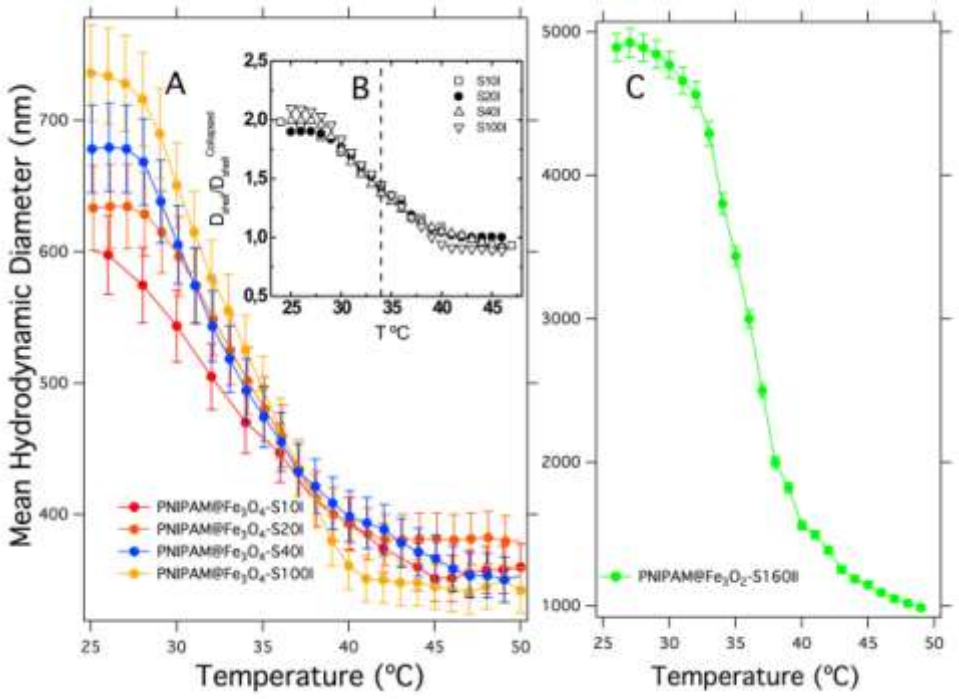

Figure 75. Swelling curves against temperature for different Fe_3O_4@PNIPAM particles.

Thus particles shrink continuously with increasing temperature as a consequence of the temperature-dependent Flory parameter.[222] Furthermore, the shrinking-swelling cycles are reversible in all cases without any significant hysteresis. For microgels with a well define magnetic core, only the PNIPAM shell manifest swelling capacity, while the inorganic core keeps constant. That has been proved by comparing the relative shell swelling for Fe_3O_4@PNIPAM with different core sizes since all curves overlap (Figure 75 inset B), indicating that the swelling of the organic shell is not influenced by the presence of the inorganic core. It is worth to point out the big difference in size exhibit by the microgels prepared with the smallest magnetic cluster, which is 4.8 μm in the swollen state. This result shows the tremendous influence that the cluster size has on the microgel formation and their architecture.

[222] S. Hirotsu, *Phase Transitions.*, **1994**, *47*, 183.

5. *Results and Discussions*

The different particle decoration obtained from the synthesis could be attributed to the different action mechanism involved in the synthesis of the hybrid microgels. Pelton et al[41] described the mechanism of the neat PNIPAM microgels production as a nucleation process of colloidal unstable nanogels, which are formed during the polymerization reaction. Due to their inherent instability, the precursor nanogels coagulate, forming a stable colloidal particle, which results in the final microgel. These nanogels have been detected using SANS.[223] In this article the authors described the presence of nanogels with a size around 22 nm above the LCST within the microgels structure.

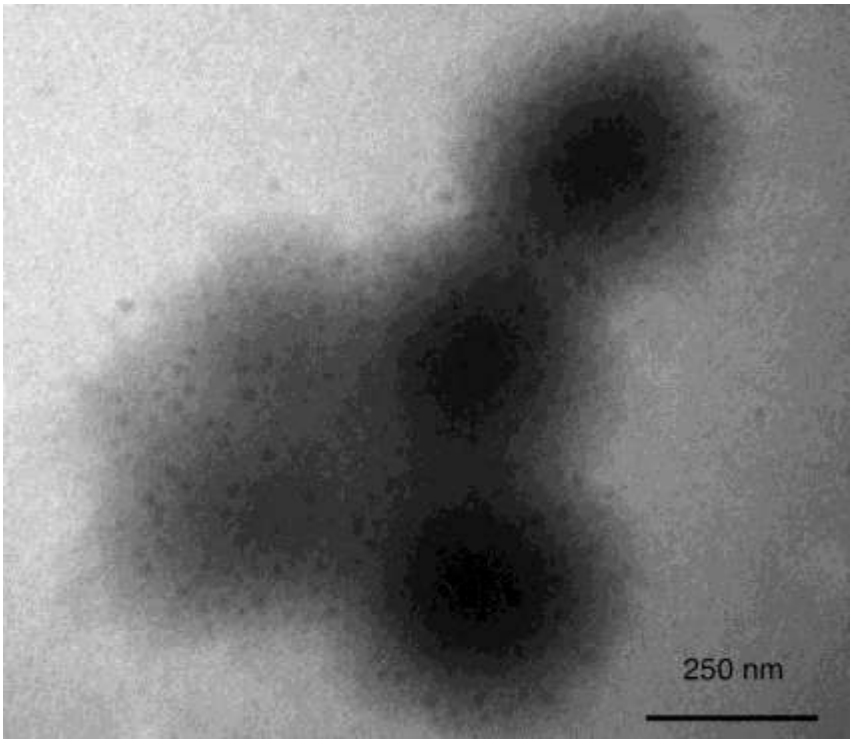

Figure 76. TEM micrograph of neat PNIPAM microgels formed by small nanogels subunits

Figure 76 shows an observation of these nanogels that appear as dark dots homogeneously distributed within the microgels. Interestingly the size of these nanogels is in the order of the SANS prediction.[223] One explanation could be that when the magnetic cores are bigger than these nanogels, the polymerization process creates a polymer shell around the cores, which

[223] A. Fernández-Barbero, A. Fernández-Nieves, I. Grillo, and E. López-Cabarcos, *Phys. Rev. E*, **2004**, *66*, 51803.

grows thanks to the excess of nanogels formed during the first stage of the polymerization. This coagulation process stops when the final microgels reach a size that provide enough colloidal stability, which is the same for all microgels produced by this way, close to 370 nm at the collapsed state (Scheme 13A).This scenario changes when the nanogels have a similar size than the magnetic clusters (Scheme 13B). Under this condition several nanogels would be required to cover a single magnetic cluster. This could provoke a rapid consumption of the nanogels that would yield to small hybrid nanogels, which are not stable enough. In order to gain colloidal stability, neighbor hybrid nanogels would aggregate each other creating the final hybrid microgel. The big different in size of S160II respect the previous hybrid microgels S100I could arise from the smaller gain of colloidal stability that the aggregation of hybrid nanogels produce in comparison with the nucleation on neat nanogels. That would provoke the growing microgels to reach a major hydrodynamic diameter to acquire colloidal stability.

Scheme 13. Microgel formation mechanism a) for magnetic cluster bigger than the nanogels and b) for magnet cluster smaller than the nanogels.

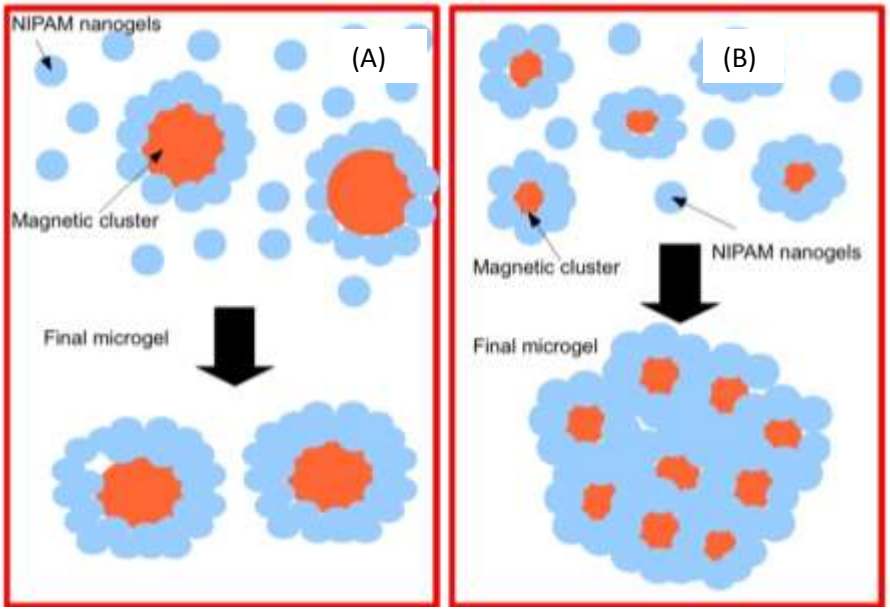

5. *Results and Discussions*

Concerning the magnetic properties of the Fe_3O_4@PNIPAM microgels, they show typical super-paramagnetic behavior with very low hysteresis. In Figure 77, one can observe that the super-paramagnetic behavior is independent of the particle swelling (sample S40I). The distances between magnetic nanoparticles are very stable into a well defined magnetic core and so insensitive to polymer network modifications. However, for sample S160II, swelling determines the magnetic material compactness (spread across the inner of the microgels) and influences the magnetic response that is stronger at high temperatures due to larger compactness.

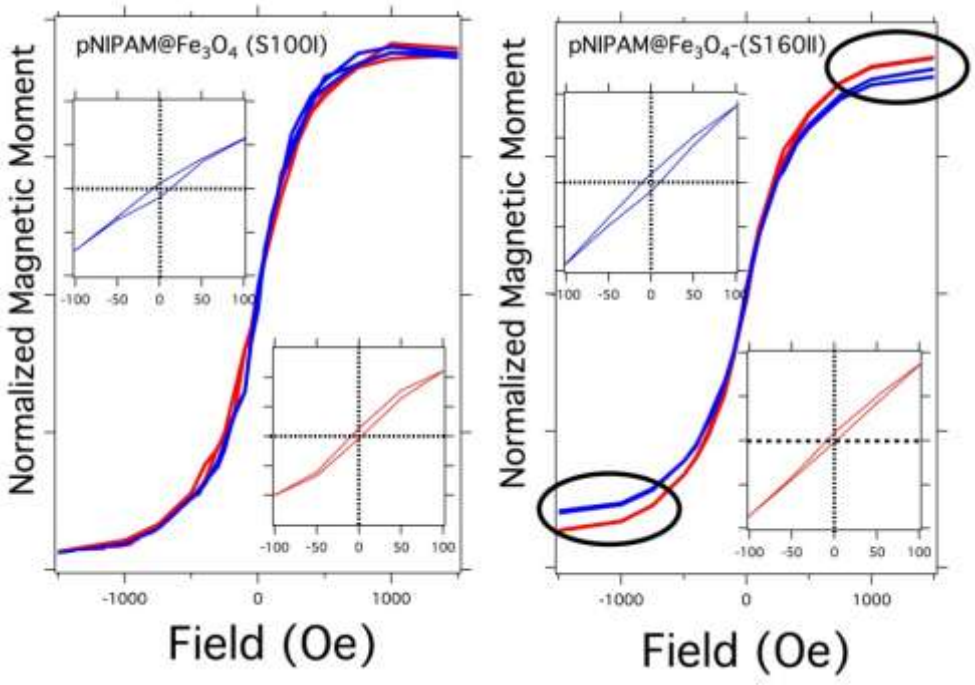

Figure 77. Magnetization for S40I and S160II. Blue and red lines correspond to experiments performed at temperatures below and above the LCST, respectively. The insets show the hysteresis found for both temperatures.

5.5.2.2 *Conclusions*

It has been developed an easy and reproducible method to encapsulate Fe_3O_4 nanoparticles into microgels in order to produce a very interesting hybrid material. The synthesis of the hybrid particles is based on the use of 3-butenoic acid to modify the magnetic cluster surface, where PNIPAM can grow. This strategy leads to controlled cluster segregation due to the extra added charge and allows PNIPAM polymerization. The 3-butenoic acid promotes terminal double-bonds formation on the nanoparticles surfaces where polymerization occurs. The final hybrid particles show two different internal architectures, consequence of a polymer coagulative nucleation. The characteristics of these growing particles are determined by the ratio between the magnetic clusters size and the PNIPAM nanoprecursors. Well defined magnetic cores become apparent when the magnetic clusters are large enough. Otherwise, hybrid microgels grow with the magnetic material spread across the polymer lattice. The transition temperature shifted to higher values due to the presence of Columbian interaction between Fe_3O_4 particles. The magnetic response for the hybrid particles under external magnetic fields is temperature independent for particles with well defined cores and depends on temperature (at sufficiently high magnetic fields) for the diffuse architecture for which the compactness of the magnetic material depends on the polymer swelling.

6. *Conclusions*

6. *Conclusions*

1. In the premicellar range, the PL emission of the CP is sharply affected by the surfactant chain length. Thus, the PL is quenched by the surfactant with the shortest tails whereas the surfactant with the longest one provokes an enhancement of the PL emission. This behavior is associated with the capacity of the longest chain surfactants that hinder the formation of p-p interchain interactions and to reduce the intrachain interaction. By contrast, at the CMC the surfactant chain length does not modify the PL emission.

2. It has been synthesized an interpenetrated microgels based on PNIPAM and PTEBS. These microgels were characterized and used to prepare reusable microsensor suitable for the detection of picric acid.

3. The HRP intermediates CoI and CoII are oxidizing agents of MPS-PPV which leads to a drop in its PL. The addition of phenolic compounds to the catalytic reaction medium leads to an increase of MPS-PPV oxidation rate. HRP was immobilized within PAA microgels to fabricate a system that can detect APAP at micromolar concentration.

4. It has been synthesized a new water-soluble conjugated polymer PTE-DMSA that exhibits very good Stern-Volmer constants for lead and mercury determination and could be used as chemosensor for those ions.

5. It has been presented a new one-pot synthesis to generate Au anisotropic nanocrystals. The CP acts as reducing and stabilizing agent and at the same time promote the formation of hybrid nanostructures when conjugated polymer PTEBS used in combination with lead nitrate and cadmium acetate.

6. It has been reported a new method to encapsulate magnetic Fe_3O_4 nanoparticles inside a PNIPAM microgel producing a core-shell hybrid material. The strategy used permits to control and obtain different architectures.

7. *Conclusiones*

7. *Conclusiones*

1. En el rango premicellar la emisión luminiscente del polímero conjugado es tremendamente afectada por la longitud de cadena del tensioactivo. Así, la luminiscencia es amortiguada por los surfactantes con la cadena más corta mientras que los de cadena más larga provocan un aumento de la fluorescencia. Por otro lado a la CMC la longitud de la cadena no afecta a la fluorescencia del polímero.

2. Se ha sintetizado un nuevo microgel interpenetrado de NIPAM y PTEBS. Estos microgeles se han caracterizados y utilizados para el desarrollo de un sensor reutilizable de compuestos nitroaromaticos.

3. Los intermediarios de la enzima HRP, CoI y CoII, son agentes oxidantes del polímero MPS-PPV, disminuyendo su fluorescencia. La adición de compuestos fenólicos al ciclo catalítico de la reacción provoca un aumento de la velocidad de oxidación del polímero. La enzima HRP ha sido inmovilizada en microgeles de PAA dando lugar a un sistema que puede detectar APAP a una concentración micromolar.

4. Se ha sintetizado un nuevo polímero fluorescente soluble en agua, PTE-DMSA, que muestra muy buenas constantes de Stern-Volmer para la detección de plomo y mercurio.

5. Se reporta un nuevo método de síntesis en un paso de nanocristales anisotrópicos de Au utilizando el polímero conjugado PTEBS con nitrato de plomo y acetato de mercurio.

6. Se reporta un nuevo método para la encapsulación de nanopartículas de Fe_3O_4 en un microgel de PNIPAM creando un material hibrido núcleo-corteza. La estrategia utilizada permite controlar y obtener diferentes arquitecturas.

8. *Table of Acronyms*

8. *Table of Acronyms*

Conjugated polymers	CPs
Photoluminescence	PL
Poly(3-ethoxy-butyl-sulfonate-thiophene-2,5-diyl)	PTEBS
N-Octylammonium Chloride	C8
N-Nonylammonium Chloride	C9
N-Decylammonium Chloride	C10
N-Dodecylammonium Chloride	C12
Critical micelle concentration	CMC
Poly(N-isopropylacrylamide)	PNIPAM
Methylene-bis-acrylamide	BA
Volume phase transition	VPT
Low critical solution temperature	LCST
Acetominophen	APAP
Horseradish peroxidase	HRP
Poly(2-methoxy-5-propyloxy-sulfonate-1,4-p-phenylene-vinylene)	MPS-PPV
Compounds I	CoI
Compounds II	CoII
Polyacrylamide	PAA
Meso-2,3-dimercaptosuccinic acid	DMSA
Poly(3-ethoxy-thiophene-2,5-diyl-dimercaptosuccinic acid)	PTE-DMSA
Au nanocrystals	AuNCs
Scanning electron microscopy	SEM
Transmission electron microscopy	TEM
High resolution TEM	HR-TEM
X-Ray Fluorescence	XRF
Nuclear magnetic resonance	NMR
Ultraviolet-Visible	UV-Vis
Dynamic light scattering	DLS
Thermalgravimetric analysis	TGA
Stern-Volmers constant	K_{SV}
N-acetyl-p-benzosemiquinonimine	NAPSQI•
Surface plasmon resonance	SPR
3-butenoic acid	3-bt

9. *Published Articles from this Thesis*

9. *Published Articles from this Thesis*

9.1 *Influence of the Surfactant Chain Length on the Fluorescence Properties of a Water-Soluble Conjugated Polymer*

Langmuir **2008**, *24*, 13321−13327

Influence of the Surfactant Chain Length on the Fluorescence Properties of a Water-Soluble Conjugated Polymer

Marco Laurenti, Jorge Rubio-Retama,* Francisco Garcia-Blanco, and Enrique López-Cabarcos

Physical Chemistry Department, Pharmacy Faculty, Complutense University, Madrid 28040, Spain

Received July 14, 2008. Revised Manuscript Received September 18, 2008

In this work, we report the influence of surfactant chain length and surfactant concentration on the photoluminescence (PL) of water-soluble π-conjugated poly(thienylethylene oxide butyl sulfonate) (PTE-BS). We have used alkylammonium surfactants with 8, 9, 10, and 12 carbon atoms per hydrocarbon chain. The surfactant concentration was varied from 0.125 the critical micelle concentration (CMC) up to 2 times the CMC. The results show that at premicellar concentrations all the surfactants promote the polymer aggregation inducing an increase in the interchain charge transfer by $\pi-\pi$ interactions, which competes with PL emission processes. However, in the premicellar range, the polymer PL emission is sharply affected by the surfactant chain length. Thus, the PL is quenched by the surfactants with the shortest tails, whereas the surfactants with the longest ones provoke an enhancement of the PL emission. This behavior has been associated with the capacity of the surfactants with the longest hydrocarbon chains to accommodate their tails inside the polymer, obstructing the appearance of $\pi-\pi$ interchain interactions during aggregation and reducing intrachain defects. By contrast, at the CMC, the surfactant chain length does not modify the PL emission, since the excess of surfactant inhibits polymer aggregation, thus enhancing the efficiency of light emissive processes.

Introduction

Photoluminescence polymers (PLPs) constitute an interesting group of materials with a wide range of applications in optoelectronics, electroactive devices, solar cells, and light emitting diodes.[1−5] In these polymers, the optoelectronics and electroactive properties can be modified easily by changing the chemical structure or the environmental conditions. This special behavior has prompted scientists to use them as sensors, since their PL properties are superb compared with other organic dyes.[6] Tiny variations in the media can provoke a dramatic change in their emission, making them highly sensitive to external stimuli such as pH, ionic strength, polarity, and so forth.[7] The so-called water dispersible PLPs, formed by $\pi-\pi$ conjugated hydrophobic backbones with charged side groups, have demonstrated to be of application to develop biosensors. In such an application, the polymer is physically or chemically bound to a biological molecule, DNA, RNA, or an antibody which, after recognizing the target, modifies the polymer configuration, inducing a change in the PL emission that permits the recognition of biological molecules with great accuracy and sensitivity.[8−10] However, the aqueous media in which these determinations are carried out induces the aggregation of the polymer hydrophobic backbone, rendering a less water-soluble material and therefore with lower emission efficiency.

The supramolecular interactions between π-conjugated polymers determine the macroscopic properties of these systems and have become one of the most challenging scientific research areas. With the aim of increasing the sensitivity of the water-soluble conjugated polymers, efforts have been made to develop methods for increasing their water solubility.[11,12] Among others, the interaction of the polymer hydrophobic backbone with surfactants seems to be a promising approach to enhance conspicuously the emission efficiency of the PLPs.[13] This phenomenon, also called surfactochromicity, was described by Haamed and co-workers[14] as a set of actions which could be summarized as follows. First, the surfactant induces the disruption of the polymer aggregates, reducing interchain quenching and increasing the PL and the quantum yield.[15] Second, the surfactant provokes changes in the polymer coil conformation,[16] extending the effective electron delocalization, which leads to red spectral shifts of the absorption and emission maxima. This effect increases the PL quantum efficiency by inhibiting the folding of the polymer chains, with the subsequent reduction of conformational disorder and of the number of defects acting as trapping and nonradiative recombination sites. Finally, incorporation of the polymer chains into micelles reduces the quenching of fluorescence by water by preventing nonradiative processes.[17]

Most of these effects have been described at surfactant concentrations above the critical micelle concentration (CMC), and only a few papers report studies performed at lower

* To whom correspondence should be addressed. E-mail: bjrubio@farm.ucm.es.

(1) Cimrová, V.; Remmers, M.; Neher, D.; Wegner, G. *Adv. Mater.* **1996**, *8*, 146.
(2) Gmeiner, J.; Karg, S.; Meier, M.; Riess, W.; Strohriegl, P.; Schwoerer, M. *Acta Polym.* **1993**, *44*, 201.
(3) Wang, F.; Gu, H.; Swager, T. M. *J. Am. Chem. Soc.* **2008**, *130*, 5392.
(4) Fan, C.; Plaxco, K.; Heeger, A. *J. Am. Chem. Soc.* **2002**, *124*, 5642.
(5) Lopez-Cabarcos, E.; Carter, S. *Macromolecules* **2005**, *38*, 4409.
(6) Najari, A.; Ruang, A. H.; Gravel, J. F.; Nobert, P.; Boudreau, D.; Leclerc, M. *Anal. Chem.* **2006**, *78*, 7896.
(7) López-Cabarcos, E.; Rubio Retama, J.; Shtoliu, V.; Carter, S. *Polym. Int.* **2007**, *56*, 588.
(8) Ho, H.; Dore, H.; Boissinot, M.; Bergeron, M.; Tanguay, R.; Boudreau, D.; Leclerc, M. *J. Am. Chem. Soc.* **2005**, *127*, 12673.
(9) Gaylord, B.; Heeger, A.; Bazan, G. *Proc. Natl. Acad. Sci. U.S.A.* **2002**, *99*, 1624.
(10) Huang, A. H.; Najari, A.; Leclerc, M. *Acc. Chem. Res.* **2008**, *41*, 168.
(11) Sato, T.; Jiang, D. *J. Am. Chem. Soc.* **1999**, *121*, 10658.
(12) Wang, Y.; Erdogan, B.; Wilson, J.; Bunz, U. *Chem. Commun.* **2003**, 1624.
(13) Knaggs, M.; Laszlo, A.; Garamus, V.; Pearson, C.; Pradhan, S.; Petty, M.; Scherf, U.; Burrows, H.; Monkman, A. *J. Phys. Chem B* **2006**, *110*, 10248.
(14) Haamed, A.; Attar, A.; Monkman, A. *J. Phys. Chem. B* **2007**, *111*, 12418.
(15) Yan, M.; Rothberg, L.; Kwock, E.; Miller, T. *Phys. Rev. Lett.* **1995**, *75*, 1992.
(16) Chen, L.; Xu, S.; McBranch, D.; Whitten, D. *J. Am. Chem. Soc.* **2000**, *122*, 9302.
(17) Chakrabarty, A.; Das, P.; Mallick, A.; Chattopadhyay, N. *J. Phys. Chem. B* **2008**, *112*, 3684.

10.1021/la802246g CCC: $40.75
Published on Web 11/08/2008

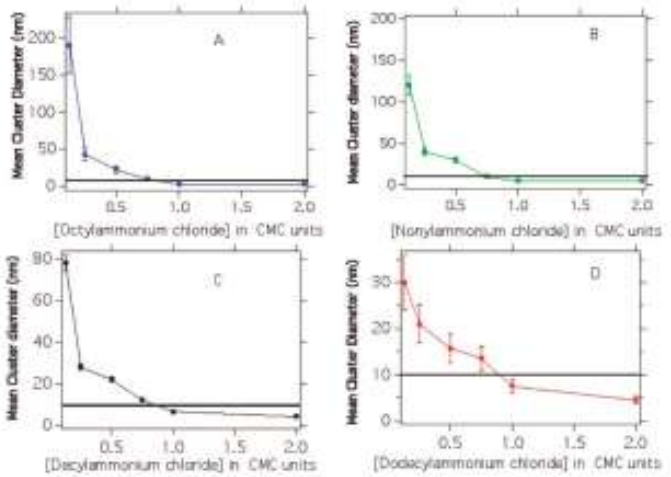

Figure 1. DLS measurements of PTE-BS solutions in the presence of surfactant at different ratios of the CMC: (A) octyl ammonium chloride (C8), (B) nonyl ammonium chloride (C9), (C) decyl ammonium chloride (C10), and (D) dodecyl ammonium chloride (C12). The continuous line in each panel represents the size of the PTE-BS particle in pure water.

concentrations.[14,16] The investigation of the influence of the surfactant chain length on the PL of poly(thienyl ethylene oxide butyl sulfonate) might help to better understand the interaction between water-soluble π-conjugated polymers and surfactants.

The results presented in this work showed that the addition of surfactant at premicellar concentrations provoked the aggregation of the polymer and the increment of the cluster polymer size. However, depending on the chain length of the surfactant, the aggregation can quench or enhance the PL emission of the polymer.

Experimental Section

Materials and Sample Preparation. The water-soluble conjugated polymer sodium poly[2-(3-thienyl)ethoxy-4-butylsulfonate] (PTE-BS, commercially called ADS2000P) was purchased from American Dye Source. The molecular weight of PTE-BS provided by American Dye Source was 269 000 g/mol with 1.4 polydispersity. Aqueous solutions of PTE-BS 1.8×10^{-5} M were prepared and purged with nitrogen for several hours. All polymer concentrations are expressed in monomer repeat units. The surfactants (dodecyl ammonium chloride (C12), decyl ammonium chloride (C10), nonyl ammonium chloride (C9), and octyl ammonium chloride (C8)) were synthesized and purified in our laboratory. The n-alkylamines were purchased from Sigma-Aldrich, and their purity was in all cases higher than 97% (for octylamine and decylamine, the purity was higher than 99%). The alkyl ammonium chlorides were prepared by passing gaseous hydrogen chloride through a solution of the n-alkylamine in diethyl ether. The resulting precipitate was washed several times with diethyl ether, subsequently crystallized from mixed solvents acetone/ethanol/diethyl ether, and finally vacuum-dried overnight. The white salts were kept in a dry atmosphere. The X-ray diffraction patterns of the powdered surfactants show a family of peaks corresponding to interdigitated bilayers without the slightest indication of contamination. The critical micelle concentration (CMC) was determined from surface tension measurements. The values obtained for CMCs were as follows: 0.195 M (C8), 0.110 M (C9), 0.055 M (C10), 0.028 M (C11), and 0.012 M (C12).[18]

Methods. Fluorescence spectra were recorded by using a PTI luminescence spectrometer. The fluorescence spectra were obtained by exciting PTE-BS surfactant solutions at 425 nm, near their respective absorption peaks. Time-resolved fluorescence measurements of the polymer−surfactant solutions were recorded using an excitation wavelength of 460 nm. The absorption spectra were taken on a UV−vis spectrometer (Cari 300 Bio). Dynamic light scattering experiments (DLS) were carried out in a Malvern Nano-ZS system equipped with a He−Ne laser working at 632.8 nm to examine the polymer and polymer−surfactant complex particle size. The time correlation function of the scattered intensity, $g(t) = \langle I(0)\, I(t)\rangle$, was measured, and the mean hydrodynamic radius was obtained using cumulant analysis. All fluorescence and DLS measurements were made at room temperature (≅20 °C). Angular-dependent scattering measurements were carried out using an ALV/DLS/SLS-5022F Compact goniometer system from ALV coupled with a 5 W laser working at 532 nm.

Results and Discussion

The size of the polymer particles and the polymer−surfactant clusters was derived from the intensity correlation function measured with DLS and is shown in Figure 1 as a function of the surfactant concentration: C8 (upper panel left), C9 (upper panel right), C10 (bottom panel left), and C12 (bottom panel right). In aqueous solution, the water-soluble photoluminescence polymers tend to form aggregates because of the inherent hydrophobicity of the thiophene moieties, which establish $\pi-\pi$ and van der Waals interactions with other thiophene groups. The resulting polymer particles have hydrophilic groups in the outer part, whereas the hydrophobic thiophene groups are buried in the inner part of the particle.[19,20] The addition of surfactant increases the PL efficiency by breaking up the aggregates and modifying the size of the polymer cluster.

As can be seen in Figure 1, the addition of surfactant produces a dual effect on the size of the polymer cluster. Independently

(18) Tenorio, A.; Gálvez Gómez, P.; López-Cabarcos, E. *Prog. Colloid Polym. Sci.* **2000**, *115*, 50.

(19) Hoeben, F.; Jonkheijm, P.; Meijer, P.; Schenning, A. *Chem. Rev.* **2005**, *105*, 1491.

(20) Martin, S.; Cudby, A.; Lane, P.; Bradley, D. *Synth. Met.* **1999**, *101*, 665.

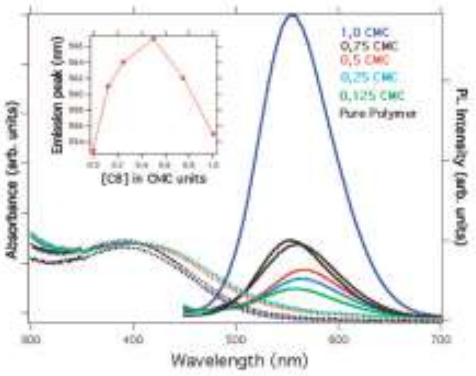

Figure 2. Absorption (dashed line) and emission (continuous line) spectra of PTE-BS in the presence of different concentrations of octyl ammonium chloride. The inset shows the shift of the PL maximum (red-shift up to 0.5 CMC followed by a blue-shift at higher surfactant concentrations) as a function of the octyl ammonium chloride concentration (in CMC units). The excitation wavelength was 425 nm.

Table 1. Half-Width at Full Maximum (HWFM) and Maximum PL Intensity of the Spectra As a Function of C8 Concentration

ratio of the surfactant concentration to the CMC	HWFM (nm)	PL intensity
0.125	56	46
0.25	53	66
0.5	52	84
0.75	50	135
1	50	598
pure polymer	49	146

of the surfactant chain length, at a low concentration of surfactant (0.125 and 0.25 times the CMC), the polymer aggregates with the surfactant, forming particles with a diameter greater than 10 nm, which is the size for the PTE-BS particles in pure water. Angular-dependent light scattering measurements show that these aggregates are spherical particles with a radius of gyration R_g = 118 nm (see the Supporting Information). This fact indicates that the increment in the hydrodynamic diameter should be due to polymer aggregation rather than to a change from coil to rod. Furthermore, it is also shown that the ability of coagulation depends on the surfactant chain length and this effect is less pronounced for the surfactant with the longest chain. This result could indicate that at low surfactant concentration the ammonium polar headgroup interacts with the sulfonate side chain of the polymer through columbic interactions, rendering a polymer−surfactant complex with low colloidal stability that tends to coagulate.[21] However, as the surfactant concentration is increased, the size of the aggregates sharply decreases, leveling at an average diameter close to 5 nm. This result indicates that at surfactant concentrations above 0.5 CMC the polymer cluster breaks up into smaller particles.

The reduction in the size of the polymer−surfactant cluster above the CMC with respect to the pure polymer would indicate that for these concentrations the polyelectrolyte charges are effectively screened by the surfactant polar headgroups which lead to the collapse of the polymer particle.

The formation of the polymer−surfactant complex modifies the absorption and emission spectra in a way that depends on

(21) MacKnight, W.; Ponomarenko, E.; Leising, G.; Tirrell, D. *Acc. Chem. Res.* **1998**, *31*, 781.

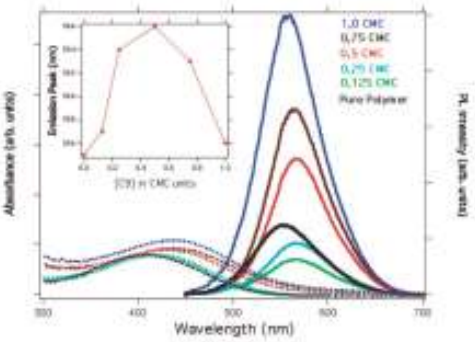

Figure 3. Absorption (dashed line) and emission (continuous line) spectra of PTE-BS in the presence of different concentrations of nonyl ammonium chloride. In the fluorescence measurements, the excitation wavelength was 425 nm. The inset shows the shift of the PL peak as a function of the nonyl ammonium chloride concentration (in CMC units).

the surfactant chain length. As is shown in Figure 2, the addition of the surfactant (0.125 CMC) provokes an abrupt decrease in the PL intensity of the polymer (see Table 1). This quenching of the PL emission as well as the red-shift at low surfactant concentrations are attributed to the aggregation of the polymer, which increases the $\pi-\pi$ interaction between neighbor thiophene rings, inducing interchain excitation quenching. Nevertheless, further increments in the surfactant concentration enhance the PL emission. Such an effect is attributed to the rupture of the polymer aggregates with the subsequent reduction of the interchain excitation quenching. These results are in agreement with the variations observed in the hydrodynamic diameter of the polymer−surfactant complex, which became smaller when the surfactant concentration increased. Furthermore, at low concentration of surfactant, one can observe a red-shift of the PL emission (see inset in Figure 2) that can be explained by the surfactant aggregation effect on the PTE-BS. However, further increments in the surfactant concentration break up the polymer cluster (see C8 panel in Figure 1), shifting the emission peak further to the red. This behavior could be attributed to the transition from coil to rod[13] in the polymer induced by the surfactant that would increase the polymer conjugation.[6,14] This explanation assumes the competition between two effects: the extension of the polymer chain and the breaking up of the polymer cluster, with the polymer chain extension being the dominant effect at premicellar concentrations. Thus, when the surfactant concentration increases, the red-shift reaches a maximum at 0.5 CMC and further increments in the surfactant concentration provoke a blue-shift that can be attributed either to the breaking up of the polymer−surfactant complex or to the enhancement of the hydrophobicity of the media.

It is worth noting that the reduction of the absorption offset and the narrowing of the emission band (see Table 1) also indicate that more ordered and homogeneous polymer configurations are obtained at higher surfactant concentrations. A similar behavior to that reported for C8 was observed after the addition of C9, as shown in Figure 3. Nevertheless, in this case, the quenching of the PL disappeared upon addition of the surfactant at concentrations above 0.25 CMC.

The sequence of processes described above (aggregation, extension, breaking up, and environmental polarity reduction) is summarized in Scheme 1, which depicts the proposed model for the

Scheme 1. Proposed Model for the Interaction between PTE-BS and Surfactant at Different C8 and C9 Concentrations

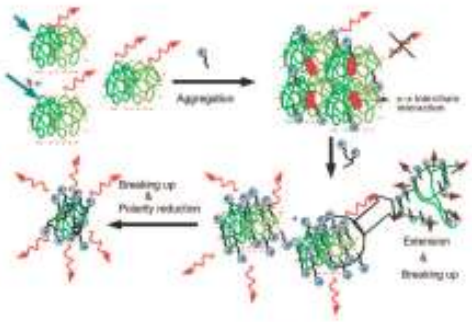

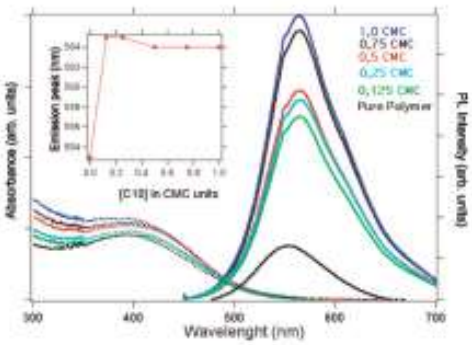

Figure 4. Absorption (dashed line) and emission (continuous line) spectra of PTE-BS in the presence of different concentrations of decyl ammonium chloride. The excitation wavelength was 425 nm.

polymer surfactant complex at different concentrations of C8 and C9.

As is illustrated in Scheme 1, the initial addition of surfactant induces the aggregation of the photoluminescent polymer, leading to the formation of a polymer cluster with low, and red-shifted, PL emission. Further increments in the surfactant concentration induce the breaking up of the polymer cluster and the extension of the polymer chain, enhancing the PL emission. Finally, at the CMC, the polymer clusters are completely disaggregated, yielding the minimum surfactant−polymer cluster size with the maximum PL emission.

The situation is different in the case of the surfactants decyl- and dodecyl ammonium chloride (see Figures 4 and 5). At low C10 concentration (0.125 CMC), the intensity increases instead of being quenched as it was in the case of C8 and C9 (Figure 4). A similar behavior was also obtained for C12 (Figure 5).

The PL red-shift is a common aggregation effect that was observed for all the surfactants investigated. Furthermore, the aggregation was confirmed by the large values of the hydrodynamic radius obtained in these systems. However, as is shown in Figure 6, at low surfactant concentrations, the behavior of the PL intensity depends on the surfactant chain length: for C8 and C9, the PL intensity decreases with respect to the PL of the pure polymer, while for C10 and C12 the PL increases.

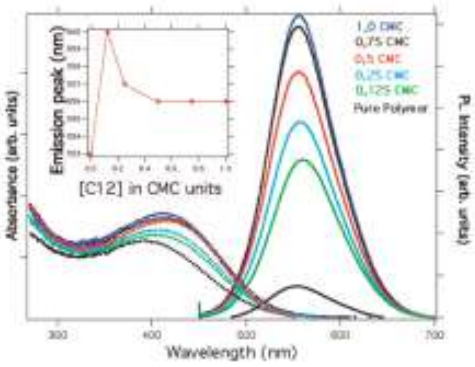

Figure 5. Absorption (dashed line) and emission (continuous line) spectra of PTE-BS in the presence of different concentrations of dodecyl ammonium chloride. The excitation wavelength was 425 nm.

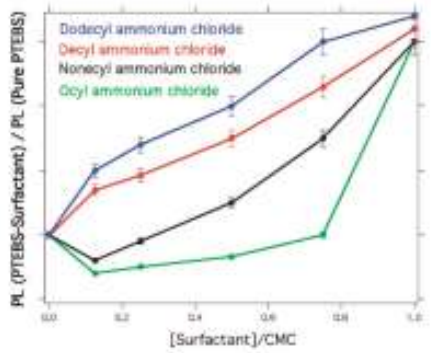

Figure 6. PL emission as a function of the ratio of the CMC for surfactants with different chain length.

In a previous work we have investigated the influence of the ionic strength of the solution on the PL of PTE-BS, and we found that the PL decreases with increasing the ionic strength. The effect was attributed to the lower solubility of the polymer at high ionic strengths due to the screening effect of monovalent cations on the polyelectrolyte charged groups.[22] Thus, the decrease of the PL intensity, with respect to the pure polymer, observed at low concentrations of C8 and C9 can be attributed to a screening effect that favors the aggregation. However, there is a threshold in the surfactant carbon chain length (around 10 carbons) for which the screening effect of the headgroup charge is overcome by the hydrophobic interactions between the surfactant tails that favor the formation of polymer−surfactant-like micelle structures that are thermodynamically stable. When the chain length increases, the aggregation capacity of the surfactants is less pronounced and the formation of hydrophobic domains reduces the number of the $\pi-\pi$ interchain interactions accounting for the quenching of the PL emission. Nevertheless, the size difference between the aggregates formed by C9 and C10 at 0.125 CMC (120 and 80 nm respectively) would not fully justify the opposite effect on the PL intensity induced by both surfactants and points to

(22) López-Cabarcos, E.; Carter, S. *Macromolecules* **2005**, *38*, 10537.

Scheme 2. Proposed Model for the Interaction between the PTE-BS and the Surfactant with Different Chain Lengths at the Premicellar and Micellar Regimes

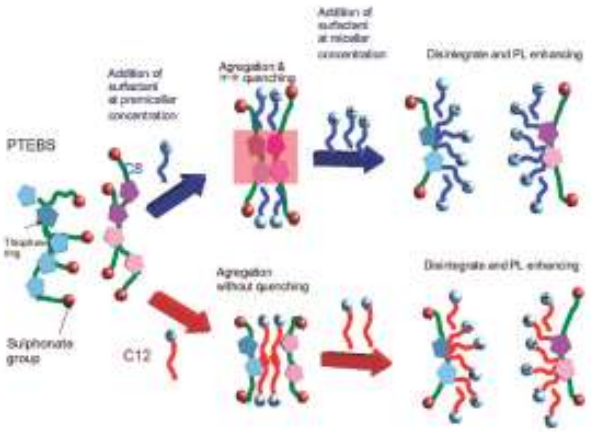

an additional effect. We can estimate the maximum length (nm) of a fully extended hydrocarbon chain from

$$l_c = 0.15 + 0.127n_c$$

where n_c is the total number of carbon atoms per chain, 0.15 is the van der Waals radius (in nm) of the terminal methyl group, and 0.127 is the carbon−carbon bond length (in nm) projected onto the direction of the chain in the *all-trans* configuration. Using this equation, we obtained a l_c value of 1.29 nm for C9 and 1.42 nm for C10. It seems that this small difference of chain length between C9 and C10 can reduce the polymer interchain charge transfer by a steric hindrance, inhibiting the self-polymer quenching and thus increasing PL intensity. Scheme 2 depicts the proposed model showing the different effects on the interchain interaction upon addition of the surfactants with the shortest and the longest tails at different concentrations.

Scheme 2 shows that at premicellar concentrations both surfactants can screen the charge of the sulfonate groups inducing the aggregation of the polymer. However, the main difference between both surfactants is that C12 could be intercalated between two thiophene moieties and C8 could not. Hence, C12 could hinder the interchain charge transfer or $\pi-\pi$ interactions, reducing the polymer quenching. By contrast, in the presence of C8, the polymer interchain interactions favor the formation of structures that compete with the light emission processes. Furthermore, the PL emission at 0.125 CMC for C10 and C12 surfactants is almost double the PL emission of the pure polymer. This result indicates that these surfactants not only prevent the formation of polymer interchain interactions during aggregation but also play a role in extending the polymer chain. The accommodation of the large hydrocarbon chains of the surfactant in the hydrophobic polymer regions could reduce the number of defects and the $\pi-\pi$ interactions that compete with the radiative emission processes.

In an attempt to further check the above hypothesis and to find out whether the chain length is a crucial parameter to understand the PL of the π-conjugated polyelectrolytes in the surfactant solutions, we carried out time-resolved fluorescence measurements. Figure 7 shows the PL intensity decay profiles for the pure polymer and the polymer−surfactant solutions.

For fitting the decay−time profiles, two exponential decay functions were necessary to describe the experimental data fit

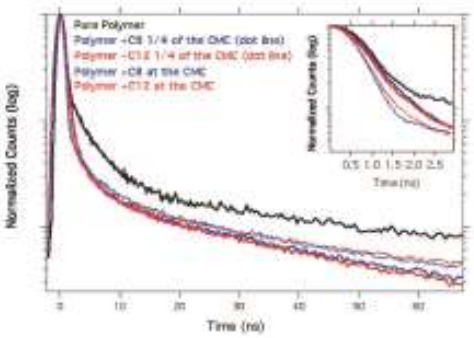

Figure 7. Selected intensity decay−time profile of pure PTE-BS (1.8×10^{-3} M) in water (black line) and PTE-BS surfactant complexes at different concentrations of C8 and C12. The inset shows the initial decay profile. $\lambda_{exc} = 460$ nm.

(χ^2 between 1.1 and 1.3, residuals <2.5%, and DW > 1.7) for all samples. This indicates that early fluorescence decay is dominated by a double exponential component. Thus, the intensity (Figure 7) is assumed to decay as the sum of individual exponential decays

$$I(t) = \sum_{i=1}^{2} A_i e^{(-t/\tau_i)}$$

where $I(t)$ is the intensity, A_i represents the amplitude of the components at $t = 0$, and τ_i is the decay time of component i.[23] Fluorescence lifetime measurements in polyelectrolytes are the result of a complex distribution of the decay times in the system. In order to get the lifetime distribution as well as the fractional contribution of each component to the steady state photoluminescence intensity,[24] we have analyzed the data using the multiexponential method. We obtained decay times for pure PTE-BS in water of 2.65 ± 0.08 and 0.78 ± 0.02 ns. The addition of surfactant changes this scenario in such a way that, at the lowest concentration of C8, when the polymer is aggregated,

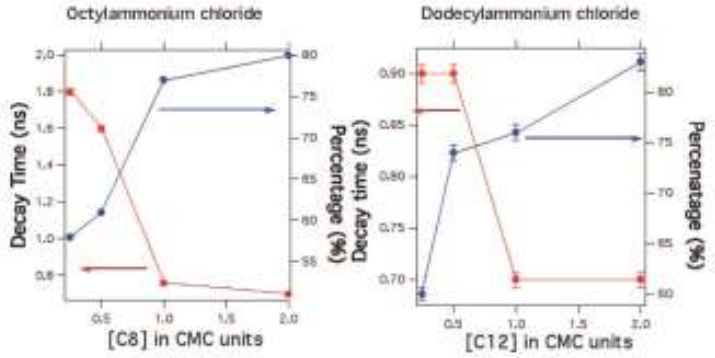

Figure 8. Slower fluorescence decay time of PTE-BS and percentage contribution to the steady state intensity as a function of the surfactant concentration: (a) PTE-BS−octyl ammonium chloride complex and (b) PTE-BS−dodecyl ammonium chloride complex.

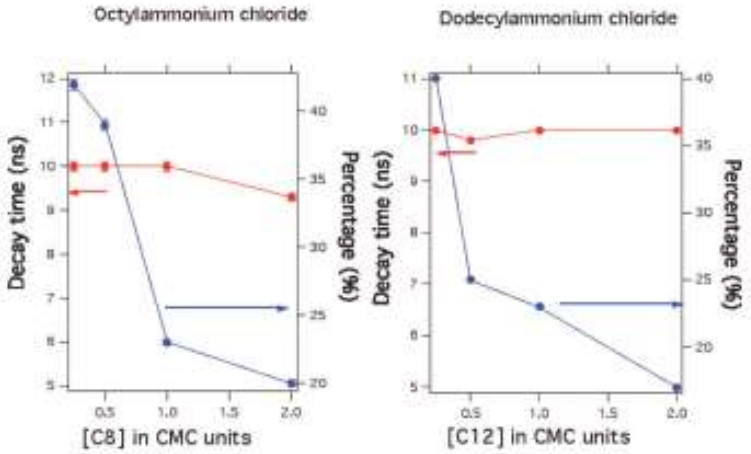

Figure 9. Profile of the higher fluorescence decay time of PTE-BS and relative contribution to the steady state intensity as a function of the surfactant concentration: (a) PTE-BS−octyl ammonium chloride complex and (b) PTE-BS−dodecyl ammonium chloride complex.

both decay times became larger: 10 ± 0.3 and 1.8 ± 0.04 ns, respectively. A similar behavior was observed upon addition of C12, for which values of 10 ± 0.3 and 0.9 ± 0.02 ns were obtained. Figure 8 shows the smaller decay time and its percentage contribution to the steady state intensity as a function of the surfactant concentration for C8 and C12.

The smaller decay times increase its relative contribution to the steady state intensity upon increasing the surfactant concentration. Figure 8 shows that the smaller lifetimes fell down from 1.8 to 0.76 ns after increasing the concentration of C8, and from 0.9 to 0.76 ns in the case of addition of C12. According to our model, this lifetime decrease would be related to the reduction of the polarity of the polymer environment, due to the increase of water screening as the surfactant concentration is increased.[25] It is interesting to note that the relative contribution of the slower lifetime increases abruptly in both samples from 55% to 80%.

The higher decay times for C8 and C12 are shown in Figure 9. They are associated with the thiophene groups that take part, via $\pi-\pi$ stacking, in the interchain interactions. The reduction of this contribution to the steady state intensity (see Figure 9) as surfactant concentration is increased is attributed to the decrease of the $\pi-\pi$ interchain interactions induced by the surfactant. The time-resolved fluorescence measurements indicate that in the polymer−surfactant complex two different fluorophore environments could account for the two exponentially decay processes observed in the time decay profile. Additionally, at premicellar concentrations, the surfactant with the longest chain length presented shorter lifetimes than those obtained upon addition of the surfactant with the smallest chain length. These results were associated with the elimination of nonradiative decay pathways as well as with increments in the media hydrophobicity. However, at the critical micelle concentration and above, the surfactant chain length loses importance, since the surfactant

(23) Lakowicz, J. R. *Principles of Fluorescence Spectroscopy*, 2nd ed.; Plenum Publishers: New York, 1999.

(24) Siemiarczuk, A.; Wagner, B.; Ware, W. *Phys. Chem. Lett.* **1990**, *94*, 1661.

(25) Achyuthan, K. E.; Bergstedt, T. S.; Chen, L.; Jones, R. M.; Kumaraswamy, S.; Kushon, S. A.; Ley, K. D.; Lu, L.; McBranch, D.; Mukundan, H.; Rininsland, F.; Shi, X.; Xia, W.; Whitten, D. G. *J. Mater. Chem.* **2005**, *15*, 2648.

breaking up process is the dominant effect that prevents the $\pi-\pi$ interchain interaction. In this regime, the size of the polymer−surfactant clusters and the decay time became independent of the surfactant chain length.

Conclusions

Our results show that, at premicellar concentrations, the surfactant chain length influences strongly the PL emission of the PTE-BS. In fact, depending on the surfactant chain length, it is possible to quench or enhance the PL emission of the polymer. At precritical micelle concentrations, the variations in PL intensity are related to the capacity of the surfactants with the shortest chain length (C8 and C9) to aggregate the PTE-BS. This effect is overcome by the hydrophobic interactions of the longer surfactant tails (C10 and C12). This scenario changes completely at the critical micelle concentration and above for which the PL increases. Under these conditions, the breaking up effect of the surfactant is maximum, and it reduces the mean polymer−surfactant cluster size and consequently the $\pi-\pi$ interactions and other effects such as chain kinks, folding, and so forth, which could be involved in quenching phenomena. In summary, we demonstrated that the polymer−surfactant interaction at premicellar concentrations plays an important role in the emission efficiency of PTE-BS, in such a way that by changing the surfactant chain length we can induce variations in the PL emission.

Acknowledgment. The authors gratefully acknowledge financial support from DGI (MAT2006-13646-C03-01) of the Spanish Science and Innovation Ministry and from the UCM Program for "Consolidation of Research Groups" (CCG UCM/MAT 2480), (CCG UCM/MAT 2681) and (CCG UCM/MAT 2481) as well as the EU for financial support through the COST Action D43. The authors also acknowledge Prof. Francisco Ortega and Dr. José Fernández (CAI de FTIR, Raman Y Correlación) for his assistance with the static light scattering experiments.

Supporting Information Available: Plot showing the inverse of the decay time of the correlation function versus the square of the scattering vector for the polymer solution with octylammonium chloride at the surfactant concentration 1/8 CMC. This material is available free of charge via the Internet at http://pubs.acs.org.

LA802246G

9.2 *Interpenetrated PNIPAM-Polythiophene Microgels for Nitro Aromatic Compound Detection*

Langmuir *Article*

pubs.acs.org/Langmuir

Interpenetrated PNIPAM−Polythiophene Microgels for Nitro Aromatic Compound Detection

M. Laurenti,[†] E. López-Cabarcos,[†] F. García-Blanco,[†] B. Frick,[‡] and J. Rubio-Retama*[,†]

[†]*Physical Chemistry Department, Faculty of Pharmacy, Complutense University, Madrid 28040, Spain, and* [‡]*Institut Laue Langevin, Grenoble, France*

Received March 11, 2009. Revised Manuscript Received April 21, 2009

In this work, we present a facile and reproducible method to obtain thermally responsive, monodisperse, fluorescent microgels with diameters smaller than 700 nm based on poly(*N*-isopropyl acrylamide) (PNIPAM) interpenetrated with poly(thiophene-ethyl buthyl sulfonate) (PTEBS). Changing the temperature and inducing the microgel volume phase transition, it is possible to modify the photoluminescence (PL) properties of the microgels. Thus, when the temperature was below the low critical solution temperature (LCST) of PNIPAM, the PL intensity was higher than that above the LCST. Time-resolved fluorescence measurements indicate that, in the swollen state, the increment of cross-linking increases the fluorescence decay time of PTEBS. By contrast, in the collapsed state, variations in the decay time were attributed to higher rigidity of the PNIPAM−PTEBS system, which was confirmed by neutron scattering measurements. Moreover, the shift in the wavelength of the fluorescence emission peak observed above the LCST indicates that the collapsed PNIPAM matrix was able to interact with the PTEBS chains hindering the formation of $\pi-\pi$ interactions. This property is envisaged for developing a picric acid microsensor based on the formation of $\pi-\pi$ interactions with the π-conjugated polymer, thus quenching its PL emission. Above the LCST of PNIPAM−PTEBS microgels, the interactions would be broken and the initial PL emission would be recovered. This property could render reusable microsensors for detection of nitro aromatic compounds.

Introduction

The interest in polymer microgels has grown rapidly over the last 10 years because their fast response to external stimuli has prompted applications as drug delivery systems, molecular entrapment matrices, oil recovery devices, or catalytic media.[1−7] Depending on the environment conditions such as pH, ionic strength, or temperature, the polymer Flory−Huggins parameter can change, leading to a steep variation of the microgel hydrodynamic radius.[8,9] In microgels, this response is fast and has been used to create smart materials of which poly(*N*-isopropyl acrylamide) (PNIPAM) is, by far, the most investigated system. PNIPAM is a water-soluble polymer with a low critical solution temperature (LCST) at 32 °C that shrinks or swells in response to changes in temperature.[10,11] Thus, PNIPAM particles swell in water at room temperature, ordering water molecules around the amide group by means of hydrogen bonding. When the temperature increases above the LCST, molecular agitation disrupts these H-bonds and leads to a breakdown of local water structure around PNIPAM chains that triggers hydrophobic attraction among isopropyl groups, with the consequent dehydration of polymer chains. Swelling of microgels depends on the type and concentration of monomer (and/or comonomer),[12] its affinity for the solvent, inclusion of nanoparticles within the microgel, and cross-linking.[1] Thus, the combination of PNIPAM with other materials (inorganic particles,[13] conducting polymers[14]) can modify the LCST, and this variation has to be taken into account when dealing with applications.

Recently, it has been reported the preparation of PNIPAM microgels that combine thermoresponsive and fluorescent properties in one material, using quantum dots (QDs) as the fluorescent emitter.[15] A different way to synthesize fluorescent microgels is polymerization of NIPAM in the presence of photoluminescent polymers to produce an interpenetrating network with the photoluminescent polymer entrapped inside the microgel. The monodispersity of PNIPAM particles allows the preparation of thermoresponsive surface coatings of controlled thickness.[16] With the interpenetrated microgels, it would be possible to fabricate fluorescent surface layers of water-soluble conjugated polymers.

This paper reports the preparation and physicochemical characterization of a novel colloidal microgel based on NIPAM polymerized, via free radical polymerization, in the presence of the water-soluble π-conjugated polymer poly(thiophene-ethyl buthyl sulfonate) (PTEBS). The amphoteric behavior of the conjugated polymer allows its interaction with PNIPAM chains

*To whom correspondence should be addressed. E-mail: bjrubio@farm.ucm.es.

(1) Benee, L.; Snowden, M. J.; Chowdhry, B. Z. *Encyclopedia of Advanced Materials*; John Wiley & Sons Ltd: New York, 2002.
(2) Hoffman, A. *J. Controlled Release* **1987**, *6*, 297.
(3) Ramkisson-Ganorkar, C.; Liu, F.; Baudys, M.; Kim, S. W. *J. Controlled Release* **1999**, *59*, 287.
(4) Snowden, M. J.; Vincent, B.; Morgan, J. C. U.K. Patent GB 226, 2117A, 1993.
(5) Serrano Ruiz, M.; Romerosa, A.; Sierra-Martin, B.; Fernandez-Barbero, A. *Angew. Chem., Int. Ed.* **2008**, *47*, 8665.
(6) Hampton, K. W.; Ford, W. T. *Abstr. Pap. Am. Chem. Soc.* **1999**, *218*, 32.
(7) Nakayama, Y. *Prog. Org. Coat.* **1998**, *33*, 108.
(8) Filipcsei, G.; Feher, J.; Zrinyi, M. *J. Mol. Struct.* **2000**, *554*, 109.
(9) Saunders, B. R.; Vincent, B. *Adv. Colloid Interface Sci.* **1999**, *80*, 1.
(10) Pelton, R. H.; Chibante, P. *Colloids Surf.* **1986**, *20*, 247.
(11) Snowden, M. J.; Chowdhry, B. Z. *Chem. Br.* **1995**, *31*(12), 943.
(12) Karg, M.; Pastoriza-Santos, I.; Rodriguez-González, B.; von Klitzing, R.; Wellert, S.; Hellweg, T. *Langmuir* **2008**, *24*, 6300.
(13) Pich, A.; Adler, H. J. P. *Polym. Int.* **2007**, *56*(3), 291.
(14) López-Cabarcos, E.; Mecerreyes, D.; Sierra-Martin, B.; Romero-Cano, M. S.; Strunz, P.; Fernandez-Barbero, A. *Phys. Chem. Chem. Phys.* **2004**, *6*, 1396.
(15) Agrawal, M.; Rubio-Retama, J.; Zafeiropoulos, N. E.; Gaponik, N.; Gupta, S.; Cimrova, V.; Lesnyak, V.; López-Cabarcos, E.; Tzavalas, S.; Rojas-Reyna, R.; Eychmüller, A.; Stamm, M. *Langmuir* **2008**, *24*, 9820–9824.
(16) Schmidt, S.; Motschmann, H.; Hellweg, T.; von Klitzing, R. *Polymer* **2008**, *49*, 749.

during the synthesis, giving microgels with entrapped PTEBS. The presence of PTEBS renders the microgels fluorescent, and this property can be modified by collapsing or swelling the PNIPAM matrix.

Materials and Methods

Materials. *N*-Isopropyl acrylamide (97% pure) and *N*,*N*-methylene bisacrylamide (99% pure) were purchased from Sigma Aldrich; ammonium peroxodisulfate (APS) was purchased from Fluka. Water-soluble conjugated polymer sodium poly[2-(3-thienyl)ethoxy-4-butylsulfonate] with an average molecular weight of 269 000 g/mol was purchased from American Dye Source.

Characterization. The microgel particles were studied using scanning electron microscopy (SEM) in a JEOL (JSM-6400) microscope. Dynamic light scattering experiments (DLS) were carried out to examine the evolution of the particle size as a function of temperature, using a Malvern Nano-ZS system equipped with a He−Ne laser working at 632.8 nm. The suspension of microgels was diluted to a concentration of 0.02% (w/w) to prevent multiple scattering and to diminish colloidal interactions. The time correlation function of the scattered intensity, $g(t) = \langle I(0)I(t)\rangle$, was measured, and the mean hydrodynamic radius was obtained as a function of the temperature. Photoluminiscence (PL) spectra were collected using a JASCO spectrofluorimeter equipped with a thermostatic bath for temperature control. Time resolved fluorescence measurements of the microgels were recorded using a QM3PH instrument from Photon Technology International, working at an excitation wavelength of 370 nm. Elemental analysis of C, H, N, and S was carried out using a LECO CHNS-932 instrument. Incoherent quasielastic neutron scattering (IQNS) experiments were carried out at the Institute Laue Langevin (ILL) in Grenoble, using the neutron backscattering spectrometer IN10. Standard ILL procedures and programs were used for corrections (empty cell), normalization, and quasielastic peak fitting.

Synthesis of PNIPAM Interpenetrated with PTEBS Microgels. PNIPAM interpenetrated microgels were synthesized using the free surfactant polymerization method[9−11] of an aqueous solution (50 mL) of NIPAM (0.1 M), PTEBS (4.3×10^{-4} M, in monomer repetitive units), and cross-linker *N*,*N*′-methylene bisacrylamide (BA). The cross-linking content, given as [BA(*g*)]/[NIPAM(*g*) + BA(*g*)] × 100, was varied between 2.5 and 10% in order to obtain microgels with different swelling properties. During the preparation of the microgels, it is extremely important to dissolve perfectly the photoluminescent polymer. Due to the low solubility of PTEBS, this was obtained at polymer concentrations between 10^{-4} and 10^{-5} M. At higher concentrations, the polymer aggregates, hampering to obtain monodispersed microgels due to the formation of PNIPAM coagulum. The solution was heated up under N_2 atmosphere, and when the temperature reached 70 °C, the polymerization was started by adding 250 mg of ammonium persulfate. The mixture was refluxed for 4 h in N_2 atmosphere, and, subsequently, the microgels were filtered and dialyzed against distilled water for 2 days. Finally, they were centrifuged at 15 000 rpm, redispersed in Milli-Q water several times, freeze-dried, and stored at room temperature.

Results and Discussion

Dynamic light scattering measurements were performed on a dispersion of PTEBS, and the results indicated that, in water, the polymer forms small particles of 10 nm mean diameter (see inset of Figure 1a). However, after the synthesis of the PNIPAM microgels in the presence of PTEBS, only microgel particles are observed as is shown in Figure 1a. The mean diameter size of the microgels depends on cross-linking, and the values obtained by DLS were 420 ± 50 nm (for 10%), 590 ± 60 nm (for 5%), and 700 ± 100 nm (for 2.5% cross-linking). These results indicate that during the microgel formation PTEBS interacts with the PNIPAM growing chains, leading to interpenetrated polymer particles in which the conjugated polymer is entrapped inside the PNIPAM matrix. The driving force for this interaction would be the inherent hydrophobicity of thiophene moieties, which permits the formation of van der Waals interactions between PTEBS and the incipient PNIPAM chains that are hydrophobic at the reaction temperature (70 °C). This sort of interaction has previously been reported for polythiophene moieties with alkyl surfactant.[17−19]

The chemical composition of PTEBS and PNIPAM is very different (see Scheme 1). This feature has been used to determine the amount of PTEBS within the microgels using elemental analysis, and it was found to be around 0.7% (w/w). The amount of PTEBS immobilized within the microgels does not depend on cross-linking percentage. We attributed this result to the fact that the growing microgels behave similar to surfactants facilitating the incorporation of PTEBS in the earlier stage of microgel formation.

Figure 1a shows that microgels with higher cross-linking rates present smaller hydrodynamic diameters. This is due to the increment of the elastic tension introduced by the cross-linker that hinders the microgel swelling and reduces its size. The SEM micrograph of the synthesized particles (see Figure 1b) showed that the microgels are spherical and quite monodispersed, with a collapsed diameter close to 250 nm. The microgels can be easily redispersed in water, giving a colloidal suspension which is stable for several days and presents fluorescence emission when illuminated by UV radiation (see Figure 2).

The swelling behavior of the interpenetrated microgels was evaluated by studying the change of the hydrodynamic diameter, D_h, as a function of temperature. Figure 3 shows that variation of D_h during the volume transition depends on the cross-linking rate of the interpenetrated microgels, as it occurred in pure PNIPAM microgels. This effect is due to the increment of the microgel rigidity introduced by the cross-linker, which hinders the polymer swelling. The inset in Figure 3 shows that, independently of the cross-linking content, the microgels present a volume transition at 34 °C, slightly higher than the LCST for pure PNIPAM. This change is attributed not only to the steric hindrances that the conjugated polymer introduces during PNIPAM chain aggregation but also to the electrostatic repulsion of the PTEBS sulfonate groups in the polymer matrix. Similar results were obtained after immobilizing nanoparticles[20,21] or introducing charged monomers inside PNIPAM microgels.[22]

Recently it has been reported, using IQNS, that PNIPAM chain dynamics exhibits striking differences in the swollen and collapsed states.[23,24] We have studied, with the backscattering spectrometer IN10, the IQNS of the interpenetrated microgels with the aim to investigate if the entrapment of PTEBS modifies the dynamics of the PNIPAM chains. Figure 4 shows the incoherent scattering function $S(Q,\omega)$ in the swollen (17 °C)

(17) Laurenti, M.; Rubio-Retama, J.; Garcia-Blanco, F.; Lopez-Cabarcos, E. *Langmuir* **2008**, *24*, 23.
(18) Chen, L.; Xu, S.; McBranch, D.; Whitten, D. *J. Am. Chem. Soc.* **2000**, *122*, 9303.
(19) Haamed, A.; Attar, A.; Monkman, A. *J. Phys. Chem. B* **2007**, *111*, 12418.
(20) Rubio-Retama, J.; Zafeiropoulos, N. E.; Serafinelli, C.; Rojas-Reyna, R.; Voit, B.; López-Cabarcos, E.; Stamm, M. *Langmuir* **2007**, *23*, 10280.
(21) Pich, A.; Adler, H. J. P. *Polym. Int.* **2007**, *56*(3), 291.
(22) Krazt, K.; Hellweg, T.; Eimer, W. *Colloids Surf., A* **2000**, *170*, 137.
(23) Rubio-Retama, J.; Frick, B.; Seydel, T.; Stamm, M.; Fernandez-Barbero, A.; López-Cabarcos, E. *Macromolecules* **2008**, *41*, 4739.
(24) Rubio-Retama, J.; Frick, B.; Seydel, T.; Lopez-Ruiz, B.; Fernandez-Barbero, A.; Lopez-Cabarcos, E. *Colloids Surf., A* **2008**, *319*, 149.

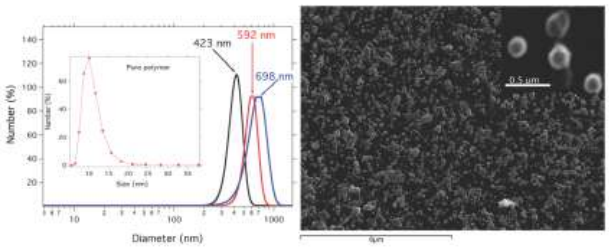

Figure 1. (a) Hydrodynamic diameter of PTEBS−PNIPAM microgels with different cross-linking rates: (black line) 10% of cross-linker, (red line) 5% of cross-linker, and (blue line) 2.5% of cross-linker. The inset depicts the hydrodynamic diameter of the PTEBS particles. (b) SEM micrograph of PTEBS−PNIPAM microgels prepared with a cross-linking rate of 10%. The inset shows microgels at high magnification.

Scheme 1. Chemical Structure of (a) PTEBS and (b) PNIPAM

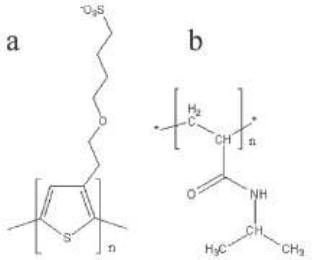

and collapsed states (54 °C) of the 5% cross-linked PTEBS-PNIPAM microgels (Q is the scattering vector and ω is the energy in $\hbar$ units). The incoherent scattering function can be written as

$$S_{inc}(Q,\omega) = \exp\left(-\langle u^2\rangle Q^2/3\right)\delta\omega \otimes \frac{1}{\pi}\frac{DQ^2}{\left(DQ^2\right)^2+\omega^2} \quad (1)$$

where ⊗ is the convolution product in ω, the displacement mean square amplitude is $\langle u^2\rangle^{1/2}$, and D is the diffusion constant. From the fitting of the quasielastic component, measured at different Q, with a Lorentzian function, we obtain the half-width at half-maximum, $\Gamma(Q)$, for the collapsed and swollen microgels. As is illustrated in the inset of Figure 4, the dependence is linear, $\Gamma = DQ^2$, and from the slope we calculated the diffusion constant of the polymer chains with respect to the microgel center of mass.

In the swollen state, we obtained $D = 1.3 \times 10^{-11}$ m^2/s, while in the collapsed state $D = 4.5 \times 10^{-13}$ m^2/s was obtained. These results are very close to those obtained for pure PNIPAM microgels,[23] indicating that the presence of the PTEBS within the PNIPAM microgels does not alter significantly the dynamics of the polymer chains. On the other hand, the big difference of the PNIPAM chain dynamics between the swollen and the collapsed states indicates that microgels present a sol-like behavior below the LCST, whereas they behave as solidlike systems[24] above the LCST.

The PL properties of the thermoresponsive interpenetrated microgels were evaluated as a function of the temperature. As can be seen in Figure 5, the PL intensity is partially quenched when PNIPAM is above the LCST and the collapsed microgel resembles a solid material. In such state, the reduction of microgel particle size with the consequent increase of its refractive index will diminish the number of photons that can reach the entrapped

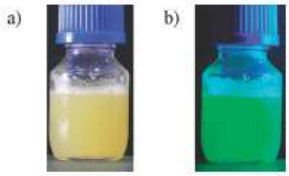

Figure 2. PTEBS−PNIPAM microgels with 10% of cross-linking rate dispersed in water (a) under visible light and (b) illuminated with a UV-lamp (excitation wavelength 350 nm).

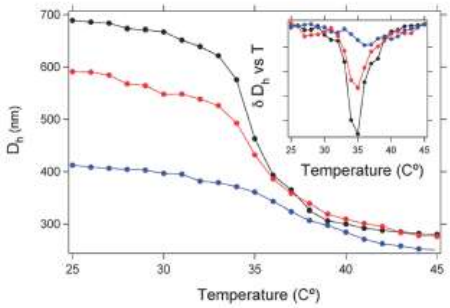

Figure 3. Hydrodynamic diameter (D_h) of microgels with different cross-linking content as a function of the temperature: (black filled circle) PTEBS-PNIPAM microgels with 2.5% of cross-linker, (red filled circle) PTEBS-PNIPAM microgels with a 5% of cross-linker, (blue filled circle) PTEBS-PNIPAM microgels with 10% of cross-linker. The inset depicts the derivative of the D_h versus temperature.

PTEBS, since a fraction of them are scattered.[25,26] Thus, the reduction of the PL emission peak is due not only to the greater chain−chain interaction between the polythiophenes in the collapsed microgel but also to the smaller amount of photons reaching the luminescent polymer. The effect is more intense when the amount of cross-linker in the microgels decreases, and this is attributed to the higher changes in the refractive index experienced by low cross-linked microgels at the volume transition.

Another consequence of the PTEBS immobilization is the shift in the PL emission of the polymer. Figure 6 shows the shift of the

(25) Hong, J. L. X.; Liu, Y.; Li, D.; Wang, Y. W.; Li, J. H.; Bai, Y. B.; Li, T. J. *Adv. Mater.* **2005**, *17*, 163.
(26) Gong, Y.; Gao, M.; Wang, D.; Möhwald, H. *Chem. Mater.* **2005**, *17*, 2648.

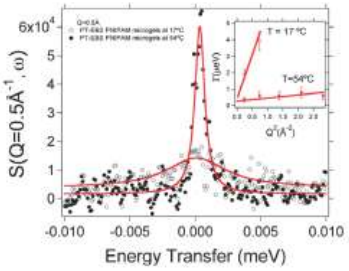

Figure 4. $S(Q,\omega)$ function clearly showing the different dynamics of the 5 wt % cross-linked PTEBS−PNIPAM network in the swollen (17 °C) and collapsed (54 °C) states. The solid lines through the points represent the fitting with a Lorentzian function. The inset shows the half-width at half-maximum of the quasielastic component as a function of Q^2 for the microgels in the swollen and collapsed states.

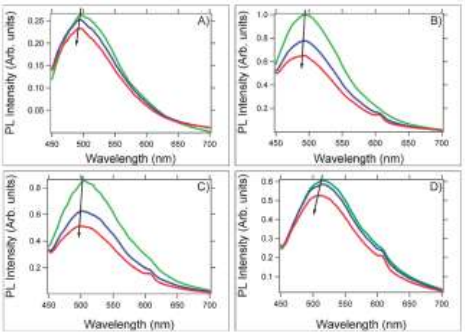

Figure 5. Emission spectra of PTEBS and PTEBS−PNIPAM microgels at different temperatures (green line, 25 °C; blue line, 35 °C; and red line, 45 °C) measured at 0.02% (w/w) concentration: (A) pure PTEBS at concentration 4.3×10^{-4}M, (B) PTEBS−PNIPAM microgels with 2.5% cross-linker, (C) PTEBS−PNIPAM microgels with 5% cross-linker, and (D) PTEBS−PNIPAM microgels with 10% cross-linker. All spectra were recorded at an excitation wavelength of 425 nm.

PL emission maximum in microgels with different cross-linking content at several temperatures. We can see that the emission peak is slightly shifted from 492 to 490 nm when the PTEBS is entrapped inside the PNIPAM microgels with 2.5% cross-linker at 25 °C. This tiny shift could be attributed to the change of polarity around the entrapped PTEBS. However, when the cross-linking content increases, the PL emission is red-shifted by an amount approximately proportional to the cross-linking. We attributed this effect to the stretching of the PTEBS chains in the hydrophobic environment provided by the higher PNIPAM concentrations inside the higher cross-linked microgels. A more stretched and consequently planar backbone will give a red-shift of the emission peak.[27−29] On the other hand, above the LCST, one would expect an intensification of the red-shift, since in this environment the volume fraction of the PNIPAM matrix increases, promoting a major structure compactness. On the

(27) López-Cabarcos, E.; Carter Sue, A. *Macromolecules* **2005**, *38*, 4409. López-Cabarcos, E.; Carter Sue, A. *Macromolecules* **2005**, *38*, 10537.
(28) Thomas, S. W.III; Joly, G. D.; Swager, T. M. *Chem. Rev.* **2007**, *107*, 1339.
(29) Hoang-A, H.; Ahmed, N.; Leclerc, M. *Acc. Chem. Res.* **2008**, *41*, 168.

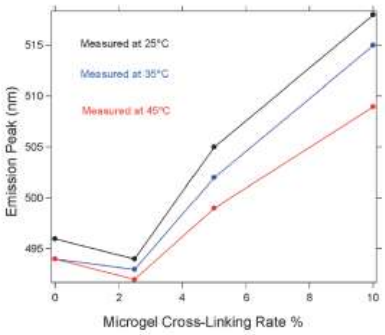

Figure 6. Position of the emission peak as a function of the cross-linking rate measured at (black filled circle) 25 °C, (blue filled circle) 35 °C, and (red filled circle) 45 °C.

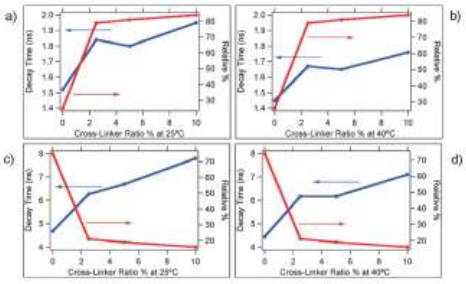

Figure 7. Two fluorescence decay times (blue) and percentage contribution to the steady state intensity (red) as a function of cross-linker content of PTEBS-PNIPAM microgels in the swollen (a, c) and collapsed states (b, d). The fast component is shown in the upper panel, and the slow one in the bottom panel.

contrary, the PL emission suffers a considerable blue-shift with the increasing temperature. This unexpected behavior could arise from the different viscoelastic properties of PNIPAM above and below the LCST. As we have previously demonstrated, the chain dynamics of the PNIPAM microgels show a sol−gel-like behavior below the LCST while above the LCST the dynamics is compatible with a solidlike behavior[24] and the collapsed microgel would hinder the rearrangement of the PTEBS chain segments. Thus, the greater flexibility of the polythiophene backbone below the LCST might facilitate a greater delocalization of the relaxed excited state (exciton). By contrast, above the LCST the tight PNIPAM environment might increase the rigidity of the polythiophene backbone reducing the length of the π-conjugated segments.[30,31] Furthermore, the hydrophobic character of the PNIPAM chains above the LCST could permit them to interact with the hydrophobic polythiophene moieties of the PTEBS, breaking up the $\pi-\pi$ intrachain interaction which would also shift the emission to the blue.[32,33]

(30) Wang, M.; Zou, S.; Guerin, G.; Shen, L.; Deng, K.; Jones, M.; Walter, G. C.; Acholes, G. D.; Winnik, M. A. *Macromolecules* **2008**, *41*, 6993.
(31) Kanemitsu, Y.; Masuda, K.; Tanaka; Ando, M.; Kushida, T; Min, K. S.; Atwater, H. A. *Phys. Status Solidi* **2002**, *190*, 529.
(32) Kwak, G.; Lee, W. E.; Jeong, H.; Sakaguchi, T.; Fujiki, M. *Macromolecules* **2009**, *42*, 20.
(33) Chen, L.; Xu, S.; McBranch, D.; Whitten, D. *J. Am. Chem. Soc.* **2000**, *122*, 9303.

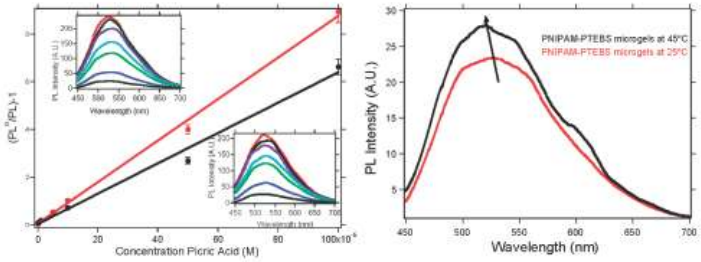

Figure 8. (a) Stern−Volmer plot for PL quenching with picric acid at 25 °C (red line) and 45 °C (black line). The upper inset shows the PL emission of PTEBS−PNIPAM microgels at different concentrations of picric acid at 25 °C, while the inset on the bottom depicts the PL emission at 45 °C for different concentrations of picric acid. (b) PL emission of the PTEBS−PNIPAM microgels in the presence of 1×10^{-4} M picric acid at 25 and 45 °C.

Scheme 2. Proposed Mechanism to Explain the Decay Time Behavior[a]

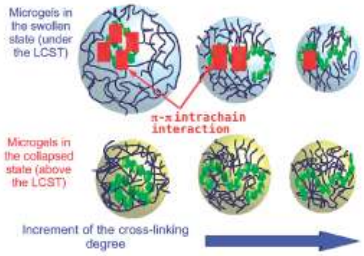

[a] Poly(thiophene) chains are hydrophobic, forming $\pi-\pi$ intrachain interactions below the LCST. The $\pi-\pi$ interactions are favored by the reduction of water content as the cross-linking increases. However, above the LCST, the PNIPAM chains become hydrophobic and interact with the poly(thiophene) moieties, breaking up the $\pi-\pi$ intrachain interactions.

Time-resolved fluorescence measurements were carried out to better understand the PL emission process of the IPNs. Two exponential decay processes were necessary for fitting the decay time profiles of all the samples. This indicates that early fluorescence decay is dominated by a double exponential component, and the intensity can be written as the sum of individual exponential decays

$$I(t) = \sum_{i=1}^{2} A_i \, e^{-t/\tau_i} \qquad (2)$$

where $I(t)$ is the intensity, A_i represents the amplitude of the components at $t = 0$, and τ_i is the decay time of the component i. In order to get the lifetime distribution as well as the fractional contribution of each component to the intensity, we have analyzed the data using the multiexponential method. Figure 7 represents the decay times obtained for the microgels with varying cross-linking rate above and below the LCST.

The existence of two decay times would indicate the presence of polythiophene moieties in two different environments. Furthermore, the decay time of entrapped PTEBS increases with respect to the nonencapsulated polymer, and the increment is proportional to the cross-linking rate. This fact could be related to the reduction of the water content inside the microgels and the consequent increase of the polymer volume fraction as the cross-linking becomes higher (see upper part of Scheme 2). Moreover, it is worth pointing out the shortening of the PL decay time when the microgel collapsed, which is attributed to the reduction of delocalization of the exciton along the PTEBS chain, due to the higher rigidity of the conjugated polymer chain in the collapsed microgel[29] (see bottom part of Scheme 2).

The detection of nitro aromatics by quenching of conjugated polymers is well established after the original work of the Swager group.[28,34,35] Above the LCST, the capacity of the PNIPAM chain to break up the $\pi-\pi$ interaction of PTEBS opens the possibility of using this system to dissociate similar interactions between polythiophene and quenching molecules such as trinitrotoluene, picric acid, or methyl viologen. For instance, below the LCST, the addition of increasing concentrations of picric acid, ranging from 1×10^{-7} to 1×10^{-4} M, to the interpenetrated microgels provokes the quenching of the PL emission (see Figure 8a), which indicates the formation of a complex between the quencher and the π-conjugated polymer.

The quenching of the PL emission by the nitro aromatic compound is 92% of its initial value at 25 °C. The quantitative measure of PL quenching is given by the Stern−Volmer constant K_{SV}, defined by

$$\frac{PL^0}{PL} = 1 + K_{SV}[A]$$

where PL^0 and PL are the intensities of fluorescence in the absence and in the presence of the quencher, respectively, and $[A]$ is the concentration of quencher. For entrapped PTEBS quenched by picric acid, $K_{SV} = 1 \times 10^5\ M^{-1}$ at 25 °C and $7 \times 10^4\ M^{-1}$ at 45 °C. These values have been compared with the nonencapsulated PTEBS, being $8 \times 10^4\ M^{-1}$ and $7 \times 10^4\ M^{-1}$ at 25 and 45 °C, respectively. As we can see, at 25 °C the differences in the K_{SV} capacity are slightly bigger in the interpenetrated microgels, which could be due to the capacity of PNIPAM to stretch the PTEBS chain below the LCST. This fact could facilitate the accessibility of quencher to the fluorophores, increasing the K_{SV} value at lower temperatures.

When the temperature of the microgels is raised above the LCST, the interactions between quencher and PTEBS are hindered due to the collapse of the microgels, and the PL emission partially recovers, even in the presence of the quencher in the microgel dispersion (see Figure 8b). This phenomenon can be used to collect the microgels free of quencher. Thus, by recovering the microgels in the collapsed state, and redispersing them in pure

(34) Andrew, T. L.; Swager, T. M. *J. Am. Chem. Soc.* **2007**, *129*, 7254.
(35) Narayanan, A.; Varnavski, O.; Swager, T. M.; Goodson, T.III *J. Phys. Chem. C* **2008**, *112*, 881.

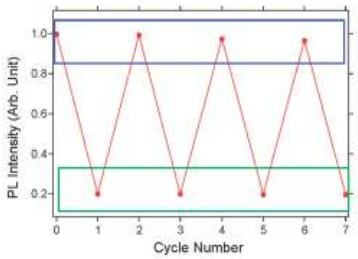

Figure 9. PL intensity measured during repeated cycles of quencher addition and subsequent recovering of collapsed microgels.

Scheme 3. Mechanism of PL Quenching and Recovering of the Initial Fluorescence of Interpenetrated Microgels

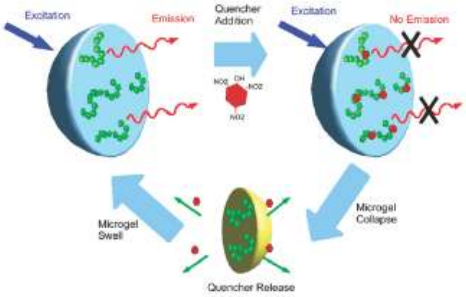

water at 25 °C, 100% of the initial PL emission is recovered (see Figure 9).

Scheme 3 summarizes the mechanism of fluorescence quenching and recovering for interpenetrated microgels. In the swollen state, the microgels are fluorescent, but after the addition of the nitro aromatic compound the PL is quenched because picric acid forms a nonfluorescent complex with the π-conjugated polymer. However, above the LCST, the PNIPAM matrix interacts with the polythiophene moieties, breaking partially the quencher−polythiophene complex and releasing the quencher. Subsequently, the microgels are collected and reswelled, recovering its initial fluorescence. The whole procedure could be use to recover the fluorescence microgels and reuse them again.

Conclusions

The present work shows an easy way for the synthesis of fluorescence microgels based on PNIPAM and PTEBS. The PL properties of the interpenetrated microgels were studied as a function of cross-linking degree, temperature, and rigidity of the polymer matrix. The results confirmed the close relationship between the environment and the PL emission of the encapsulated π-conjugated polymer. Furthermore, it was observed that above the LCST the PNIPAM chain was able to interact with the π-conjugated polymer, breaking $\pi-\pi$ interactions. This characteristic was used to prepare a reusable microsensor suitable for detecting nitro aromatic compounds.

Acknowledgment. This work was supported by the Ministry of Science and Technology (MAT2006-13646-C03-01) and the BSCH-UCM program for research groups. Marco Laurenti thanks the "Comunidad de Madrid" and E.U. for cofunding a Ph.D. fellowship to perform this work. Partial support of COST Action D43 is also acknowledged.

9.3 Fluorescence Decrease of Conjugated Polymers by the Catalytic Activity of Horseradish Peroxidase and Its Application in Phenolic Compounds Detection

BioMACROMOLECULES

ARTICLE

pubs.acs.org/Biomac

Fluorescence Decrease of Conjugated Polymers by the Catalytic Activity of Horseradish Peroxidase and Its Application in Phenolic Compounds Detection

M. I. González-Sánchez,[†] M. Laurenti,[‡] J. Rubio-Retama,[‡] E. Valero,*[,†] and E. Lopez-Cabarcos[‡]

[†]Physical Chemistry Department, School of Industrial Engineering, University of Castilla-La Mancha, Albacete 02071, Spain

[‡]Physical Chemistry Department, Faculty of Pharmacy, Complutense University of Madrid, Madrid 28040, Spain

ABSTRACT: We report the fluorescence decrease of the water-soluble $\pi-\pi$-conjugated polymer poly(2-methoxy-5-propyloxy sulfonate phenylene vinylene, MPS-PPV) by the catalytic activity of horseradish peroxidase in the presence of H_2O_2. MPS-PPV acts as a donor substrate in the catalytic cycle of horseradish peroxidase where the electron-deficient enzymatic intermediates compounds I and II can subtract electrons from the polymer leading to its fluorescence decrease. The addition of phenolic drug acetaminophen to the former solution favors the decrease of the polymer fluorescence, which indicates the peroxidase-catalyzed co-oxidation of MPS-PPV and acetaminophen. The encapsulation of horseradish peroxidase within polyacrylamide microgels allows the isolation of intermediates compound I and compound II from the polymer, leading to a fluorescence decrease that is only due to the product of biocatalytic acetaminophen oxidation. This system could be used to develop a new device for phenolic compounds detection.

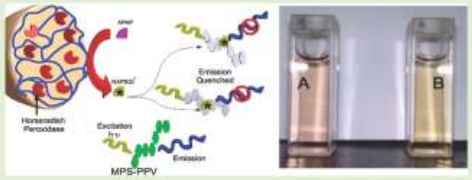

INTRODUCTION

Fluorescent-conjugated polymers (CPs) are one of the most attractive areas of research for a variety of applications such as light-emitting diodes,[1] laser diodes,[2] fluorescent polarizers,[3] chemical sensors,[4−6] and photovoltaic devices.[7] Besides, water-soluble CPs are of particular interest for applications in chemical and biological detection[8] for the following reasons: (i) they exhibit the property of their fluorescence being quenched by an ultralow concentration of quenchers,[9] (ii) their fluorescence is enhanced (by several orders of magnitude upon addition of surfactants),[10,11] and (iii) they provide a new environment to investigate the properties of π-conjugated polymers. Moreover, fluorescence methods are highly sensitive, are easy to operate, and are a good tool to investigate how the electronic states of the luminescent polyelectrolyte are affected by the geometrical changes of the solvated photoluminiscent polymer. For these reasons, water-soluble CPs are being investigated with a view to developing optical biosensors.[9−15]

Chen et al.[9] proposed a novel fluorescent biosensor based on the luminescent polyelectrolyte poly(2-methoxy-5-propyloxy sulfonate phenylene vinylene) (MPS-PPV). They showed that the photoluminescence (PL) of MPS-PPV was very efficiently quenched by an electron acceptor (methyl viologen). By tethering the quencher to a ligand that is sequestered by binding it to a specific biorelevant target, they created a novel and sensitive class of biosensors. More recently, Fan et al.[12] reported that cytochrome *c* (cyt c) acts as an efficient PL quencher of poly[lithium 5-methoxy-2-(4-sulfobutoxy)-1,4-phenylenevinylene], which is an example of fluorescence quenching of CPs by a protein. These authors attributed the high efficiency of the polymer fluorescence decrease to a combination of photoinduced electron transfer (PET) between cyt c and the CP, and also to the formation of the polymer−quencher complexes driven by attractive Coulomb interactions.

In this work, we propose a mechanism to detect phenolic compounds based on the oxidation of MPS-PPV by the catalytic activity of horseradish peroxidase (HRP) in the presence of H_2O_2, which brings about a conspicuous drop in PL. The heme-containing protein HRP (donor:hydrogen-peroxide oxidoreductase, EC 1.11.1.7) catalyzes the oxidation of substrates at the expense of H_2O_2 or lipid peroxides. The enzyme catalytic cycle is initiated by the rapid $2e^-$ oxidation ($k > 10^7\ M^{-1}\ s^{-1}$)[16] of the met enzyme (i.e., in the Fe(III) heme state, native enzyme, metHRP) by hydrogen peroxide to give a green enzymatic intermediate, compound I (CoI), with the heme iron oxidized to the oxyferryl state (Fe^{IV}=O) and a π-cation radical on the porphyrin ring. Phenols or aromatic amines reduce CoI in a one-electron step to compound II (CoII), and CoII back to the native enzyme in a sequential one-electron step, as shown in Scheme 1.

However, in the presence of an excess of H_2O_2, CoII transforms to compound III (CoIII) (formal oxidation state of +6), which involves a protective mechanism against the suicide inactivation of HRP.[17] Donor substrates also show a protective effect on the H_2O_2-induced suicide inactivation of HRP, as long as the [substrate]/[H_2O_2] ratio is high.[17] Thus, rich electron molecules such as $\pi-\pi$-conjugated polymers may act as substrates in the HRP action mechanism to provide a protective effect.

Received: January 19, 2011
Published: February 22, 2011

   dx.doi.org/10.1021/bm200091m | Biomacromolecules 2011, 12, 1332–1338

Scheme 1. Classic Peroxidase Cycle Using H_2O_2 as an Oxidizing Substrate[a]

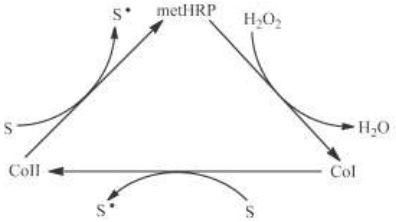

[a] S is a reducing substrate and S• is the free radical product.

Polymer oxidation conveys an increase in the polymer HOMO−LUMO band gap by decreasing fluorescence quantum efficiency and provoking a blue shift of the signal. The change in fluorescence emission offers the possibility of detecting the radical molecules generated by a peroxidase-like activity, which can occur in living organisms under oxidative stress conditions.

For instance, HRP catalyzes the one-electron oxidation of the analgesic and antipyretic drug acetaminophen (APAP), which is safe for humans at normal doses but can lead to liver damage and renal impairment if ingested in excess.[18] The HRP-catalyzed oxidation of APAP in the presence of H_2O_2 yields *N*-acetyl-*p*-benzosemiquinonimine (NAPSQI•), a very reactive radical[19,20] that lowers the polymer's fluorescence emission and makes it possible to detect APAP at micromolar concentrations. This feature may lead to the development of new sensory devices that use the optical and electronic properties of CPs.

EXPERIMENTAL SECTION

Chemicals and Buffers. Acrylamide (AA) 99%, *N*,*N*′-methylenebisacrylamide (BIS) 99%, *N*,*N*,*N*′,*N*′-tetramethylenediamine (TEMED), dodecane 99%, HRP, and APAP were purchased from Sigma Aldrich (Madrid, Spain). Ammonium peroxodisulfate and surfactant Span 80 were purchased from Fluka (Madrid, Spain). Hydrogen peroxide was obtained from Panreac (Barcelona, Spain). MPS-PPV with a molecular weight of $(1-5) \times 10^5$ Da (≈1000 monomer repeat units) was first synthesized by Fred Wudl (UCLA).[9] In this work, MPS-PPV concentrations are expressed in monomer units (M_w = 276.2 Da). All the solutions were prepared using 50 mM sodium phosphate buffer at pH 7. A stock solution of 100 μM MPS-PPV was prepared by dissolving 2.8 mg of MPS-PPV in 100 mL of buffer.

All the reagents were used as received without further purification. Solutions were prepared with demineralized water which was purified in a Milli-Q purification system (18.2 MΩ·cm) (Millipore Corp., Bedford, MA).

Microgels Synthesis. Polyacrylamide microparticles (PAA) with BIS as a cross-linker and HRP entrapped (HRP-PAA) were prepared using the concentrated emulsion polymerization method.[21,22] The cross-linking degree, η, given as the ratio between the cross-linker (BIS) weight and the monomer (AA), was 8%.[22] The concentrated emulsion was prepared with 16.67% of the oil phase (the continuous phase) and 83.33% of the aqueous phase (dispersed phase). To obtain the W/O concentrated emulsion, 5 mL of an aqueous solution, consisting of 1.25 g of AA, 100 mg of BIS, 9 mg of ammonium persulfate, and 1.4 mg of HRP, was added by dropwise addition using a syringe until the continuous oil phase (750 μL of dodecane and 250 μL span 80). The emulsion was homogenized by magnetic stirring and purged with nitrogen to remove residual oxygen. Polymerization was started by adding 63 μL of TEMED to the emulsion. Polymerization of the gel-like emulsion produced entrapped enzyme microgels. During polymerization, the temperature was controlled and kept below 35 °C to maintain enzyme activity and to avoid protein denaturation. At 1 h postreaction, microgel particles were precipitated and washed several times with phosphate buffer at pH 7 until no enzymatic activity was detected in the supernatant. Subsequently, they were isolated by centrifugation (10 000 rpm) for 10 min at 8 °C and freeze-dried. This protocol generated PAA microparticles with diameters of between 1 and 32 μm.

Microgel particles were examined using scanning electron micrographs (SEM) under a JEOL (Tokyo, Japan) JSM-6400 microscope operating at an acceleration voltage of 20 kV.

To study size distribution, freeze-dried microgels were dispersed in water for 24 h and observed with an optical microscope. Two hundred particles were picked up randomly from optical microscope photographs, while their diameters were measured using the UTHSCSA ImageTool (V.3.0) to calculate the average diameter and the size distribution of the microgels.

Fluorimetric and Spectrophotometric Assays. Fluorescent spectra were taken with a JASCO (Tokyo, Japan) FP 6300 fluorometer, by exciting at 466 nm near the absorption peak of MPS-PPV. Absorption spectra were taken with a Varian Cary (Amsterdam, The Netherlands) 300 Bio UV−vis spectrophotometer. Temperature was controlled at 25 °C using a Hetofrig Selecta (Barcelona, Spain) circulating bath with a heater/cooler and was checked with a Checktemp 1 pocket digital thermometer from Hanna Instruments (Guipúzcoa, Spain) with a resolution of 0.1 °C. All the assays were initiated by the addition of H_2O_2.

The H_2O_2 and APAP concentrations in the stock solutions were spectrophotometrically determined at 240 nm using the following molar extinction coefficients: 39.5[23] and 9.7 × 10^3 M^{-1} cm^{-1},[20] respectively. The HRP concentration was calculated at 403 nm using a molar extinction coefficient of 1.02 × 10^5 M^{-1} cm^{-1}.[24]

RESULTS

We investigated the PL decrease of MPS-PPV by the catalytic activity of HRP in the presence of H_2O_2. The emission spectrum of an MPS-PPV solution (80 μM) was measured in both the absence and presence of H_2O_2 (Figure 1A), and no difference between them was observed. The emission spectrum of an MPS-PPV solution in the presence of HRP is shown in Figure 1B (curve 1) and, in comparison with Figure 1A, no shift of the maximum wavelength or decrease in the fluorescence of MPS-PPV was observed. However, when H_2O_2 was added to this solution, fluorescence intensity decreased conspicuously as a function of time, as shown in Figure 1B. Moreover, this decrease of PL intensity was concomitant with a blue shift of the maximum from 547 to 517 nm (Figure 1B). Polymer fluorescence was not restored after the end of the biocatalytic reaction, which suggests a permanent change in the MPS-PPV structure.

Figure 2 shows the UV−vis spectrum of native HRP in an aqueous solution (curve 1) with an intense peak at 403 nm (Söret band), which is characteristic of pigmented heme-containing moieties, and three weak bands assignable to Q_x, Q_0, and porphyrin → iron charge-transfer bands at 504, 537, and 645 nm, respectively.[25] The absorbance spectrum of MPS-PPV in the aqueous solution (curve 2) shows two maxima at 358 and 453 nm. Curve 3 in Figure 2 corresponds to the absorbance spectrum of a solution of HRP and MPS-PPV. This curve coincides with the sum of curves 1 and 2, indicating there is no reaction between the polymer and the protein. However, when an excess of H_2O_2 is added to this latter solution, the maximum

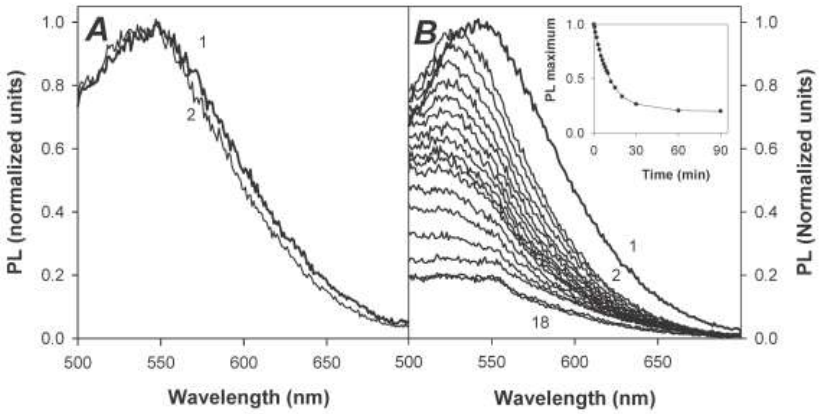

Figure 1. (A) Emission spectra of 80 μM MPS-PPV (curve 1) and 80 μM MPS-PPV plus 0.5 mM H_2O_2 (t = 5 min after the addition of H_2O_2, curve 2). (B) Repetitive emission spectra of 80 μM MPS-PPV in the presence of HRP and H_2O_2. Curve 1 corresponds to the emission spectrum of a solution of 80 μM MPS-PPV and 3.0 μM HRP. Curves 2−18 are the emission spectra of 80 μM MPS-PPV and 3.0 μM HRP taken after the addition of 0.5 mM H_2O_2 at the times indicated in the inset where we show the evolution of the PL maximum as a function of time. Scan speed was 600 nm/min. The excitation wavelength was 466 nm.

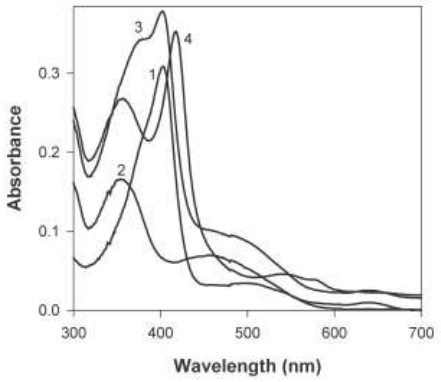

Figure 2. Absorption spectra of an aqueous solution of 3.0 μM HRP (curve 1), 80 μM MPS-PPV (curve 2), 3.0 μM HRP with 80 μM MPS-PPV (curve 3), and 3.0 μM HRP with 80 μM MPS-PPV, 1 min after the addition of 0.5 mM H_2O_2 (curve 4). Scan speed was 1000 nm/min.

wavelength of the Söret band of HRP red-shifted from 403 to 417 nm (curve 4) owing to the formation of CoIII (Söret band at 418 nm and two absorbance peaks at 544 and 577 nm) under the condition of an excess of H_2O_2 used in this experiment.[26] In addition, the 453 nm peak corresponding to MPS-PPV disappeared at 1 min after the addition of H_2O_2.

The change in absorbance during the reaction of HRP with H_2O_2 is shown in the insets of Figure 3 in both the absence (A) and presence (B) of MPS-PPV. Given our aim to better illustrate the evolution of absorbance during the reaction, we present in Figure 3 the results obtained in both cases from a spectral differential analysis. Upon the addition of H_2O_2 to native HRP, the Söret band shifted from 403 (Figure 2, curve 1) to 417 nm (curve 2 in the inset of Figure 3A,B) due to the predominance of species CoIII under the experimental conditions described herein. The characteristic CoIII spectrum reached its maximum at 2 min after the reaction began (insets in Figure 3A,B, curve 2) and subsequently decayed with time (Figure 3A,B). In the absence of the polymer (Figure 3A), CoIII evolved toward the formation of the inactive species of HRP, as observed by the increase in absorbance at 670 nm, and the CoII spectrum could be seen at longer reaction times (Söret band at 420 nm and two absorbance peaks at 527 and 554 nm) (Figure 3A inset, curve 39). When MPS-PPV was included in the reaction medium, the absorbance at 417 nm showed faster decay (Figure 3B). Moreover, no increase in absorbance was observed at 670 nm, indicating a protective effect of the polymer on H_2O_2-induced HRP suicide inactivation. During the course of the reaction, an isosbestic point at 393 nm was maintained, indicating the coexistence of species CoI and CoII (Figure 3B).[27] The characteristic CoII spectrum could be seen at longer reaction times (Figure 3B inset, curve 39).

Based on these results, it is feasible to decrease polymer fluorescence using the free radicals generated by enzymatic oxidation of aromatic compounds to therefore detect those molecules that are substrates of HRP. In the presence of H_2O_2, HRP catalyzes the oxidation of APAP to NAPSQI$^{\bullet}$,[19,20] an electron-deficient molecule which reacts with nucleophilic molecules (Scheme 2).

To prove the effect of NAPSQI$^{\bullet}$, we measured the fluorescence emission of MPS-PPV in the presence of HRP, H_2O_2, and APAP. The results are shown in Figure 4.

If we compare the inset in Figure 4 with the inset in Figure 1, we can see that the presence of APAP yielded an almost instantaneous fluorescence decrease, which indicates the appearance of NAPSQI$^{\bullet}$. In addition, the color of the samples changed from pale pink to orange as a result of the reaction (Scheme 3). Under these experimental conditions, there were three molecules responsible for the decrease in fluorescence: CoI, CoII, and

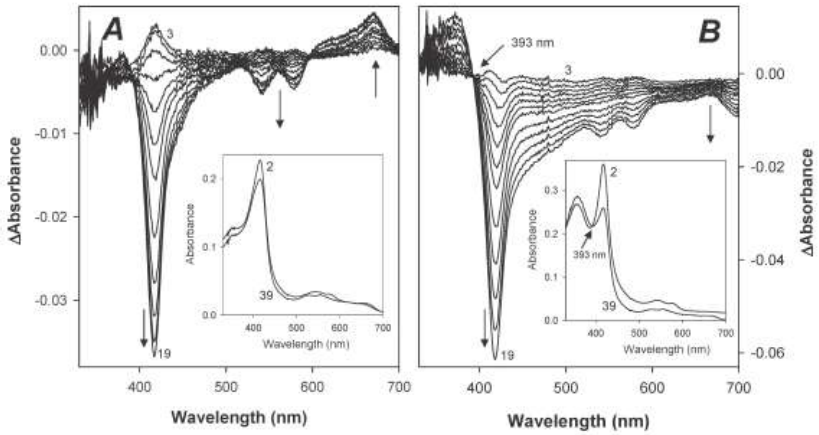

Figure 3. Spectral differential analysis of the reaction of native ferric HRP (metHRP) (3.1 μM) with H_2O_2 (0.5 mM) in the absence (A) and presence (B) of MPS-PPV (80 μM). The spectrum obtained 2 min after the addition of H_2O_2 has been subtracted from all the spectra to show maxima differences. (A) Spectra were taken at 1 min intervals from t = 3 min (spectrum 3) up to 9 min after the addition of H_2O_2, and at 2 min intervals from t = 11 min up to 19 min (spectrum 19). The scan speed was 1000 nm/min. The inset shows the direct spectra obtained at 2 min (curve 2, predominance of CoIII) and 39 min (curve 39, predominance of CoII) after the addition of H_2O_2. (B) The spectra shown were taken as in (A). The inset shows the direct spectra obtained at 2 min (curve 2, predominance of CoIII) and 39 min (curve 39, predominance of CoII) after the addition of H_2O_2.

Scheme 2. Production of NAPSQI$^•$ from APAP via HRP-Catalyzed Oxidation in the Presence of H_2O_2

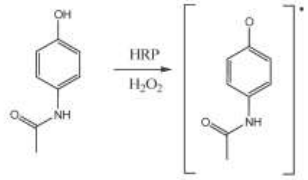

Acetaminophen (APAP) — N-acetyl-*p*-benzosemiquinone imine (NAPSQI$^•$)

NAPSQI$^•$. For the purpose of isolating the contribution of the different agents, HRP was immobilized in poly(acrylamide) microgels (PAA) with 8% of the cross-linking degree.[22] Figure 5A depicts an SEM micrograph of the microgels with HRP entrapped inside. Microgels were spherical in shape with a mean hydrodynamic diameter of 6.8 μm when dispersed in water (Figure 5B).

HRP immobilization within the microgels prevents contact between both ferryl states of HRP (CoI and CoII intermediates) and MPS-PPV, thus avoiding the effect of the activated enzyme on the CP. At the same time, the reticulated polymer microgel allows a good diffusion of small molecules such as H_2O_2 and APAP which, after being transformed within the microgel into NAPSQI$^•$, can diffuse to the bulk solution where MPS-PPV is dissolved. In this scenario, fluorescence intensity reduction is related with the presence of NAPSQI$^•$ in the bulk solution.

To prove the isolation of the enzyme from MPS-PPV, the fluorescence emission spectrum of MPS-PPV in the presence of the HRP encapsulated in the microgels (HRP-PAA) was

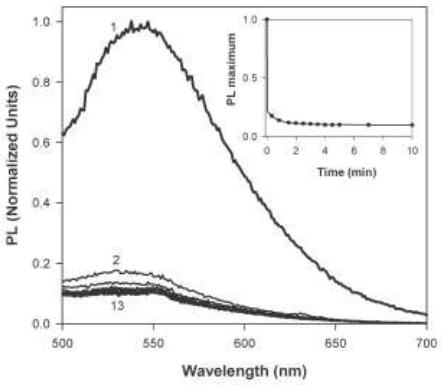

Figure 4. Curve 1 is the fluorescence spectrum of a solution containing 80 μM MPS-PPV, 3 μM HRP, and 0.6 mM APAP. Curves 2−13 correspond to the spectra of the previous solution after the addition of 0.5 mM H_2O_2 at the times indicated in the inset. The scan speed was 600 nm/min. The excitation wavelength was 466 nm.

measured in both the absence (Figure 6A, curve 1) and presence of H_2O_2 (Figure 6A, curve 2); the difference was negligible. The corresponding variation of fluorescence emission at the maximum wavelength as a function of time is shown in Figure 6B, curves 1 and 2, respectively. Both time courses were in parallel, indicating that, under these conditions, the effect of H_2O_2 on the fluorescence emission was slight and, therefore, the confinement of HRP inside the PAA microgels was effective.

Subsequently, H_2O_2 was added to different solutions consisting of HRP-PAA, MPS-PPV, and a range of APAP concentrations,

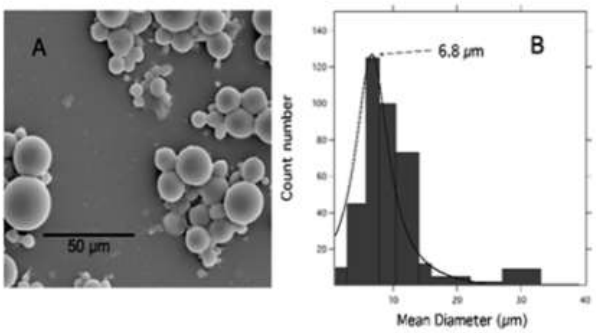

Figure 5. (A) SEM micrograph of microgels with HRP entrapped inside with a cross-linking degree of 8%. (B) Size distribution of the microgels dispersed in the aqueous solution.

Scheme 3. Summary of the APAP Detection Mechanism

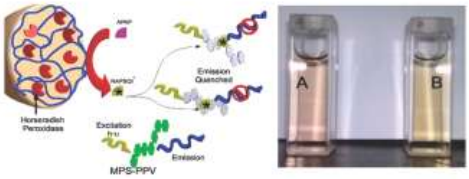

while fluorescence emission was measured as a function of time (Figure 6B, curves 3−11). The degree of PL decrease is dependent upon the APAP concentration, a fact that could be used to detect APAP (or other phenolic compounds substrates of HRP) by optical means. Thus, setting the detection limit to equal 3 times the fluctuation of the signal is possible to be able to detect APAP concentrations above 1×10^{-7} M under the experimental conditions described herein.

DISCUSSION

The water-soluble $\pi-\pi$-conjugated polymer MPS-PPV is able to act as a donor substrate in the catalytic cycle of HRP in the presence of H_2O_2. There are two facts that support this statement: (i) MPS-PPV has electron donor character[28] and (ii) the active HRP site offers good accessibility,[29] which facilitates interaction with the polymer. Thus, MPS-PPV behaves as a substrate of HRP by reducing both CoI and CoII in agreement with the action mechanism of HRP[27] (Scheme 1). Both intermediates, CoI and CoII, are powerful oxidants with redox potentials close to +1 V,[30] and each one can subtract an electron from the polymer, provoking its oxidation and decreasing its fluorescence. In CPs, there is a red shift of the emission spectra when the electron density is injected into the polymer chain, and a blue shift when the electron density is removed.[31,32] Therefore, the blue shift observed from 547 to 517 nm (Figure 1) correlates with both the oxidation of the polymer chain and the corresponding decrease of $\pi-\pi$ conjugation. Oxidation of MPS-PPV would explain not only the blue shift of the PL maximum reported in Figure 1 but also the disappearance of the maximum at 453 nm in the absorbance spectra (Figure 2, curve 4). Furthermore, the isoelectric point of HRP is 7.2,[33] which means that HRP is not charged under our experimental conditions (pH 7.0). For this reason, the decrease in fluorescence could not be attributed to the formation of a polymer−protein complex driven by attractive Coulomb interactions.

The spectra shown in Figure 3B indicate that MPS-PPV has a protective effect against the H_2O_2-induced inactivation of HRP. This behavior is characteristic of electron donors that reduce CoI and CoII to the so-called met state of the protein.[17,20] Moreover, the CoII spectrum is clearly noted with long reaction times (Figure 3A,B, insets), thus providing proof that CoI has been reduced. The reduction of CoII back to the ferric state of the protein usually takes place at a slower rate than the reduction of CoI,[34] thus the rate-limiting step in the catalytic cycle of HRP. A feasible model in which MPS-PPV behaves as a substrate of HRP would be the following:

$$\text{HRP (Fe(III))} + H_2O_2 \rightarrow \text{CoI} + H_2O \quad (1)$$

$$\text{CoI} + \text{MPS-PPV} \rightarrow \text{CoII} + \text{MPS-PPV}^{\bullet} \quad (2)$$

$$\text{CoII} + \text{MPS-PPV} \rightarrow \text{HRP (Fe(III))} + \text{MPS-PPV}^{\bullet} \quad (3)$$

where MPS-PPV$^{\bullet}$ stands for the oxidized state of MPS-PPV.

When APAP was included in the reaction medium, an almost instantaneous fluorescence decrease took place. There have been reports that in the peroxidase-catalyzed oxidation of two substrates, activation (or inhibition) of the reaction of one substrate for another is often observed (co-oxidation).[35] For example, the oxidations of both NADPH[36] and rifampicin[37] catalyzed by HRP and H_2O_2 are markedly increased by the presence of APAP. This phenomenon is explained by an electron-transfer mechanism of the following type:

$$S_1^{\bullet} + S_2 \rightarrow S_1 + S_2^{\bullet} \quad (4)$$

where S_1 and S_2 are substrates of HRP, and $S_1^{\bullet}$ and $S_2^{\bullet}$ are their corresponding oxidized products. In such cases, the better substrate (S_1) is oxidized first by CoI and CoII, and its product ($S_1^{\bullet}$) is the oxidizing agent for the second substrate (S_2). In our case, S_1 in eq 4 is APAP, while S_2 is MPS-PPV since APAP is oxidized by HRP with good catalytic efficiency.[19,20] Furthermore, the accessibility of MPS-PPV to the active site of the enzyme is

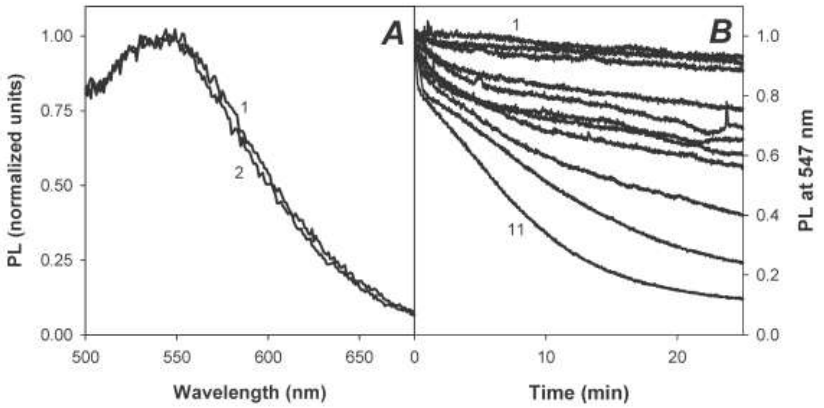

Figure 6. (A) Emission spectra of an MPS-PPV aqueous solution (80 μM) in the presence of 1 mg of HRP-PAA (curve 1), 1 mg of HRP-PAA and H_2O_2 0.5 mM (t = 10 min after the addition of H_2O_2, curve 2). (B) Fluorescence intensity at 547 nm of 80 μM MPS-PPV aqueous solutions recorded in the presence of 1 mg of HRP-PAA at a fixed H_2O_2 concentration (0.5 mM) and different APAP concentrations. Curve 1 corresponds to a solution containing 80 μM MPS-PPV and 1 mg of HRP-PAA, in the absence of H_2O_2. Curves 2−11 were obtained in the presence of H_2O_2 at the following APAP concentrations: 0, 6×10^{-8} M, 1×10^{-7} M, 6×10^{-7} M, 1×10^{-6} M, 6×10^{-6} M, 1×10^{-5} M, 3×10^{-5} M, 6×10^{-5} M, and 1×10^{-4} M.

more difficult. The encapsulation of HRP inside poly(acrylamide) microgels confirms this surmise since it prevents any contact between the protein and the CP, and consequently, no drop in fluorescence was observed in the absence of APAP (Figure 6A). However, small molecules such as H_2O_2 and APAP can diffuse through the microgel and reach the enzyme catalytic site to generate NAPSQI$^{\bullet}$, which then diffuses outward the microgel, oxidizing MPS-PPV and decreasing the fluorescence emission.

In Scheme 3, we summarize the steps involved in the fluorescence decrease of MPS-PPV using HRP-PAA in the presence of H_2O_2 and APAP.

CONCLUSIONS

In this work, we show that the HRP intermediates CoI and CoII act as efficient one-electron oxidizing agents of MPS-PPV, which lead to a drop in its fluorescence emission. This is an example of photoluminescence decrease of a CP due to the catalytic action of HRP, which can be applied to the detection of specific molecules. The addition of a phenolic compound to the reaction medium, such as APAP, leads to an increased MPS-PPV oxidation rate due to the phenomenon of substrate−substrate activation, which is typical of HRP-catalyzed reactions (co-oxidation). For the purpose of substantiating our model, HRP has been immobilized within PAA microgels to separate the protein from the polymer. This new system can be used to detect phenolic compounds since it responds to APAP at micromolar concentrations.

ACKNOWLEDGMENT

We acknowledge financial support from the Spanish Ministry of Science and Innovation (grant MAT2010-15349), the UCM-BSCH program for "Consolidation of Research Groups" (Group 911033), the COST Action D43, and the Regional Ministry of Science and Technology (Consejería de Ciencia y Tecnología; JCCM, Spain) (grants PAI-08-0175-8618 and POII-10-0235-8597). M.L. acknowledges the Autonomous Community of Madrid for a fellowship to perform this work.

REFERENCES

(1) Liu, H. F.; Fong, L. Y.; Yang, Y. *Appl. Phys. Let.* **2002**, *80*, 1891–1893.
(2) McGehee, M. D.; Grupta, R.; Miller, E. K.; Heeger, A. J. *Synth. Met.* **1999**, *102*, 1030–1033.
(3) Yanagi, H.; Morikawa, T.; Hotta, S.; Yase, K. *Adv. Mater.* **2001**, *13*, 313–317.
(4) McQuade, D. T.; Pullen, A. E.; Swager, T. M. *Chem. Rev.* **2000**, *100*, 2537–2574.
(5) Laurenti, M.; López-Cabarcos, E.; García-Blanco, F.; Frick, B.; Rubio-Retama, J. *Langmuir* **2009**, *25*, 9579–9584.
(6) Thomas, S. W., III; Joly, G. D.; Swager, T. M. *Chem. Rev.* **2007**, *107*, 1339–1386.
(7) Tang, C. W. *Appl. Phys. Lett.* **1986**, *48*, 183–185.
(8) Montaño, G. A.; Dattelbaum, A. M.; Wang, H. L.; Shreve, A. P. *Chem. Commun.* **2004**, *10*, 2490–2491.
(9) Chen, L.; McBranch, D. W.; Wang, H. L.; Helgeson, R.; Wudl, F.; Whitten, D. G. *Proc. Natl. Acad. Sci. U.S.A.* **1999**, *96*, 12287–12292.
(10) López-Cabarcos, E.; Rubio-Retama, J.; Sholin, V.; Carter, A. *Polym. Int.* **2007**, *56*, 588–592.
(11) Sholin, V.; López-Cabarcos, E.; Carter, A. *Macromolecules* **2006**, *39*, 5830–5835.
(12) Fan, C.; Plaxco, K. W.; Heeger., A. J. *J. Am. Chem. Soc.* **2002**, *124*, 5642–5643.
(13) Jiang, H.; Taranekar, P.; Reynolds, J. R.; Schanze, K. S. *Angew. Chem., Int. Ed.* **2009**, *48*, 4300–4316.
(14) Liu, Y.; Ogawa, K.; Schanze, K. S. *J. Photochem. Photobiol. C—Photochem. Rev.* **2009**, *10*, 173–190.
(15) López-Cabarcos, E.; Carter, S. A. *Macromolecules* **2005**, *38*, 4409–4415.
(16) Rodríguez-López, J. N.; Hernández-Ruiz, J.; García-Cánovas, F.; Torneley, R. N. F.; Acosta, M.; Arnao, M:B. *J. Biol. Chem.* **1997**, *272*, 5469–5476.
(17) Hernández-Ruiz, J.; Arnao, M. B.; Hiner, A. N.; García-Cánovas, F.; Acosta, M. *Biochem. J.* **2001**, *354*, 107–114.

(18) Thomas, S. H. *Pharmacol. Ther.* **1993**, *60*, 91–120.
(19) Potter, D. W.; Hinson, J. A. *Drug. Metab. Rev.* **1989**, *20*, 341–358.
(20) González-Sánchez, M. I.; Manjabacas, M. C.; García-Carmona, F.; Valero, E. *Chem. Res. Toxicol.* **2009**, *22*, 1841–1850.
(21) Rubio-Retama, J.; López-Ruiz, B.; López-Cabarcos, E. *Biomaterials* **2003**, *24*, 2965–2973.
(22) González-Sánchez, M. I.; Rubio-Retama, J.; López-Cabarcos, E.; Valero, E. *Biosen. Bioelectron.* **2011**, *26*, 1883–1889.
(23) Nelson, D. P.; Kiesow, L. A. *Anal. Biochem.* **1972**, *49*, 474–478.
(24) Sakurada, J.; Sekiguchi, R.; Sato, K; Hosoya, T. *Biochemistry* **1990**, *29*, 4093–4098.
(25) Huang, Q.; Al-Azzam, W.; Griebenow, K.; Schewertzer-Stenner, R. *Biophys. J.* **2003**, *84*, 3285–3298.
(26) Ximenes, V. F.; Catalani, L. H.; Campa, A. *Biochem. Biophys. Res. Commun.* **2001**, *287*, 130–134.
(27) Dunford, H. B. *Peroxidases and Catalases. Biochemistry, Biophysics, Biotechnology and Physiology*, 2nd ed.; John Wiley & Sons: New York, 2010.
(28) Toal, S. J.; Trogler, W. C. *J. Mater.Chem.* **2006**, *16*, 2871–2883.
(29) Ortiz de Montellano, P. R. *Annu. Rev. Pharmacol. Toxicol.* **1992**, *32*, 89–107.
(30) Veitch, N. C. *Phytochemistry* **2004**, *65*, 249–259.
(31) Thomas, S. W., III; Swager, T. M. *Macromolecules* **2005**, *38*, 2716–2721.
(32) Lakowicz, J. R. *Principles of Fluorescence Spectroscopy*, 2nd ed.; Kluiwer Academic/Plenum Publishers: New York, 1999.
(33) Maehly, A. C. *Arch. Biochem. Biophys.* **1955**, *56*, 507–524.
(34) Dunford, H. B.; Stillman, J. S. *Coord. Chem. Rev.* **1976**, *19*, 187–251.
(35) Lebedeva, O. V.; Ugaroya, N. N. *Russ. Chem. Bull.* **1996**, *45*, 18–25.
(36) Keller, R. J.; Hinson, J. A. *Drug Metab. Dispos.* **1991**, *19*, 184–187.
(37) Dos Santos, F. J. N.; Ximenes, V. F.; Da Fonseca, L. M.; De Faria Oliveira, O. M.; Brunetti, I. L. *Biol. Pharm. Bull.* **2005**, *28*, 1822–1826.

9.4 *Synthesis of the Water-Soluble Conjugated Polymer poly(3-ethoxy-thiophene-2,5-diyl-dimercaptosuccinic-acid) and its Application in Heavy Metal Ions Detection*

The article derived from Chapter 5.4 of this manuscript has been submitted to *Macromolecules.*

9.5 *Synthesis of Anisotropic Gold Nanocrystals Mediated by Lead, Cadmium and Water Soluble Conjugated Polymers*

The article derived from Chapter 5.5.1 of this manuscript is in preparation and will be submitted to *Langmuir.*

9.6 *Synthesis of Thermosensitive Core-Shell Hybrid Microgels with Tunable Magnetic Core Size*

The article derived from Chapter 5.5.2 of this manuscript has been submitted to *Langmuir.*